Plasma chemistry modelling for the conversion of CO_2 and CH_4 into value-added chemicals under atmospheric pressure plasma conditions

Joachim Slaets

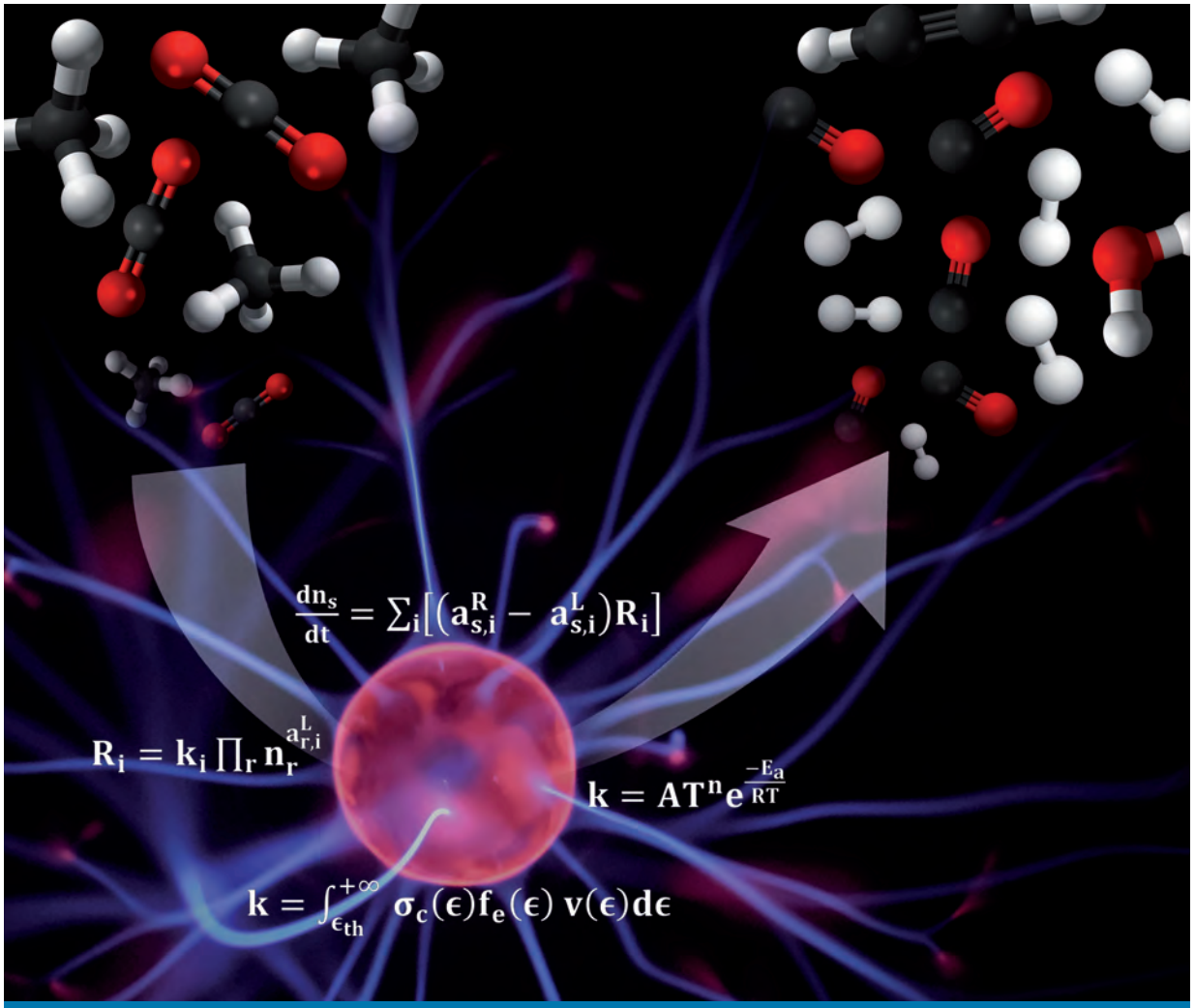

Supervisor **prof. dr. Annemie Bogaerts**

Thesis submitted for the degree of Doctor of Sciences
Faculty of Science | Department of Chemistry | University of Antwerp, 2024

University of Antwerp

Faculteit wetenschappen

Departement Chemie

Plasma chemistry modelling for the conversion of CO_2 and CH_4 into value-added chemicals under atmospheric pressure plasma conditions

Proefschrift voorgelegd tot het behalen van de graad van Doctor in de Wetenschappen: Chemie

Aan de Universiteit Antwerpen te verdedigen door

Joachim Slaets

Antwerpen 2024

Promotor: prof. dr. Annemie Bogaerts

Members of the Jury

- Prof. dr. Erik Neyts (Chair)
  Modelling and Simulation in Chemistry, University of Antwerp

- Prof. dr. Annemie Bogaerts (Promotor)
  Plasma Lab for Applications in Sustainability and Medicine - Antwerp, University of Antwerp

- Prof. dr. Siegfried Denys
  Antwerp engineering, PhotoElectroChemistry & Sensing, University of Antwerp

- Prof. dr. Patrice Perreault
  Laboratorium voor de elektrificatie van chemische processen en waterstof, University of Antwerp

- Prof. dr. Jan van Dijk
  Elementary Processes in Gas Discharges, Eindhoven University of Technology

- Prof. dr. Gerard van Rooij
  Circular Chemical Engineering - Plasma Chemistry, Maastricht University

- dr. Ramses Snoeckx
  Empa, Swiss Federal Laboratories for Materials Science and Technology

Acknowledgements

The last years I embarked on this challenging PhD journey which certainly had its ups and downs. I even had some moments I didn't think I would get here, but look, I finally made it. Those who know me well know that I'm not great with words and not the best at expressing thanks, so I'll keep this brief.

Firstly, I would like to thank my promotor Annemie for giving me the opportunity to do this PhD and for the support and guidance along the way. Over the years I shared an office with a lot of people; Vincent, Fanny, Charlotta, Kristof, Josh, Omar, Matthew, Yury, Callie, Joran and Elli, thank you all for the great atmosphere. Also, I would like to thank all the people I met, worked with at PLASMANT; Bart, Rani, Colin, Ivan, Roel, Hamid, Stein, Stijn, Mathias, Mahdi, Shangkun, Eduardo, Greg, Igor, Robin, Sara, Sarah, Helder, Pepijn, Cedric, Luc, Karen, Karel, Priyanka, Maryam, James, Sean, Yannick, Stijn, Yannick, Kevin. You all made it a great place to work and all of you helped me achieve this milestone. I am truly thankful for getting to know you all.

In het bijzonder wil ik Senne, Elise, Eline en Claudia bedanken om mij met open armen te verwelkomen, wegwijs te maken in de groep en altijd bij jullie terecht te kunnen. Dan is er ook nog Björn, de 2^{e} helft van het duo, het was geweldig om samen met jou aan dit avontuur te beginnen na samen gestudeerd te hebben. Na bijna 10 jaar zal het toch ook wel wennen worden om niet meer samen te werken.

Ook wil ik mijn mama, papa en zus bedanken voor alle steun en het vertrouwen dat jullie in mij hadden. Zonder alles dat jullie voor mij gedaan hebben had ik nooit de weg kunnen afleggen om tot op dit punt te komen. Dante, Matthias & Yannick, Céderic en Elien, bedankt dat ik bij jullie af en toe mijn frustraties kon uiten en ook de positieve momenten kon delen. Annick, Paul, Margaux en Junior danku voor alle dagen die ik bij jullie heb doorgebracht. Jullie hebben me geholpen mijn gedachten te verzetten en ik voelde me altijd welkom.

Manou je bent er altijd voor mij geweest, al die jaren heb je toch wel wat afgezien met mij, als ik weer een hele avond gefrustreerd bezig was met uitzoeken waarom iets weeral niet werkte. Maar ondanks alles kon ik altijd bij jou terecht en bleef je in mij geloven.

Summary

Global CO_2 concentrations in the atmosphere have reached unprecedented levels, driven primarily by anthropogenic emissions. This alarming rise in greenhouse gases (GHGs) presents a significant challenge to global climate stability, with CO_2 being the primary contributor to climate change. Industrial activities are major sources of these emissions, highlighting the urgent need for innovative and sustainable solutions. One promising approach to mitigate CO_2 emissions involves the utilization of CO_2 as a feedstock or raw material, transforming waste carbon into valuable products, a concept known as carbon capture and utilization (CCU).

Among the various CCU technologies, plasma technology emerges as particularly promising. Plasma creates a highly reactive environment through the presence of high-energy electrons. By leveraging such processes, CO_2 can be transformed into useful chemicals, contributing to both emissions reduction and resource circularity. A key advantage of plasma-based processes is their compatibility with electrification, particularly when powered by renewable energy sources like solar or wind. This not only reduces the carbon footprint of chemical processes but also aligns with the global transition towards renewable energy.

One interesting reaction, which can be carried out in a plasma environment, is the dry reforming of methane (DRM). DRM is a process that utilizes CO_2 and methane (CH_4) to produce a mixture of carbon monoxide (CO) and hydrogen (H_2), which can be used to synthesize a variety of chemicals and fuels. This makes DRM a versatile and valuable process in the context of CCU.

This thesis delves into the chemistry of plasma-based DRM, with a focus on understanding and optimizing the process through chemical kinetics modelling. The extended introduction in chapter 1 provides a comprehensive overview of the principles and potential of this technology. This is followed by a description of the simulations performed to model the chemical kinetics of DRM in chapter 2.

Chapter 3 investigates the effect of nitrogen (N_2) on plasma-based DRM, using the model to support experimental results and demonstrate the role of N_2 in

the conversion process within a gliding arc plasmatron (GAP) reactor. This concludes that a small fraction of N_2 can actually improve the energy efficiency of the process.

In chapter 4, a wide range of conditions is explored using the model to understand the core chemical kinetics of DRM in warm plasmas. This chapter highlights the limitations of different gas mixtures and examines the performance of the process across a wide temperature range. The findings demonstrate where plasma-specific kinetics diverges from thermal gas-phase chemistry, offering new insights into the unique behaviour of plasma-driven reactions.

After the plasma has converted the gas molecules, further chemical changes can still occur, influencing the overall efficiency and product distribution. Chapter 5 investigates these post-plasma reactions, showing that quenching the gas temperature does not generally improve performance, except in CO_2-rich mixtures where certain reactions are influenced by the cooling process, leading to notable changes in the product distribution. The chapter also explores the benefits of combining the hot plasma effluent with unconverted gas, where the residual heat from the plasma can be reused to drive additional reactions, thereby improving the overall efficiency of the process.

The findings presented in this thesis contribute to a deeper understanding of plasma-based DRM technology, forming a foundation for further experimental and theoretical studies.

These insights pave the way for the development of more advanced and complex models, which, in turn, can support experimental work aimed at further optimizing and scaling up this promising technology for industrial applications. By advancing plasma-based CCU processes, this research contributes to the broader goal of reducing GHG emissions and supporting the transition to a sustainable, low-carbon future.

Samenvatting

De wereldwijde CO_2-concentraties in de atmosfeer hebben ongekende niveaus bereikt, voornamelijk door menselijke uitstoot. Deze alarmerende toename van broeikasgassen vormt een aanzienlijke bedreiging voor de stabiliteit van het klimaat, waarbij CO_2 de belangrijkste bijdrage levert aan deze klimaatverandering. Industriële activiteiten zijn een grote bron van deze emissies, waardoor er dringend nood is aan innovatieve en duurzame oplossingen. Het gebruik van CO_2 als grondstof of basismateriaal, is een veelbelovende manier om CO_2-emissies te verminderen. Hierbij wordt een afvalstroom omgezet in waardevolle producten, een concept dat bekend staat als koolstofopvang en -gebruik (CCU).

Onder de verschillende CCU-technologieën komt plasmatechnologie naar voren als veelbelovend. Plasma creëert een zeer reactieve omgeving door de aanwezigheid van hoog-energetische elektronen. Door gebruik te maken van dergelijke processen, kan CO_2 worden omgezet in bruikbare chemicaliën, wat bijdraagt aan zowel emissiereductie als circulaire economie. Een belangrijk voordeel van plasmaprocessen is het gebruik van elektriciteit, vooral wanneer ze worden aangedreven door hernieuwbare energiebronnen zoals zonne- of windenergie. Hierdoor vermindert niet alleen de ecologische voetafdruk van chemische processen, maar sluit dit ook aan bij de wereldwijde overgang naar hernieuwbare energie.

Een interessante reactie, die kan uitgevoerd worden in een plasma omgeving, is de droge reforming van methaan (DRM). DRM is een proces waarbij CO_2 en methaan (CH_4) worden gebruikt om een mengsel van koolstofmonoxide (CO) en waterstof (H_2) te produceren, wat gebruikt kan worden voor de synthese van verschillende chemicaliën en brandstoffen. Dit maakt van DRM een veelzijdig en waardevol proces in de context van CCU.

Deze thesis verdiept zich in de chemie van plasma-gebaseerde DRM, met een focus op het begrijpen en optimaliseren van het proces door middel van chemische kinetische modellering. De inleiding in hoofdstuk 1 biedt een uitgebreid overzicht van de principes en mogelijkheden van deze technologie. Hierna volgt in hoofdstuk 2 een beschrijving van de uitgevoerde chemisch kinetische simulaties van DRM.

Hoofdstuk 3 onderzoekt het effect van stikstof (N_2) op plasma-gebaseerde DRM, waarbij het model wordt gebruikt ter ondersteuning van experimentele resultaten en om de rol van N_2 in het conversieproces binnen een 'gliding arc plasmatron' (GAP) reactor aan te tonen. Dit onderzoek concludeert dat een kleine fractie N_2 de energie-efficiëntie van het proces kan verbeteren.

In hoofdstuk 4 wordt met behulp van het model een brede waaier aan condities bestudeerd om de fundamentele chemische kinetiek van DRM in warme plasma's te begrijpen. Dit hoofdstuk belicht de beperkingen van verschillende gasmengsels en onderzoekt de prestaties van het proces over een breed temperatuurbereik. De bevindingen tonen aan waar plasma-specifieke kinetiek afwijkt van thermische gasfase-chemie en bieden nieuwe inzichten in de unieke eigenschappen van plasma-gestuurde reacties.

Nadat het plasma de gasmoleculen heeft omgezet, kunnen verdere chemische veranderingen nog steeds optreden, die de algehele efficiëntie en productverdeling beïnvloeden. Hoofdstuk 5 onderzoekt deze post-plasmareacties, waarbij wordt aangetoond dat het afkoelen van de gastemperatuur over het algemeen niet tot prestatieverbetering leidt, behalve in CO_2-rijke mengsels waar bepaalde reacties worden beïnvloed door het afkoelingsproces, wat leidt tot merkbare veranderingen in de productverdeling. Dit hoofdstuk onderzoekt ook de voordelen van het combineren van het warme plasma-effluent met koud niet-omgezet gas, waarbij de restwarmte van het plasma opnieuw kan worden gebruikt om extra reacties aan te drijven, wat de efficiëntie van het proces verbetert.

De bevindingen in deze thesis dragen bij aan een beter inzicht in plasma-gebaseerde DRM technologie, en vormen een basis voor verdere experimentele en theoretische studies. Deze inzichten effenen de weg voor de ontwikkeling van meer geavanceerde en complexe modellen, die op hun beurt experimenteel werk kunnen ondersteunen dat gericht is op het verder optimaliseren en opschalen van deze veelbelovende technologie voor industriële toepassingen. Door plasma-gebaseerde CCU-processen te bevorderen, draagt dit onderzoek bij aan het bredere doel van het verminderen van broeikasgasuitstoot en het ondersteunen van de overgang naar een duurzame, koolstofarme toekomst.

Table of Contents

1 Introduction

1.1 From Industrial Revolution to Circular Economy

Many of the technological masterpieces that are taken for granted in the 21st century, from cars and airplanes to computers and smartphones, owe their existence to the profound transformations that began during the Industrial Revolution. Spanning from the late 18th to the early 19th century, this era marked a pivotal turning point in human history. Factories sprung up, powered by steam engines that utilized coal, and a surge in productivity and technological innovation ensued. Amid this period of rapid advancement, the mid-19th century discovery of oil ushered in a new age of energy. Oil, with its superior energy density, became the lifeblood of modern civilization, enabling unprecedented growth and innovation. The widespread use of the internal combustion engine in the late 19th century exponentially increased oil's value. This engine, which efficiently converted fuel into mechanical energy, revolutionized transportation and industry. The widespread adoption of gasoline and diesel-powered cars, airplanes, and ships made these modes of transportation omnipresent, advancing globalisation and accelerating economic growth. However, these advancements came with a hidden cost that would only become apparent later.

With the widespread use of internal combustion came also the emissions of greenhouse gases (GHGs), namely CO_2, for which the atmosphere levels increased from below 300 ppm in the 19th century to currently above 410 ppm.[1] The main CO_2 emissions originate from the use of fossil fuels (coal, oil and natural gas) for energy production and transportation.[2] The CO_2 in the atmosphere is involved in the greenhouse effect, which traps heat originating from solar radiation in the atmosphere, raising the temperature. Aside from CO_2, also other gases contribute to this enhanced greenhouse effect, such as CH_4 which is in fact a much stronger GHG, with a warming potential about 25 times higher compared to CO_2 over a 100-year period.[3] CH_4 is emitted through various sources, mainly fossil fuel extraction, agriculture (ruminant livestock and rice production) and waste/waste water.[2] While the greenhouse effect is a natural phenomenon, which is necessary to allow and sustain life on our planet,

the large amount of anthropogenic GHGs enhances this effect, trapping more heat and further raising the overall temperature. This is correlated to climate changes, e.g. rising of the sea level, disruptions of ecosystems and more extreme weather events.[1,4–7] Large scale efforts are needed to mitigate the emission of GHGs and thus limit global warming and avoid these disastrous effects of climate change. One important part is by shifting away from fossil fuels and replacing them with renewable energy sources such as solar or wind.

Further, aside from for energy production, fossil sources are also widely used as raw materials in chemical industry. It would be opportune if these could be substituted for more sustainable sources. When combining this with the goal of reducing emissions, the concept of carbon capture and utilization (CCU)[8] comes into play, aiming to recycle waste CO_2 to be used as a new feedstock for the production of chemicals instead of being emitted into the atmosphere. This also contributes to a circular economy and the cradle-to-cradle principle.[9] To achieve this, new chemical processes are needed to break down these GHGs into viable building blocks that can be used in new or existing processes for the synthesis of various chemicals, fuels, or plastics. This should thereby lead to the integration of multiple production processes reducing the overall emissions.[10] However, dedicated effort is needed to develop such processes that transform CO_2 from a waste product to a building block that can be used in new value chains.

1.2 Plasma technology

A possible route for this GHG utilization is through the use of plasma technology. Plasma is defined as a (partially) ionized gas, containing neutral gas molecules, radicals and excited species along with ions and free electrons. Between these species a wide range of ionization, excitation, dissociation or association reactions can occur, creating an interesting reactive environment from a chemical point of view.[11,12]

Plasma can be created by applying a potential difference across two electrodes, creating an electric field which accelerates the lighter electrons in this field, increasing their kinetic energy, or in other words, their temperature. These electrons can create new electrons and ions through ionizing collisions with

other species, thus sustaining the plasma. Also, during collisions with heavy species, a faction of their energy is transferred to them. If enough energy is transferred, a state of local thermodynamic equilibrium (LTE) is reached, in which all species can be described by the same temperature.[11,12] This is also often referred to as thermal plasmas, which can be achieved at very high temperatures or high pressures. They are for example used in welding or found in fusion plasmas like occurring in stars.

On the contrary, when there is a large discrepancy between the temperature of different plasma species, this is a non-LTE or non-thermal plasma.[11,12] This refers to the unequal distribution of energy across the degrees of freedom (translations, rotations, vibrations and electronic excitations), i.e., the plasma can be described by multiple temperatures.[12] The electron temperature is often much higher, reaching several eV (1 eV = 11605 K), while the heavy species temperature remains much lower, closer to room temperature. The lowest energy modes are usually shared between the ions and the translational and rotational degrees of freedom, all having a similar temperature, while the temperature of vibrationally excited species can be higher, yet still much lower than the electron temperature. The high energy electrons can also excite and even dissociate stable molecules, such as CO_2 or N_2, thereby creating radicals. This makes non-LTE plasmas chemically very reactive. These non-LTE plasmas find multiple applications in for example etching, thin layer deposition and the breakdown of small molecules.[11,12]

Non-thermal plasmas in which the heavy species reach gas temperatures of several 1000 K are sometimes classified as warm plasmas.[13] In these plasmas, all degrees of freedom are equilibrated, except for the electron temperature (typically obtained for pressures close to or above atmospheric pressure). These plasmas share the same high energy electron processes with non-LTE plasmas, while the elevated gas temperature also influence the gas kinetics. Examples of these warm plasmas are gliding arc (GA), microwave (MW), atmospheric pressure glow discharges (APGDs) or nanosecond pulsed discharges (NPDs).[11,13]

1.2.1 Plasma for gas conversion

While plasma technology is gaining increasing interest from industry[14,15], there are still technological hurdles to overcome. This requires further scientific

research to better understand the chemical processes at hand and optimize operating conditions to improve competitiveness with other technologies.[16] To achieve robust industrial applications, also optimisation of reactor design and materials, specifically for scale up and durability for extended operation, is needed.[17]

Electrification of chemical production through the use of renewable energy sources, such as solar and wind, is also a major challenge and necessary to reduce the environmental impact.[14,17] However, electricity production of these renewable sources can vary significantly as they are depending on environmental factors, leading to fluctuations in the electricity grid. It is there that the full electric nature of plasma processes and the relative ease with which they can be turned on and off, allows them to quickly adapt to overproduction and capitalize on the resulting drop in electricity prices. Therefore, plasma technology can be used for peak shaving and help balance the electricity grid.[17] This creates the opportunity for a collaborative operation of the chemical and energy industry, beneficial for both parties.

1.2.2 Gliding arc plasma

This thesis studies plasma-based conversion in a wide range of conditions typical for warm plasmas, but chapter 3 focusses more in dept on the process in a GA plasma. Therefore, here we explain its operational principle in a bit more detail. Traditionally, in their simplest configuration, GA plasmas consist of a gas flow between diverging electrodes.[18] A discharge is achieved at the shortest distance, which travels along the electrodes following the gas flow. The arc lengthens until it eventually becomes too long and can no longer be supported and the arc extinguishes. Then, a new arc is formed at the shortest distance, and the whole process is repeated. This two-dimensional design of a traditional GA geometry has certain disadvantages. The arc is not stationary, i.e., continuously moving along the electrodes, extinguishing and reigniting, and therefore only a portion of the gas can pass through the arc and be treated. Additionally, this also leads to short residence times, further limiting its applicability for gas conversion.

To address these limitations, different GA reactor geometries are being developed, one of which is the gliding arc plasmatron (GAP).[19,20] This novel type

of GA reactor was developed at Drexel University by Nunnally et al.[19] to overcome the non-uniform gas treatment of a classical two-dimensional (2D) GA. It utilizes a reverse vortex flow design, comprised of two separate vortex flows moving in opposing directions (as depicted in Figure 1.1). The six tangential inlets create an initial vortex (yellow arrow in Figure 1.1) that is forced upward along the reactor wall, which functions as the cathode. When the gas reaches the end of this reactor wall, it reverses direction, forming a second, narrower inner vortex (blue arrow in Figure 1.1) that moves toward the reactor outlet, which also serves as the anode, and exits the reactor. A potential difference is applied between the cathode and anode, initiating the discharge at the point of shortest distance between them, close to the gas inlets. The gas flow carries the arc until it reaches the end of the cathode, similar to a traditional GA. However, this positions the arc along the reactor's length and is stabilized in the centre by the inner vortex flow, as depicted in red in Figure 1.1. The combination of inner and outer vortex flows not only stabilizes the arc but also allows more gas to pass through it and creates an insulating effect against the reactor walls.

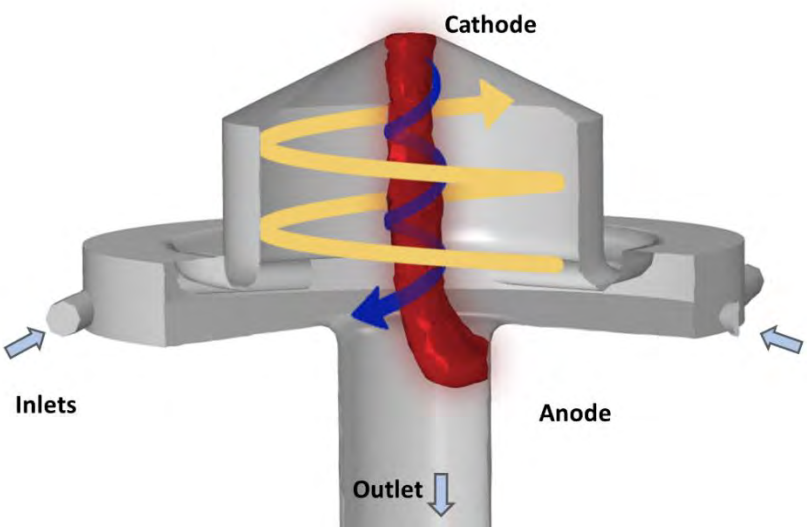

Figure 1.1 Schematic picture of the GAP reactor, with illustration of the outer and inner vortex gas flows (yellow and blue arrows), and the plasma arc (red). The reactor body is at cathode potential while the outlet functions as anode. The arc is formed between the top of the cathode (top of the reactor body) and the anode (outlet). The tangential gas inlets and the outlet of the reactor are indicated with arrows.

1.3 The dry reforming of methane

The simplest way to process CO_2 is through direct splitting into CO and O_2; however, this is limited in its applications for further processing. Instead, adding H_2 to the formed CO creates a mixture known as syngas. This is a versatile feedstock, which can be utilized in various synthesis routes for a wide range of value-added chemicals. Most notably, the Fisher-Tropsch process converts syngas into a variety of hydrocarbons, which can be refined into liquid fuels, such as diesel and gasoline.[21–23] Alternatively, syngas can also be used to produce alcohols (methanol, ethanol), ethers (dimethyl ether) or aldehydes (formaldehyde) through oxo synthesis.[24]

Therefore, adding a hydrogen source to CO_2 before splitting can enable the direct formation of syngas in a one step process. One possible H-containing reactant is CH_4. The combined conversion of CO_2 and CH_4 is otherwise known as the dry reforming of methane (DRM) (R1.1). This allows for the co-creation of CO and H_2 with a theoretical syngas ratio of 1, which is useful for the formation of formaldehyde or simple linear alcohols.[24]

$$\mathrm{CO_{2(g)} + CH_{4(g)} \rightarrow 2\ CO_{(g)} + 2\ H_{2(g)} \quad \Delta H^0 = 247\ kJ\ mol^{-1}} \qquad \text{(R1.1)}$$

Compared to pure CO_2 splitting ($\Delta H^0 = 283$ kJ/mol), this DRM reaction also has a lower reaction enthalpy (36 kJ/mol), making it slightly more thermodynamically favorable. The use of CH_4 is also beneficial from an environmental point of view, as this creates value from a second and more potent GHG (see section 1.1). Lastly, this conversion process can also trigger alternative pathways that directly form other byproducts, such as small hydrocarbons (ethane, ethene, acetylene) or oxygenates (methanol, formaldehyde).[13] The direct generation of these value-added chemicals can be beneficial in terms of valorization.

1.3.1 Plasma-based DRM

When the DRM reaction is performed in a plasma environment, it offers several advantages, as discussed in section 1.2. It allows for the use of renewable energy sources, with great adaptability to the variable electricity supply from these sources. Plasma-based DRM has been explored in a wide variety of

plasma types under a broad range of conditions. In so-called warm plasmas, such as gliding arc (GA), microwave (MW), atmospheric pressure glow discharges (APGDs) or nanosecond pulsed discharges (NPDs), where the gas temperature can reach up to 4000 K or even higher, the main reaction product is indeed syngas.[25,26,35–38,27–34] Cold plasmas, on the other hand, like dielectric barrier discharges (DBDs), also produce mainly syngas, but they also allow the formation of additional side products, such as C2- and C3-hydrocarbons and oxygenates, like methanol, ethanol or formaldehyde, especially when catalysts are integrated in the plasma zone.[39–45]

Although the reaction equation suggests equal ratios of CO_2 and CH_4, in practice, the ratio is often adjusted, typically with an excess of CO_2. This is done for stability reasons, as mixtures with a high CH_4 content tend to produce excessive solid carbon, making them more difficult to handle in practice.[34–38]

The extensive literature search by Snoeckx and Bogaerts[13] evaluated a wide range of plasma types based on experimentally obtained conversion and energy cost for DRM. They concluded that GA and APGD reactors were the most promising, as they can meet the proposed energy cost target of 4.27 eV/molecule (412 kJ/mol) to be competitive with other gas conversion technologies. GA plasmas generally achieve lower conversions compared to APGDs, while the latter can attain both high conversions and low energy cost. The best overall result was reported by Li et al.[46] using an APGD plasma, achieving a total conversion of 89% at an energy cost of only 1.2 eV/molecule. Questions arise however on these findings, because of the low power measurements, as discussed by Wanten et al.[33] In the latter paper, the literature overview was further updated, showing promising results for MW reactors as well, with Chun et al.[47] reaching an energy cost of 3.4 eV/molecule with a CO_2 and CH_4 conversion of 68 and 97%, respectively. Furthermore, Sun et al.[48] improved upon this, obtaining an energy cost of around 3.0 eV/molecule with conversions above 90%. It should be noted that these results are all obtained for warm plasma types, indicating their great potential for high conversion combined with energy-efficient DRM.

1.3.2 DRM kinetics modelling

While experiments are invaluable for the further development of plasma-based DRM, the obtained information is mostly limited to the effects of reactor design and operating conditions on the overall reaction performance, such as energy efficiency, reactant conversion and product yields. This only gives limited insights into the underlying chemical processes. Therefore, additional information can be obtained through kinetics modelling of the experimental setups, gaining important insights in the chemical reactions related to the performance of specific plasma types, reactor designs and the effects of experimental parameters (e.g., flow rate, plasma power, gas mixture). However, this is also a limitation, as the model only considers the specific experimental conditions, determined by e.g., flow dynamics and heat transfer, providing information relevant only for that specific reactor design and operating conditions. For example, studies by Cleiren et al.[31] and Wanten et al.[33] consider DRM in GA and APGD plasmas, respectively, but their modelling is limited to gas temperatures between 2000 – 2700 K in the plasma. The most notable restriction is the maximum CH_4 fraction of only 35%, because of experimental limitations. They also consider a thermal reaction zone with a lower temperature between 1600 – 2200 K, to obtain a better approximation of their experimental reactor. The modelling work performed by Liu et al.[49] does cover a wider range of gas mixtures, up to 50% CH_4 fraction, but it still only considers a gas temperature of 2500 K in the plasma. However, they showed that within plasma systems, thermal chemistry can be an important contributor to the conversion process, thereby showing the effectiveness of the high gas temperatures in warm plasmas. These works show experimentally that CO, H_2 and H_2O are the main products for these gas mixtures, with much smaller and trace amounts of C_2H_2, C_2H_4, C_2H_6 and O_2. Other studies consider DRM with the addition of other gases, such as O_2 or N_2 as major components or impurities in the gas mixture.[32,50] There are also kinetic studies that consider a broader range of operating conditions for plasma-based DRM, but these studies are limited to low temperature DBD plasmas.[51,52] Hence, there is a need for further and more comprehensive studies in this area, to better understand the underlying chemistry in a very broad range of conditions.

1.4 Post-plasma quenching effects

It has been revealed that the downstream gas temperature (i.e., the afterglow or post-plasma region, outside of the plasma zone) in warm plasmas may still be sufficiently high to enable reaction pathways that can influence reactor performance in different manners. For instance, this effect could trigger reverse reactions, reducing the overall conversion and altering the product distribution.[12] On the other hand, it can also be used to enhance the conversion and product yield.

Three different modes can be identified for post-plasma quenching.[12] First, in absolute quenching, the plasma-generated product molecules are preserved, while the radical species recombine to reform the reactants, i.e., leading to a net reduction in the conversion. Second, in ideal quenching, the conversion achieved in the plasma zone is retained by inducing the radicals to react towards products. The third quenching mode is called super-ideal quenching, where not only the high conversions are maintained, but they can be further boosted. Super-ideal quenching can be achieved when the gas is cooled faster than the time required for vibrational-translational (VT) relaxations to occur, creating a VT non-equilibrium.[12] The vibrational energy trapped in the gas molecules can stimulate endothermic reactions, allowing for conversion gains during the quenching.

Thus, recent studies have increasingly focussed on the post-plasma region of these reactors, to build a better understanding of the effects at play and improve the overall performance. Applying this to CO_2 plasmas, it has been demonstrated that CO_2 conversion locally within the plasma can approach 100%.[53,54] However, reverse reactions in the post-plasma region (namely recombination of CO with O radicals) have been found to reduce this significantly, with measured conversions as low as 25%.[53,54] Rapid quenching of the high gas temperature has been shown to be a successful strategy to curtail these reverse reactions.[55–58] This super-ideal quenching mode could even be achieved under specific conditions and in systems with a strong VT non-equilibrium character.[54]

There is a diverse range of quenching methods and several studies have investigated the use of a constricting nozzle, for example.[56–58] This device can

cool down the gas by rapid expansion, creating eddies in the fluid flow which improve gas mixing and heat transfer.[57–59] For CO_2, the conversion gain from this strategy can vary significantly (between 2 and 30%), depending strongly on the operating conditions and nozzle design. The largest additional conversion was seen by Hecimovic et al.[58] who measured an increase in CO_2 conversion from 5 to 35%, following nozzle implementation. Subsequently, this setup was modelled by Van Alphen et al.[60] confirming these findings, indicating that a cooling rate of ~ 10^7 K/s was achieved, significantly enhancing CO_2 conversion. A similar nozzle approach was modelled by Yang et al.[59], reaching the same conclusions.

Further research attempted quenching using liquid-cooled devices to reduce the temperature of the gas stream from the plasma region. A two-stage cooling system used by Wang et al.[61] improved the CO_2 conversion from 6.6 to 19.5%. Another design, which uses a liquid-cooled rod in the reactor outlet to achieve the post-plasma cooling, was used by Kim et al.[55] who reported that the CO_2 conversion increased from 30.1 to 36.1% upon implementation of this strategy. The same approach was also tested for DRM, leading to interesting findings: both the CO_2 and CH_4 conversion were observed to drop compared to the uncooled plasma reactor.[37] The reported maximum decrease in total conversion occurred at a CO_2/CH_4 ratio of 3/1, from 23.4 to 22.6%. On the other hand, upon employing the quenching rod, selectivity towards H_2 was boosted, while that towards H_2O dropped. The selectivity effect was attributed to the inhibition of the reverse water gas shift (RWGS) in the colder post-plasma region, preventing CO_2 and H_2 from reacting to CO and H_2O. While the drop in conversion has a negative effect on the energy cost, the selectivity gain towards H_2 (observed for mixtures with higher CH_4 fractions) can outpace the negative effect on conversion, resulting in a lower energy cost for syngas production.

Another approach to consider is the introduction of new gas in the afterglow region, such as through a secondary inlet. Cho et al.[62] injected cold CH_4 in the afterglow of a CO_2 plasma to achieve conversion, effectively separating the DRM reaction into a two step process. They claim the main advantage of this method is the increase in energy consumption selectivity. The energy injected through the plasma decomposes only CO_2 rather than CH_4, yielding higher CO_2 conversion and higher syngas energy conversion efficiency compared to the

direct DRM reaction in the plasma. While their work specifically focusses on this two step DRM process, this secondary inlet can be an interesting strategy to apply, even without changing the overall gas mixture. The remaining heat in the plasma effluent can be recovered and used to convert the newly introduced gas, potentially improving the performance of the system, while it also provides cooling to the afterglow.

1.5 The aim of this thesis

The overarching aim of this thesis is to obtain a better understanding of the chemical reactions and processes that occur in warm plasmas used for DRM, through chemical kinetics modelling. The different aspects investigated and the obtained insights can lead to potential improvements, to be used in new reactor designs for further advancement of plasma-based DRM technologies.

In **chapter 3** the effect of N_2 on plasma-based DRM is investigated to optimize the N_2 content in the feed gas, to achieve maximal performance for a GAP reactor. The effect of different N_2 fractions on conversion, product selectivity and yield, energy cost and energy efficiency are being investigated through chemical kinetics modelling, while evaluating the modelling output against experimental results.

Chapter 4 presents a very broad kinetics study on the core chemical kinetics of DRM in warm plasmas, such as found in GA, MW, APGDs and NPDs, because they give rise to much better energy efficiency. However, this is not limited to a specific reactor design or narrow operating conditions, as this hinders finding opportunities for further optimization of the conversion process. Instead, general plasma conditions are considered with a wider range of gas temperature, plasma power density, and most importantly, a full range of CO_2/CH_4 gas mixtures, ranging from 90% CO_2 to 90% CH_4. Also, the kinetics of thermal gas chemistry is compared with that of plasma-based conversion to illustrate the differences and similarities between them.

Continuing on this, in **chapter 5** the focus shifts towards the afterglow or post-plasma region, with a specific interest in the downstream gas temperature for DRM plasmas. Kinetics modelling reveals the effect of two distinct approaches to post-plasma quenching: (i) heat removal from the system (emulating the

introduction of a cooled rod, hence conductive cooling), and (ii) the mixing of cold gas in the post-plasma region (emulating the introduction of a nozzle, or simply adding cold gas in the afterglow). In the interest of model versatility and relevance, the work is again not limited to specific reactor designs or operating conditions. Instead, like in previous chapter, general warm plasma conditions are studied with a wide range of plasma temperatures between 2000 – 4000 K and three different CO_2/CH_4 ratios, i.e., stoichiometric (50/50), excess CH_4 (30/70) and excess CO_2 (70/30). Different degrees of gas cooling are explored, achieved with both methods, and the effects of the ensuing temperature drop on conversion, selectivity and energy cost are evaluated.

2 Methodology

2.1 Kinetics modelling

Chemical kinetics modelling is a useful tool for understanding the behaviour of complex chemical systems. In this chapter we explain the use of 0D kinetics models to simulate plasma processes. This type of model considers a homogeneous system, i.e., no spatial gradients, in terms of temperature, power density or species concentrations. It can efficiently handle a large number of species and reactions, making it ideal for simulating these complex processes. Despite the complexity of the underlying chemistry, the model setup is straightforward, and calculations are performed in a reasonable time.

The plasma chemistry in this PhD thesis is described with the Zero-Dimensional Plasma Kinetics solver (ZDPlasKin).[63] In this model the mass conservation equations for all individual species are solved. Every species in the plasma has a certain number density, which changes as a result of the occurring plasma reactions. Part of the species will be consumed by reactions (loss term) and part will be formed from other reactions (production term). This change in number density n of species s with respect to time t is calculated using Eq. 2.1, in which $a^R_{s,i}$ and $a^L_{s,i}$ are the coefficients of species s on the right and left side of the reaction i, respectively, and R_i is the corresponding reaction rate. The reaction rate of reaction i, given by Eq. 2.2, is the product of the rate coefficient k_i and number densities of the reactants n_r.

$$\frac{\mathrm{dn_s}}{\mathrm{dt}} = \sum_{\mathrm{i}}\left[\left(\mathrm{a}^{\mathrm{R}}_{\mathrm{s,i}} - \mathrm{a}^{\mathrm{L}}_{\mathrm{s,i}}\right)\mathrm{R_i}\right] \tag{2.1}$$

$$\mathrm{R_i} = \mathrm{k_i}\prod_{\mathrm{r}} \mathrm{n}_{\mathrm{r}}^{\mathrm{a}^{\mathrm{L}}_{\mathrm{r,i}}} \tag{2.2}$$

For the electron impact reactions, the rate coefficients are calculated using Eq. 2.3, where ϵ is the electron energy, σ_c the collision cross section, f_e the electron energy distribution function (EEDF) and v the electron velocity. This electron velocity is given by Eq. 2.4, in which m_e is the mass of an electron (9.10938×10^{-31} kg).

$$\mathrm{k} = \int_{\epsilon_{\mathrm{th}}}^{+\infty} \sigma_{\mathrm{c}}(\epsilon)\mathrm{f_e}(\epsilon)\,\mathrm{v}(\epsilon)\mathrm{d}\epsilon \tag{2.3}$$

$$v(\epsilon) = \sqrt{\frac{2\epsilon}{m_e}} \tag{2.4}$$

The EEDF is calculated by a Boltzmann solver, BOLSIG+[64], which is integrated in the ZDPlasKin code. BOLSIG+ uses the two-term approximation to calculate the EEDF from the reduced electric field (*E/N*), which is obtained from Eq. 2.5, with n_{tot} the total species number density, *P/V* the power density (given as input to the model) and σ the plasma conductivity. The latter is calculated by Eq. 2.6, with μ the electron mobility, also obtained from BOLSIG+, n_e the electron density and *e* the elementary charge (1.60217662x10^{-19} C).

$$\left(\frac{E}{N}\right) = \frac{1}{n_{tot}}\sqrt{\frac{P/V}{\sigma}} \tag{2.5}$$

$$\sigma = \frac{\mu}{n_{tot}} \cdot n_e \cdot e \tag{2.6}$$

For the other reactions, by the so-called heavy species (i.e., all species besides the electrons), the rate coefficients are given by analytical equations, e.g., modified Arrhenius equations or fall-off functions. The modified Arrhenius equation (Eq. 2.7) gives an empirical relation between temperature and reaction rate coefficient, in which *A* is the pre-exponential factor, *T* the temperature, T^n describes the temperature dependence of the pre-exponential factor, E_a is the activation energy of the reaction and *R* the universal gas constant.

$$k = AT^n e^{\frac{-E_a}{RT}} \tag{2.7}$$

Alternatively, the Lindemann expression can be used to describe the pressure dependence of a reaction, which at low pressure is dependent on the concentration of neutral species [M], while at high pressure this is independent of [M].[65,66] To give a more accurate representation of the transition between these high and low pressure limits, an extra term is added to the equation, using the fall-off expression.[65,66] The rate coefficient is calculated using Eq. 2.8, with k_0 the rate coefficient at the lower pressure limit, k_∞ the rate coefficient at the high pressure limit, *[M]* the concentration (or number density in the case of gas kinetics modelling) and *F* the broadening factor. Several different approximations can be used for the broadening factor, a commonly used

expression is given in Eq. 2.9, with *N* calculated as $N = 0.75 - 1.27 \log F_c$ and F_c an empirical function depending on temperature.[65,66]

$$\mathrm{k} = \frac{\mathrm{k_0[M]k_\infty}}{\mathrm{k_0[M]+k_\infty}} \mathrm{F} \tag{2.8}$$

$$\log \mathrm{F} = \frac{\log \mathrm{F_c}}{1+\left[\frac{1}{\mathrm{N}} \log(\mathrm{k_0[M]/k_\infty})\right]} \tag{2.9}$$

Most rates coefficients can be obtained directly from literature sources, with some exceptions. For reverse processes of reactions between neutral species for which no reliable source can be found in literature, detailed balancing can be used to obtain the rate coefficients. The equilibrium constant K_{eq} is calculated using Eq. 2.10, with *p* the reference pressure (1 bar), Δv the change in number of species in the reaction ($\Delta v = \sum \mu_P - \sum \mu_R$) and ΔG_r the Gibbs free energy of the reaction, calculated using thermodynamic data from McBride et al.[67] and Burcat et al.[68].

$$\mathrm{K_{eq}} = \left(\frac{\mathrm{p}}{\mathrm{RT}}\right)^{\Delta \mathrm{v}} \mathrm{e}^{\left(\frac{-\Delta \mathrm{G_r}}{\mathrm{RT}}\right)} \tag{2.10}$$

From this equilibrium constant, the rate coefficient can be calculated, which is given in Eq. 2.11, assuming the derived reaction is the forward reaction ($k_{forward}$), K_{eq} is given by Eq. 2.10, and $k_{reverse}$ is the known reaction rate coefficient.

$$\mathrm{k_{forward}} = \mathrm{K_{eq} k_{reverse}} \tag{2.11}$$

This type of model depends on the reliability and accuracy of the included rate coefficients, with uncertainties typically expected in the order of 10 – 30%, but they can also be higher than 100%. It is generally established that chemical kinetics models can have a large uncertainty.[69–72] Wang et al.[72] quantified the uncertainties for their DBD model for DRM and obtained uncertainties up to 33% for the conversion and up to 28% for the syngas yield. Therefore, the trends and relative values of the species densities predicted by the model are more important than the absolute values.

In principle, ZDPlasKin considers a batch reactor, calculating the species number densities only as a function of time, by solving the conservation equations (Eq. 2.1). However, the total number density is affected by temperature and chemical reactions, requiring a modification to account for these changes and

to maintain constant (atmospheric) pressure. Therefore, at each timestep, the number densities calculated by ZDPlasKin for all species are multiplied with a correction factor β (Eq. 2.12) to maintain the total number density corresponding to the ideal gas law at atmospheric pressure and the simulated temperature.[54] This approach can be considered a batch reactor operating at constant pressure. In a flow reactor, this correction would be equivalent to contraction or expansion of the gas volume due to chemical reactions, and correspondingly a decrease or increase of the velocity through the plasma.

$$\beta = \frac{\mathrm{T_g}(0)\sum_i n_i(0)}{\mathrm{T_g(t)}\sum_i n_i(t)} \tag{2.12}$$

This expansion also needs to be accounted for when evaluating the simulation output, and therefore the gas expansion factor α is calculated (Eq. 2.13) which represents the ratio of the mass density at the start of the simulation (ρ) and the end (ρ_0). The mass density is the summation of the products of the number density n_j and mass m_j of each species *j* in the model.

$$\alpha = \frac{\rho_0}{\rho} = \frac{\sum_\mathrm{j}[\mathrm{n_{j,0}m_j}]}{\sum_\mathrm{j}[\mathrm{n_j m_j}]} \tag{2.13}$$

2.2 Definitions of calculated conversion, product selectivities and yields, energy cost and energy efficiency

To evaluate the chemical processes that occur in the evaluated plasma systems, several different parameters are considered, e.g., reactant conversion, product selectivity, product yield, energy cost of conversion and energy efficiency.

The absolute conversion (χ_{abs}) is calculated for the reactants, i.e. CO_2 and CH_4, using Eq. 2.14, in which c^{in} and c^{out} are the concentration of the reactant *i* before and after the plasma process, respectively, and α is a factor to account for gas expansion.

$$\chi_{\mathrm{abs}_i} = 1 - \frac{\alpha\, \mathrm{c}_i^{\mathrm{out}}}{\mathrm{c}_i^{\mathrm{in}}} \tag{2.14}$$

In addition, due to dilution with other molecules in the initial mixture (e.g. N_2), we also define the effective conversion (Eq. 2.15), which accounts for the fraction of the reactant *i* in the initial gas mixture.

$$\chi_{\mathrm{eff}_i} = \chi_{\mathrm{abs}_i} \cdot \mathrm{fraction}_i \tag{2.15}$$

The total conversion χ_{total} is calculated in Eq. 2.16 as the sum of the effective conversions of all reactants *i*.

$$X_{\mathrm{total}} = \sum_i X_{\mathrm{eff}_i} \tag{2.16}$$

The product selectivity is calculated using Eq. 2.17, where A is the base-atom (e.g. C, H or O) and μ_s^A and μ_i^A are the numbers of the base-atom in product *s* and reactants *i*, respectively. The base-atom is required to differentiate between the number of each atom type in the gas mixture, which eventually become the products. For the DRM reaction for example, the selectivity of CO can be calculated relative to the amount of C (from CO_2 and CH_4) or O (from CO_2) present in the mixture. Therefore, multiple selectivity values can be calculated for one product.[73,74] By definition, the sum of all selectivity values must be 100%, which is the case for each base-atom.

$$\mathrm{S}_{\mathrm{S}}^{\mathrm{A}} = \frac{\mu_{\mathrm{S}}^{\mathrm{A}}\, \alpha\, \mathrm{n}_{\mathrm{S}}^{\mathrm{out}}}{\sum_{\mathrm{i}}[\mu_{\mathrm{i}}^{\mathrm{A}}(\mathrm{n}_{\mathrm{i}}^{\mathrm{in}} - \alpha\, \mathrm{n}_{\mathrm{i}}^{\mathrm{out}})]} \tag{2.17}$$

The same logic applies to the yield (*Y*) of the different products (Eq. 2.18), which represents the actual amount of product relative to theoretical maximum amount (based on the chosen base-atom).

$$\mathrm{Y}_{\mathrm{S}}^{\mathrm{A}} = \frac{\mu_{\mathrm{S}}^{\mathrm{A}}\, \alpha\, \mathrm{n}_{\mathrm{S}}^{\mathrm{out}}}{\sum_{\mathrm{i}} \mu_{\mathrm{i}}^{\mathrm{A}} \mathrm{n}_{\mathrm{i}}^{\mathrm{in}}} \tag{2.18}$$

Further, the specific energy input (*SEI*) is calculated using Eq. 2.19, in which P_{plasma} is the applied plasma power and Q_{flow} is the total volumetric gas flow rate.

$$\mathrm{SEI} = \frac{\mathrm{P}_{\mathrm{plasma}}}{Q_{\mathrm{flow}}} \tag{2.19}$$

The energy cost of the conversion (*EC*) is calculated from the total conversion and the specific energy input using Eq. 2.20.

$$\mathrm{EC} = \frac{\mathrm{SEI}}{\mathrm{X}_{\mathrm{total}}} \tag{2.20}$$

The energy efficiency (*EE*) is calculated with Eq. 2.21, with *j* the products, *i* the reactants, α the gas expansion factor, $H_{f,j}$ and $H_{f,i}$ the enthalpy of formation of the products (*j*) and reactions (*i*), χ_{abs} the absolute conversion, c^{in} and c^{out} the

concentration at the inlet and outlet, respectively, SEI the specific energy input and V_{mol} the molar volume (24.5 L mol^{-1} at 293 K).

$$EE = \frac{\alpha \cdot \sum_j \left[c_j^{out} \cdot H_{f,j}^{out} \left(\frac{kJ}{mol} \right) \right] - \sum_i \left[\chi_{abs_i} \cdot c_i^{in} \cdot H_{f,i}^{in} \left(\frac{kJ}{mol} \right) \right]}{SEI(kJ\ L^{-1}) \cdot V_{mol}(L\ mol^{-1})} \quad (2.21)$$

3 Effect of N_2 on CO_2-CH_4 conversion in a gliding arc plasmatron: Can this major component in industrial emissions improve the energy efficiency?

The results presented in this chapter are published in:

- Van Alphen, S.*; Slaets, J.*; Ceulemans, S.; Aghaei, M.; Snyders, R.; Bogaerts, A. Effect of N_2 on CO_2-CH_4 conversion in a gliding arc plasmatron: Can this major component in industrial emissions improve the energy efficiency? Journal of CO2 Utilization **2021**, 54, 101767. https://doi.org/10.1016/j.jcou.2021.101767.

* shared first author

3.1 Introduction

In this chapter we investigate the effect of N_2 on plasma-based DRM and we optimize the N_2 content in the gas feed to achieve maximal performance for a GAP reactor (described in section 1.2.2). Some studies also explored the addition of N_2 to CO_2 or CO_2-CH_4 plasmas, either to create a more stable plasma or to mimic realistic emissions from industrial plants.[32,50,75–77] Vice versa, CH_4 addition to CO_2/N_2 plasma has also been shown to have beneficial effects, like suppressing NO_x formation.[78] Most industrial gas emissions contain significant amounts of N_2, and separation is financially costly.[79] The addition of N_2 thus creates a more realistic situation for the industrial application of plasma-based DRM.[80] For this purpose, more insight is needed in the effect of N_2 on the plasma chemistry and the performance of plasma-based DRM. While adding N_2 inevitably leads to electric power being wasted into excitation, ionization and dissociation of N_2, it has already been demonstrated for pure CO_2 conversion that N_2 assists the CO_2 splitting process,[75–77] raising the question if N_2 could also be a useful admixture for DRM.

The previously mentioned GAP reactor (section 1.2.2) has already delivered promising results for pure CO_2 splitting,[26] as well as for DRM in CO_2-CH_4[73] and CO_2-CH_4-N_2-O_2[32] mixtures. In the latter case, N_2 was also present, but in large amounts (60-80%) to create a more stable plasma, and the focus was on the effect of O_2 addition, while the effect of N_2 on the chemistry and performance was not investigated. N_2 addition to pure CO_2 plasma showed promising results,[77] but the effect of N_2 addition for DRM in the GAP has not been studied yet. Therefore, the aim is to optimize the performance of the GAP for DRM in a wide range of N_2 fractions and provide insight in both the physical and chemical effects of varying the N_2 fraction in the plasma. The N_2 fractions are varied between 0% and 80%, in which the CO_2:CH_4 ratio is kept at 1:1.

This chapter focusses mainly on the underlying chemistry of this conversion, obtained through a quasi-1D plasma chemical kinetics model. These simulations take input from three different computational models, i.e., a 3D turbulent gas flow model, a 3D thermal plasma model and particle tracing simulations, using the experimental input gas mixture, plasma power, and reactor geometry as input. This is done to mimic the experimental conditions in the quasi-1D model, of which the output is compared with the experiments by evaluating energy cost, energy efficiency, the conversion of CO_2 and CH_4, and the product yields and selectivities. This modelling approach is introduced by Van Alphen et al.[81], who also performed the 3D computations used in this study. However, the scope of this chapter is limited only to the quasi-1D model, being my contribution in this work.

3.2 Experimental details

The experimental setup consists of three main parts, the reactor, the electric circuit, and the gas analysis system. The gas flow of the different inlet gases (i.e. CO_2, CH_4 and N_2) is regulated by mass flow controllers (MFC) (Bronkhorst), that are controlled by a computer and mix in the inlet tube leading to the reactor. This reactor is described in more detail in the chapter 1 (section 1.2.2). The gas mixture at the outlet is analyzed by a gas chromatograph (GC) (Thermo Scientific trace 1310 GC) using two porous polymer columns (Rt-Q-BOND) and a molecular-sieve column (Molsieve 5Å) for gas separation, helium as the carrier gas and a thermal conductivity detector for gas detection. The power supply

(Advanced Plasma Solutions, PA, USA) is connected to the electrodes. The electrical current is controlled and held at 0.3 A, while the voltage is regulated by the power supply itself (1200 – 1800 V), delivering a certain power (360 – 540 W). The plasma power is measured using an oscilloscope (Tektronix TDS2012C), by integrating the product of voltage and current over a certain period of time. The voltage is measured using a high voltage probe (Testec) connected to the cathode. The current is obtained by measuring the voltage across a known resistance (3 Ohm) that is placed in the grounding wire. The oscilloscope registers this as a voltage, which is converted to a current using Ohm's law.

Before each experiment the setup is flushed for 10 min with the gas mixture, after which the plasma is ignited, and another 10 min is given to stabilize. The exhaust gases are stored in sample loops, each with a 100 µL volume. After the filling process, the content of the sample loops is injected in the set of three columns with helium as carrier gas. For statistical analysis, every experiment is repeated three times, with four sample loops analyzed for each repeat, thus creating 12 data points. For every gas mixture a blank measurement without plasma is performed, needed to calculate the CO_2 and CH_4 conversion.

DRM leads to an expansion of gas due to the increasing number of molecules after the reaction (see R1.1 in chapter 1), which increases the volumetric flow rate. However, the sample loops in the GC have a constant volume and operate at atmospheric pressure, which means part of the gas is lost before injecting in the GC. This results in a lower number of molecules (e.g., of CO_2 or CH_4) being detected compared to the number of molecules in the outlet of the reactor.

Not accounting for this leads to wrong results, such as an overestimation of the conversion, which is described by Pinhão et al.[82] and further expanded upon by Wanten et al.[74] A factor to account for this can be determined by adding an internal standard, such as N_2, He or Ar, to the outflow gas stream after the gas has passed through the reactor.[82] This expansion factor α is calculated using Eq. 3.1, as the ratio of the peak area of this internal standard from the blank (A_{blanc}) to the plasma measurement (A_{plasma}), and factor β to account for increased gas flow rate because of the internal standard. The latter is calculated in Eq. 3.2, in which Q_{plasma} and $Q_{standard}$ are the flow rate of the gas through the plasma and the standard, respectively.

$$\alpha = \frac{A_{blanc}}{A_{plasma}}(1+\beta) - \beta \quad (3.1)$$

$$\beta = \frac{Q_{standaard}}{Q_{plasma}} \quad (3.2)$$

In our setup, He cannot be used as this is the carrier gas in the GC, and neither can Ar, because the peak overlaps with the one of O_2. Therefore, a N_2 flow of 1 L/min is added after the plasma as internal standard for pure CO_2-CH_4 mixtures. For the gas mixtures already containing N_2, no extra N_2 flow is added after the plasma. The N_2 in the mixture is barely converted in the GAP (< 0.05%) and can therefore be used as internal standard. In those cases, the formulas still apply as the β factor becomes zero.

These correction factors are further used in the calculation of the concentrations c^{blanc} and c^{plasma}, through Eq. 3.3 and 3.4, respectively, in which c_m is the measured concentration obtained from the GC.[82]

$$c^{blanc} = c_m^{blanc}(1+\beta) \quad (3.3)$$

$$c^{plasma} = c_m^{plasma}\left(1+\frac{\beta}{\alpha}\right) \quad (3.4)$$

Further calculation of the experimental results is done through the formulas explained in section 2.2, using the corrected concentrations and gas expansion factor as explained in this section. The CO_2 and CH_4 conversion are measured, as well as the H_2 and CO yield, the energy cost and energy efficiency of the conversion process. This energy efficiency presented here only considers the main DRM products, CO and H_2 ($H_f(CO)$ = -110,5 kJ mol^{-1}; $H_f(CH_4)$ = -74,8 kJ mol^{-1}; $H_f(CO_2)$ = -393,5 kJ mol^{-1}; $H_f(H_2)$ = 0 kJ mol^{-1}), however a more accurate value could be calculated when side products would be considered, e.g. H_2O, C_2H_2 or other hydrocarbons. These were not included because they could not be quantified with the current experimental setup, but based on the model, they are not formed in large amounts, so the effect of neglecting them in the formula would be minor anyway.

3.3 Computational details

We used ZDPlasKin[63], which was explained in section 2.1. 177 species are taken into account in the model, which can be formed from the gas mixture of N_2, CO_2, CH_4, and they are listed in Appendix A (Table A-1). This includes various molecules, radicals, excited species and ions, as well as the electrons. These species interact with each other in 15987 reactions, i.e., various electron impact reactions, electron-ion recombination reactions, ion-ion, ion-neutral, and neutral-neutral reactions, as well as vibrational-translational and vibrational-vibrational relaxation reactions. The reactions (and corresponding rate coefficients) between CH_4 and CO_2 derived species (hence including also those between CH_4 and O_2 derived species) were taken from Cleiren et al.[73], the reactions between CO_2 and N_2 derived species (including also those between O_2 and N_2 derived species) were adopted from Ramakers et al.[77], and those between CH_4 and N_2 from Snoeckx et al.[83] Note that the number of species and chemical reactions in this model is much larger than what is actually needed for the purpose of this study, as we are in first instance interested in the conversion of CH_4 and CO_2, and the effect of N_2 on these conversions, but not in the formation of all possible reaction products. However, this chemistry set was developed to be as complete as possible, because it is not *a priori* known which species and chemical reactions are important in the conversion process. For instance, the model contains a large number of (electronically and vibrationally) excited levels, which can be important for energy-efficient CO_2 conversion.[84]

We used ZDPlasKin as a quasi-1D chemical kinetics model. In principle, this is a 0D model, without spatial dimensions, and in which the plasma is modeled in a single point. Hence, the plasma properties (like species densities) only change as a function of time, allowing for the incorporation of an extensive plasma chemistry set, without suffering from long calculation times. However, in order to better account for spatial variations within the GAP reactor, a modelling strategy based on four complementary models is used.[81,85] This consists of a 3D turbulent gas flow model, followed by a 3D plasma arc model and particle tracing simulations and lastly the quasi-1D chemical kinetics model. This chapter only discusses the last model, the preceding calculations were caried out by a fellow PhD student (S. Van Alphen). These models are solved sequentially, in which each model builds further on the results of the previous

model. In short, the gas flow model describes the complex vortex flows in the GAP reactor, with the arc model adding the arc dynamics and gas heating in the plasma. The latter utilizes the plasma power measured in the experiments, with the energy efficiency applied to determine the fraction of energy directed towards gas heating (1 – EE) rather than chemical changes. The physical properties (heat capacity, ratio of specific heat, dynamic viscosity and thermal conductivity) are calculated based on the CO_2-CH_4-N_2 composition to account for the effects of the different gas mixtures.

These models revealed that the gas temperature is heavily influenced by the composition of the gas mixture. This is illustrated in Figure 3.1, which presents the maximum gas temperatures achieved in the arc across the different gas mixtures, as calculated by the arc plasma model. In general, the temperature in the arc increases upon N_2 addition, reaching up to 4400 K for a N_2 fraction of 80%. This is attributed to the higher overall heat capacity upon N_2 addition, as illustrated by the isobaric heat capacity of the different CO_2-CH_4-N_2 mixtures at 3000 K (i.e. a typical plasma gas temperature) in Figure 3.1 (right y-axis).

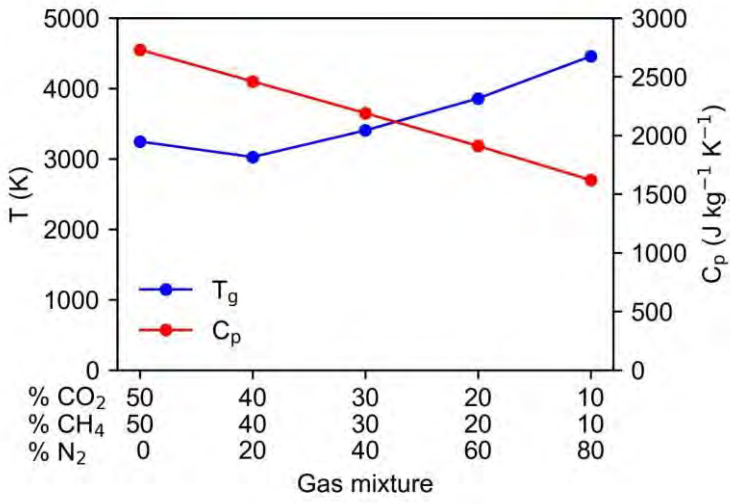

Figure 3.1 Maximum calculated gas temperature in the plasma (arc centre) (blue) and isobaric heat capacity of the CO_2-CH_4-N_2 gas mixture at 3000 K (red), as a function of the N_2 fraction.

The higher gas temperature resulting from N_2 addition has also been observed experimentally in a CH_4 plasma by Zhang et al.[27] for a rotating gliding arc reactor. Using optical emission spectroscopy, the authors observed an increase of more than 300 K when the molar CH_4/N_2 ratio was reduced from 1.20 to 0.05.

Subsequently, after obtaining the results by the 3D gas flow and 3D plasma arc model, the particle tracing simulations are used to convert the calculated plasma parameters of the 3D models to a time-based input for the chemical kinetics model. These trajectories are used to divide the reactor into four different zones, for which the temperature as a function of time is obtained from the gas flow and arc model. This serves as input for the 0D model, thereby enabling the development of a quasi-1D model. This simplified approach does improve the ability to capture spatial variations compared to a single quasi-1D model. Considering the non-uniformity of the plasma and the decoupling of the different models, deviations are possible, however, we believe that it is an acceptable approximation for this study.

Because of the separation into multiple zones, the results of different calculations need to be combined into a single overall result. The overall concentration of plasma species *i* at the end of each simulation is combined through Eq. 3.5, which first weighs the number density *n* in each zone to the contribution *fr* of each zone *z*, after which this is divided by the total sum of all species in the model *j*. The overall gas expansion α is also determined by weighing all zones through Eq. 3.6, in which n_j^{in} and n_j^{out} are the densities of species *j* at the start and end of the simulation, respectively. Note the absence of the gas expansion in the denominator, which is equal to 1 at the start of the simulation.

$$c_i = \frac{\sum_z fr_z \, \alpha_z \, n_{i,z}}{\sum_j \sum_z fr_z \, \alpha_z \, n_{j,z}} \tag{3.5}$$

$$\alpha = \frac{\sum_j \sum_z fr_z \, \alpha_z \, n_{j,z}^{out}}{\sum_j \sum_z fr_z \, n_{j,z}^{in}} \tag{3.6}$$

These values are further used in the calculation of the conversion, yield, selectivity, energy cost of conversion and energy efficiency, using the formulas described in section 2.2.

3.4 Results and discussion

3.4.1 Absolute and effective CO_2 and CH_4 conversion

To analyse the effect of N_2 on the performance of DRM, we evaluated five different N_2 fractions (i.e. 0, 20, 40, 60 and 80%), while the CO_2:CH_4 ratio was kept constant at 1:1. The total flow rate and electrical current were kept at 10 L min^{-1} and 0.3 A. To quantify the CO_2 and CH_4 conversion, we define both the absolute and the effective conversion. The absolute conversion, or simply "conversion", allows easy comparison between different mixtures, while the effective conversion takes into account the dilution of CO_2 and CH_4 in N_2. It is obtained by multiplying the absolute conversion with the CO_2 or CH_4 fraction in the mixture.

Figure 3.2 presents the (absolute) CO_2 and CH_4 conversion as a function of N_2 fraction in the mixture, obtained in the experiments and the model. Without N_2, a conversion of 23.9% is measured for CO_2 and 31.4% for CH_4. These values rise notably upon N_2 addition, up to 47.7% for CO_2 and 61.2% for CH_4 at 80% N_2. The calculated conversions are in satisfying agreement with the experimental values, except at 0% N_2, where the calculated values are somewhat overestimated, and they drop towards 20% N_2, while experimentally a rise in conversion is observed. This is attributed to the gas temperature (see section 3.3), which may be somewhat overestimated in the input data at 0% N_2 and underestimated at 20% N_2. We believe the agreement is reasonable, within the limitations and approximations of the model.

In general, our results demonstrate that the addition of N_2 benefits the conversion of CO_2 and CH_4. The reason is that N_2 does not actively participate in the DRM chemistry and essentially remains unconverted (i.e. less than 0.05% conversion) in the plasma. As the energy acquired by N_2 molecules through inelastic collisions with electrons does not lead to chemical reactions, this energy eventually relaxes to gas heating, which accelerates the DRM reactions.

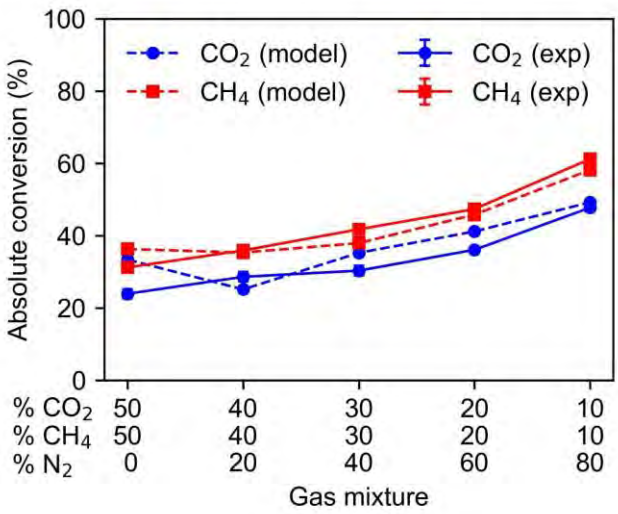

Figure 3.2 Experimental and calculated absolute CO_2 and CH_4 conversion as a function of N_2 fraction. The experiments were performed in triplicate, but the error bars on the experimental results are mostly too small to be visible.

Note that by adding N_2, the total amount of CO_2 and CH_4 present in the gas mixture are lowered from 100% (50%-50%) to 20% (10%-10%). This means that the effective conversion of CO_2 and CH_4, which is calculated based on the initial fraction of each gas in the mixture is expected to decrease upon adding more N_2. The effective CO_2, CH_4 and total (overall) conversion as a function of N_2 fraction are plotted in Figure 3.3. The values drop from 12.0 to 4.8% for CO_2, from 15.6 to 6.1% for CH_4, and from 27.6 to 10.9% for the total conversion, upon increasing N_2 fraction. Hence, while the absolute conversion increases upon N_2 addition, the effective and total conversion decreases, meaning that less CO_2 and CH_4 can be converted overall upon dilution, simply because there is less CO_2 and CH_4 present in the mixture. However, the drop in conversions is not linear: it is less steep at low N_2 fractions and becomes a bit more significant as more N_2 is added. This implies that at low N_2 fractions, the dilution effect is less important than the beneficial effect of N_2 on the (absolute) conversion, observed in Figure 3.2.

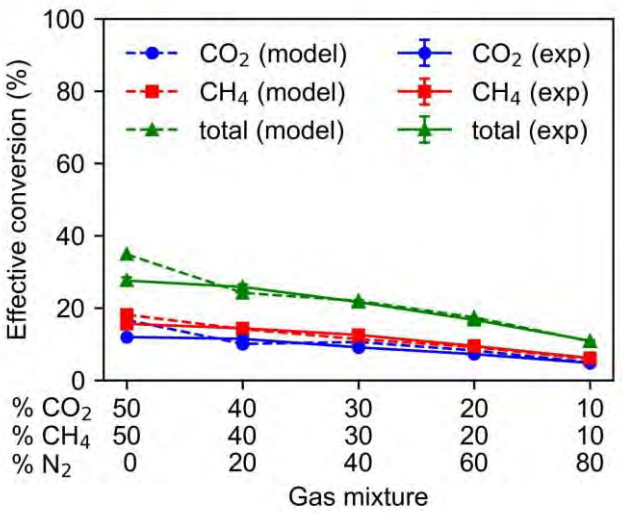

Figure 3.3 Effective CO_2 and CH_4 conversion, as well as the total conversion, as a function of N_2 fraction. The experiments were performed in triplicate, but the error bars on the experimental results are mostly too small to be visible.

3.4.2 Product yields

The measured and calculated product yields for different N_2 fractions are presented in Figure 3.4(a). The CO yield rises from 26.1 to 42.1%, while the H_2 yield rises from 25.2 to 49.8%, upon increasing N_2 fraction. The calculated values are in satisfying agreement with the experiments. The model also predicts H_2O and C_2H_2 as important products, but they could not be measured by our GC. The CO and H_2 yields follow the same trend as the (absolute) conversion, which is logical. Figure 3.4(b) illustrates the measured and calculated product selectivities. While the CO selectivity drops from 92.4 to 77.4% upon increasing N_2 fraction, the H_2 selectivity first drops from 79.0 to 72.4% when 20% N_2 is added and then increases again to 81.2% upon 80% N_2 addition. Our model also predicts the drop in selectivity when 20% N_2 is added, but the drops is much more pronounced and occurs for both CO and H_2. Our model suggests that for this mixing ratio, the selectivity towards C_2H_2 increases, which lowers the selectivity towards CO and H_2. As this drop is not so pronounced in the experiments, some reaction towards C_2H_2 may be slightly overestimated in the model at these low N_2 fractions, probably attributed to the somewhat underestimated gas temperature (see section 3.3), already mentioned in relation to the conversion (see previous section).

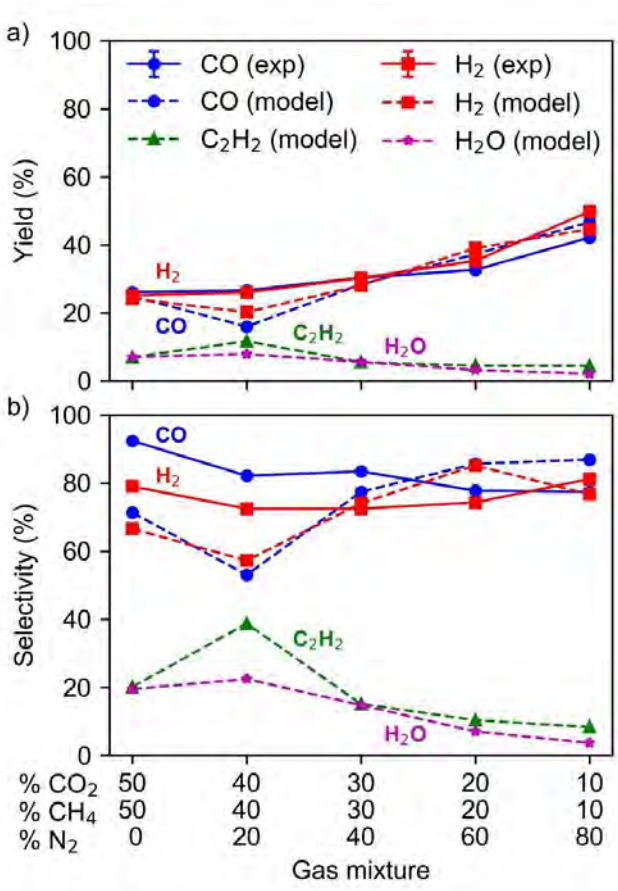

Figure 3.4 Experimental and calculated product (a) yields and (b) selectivities, as a function of N_2 fraction. The experiments were performed in triplicate, but the error bars on the experimental results are too small to be visible.

3.4.3 Energy cost and energy efficiency

Besides conversion, product yields and selectivities, the other important criteria in defining the optimal gas composition for plasma-based DRM are the energy cost and energy efficiency, as they also define the performance of the process in an industrial context, where processes must be cost- and energy-efficient to be competitive. The experimental SEI across the different gas mixtures is presented in Figure 3.5(a). It is clear that the SEI significantly decreases when N_2 is initially added to the gas mixture, from 0.82 to 0.55 eV/molec (or from 3.2 to 2.2 kJ/L) when only 20% N_2 is added to a pure CO_2-CH_4 mixture. Further addition of N_2 only induces a slight drop in SEI. The fact that less power is required to achieve a stable plasma at a fixed plasma current when N_2 is added,

explains why N_2 is often added to pure CO_2, CH_4 or CO_2-CH_4 mixtures to achieve a more stable plasma discharge. While the origin of this effect will be explained further by the computational model in section 3.4.5, we will now discuss the implication of this effect on the energy cost and energy efficiency.

Figure 3.5(b) depicts the energy cost (both in eV/molec and kJ/L) as a function of the N_2 fraction, obtained in the experiments and the model. Across the different gas mixtures, the energy cost ranges from 2.2 to 5.0 eV/molec (or 8.7 to 19.8 kJ/L) and has a minimum for an N_2 fraction of 20%. The latter is attributed to the limited reduction in effective conversion at 20% N_2 (i.e. only 2% loss), as seen in Figure 3.3), while it corresponds to a significantly lower SEI for stable plasma operation, as observed in Figure 3.5(a), thus resulting in an overall lower energy cost. This minimum energy cost at the 20% N_2 fraction corresponds to the maximum energy efficiency of 58% as shown in Figure 3.5(c), where the energy efficiency is plotted across the different gas mixtures. The calculated energy cost and energy efficiency are in reasonable agreement with the measured values, except for the slope from 0% to 20% N_2. Indeed, the energy cost at 0% N_2 seems to be underestimated in the model (Figure 3.5(b)), and the energy efficiency is somewhat overestimated (Figure 3.5(c)). This is both related to the aforementioned overestimation in calculated CO_2 and CH_4 conversion at 0% N_2, attributed to the possible overestimated gas temperature (see section 3.3). In general, however, the agreement is reasonable, given the approximations in the models. Taking it all together, our results indicate that 20% N_2 addition yields the best performance, i.e., the lowest energy cost of 2.2 eV/molec (or 8.7 kJ/L) and highest energy efficiency of 58%, for a CO_2 and CH_4 (absolute) conversion of 28.7 and 35.9%, and a total conversion of 25.8%.

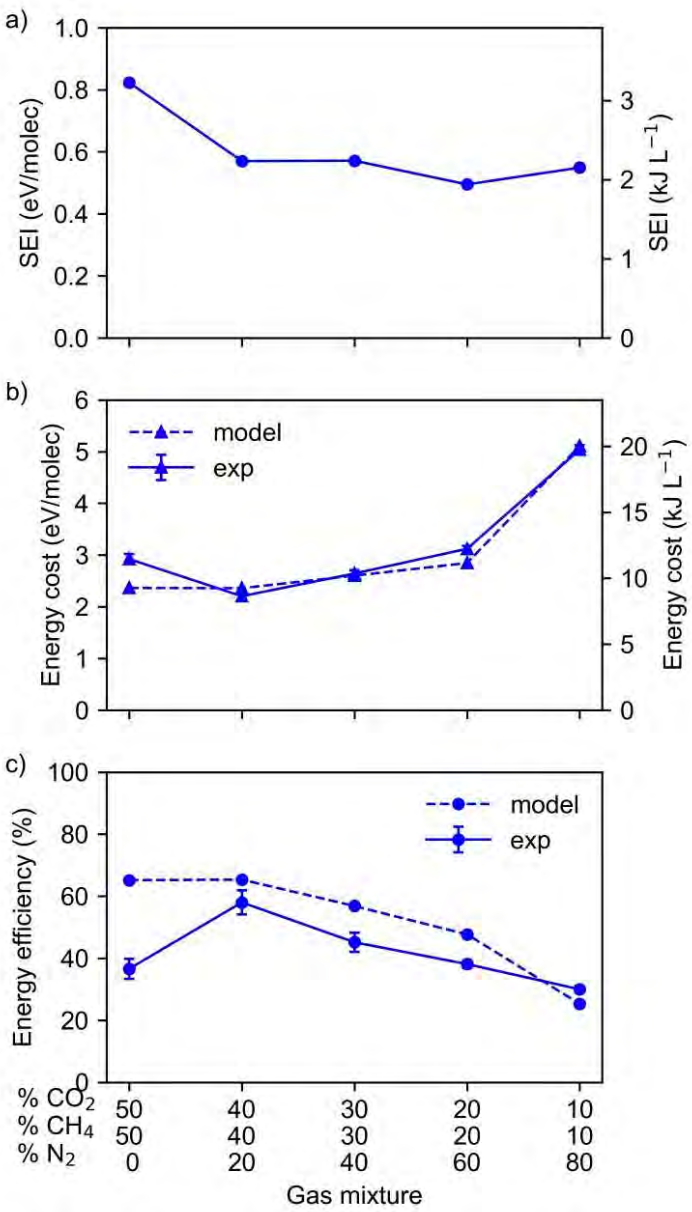

Figure 3.5 (a) Experimental SEI at a constant plasma current of 0.3 A, (b) experimental and calculated energy cost, and (c) experimental and calculated energy efficiency, as a function of N_2 fraction. The experiments were performed in triplicate, but the error bars on the experimental results are mostly too small to be visible.

3.4.4 Comparison with other plasma reactors

In Figure 3.6, we benchmark our results to an extended range of DRM data of several different plasma reactor types collected by Snoeckx and Bogaerts[13]. Our data points are added to this figure as orange stars. Except for the mixture with the highest N_2 fraction, they are all located above the energy cost target of 4.27 eV/molecule (cf. green dash-dotted line indicated as "efficiency target"), which was calculated by Snoeckx and Bogaerts[13] as the target energy cost to be competitive in terms of syngas production with other technologies. Our results perform well in terms of energy cost, i.e., better that DBD, MW and corona discharges, which can achieve high conversions up to 90%, but always at an energy cost above 10 eV/molecule. Nevertheless, our results do not yet reach the best data obtained by some APGD and other GA discharges, but we believe there is room for future improvements of our GAP reactor. Indeed, increasing the fraction of gas that is treated by the plasma arc, through changes in the reactor design, would significantly increase the conversion, and hence also the energy efficiency of the GAP.

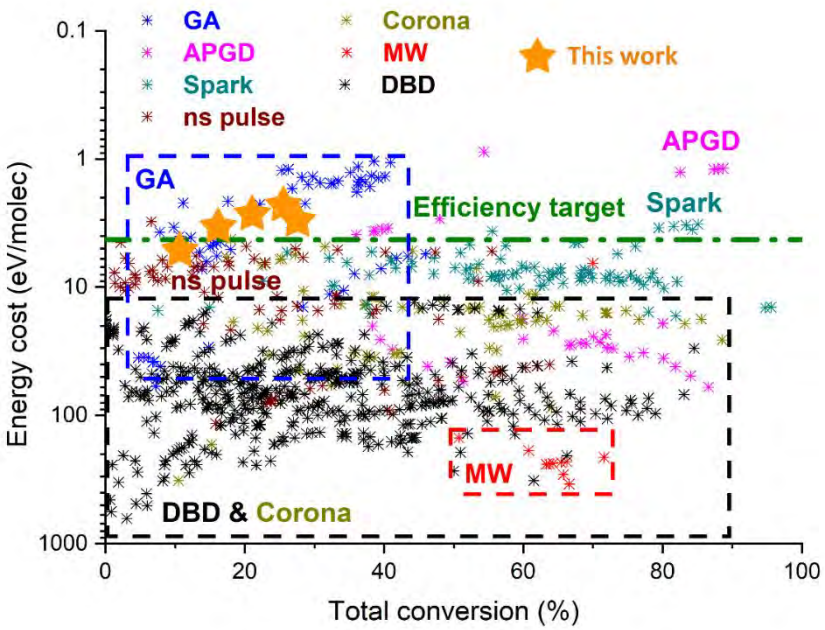

Figure 3.6 Comparison of energy cost as a function of total conversion for DRM, in various types of plasma reactors from literature. Original figure obtained from Snoeckx and Bogaerts.[13] Our results are added to the graph as orange stars. Note that the y-axis is reversed, from the highest to the lowest energy costs (i.e., the best values are at the top).

3.4.5 Explanation of the performance by means of the model

3.4.5.1 N_2 addition enhances the electron density, affecting the plasma conductivity, plasma power and SEI

As illustrated in Figure 3.5(a) above, the measured SEI in the CO_2-CH_4 mixture drops significantly when 20% N_2 is added, due to the lower power needed to ignite and sustain the plasma at a fixed plasma current. Our model reveals that this is attributed to the increasing electron density upon adding N_2 to the mixture, as illustrated in Figure 3.7 (black line, left y-axis). This figure also presents the dominant electron formation reactions in the mixture (coloured bars, right y-axis), as calculated by the model. Note that this model was run for a constant temperature of 3500 K and power density of 4.5 kW cm^{-3}, to clearly isolate the effect of the changing gas composition (independent from the effect of the gas temperature) on the plasma chemistry. Without N_2, electron formation mainly occurs through recombination of H_2 and O^- to H_2O (reaction 5), and of CO and O^- to CO_2 (4), as well as by electron impact ionization of CO_2 (reaction 1). When N_2 is added, ionization of N_2 (especially electron impact ionization of ground state N_2 (reactions 7 and 8), but also associative ionization by two electronically excited molecules, $N_2(A^1\Sigma_u)$ (reaction 9) and $N_2(A^3\Sigma_u)$ (reaction 10), take over as the main electron formation processes, explaining the rising electron density in the plasma. In other words, through the addition of N_2 a new gas is introduced to the plasma, which, unlike CO_2 and CH_4, does not react away easily by other (chemical) reactions due to its strong triple bond, and is thus always available for ionization. The electron density enhances the conductivity of the plasma, thus reducing the power needed to achieve a certain plasma current. Hence, this explains the drop in plasma power, and thus in SEI (cf. Figure 3.5(a)) upon N_2 addition, contributing to the low energy cost of the 20% N_2 mixture.

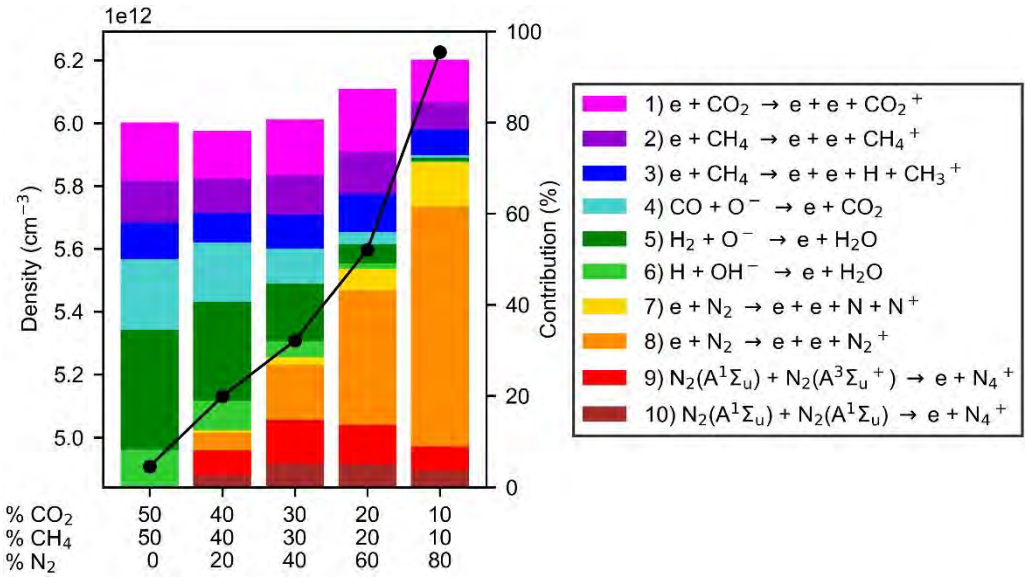

Figure 3.7 Calculated electron density (black line, left y-axis) as a function of N_2 fraction, at a constant gas temperature of 3500 K and power density of 4.5 kW cm^{-3}. The coloured bars (right y-axis) show the contribution of the dominant electron formation reactions across the different gas mixtures. The values are determined for a plasma residence time of 1 ms, which is comparable to the residence time in the plasma obtained in the 3D simulations (performed by a fellow PhD student) based on the experimental conditions.

3.4.5.2 Underlying reaction pathways in DRM

A general reaction scheme, as predicted by our quasi-1D simulations, is presented in Figure 3.8, indicating the important reactions involved in the conversion processes of CO_2 and CH_4 and their link to the formation processes of the most abundant products, i.e., CO, H_2, H_2O and C_2H_2. The figure applies to the CO_2:CH_4:N_2 mixture with 40% N_2, which is intermediate, and thus representative for the various N_2 fractions. The thickness of the arrows is indicative of the total time-averaged rate (averaged over the residence time in the plasma) and thus marks the importance of the reaction within the DRM process. Note that these are all net rates, balancing the rates of the forward and reverse reactions. The reactants of the dominant reactions are placed next to the arrows.

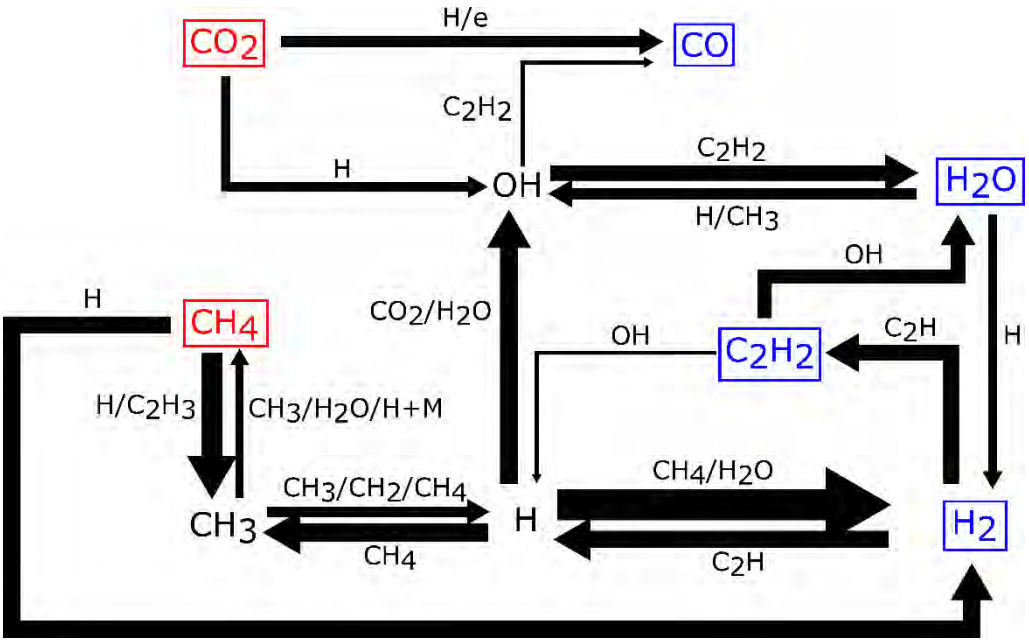

Figure 3.8 Schematic overview of the most important reactions for the conversion of CO_2 and CH_4 and the formation of CO, H_2, C_2H_2 and H_2O, based on the time-averaged net reaction rates for the CO_2-CH_4-N_2 gas mixture with 40% N_2. The arrow thickness is indicative of the net reaction rate of the reactions involved. The arrows towards CO are clearly thinner than towards H_2, while nearly equal amounts of CO and H_2 are formed. The reason is that loss processes for CO are less important than for H_2 (see scheme). Note that N_2 does not play a direct role in this chemistry, except as neutral molecule (M), but it has an important indirect contribution, through the enhanced gas temperature and electron density (see before).

The scheme in Figure 3.8 shows that CH_4 conversion is mostly driven by reactions with H and C_2H_3 to form CH_3 (R3.1, R3.2) and H_2 (R3.1). CH_4 is also converted upon reactions with O or electrons, but because of their lower contribution (< 3%), these reactions are not displayed in the scheme. The relative importance of electron impact reactions decreases with increasing N_2 fraction, in spite of the higher electron density. This is because the contribution of the heavy species reactions increases strongly at the high gas temperatures. This higher gas temperature is the result of a decreasing isobaric heat capacity of the mixture with increasing N_2 fraction. Higher N_2 fractions thus promote the thermal DRM chemistry, rather than electron-induced reactions.

$$CH_4 + H \rightarrow CH_3 + H_2 \qquad \text{(R3.1)}$$

$$CH_4 + C_2H_3 \rightarrow CH_3 + C_2H_4 \qquad \text{(R3.2)}$$

CH_3 can react back to CH_4 through three-body recombination with H and M (representing any neutral molecule) (R3.3) or upon reactions with CH_3 or H_2O (R3.4, R3.5). In addition, it can react further with CH_3, CH_2 and CH_4, creating H atoms and multiple C_2H_x species (R3.6-3.8). The formation to H_2 occurs upon reaction of H atoms with CH_4 (R3.1) or with H_2O (R3.9). Recombination of 2 H atoms into H_2 occurs as well, but at a much lower rate.

$$CH_3 + H + M \rightarrow CH_4 + M \quad \text{(R3.3)}$$

$$CH_3 + CH_3 \rightarrow CH_4 + CH_2 \quad \text{(R3.4)}$$

$$CH_3 + H_2O \rightarrow CH_4 + OH \quad \text{(R3.5)}$$

$$CH_3 + CH_3 \rightarrow H + C_2H_5 \quad \text{(R3.6)}$$

$$CH_3 + CH_2 \rightarrow H + C_2H_4 \quad \text{(R3.7)}$$

$$CH_3 + CH_4 \rightarrow H + C_2H_6 \quad \text{(R3.8)}$$

$$H + H_2O \rightarrow H_2 + OH \quad \text{(R3.9)}$$

The main conversion pathway for CO_2 proceeds through reactions with H and (to a smaller extent) electrons (R3.10, R3.11), creating CO and OH (or O). Like for CH_4, the relative contribution of electron impact dissociation of CO_2 decreases upon higher N_2 fractions, as the higher gas temperature promotes the thermal reactions between the heavy species. While dissociation from CO_2 is the most important formation reaction for CO, another (less important) CO formation pathway is by reaction of OH and C_2H_2 (R3.12). Several loss reactions of CO exist towards CO_2, O and CH_3, but they are not added to the scheme, because their rates are several orders of magnitudes lower than the formation pathways.

$$CO_2 + H \rightarrow CO + OH \quad \text{(R3.10)}$$

$$CO_2 + e \rightarrow CO + O + e \quad \text{(R3.11)}$$

$$OH + C_2H_2 \rightarrow CO + CH_3 \quad \text{(R3.12)}$$

C_2H_2 is mainly formed upon reaction of H_2 with C_2H (R3.13), which is also the major loss reaction for H_2. C_2H_2 has two different loss reactions with OH, i.e., a small fraction forms H (R3.14) while the majority is lost towards H_2O (R3.15).

The latter reaction is also the major loss process of OH. Finally, H_2O is converted again to H_2 upon reaction with H (R3.9), and to OH upon reactions with CH_3 or H (R3.5, R3.9).

$$H_2 + C_2H \rightarrow H + C_2H_2 \quad \text{(R3.13)}$$

$$C_2H_2 + OH \rightarrow H + CH_2CO \quad \text{(R3.14)}$$

$$C_2H_2 + OH \rightarrow H_2O + C_2H \quad \text{(R3.15)}$$

3.5 Conclusions

In this chapter, we investigated the effect of N_2 on plasma-based DRM in a GAP, by means of experiments and a computational model. Overall, a N_2 content of 20% was found to be optimal in terms of overall performance, achieving a total conversion of 25.8%, and (absolute) conversions of 28.6% for CO_2 and 35.9% for CH_4 at a total energy cost of 2.2 eV/molec (or 8.7 kJ/L) and energy efficiency of 58%. The syngas components (CO and H_2) are the major products, but the model reveals that some C_2H_2 (and H_2O) are also formed. The computational model reaches reasonable agreement with the experimental conversions, product yields and selectivities, energy cost and energy efficiency, and can thus be used to elucidate the underlying mechanisms and explain the trends of N_2 addition.

As N_2 remains largely unconverted, virtually all plasma energy taken up by N_2 molecules through inelastic collisions with electrons is eventually being distributed to the translational degrees of freedom. The addition of N_2 to the mixture also lowers the isobaric heat capacity of the overall mixture. Combined this leads to higher maximum gas temperatures reached in the plasma, from around 3200 K without N_2, up to 4400 K upon 80% N_2 addition. This higher temperature is shown by the chemical kinetics model to significantly accelerate the DRM reactions, enhancing the (absolute) conversions of CO_2 and CH_4.

Indeed, our models reveal that the addition of N_2 promotes the conversion of CO_2 and CH_4 through thermal conversion reactions, rather than through electron impact reactions. The addition of N_2 also reduces the power that is needed to achieve a certain plasma current, and thus the plasma can operate at lower SEI, for a constant gas flow rate. Indeed, the N_2 molecules are virtually

not dissociated (and thus not converted in chemical reactions), but they only undergo ionization (and excitation). This enhances the electron production rate due to the extra ionization channels, thus increasing the electron density. A higher electron density leads to a higher plasma conductivity, so less power is required to achieve the fixed plasma current in the experiments when more N_2 is present, thereby reducing the SEI of the process.

Hence, both the higher absolute conversion and lower SEI at increasing N_2 fractions are beneficial, but on the other hand, diluting the CO_2-CH_4 fraction reduces the effective conversion of CO_2 and CH_4. However, at N_2 fractions around 20%, the advantages of adding N_2 outweigh the dilution effect, improving the energy efficiency of the process with respect to pure CO_2-CH_4 mixtures, by 21%, i.e., from 37 to 58%, and reducing the energy cost from 2.9 to 2.2 eV/molec (or from 11.5 to 8.7 kJ/L).

In conclusion, we have shown that the addition of N_2, a component in many industrial emissions, can significantly improve the energy efficiency of plasma-based DRM, thus bringing this plasma-based process a step closer towards real applications.

4 Plasma-based DRM: Plasma effects vs. thermal conversion

The results presented in this chapter are published in:

- Slaets, J.; Loenders, B.; Bogaerts, A. Plasma-based dry reforming of CH_4: Plasma effects vs. thermal conversion. *Fuel* **2024**, *360*, 130650. https://doi.org/10.1016/j.fuel.2023.130650.

4.1 Introduction

As discussed previously in section 1.3.2, there are still gaps and limitations to the understanding of the chemical kinetics of DRM. Therefore, this chapter aims to gain a broader understanding of the effects of plasma parameters on the core chemical kinetics under warm plasma conditions. Further, this chapter is not specifically limited to a specific reactor design, but we study a general plasma setting with a wider range of gas temperature, plasma power density, and most importantly, a full range of gas mixtures, ranging from 90% CO_2 to 90% CH_4, which has not been demonstrated before for warm plasmas. We compare the kinetics of thermal gas chemistry with that of plasma-based conversion and illustrate differences and similarities between them. It has indeed been shown that within plasma systems, thermal chemistry can be an important contributor to the conversion process.[49] Importantly, we constructed a new chemical kinetics scheme for this broad study, which serves as an updated/revised version of the previous works from our group PLASMANT.[31,32,88,33,50–52,75,83,86,87] Improvements are made by careful literature review of the original sources and the use of detailed balancing to fill gaps in the chemistry. We also specifically improved the kinetics scheme by comparing the steady state concentrations from our model to thermodynamic equilibrium, which was never considered as a validation tool in previous works.

4.2 Computational details

The focus of this chapter is to study the influence of various parameters, i.e., gas temperature, plasma power and CO_2/CH_4 ratio, on the chemical composition in the plasma, independent of a specific reactor configuration. This makes a (zero-dimensional) chemical kinetics model ideal for this study. The simple model setup allows a wide range of parameters to be studied with reasonable calculation times. We used the ZDPlasKin code for these calculations.[63] Detailed explanation on this model was given in section 2.1.

Both plasma power and gas temperature are considered as separate input parameters, independent of each other, and they are both kept constant at fixed values throughout the simulation. This means that the gas temperature is not calculated time-dependently using the heat balance equation, and therefore, the plasma power is not responsible for gas heating, i.e., gas temperature and plasma power are fully decoupled parameters. This has the benefit that we can evaluate their effect, independent from each other, providing more insight in the effect of individual parameters. In reality, however, the gas temperature depends on the applied plasma power and heat capacity of the gas mixture, as well as heat losses to for example the reactor walls. Hence, either external heating or cooling may be required to obtain a specific combination of plasma power and gas temperature, used as input in this study. However, this work aims to gain a better understanding of the effects of these external parameters on the chemical kinetics, without focusing on a specific experimental condition, which justifies this approach. Even more, it provides a broad picture of the overall chemistry, and thus allows to discover possible improvements in the chemical conversion process.

4.2.1 Chemistry

The kinetics scheme considers 70 different plasma species, i.e., 40 different neutral species, 24 different positive ions, 5 different negative ions, and the electrons, which react through 1469 reactions. A list of the species included in the model is given in Table 4.1 and a full list of the chemical reactions with the corresponding rate coefficients and the references where the data is adopted from, is provided in Appendix D (Table D-1).

In total, 336 different electron impact reactions are taken into account for the calculation of the EEDF (see Appendix; Tables D-1 and D-2), including 123 electron impact excitation reactions. However, the excited species formed in this way are not included in our kinetics scheme. Indeed, our model does not consider a state-to-state chemistry, but instead it assumes a vibrational-translational equilibrium, i.e., the vibrational temperature is equal to the gas temperature, and there is no overpopulation of the vibrationally excited levels. As an indication, it has been demonstrated that a vibrational-translational non-equilibrium can only be sustained for very short timescales, reaching equilibrium in less than 0.1 ms for pressures of 25 mbar.[89] With increased pressure, the higher collision frequency between species will result in even faster vibrational-translational relaxation. As our study is focused on atmospheric pressure plasmas and residence times up to 10 ms, we can reasonably assume that relaxation is sufficiently fast to result in a thermal vibrational distribution function (VDF) and a negligible influence of vibrational-translational non-equilibrium on the kinetics.

Table 4.1 Overview of species included in the chemical kinetics set, excluding the electrons.

Neutral species	**Ions**
C	C^+
O, O_2, O_3	O^+, O_2^+, O^-, O_2^-, O_3^-
H, H_2	H^+, H_2^+, H_3^+, H^-
CO, CO_2	CO^+, CO_2^+
CH, CH_2, CH_3, CH_4, C_2H, C_2H_2, C_2H_3, C_2H_4, C_2H_5, C_2H_6	CH^+, CH_2^+, CH_3^+, CH_4^+, CH_5^+, C_2H^+, $C_2H_2^+$, $C_2H_3^+$, $C_2H_4^+$, $C_2H_5^+$, $C_2H_6^+$
OH, H_2O, HO_2, H_2O_2	OH^+, H_2O^+, H_3O^+, HO_2^+, OH^-
CH_2CH_2OH, CH_2CO, CH_2OH, CH_3CH_2O, CH_3CH_2OH, CH_3CHO, CH_3CHOH, CH_3CO, CH_3COOH, HCCO, CH_3O, CH_3OH, CH_3OO, CH_3OOH, COOH, HCHO, HCO, HCOOH	HCO^+

Furthermore, some assumptions were made in the kinetics scheme or reactions involving electrons. The associative ionization rate coefficients (reactions 549-551, 1084, 1085, 1156, 1157, 1201 in Table D-1) are taken equal to the values of Park et al.[90] for O + O (forming O_2^+ + an electron). Indeed, they could prove important in the higher temperature range for the formation of electrons, as stated by Vialetto et al.[91]. The electron detachment reaction from OH^- ions (reaction 457 in Table D-1) is estimated to be equal to the detachment process of O^- ions and was found to be an important reaction to balance the anions in the plasma. The electron-ion three-body recombination rate coefficients for CO^+ and CO_2^+ were also estimated based on the generalized formulation of Kossyi et al.[92], although these reactions turn out to have minimal impact on the overall scheme (reactions 1159-1162 in Table D-1).

4.2.2 Simulation details

In this chapter, we focus specifically on the kinetics in the active plasma region, without considering an afterglow or post-plasma effects, which are studied in next chapter. We varied the gas temperature between 1000 and 4000 K, which is in the typical range for warm plasmas[13], for five different CO_2/CH_4 ratios (10/90, 30/70, 50/50, 70/30, 90/10). We also conducted four sets of simulations for the power density, further referred to as thermal (0 W/cm^3) and plasma (500, 1000, 1500 W/cm^3) simulations. These power densities are typical for warm plasmas, as obtained from different literature sources[26,28,31–33,93–97] (see comparison in Table 4.2).

“Thermal” represents purely thermal decomposition of molecules in the gas-phase because of the high gas temperature, in which no electrons or ions are considered, but only neutral species. The comparison with the plasma simulations is performed for a residence time of 10 ms. This estimate of residence time is realistic based on the work of Van Alphen et al.[81], where a residence time distribution up to 17.5 ms was reported based on CFD simulations of their arc reactor. Additionally, Dahl et al.[98] also used a residence time of 10 ms in solar-thermal DRM operating at 2000 K. On the other hand, we also conducted the thermal simulations up to an extremely long simulation time (10^{10} s, approximately 3169 years). This is of course unrealistic in practice, but it allows the heavy species kinetics to reach a steady state. The concentrations

of the neutral species can then be evaluated against thermodynamic equilibrium concentrations for the corresponding conditions, which are calculated as described by Biondo et al.[99] This comparison provides a first validation of our heavy species kinetics. However, it is important to note that this only applies to the steady state concentrations themselves, and not the kinetic pathways to obtain them, neither the timescales in which they are obtained. The accuracy of the model for those aspects is related to the accuracy of the reaction rate coefficients used in the model. These uncertainties are typically in the order of 10 – 30%, but can be higher than 100%. Therefore, it is generally established that chemical kinetics models can have a large uncertainty.[69–72] Wang et al.[72] quantified the uncertainties for their DBD model for DRM and obtained uncertainties up to 33% for the conversion and up to 28% for the syngas yield. Therefore, the trends and relative values of the species densities predicted by the model are more important than the absolute values.

Table 4.2 Overview of estimated power density from various literature sources. The plasma volume is not specifically measured in these sources and therefore, we could only make a rough estimate of the power density. Despite some outliers above 1500 W cm^{-3}, our chosen power density values (500, 1000 and 1500 W cm^{-3}) provide good coverage of this literature data.

Plasma	Power (W)	Volume (cm^3)	Power density (W cm^{-3})	Ref.
GAP	500	0.37	1351	31
GAP	224	0.383	585	95
GAP	225 – 475	0.13	1731 – 3653	26
APGD	90 – 160	0.43*	209 – 372	28
cAPGD	100	0.43*	233	28
cAPGD	80 – 125**	0.43*	186 – 291	33
GAP	349 – 472	0.14*	2415 – 3266	32
MW	900 – 1400	1.08 – 2.19*	639 – 833	94
MW	550 – 700	0.71*	772 – 982	97
GA	1300	0.68*	1916	96
GA	1000	0.75*	1326	93

* Estimated based on the reactor geometry

** Estimated from figures

When comparing our thermal and plasma simulations and thermodynamic equilibrium calculations, we define the deviation between the species concentrations using the equation for mean absolute deviation. The large number of species with very low density reduces the value of the mean significantly, and therefore a weighted mean is employed to focus on the higher density species. This weighted mean absolute deviation (*wMAD*) is calculated by Eq. 4.1, with Δc_s the concentration difference for species *s* between the results that are compared and w_s the weight for species *s*. When we compare with thermodynamic equilibrium concentrations, we use the latter as weights in the equation. When we compare thermal and plasma simulations, the weights are taken as the thermal concentrations.

$$\mathrm{wMAD} = \frac{\sum_s (w_s \cdot |\Delta c_s|)}{\sum_s w_s} \tag{4.1}$$

4.3 Results and discussion

4.3.1 Validation of the thermal chemistry

First, we quantify the deviation between the calculated species concentrations for the thermodynamic equilibrium and thermal kinetics simulations, to validate in first instance the thermal chemistry in our model, for the five different DRM mixtures, using the *wMAD* (Eq. 4.1), shown in Figure 4.1. The corresponding species concentrations (comparison of thermodynamic equilibrium vs. thermal kinetics simulations) for the 50/50 mixture are plotted in Figure 4.1(b), as a reference. The comparison at the other mixing ratios is presented in the Appendix, Figure B-1.

Good agreement is reached between 1700 and 2700 K, with a deviation (*wMAD*) of less than 1%. At lower temperature, a larger deviation, up to 1.5% for 1000 K, is obtained. At higher temperatures, the deviation also rises, but remains below 4%. Hence, the steady state compositions for this kinetics scheme are in good agreement with those at thermodynamic equilibrium, which serves as a validation of the thermal chemistry in our model. This comparison only confirms the model's ability to reproduce the chemical composition at equilibrium. It does not validate the chemical reactions included or the associated rate constants on an individual basis, which may still be

subject to uncertainty. As a result, the timescales at which specific reactions or pathways occur may deviate, potentially leading to an over- or underrepresentation of intermediate species. Additionally, the residence time at which intermediates are formed or steady state is reached could be different. Nevertheless, this analysis does provide us with additional confidence in the overall chemistry set.

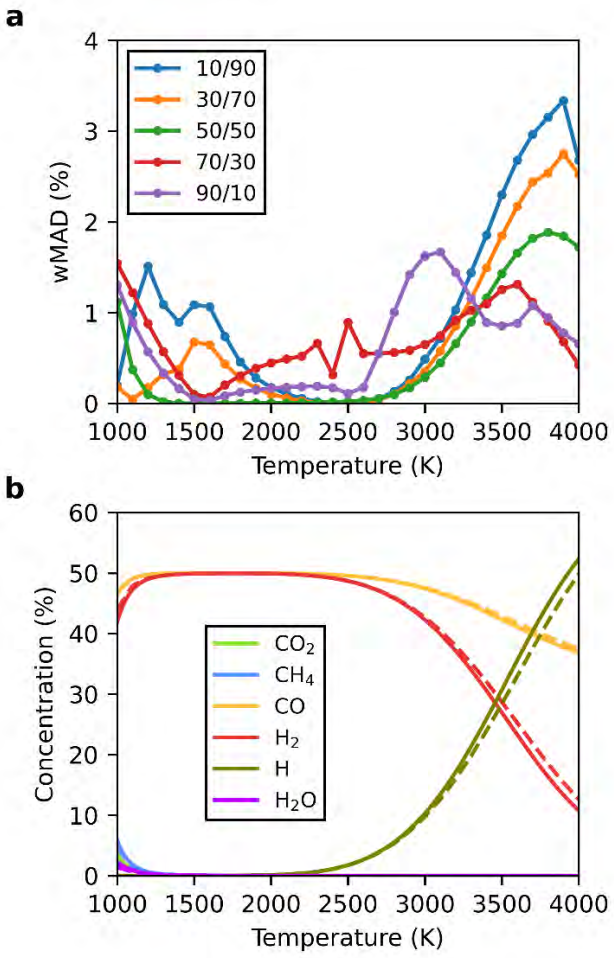

Figure 4.1 (a) Weighted mean absolute deviation (wMAD) between the calculated species concentrations of the thermal simulations (for t = 10^{10} s) and the thermodynamic equilibrium concentrations, in the temperature range of 1000 to 4000 K, for five different CO_2/CH_4 ratios (90/10, 70/30, 50/50, 30/70, 10/90). (b) Corresponding species concentrations, calculated at thermodynamic equilibrium (solid) vs. thermal kinetics simulations (dashed) for the 50/50 mixture. Note that at thermodynamic equilibrium (or steady state) nearly all CO_2 and CH_4 is converted into CO and H_2, even at/above 1000 K, while above 2500 K, H_2 starts to be dissociated.

4.3.2 Comparison of plasma and thermal kinetics

4.3.2.1 Plasma species concentrations as a function of temperature

For further characterization of the DRM chemistry, we compare different cases with and without plasma power, to compare the plasma and thermal kinetics, with timescales limited to the millisecond range. The concentrations of the main species, for both the thermal and plasma simulations, at a residence time of 10 ms and for the stoichiometric ratio of 50/50 CO_2/CH_4, are plotted in Figure 4.2. It is clear that, above 2400 K, also the plasma concentrations agree with the thermodynamic equilibrium concentrations plotted in Figure 4.1(b). Below 2400 K, CO_2 and CH_4 are not yet dissociated within this short residence time (Figure 4.2(a)), and H_2O, C_2H_2 and C_2H_4 are formed to some extent (Figure 4.2(b)), which will react away before thermodynamic equilibrium is established.

The thermal conditions show no conversion below 1400 K, and thus CO_2 and CH_4 are the only species present. The corresponding plasma conditions do show clear conversion already in this temperature range, being somewhat higher for CH_4 than for CO_2, which is logical, based on the C-H vs C=O bond strength (i.e., 439 vs 532 kJ mol^{-1})[100]. Both CO_2 and CH_4 conversion increase significantly towards 1600 K, which results in the formation of H_2, CO, C_2H_2 and H_2O (and a limited amount of C_2H_4), for both thermal and plasma conditions. While syngas (CO and H_2) is the dominant product (Figure 4.2(a)), the formation of H_2O is also quite important (Figure 4.2(b)), and most significant at 1800 K, competing with H_2 formation. This results in a small dip (i.e., 4.5% and 3.9% lower concentration) for H_2 at 1800 K compared to at 1700 K, for the thermal and plasma conditions, respectively. For higher temperatures, the concentrations of C_2H_2 and H_2O drop and become negligible around 2400 K. Simultaneously, the CO_2 and CH_4 conversions reach 100% at this temperature, leading to the maximum concentrations of 49 and 50% for H_2 and CO, respectively. The calculated species concentrations of the thermal and plasma conditions (dotted and full lines) fully coincide above 2000 K.

For temperatures above 2400 K, the concentration of H radicals becomes increasingly important, at the cost of H_2, leading to H_2 and H concentrations of 13 and 50%, respectively, at 4000 K, for both the thermal and plasma conditions. The concentration of CO also drops slightly, but this is simply due to

the splitting of H_2, which increases the number of species, effectively diluting CO. The other free radicals, C, O and OH, are much less significant, with calculated concentrations of 0.03% or less. It should be noted that all radicals will recombine in the afterglow region, where the gas cools down, but this is not considered in our model.

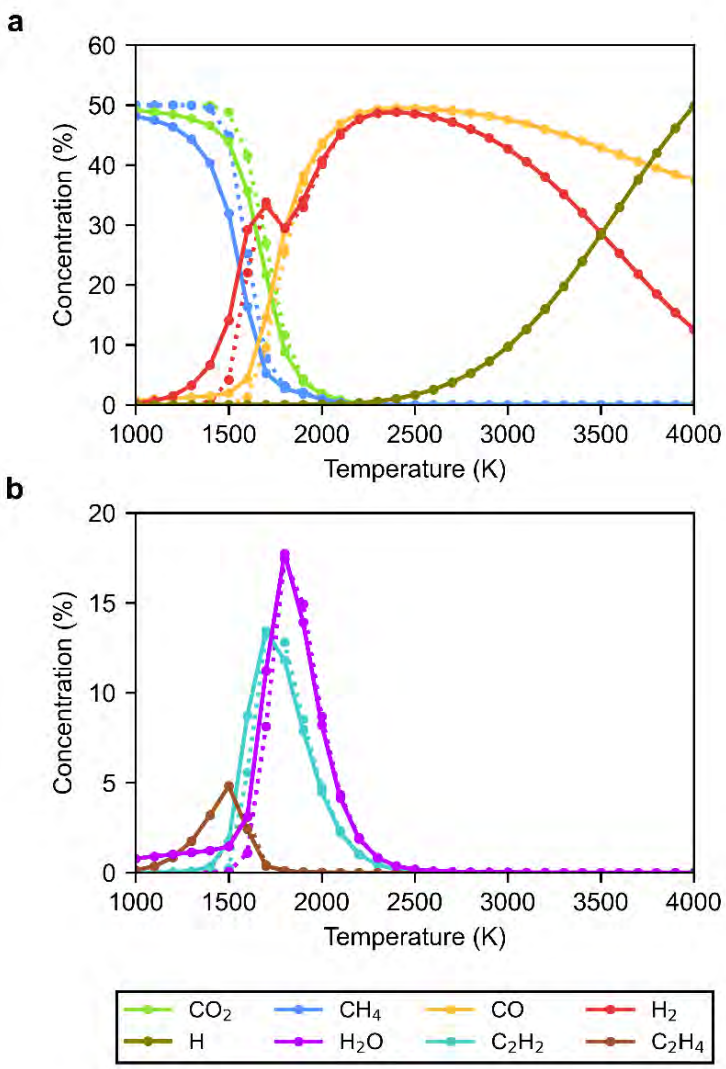

Figure 4.2 Calculated concentrations of the main plasma species for the temperature range of 1000 to 4000 K and a 50/50 CO_2/CH_4 ratio, at a residence time of 10 ms, for both thermal (dotted lines) and 1000 W/cm^3 plasma conditions (solid lines).

In summary, the plasma activates the chemistry at low temperature (below 1700 - 1800 K), yielding higher conversion than the pure thermal process. As the conversion process is initiated by electron impact reactions through the creation of radicals. Even more, below 1400 K, plasma reactions already give rise to a clear conversion, whereas thermal reactions alone cannot. Above 1500 K, the differences between thermal and plasma kinetics gradually become smaller, and thus, thermal reactions start to dominate. As temperature increases, thermal reactions are accelerated, thus contribute more to the initial creation of radicals and causing conversion on even shorter timescales compared to electron impact reactions. Above 2000 K, the thermal and plasma kinetics coincide, so the chemistry becomes purely thermal. Finally, above 2400 K, the concentrations follow thermodynamic equilibrium (cf. Figure 4.1(b)), indicating that the kinetics is fast enough to reach steady state within the simulation time of 10 ms.

4.3.2.2 Deviation between plasma and thermal kinetics

We use the deviation between the simulations with and without plasma power to quantify the influence of plasma-specific reactions compared to thermal kinetics. Figure 4.3 presents the deviation (*wMAD*) between the thermal and plasma concentrations for the 50/50 ratio, between 0.1 and 10 ms, for an applied power density of 1000 W/cm^3. For a residence time of 0.1 ms, the difference between thermal and plasma concentrations is very small, with a *wMAD* of less than 0.4%, but after 1 ms, the difference increases, resulting in a maximum *wMAD* of 1.8% at a gas temperature of 1700 K. At still longer residence times of 10 ms, the maximum *wMAD* increases to 8.7%, and shifts to a lower gas temperature of 1500 K. This larger deviation with time is logical, as a longer residence time simply allows for more reactions to occur.

The deviation obtained for low temperatures near 1000 K is due to the very small, almost negligible thermal conversion, while the plasma power activates electron impact dissociation, enabling more conversion. This is explained in more detail in section 4.3.2.3. Raising the temperature up to 2000 K accelerates the thermal reactions, allowing the products from electron impact dissociation to react away faster. This drives the conversion process even more forward and increases the deviation compared to pure thermal conversion, where the initial

dissociation of the reactants can only occur from thermal kinetics. The deviation reaches a maximum around 1500 - 1700 K, after which the thermal kinetics increases further, taking over the conversion process. Above 2000 K, thermal chemistry fully controls the conversion, resulting in a negligible deviation between the thermal and plasma conditions, with a *wMAD* below 0.2%.

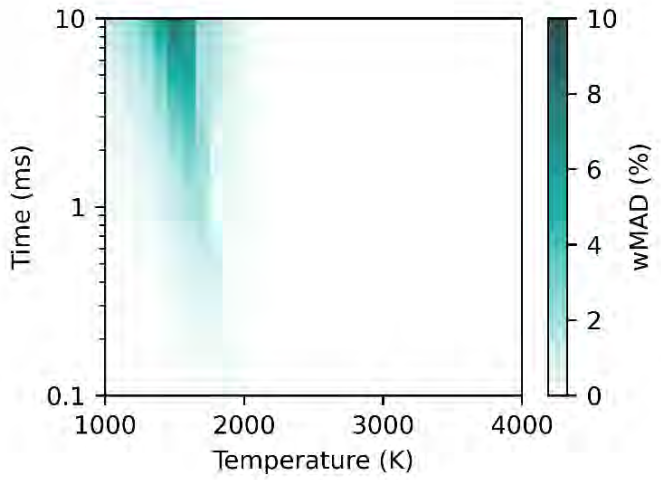

Figure 4.3 Weighted mean absolute deviation (wMAD) between the calculated species concentrations for thermal and plasma kinetics (1000 W/cm^3) as a function of residence time (0.1 to 10 ms) and gas temperature (1000 to 4000 K), for a stoichiometric (50/50) CO_2/CH_4 ratio.

A similar behavior is observed for the other CO_2/CH_4 ratios, for which the deviation also rises and shifts towards slightly lower gas temperatures with increasing residence time. In our further discussion, we only consider a residence time of 10 ms, typically giving rise to the largest deviation. The deviation between plasma and thermal kinetics depends on the gas mixture, as shown in Figure 4.4. For mixtures with an excess of CH_4 (i.e., 30/70 and 10/90 CO_2/CH_4), the *wMAD* reaches maxima of 11 and 13%, respectively, at 1500 K. For mixtures with excess CO_2, the maxima are obtained at slightly higher gas temperatures, i.e., at 1600 K for the 70/30 ratio (8.1%) and at 1700 K for the 90/10 ratio (12%). Similar to the 50/50 CO_2/CH_4 mixture, the *wMAD* between the thermal and plasma kinetics is negligible (< 0.2%) above 2000 K. An exception to this is the 90/10 mixture, showing a small deviation between 2000 and 3000 K, with a maximum of 0.71% at 2500 K, which will be discussed in section 4.3.4.1. As expected, the difference between thermal and plasma kinetics slightly rises with the applied power density. The maximum *wMAD* for

the different mixtures ranges between 4.1 and 6.4% for 500 W/cm^3, while for 1500 W/cm^3, it is between 12 and 19%, see the Appendix (Figure B-2). In the rest of this chapter, we will focus only on the 1000 W/cm^3 case, being the intermediate power density.

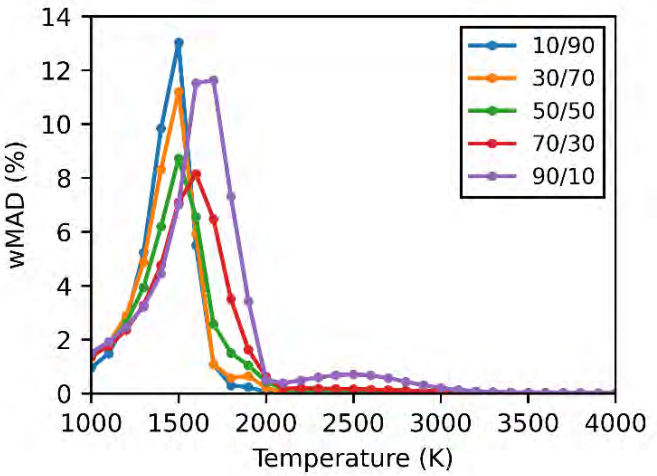

Figure 4.4 Weighted mean absolute deviation (wMAD) between the calculated species concentrations for thermal and plasma kinetics (1000 W/cm^3) at a residence time of 10 ms, in the temperature range of 1000 to 4000 K, for five different CO_2/CH_4 ratios (90/10, 70/30, 50/50, 30/70, 10/90).

From these results we can conclude again the importance of the plasma kinetics for the DRM reaction below 2000 K. Moreover, the deviation (*wMAD*) for the thermal and plasma kinetics becomes larger with longer residence times and higher power densities. On the other hand, at temperatures above 2000 K, the chemistry is almost purely thermal. These results suggest that for warm plasma conditions characterized by temperatures (largely) above 2000 K, being typical for GA, MW and APGDs, the DRM process can reasonably be described by only considering the thermal kinetics. It should be noted, however, that the energy balance is not solved in this study and electron impact collisions can still influence the plasma heating mechanisms.

4.3.2.3 Product formation as a function of time

In Figure 4.2 we observed only some differences in absolute values of the species concentrations between the thermal and plasma kinetics (below 2000 K), without any drastic changes in product distribution. When comparing the

species concentrations at different timepoints in the simulations, we observe a clear relation with gas temperature, as the product concentrations shift towards higher gas temperatures for shorter residence times (presented in Appendix B, Figure B-3). This is logical as, for the same temperature, a shorter residence time results in less reaction, i.e., higher reactant concentrations and lower product concentrations. However, above 3000 K, thermodynamic equilibrium concentrations are already reached for a residence time of 0.1 ms. Indicating that the conversion process occurs on a much shorter time scale compared to typical residence times in warm plasma systems.

To explain this in more detail and to obtain a better picture of the kinetics responsible for the conversion process, the concentrations of the major species are plotted as a function of time in Figure 4.5, for a gas temperature of 1500, 2000 and 4000 K, and for both thermal and (1000 W/cm^3) plasma conditions, at a 50/50 CO_2/CH_4 ratio.

Figure 4.5(a) presents the time evolution at 1500 K, where the effects of the plasma kinetics were most significant, according to Figures 4.2 - 4.4. It is clear that the temporal concentration profiles (i.e., rise or drop as a function of time) are similar in both thermal and plasma kinetics, but the time-evolution occurs faster for the plasma condition. As both cases are still in the early stages of conversion at the residence time of 10 ms, we show an extended timescale to clearly indicate this shift in timescale between both conditions. Indeed, the product species reach a local maximum in concentration at a specific point in time, which is similar in absolute values, but the maximum is located earlier in time for the plasma case. For example, the maximum concentration reached for H_2O is 16% for the thermal conditions after 760 ms, while it is 14% for the plasma condition and reached after only 142 ms. Hence, we can conclude that the plasma generally accelerates the conversion process, rather than altering the overall kinetic pathways and intermediate products. This suggests that electron impact reactions are important in the initial dissociation step, and much less in further reactions of the dissociation products.

Figure 4.5(b) illustrates the species concentrations as a function of time at 2000 K, where the plasma and thermal kinetics exhibit a negligible deviation; cf. Figures 4.2 - 4.4 (with a *wMAD* of only 0.44%). Compared to Figure 4.5(a) (at 1500 K), the temporal concentration profiles look similar, but they are shifted

to shorter timescales. Indeed, a higher temperature allows for faster reactions, so the simulations reach a further point in the reaction pathway at higher temperature. This allows the heavy species (thermal) kinetics to compete and even take over from the plasma-specific reactions, as will be further discussed in section 4.3.3.

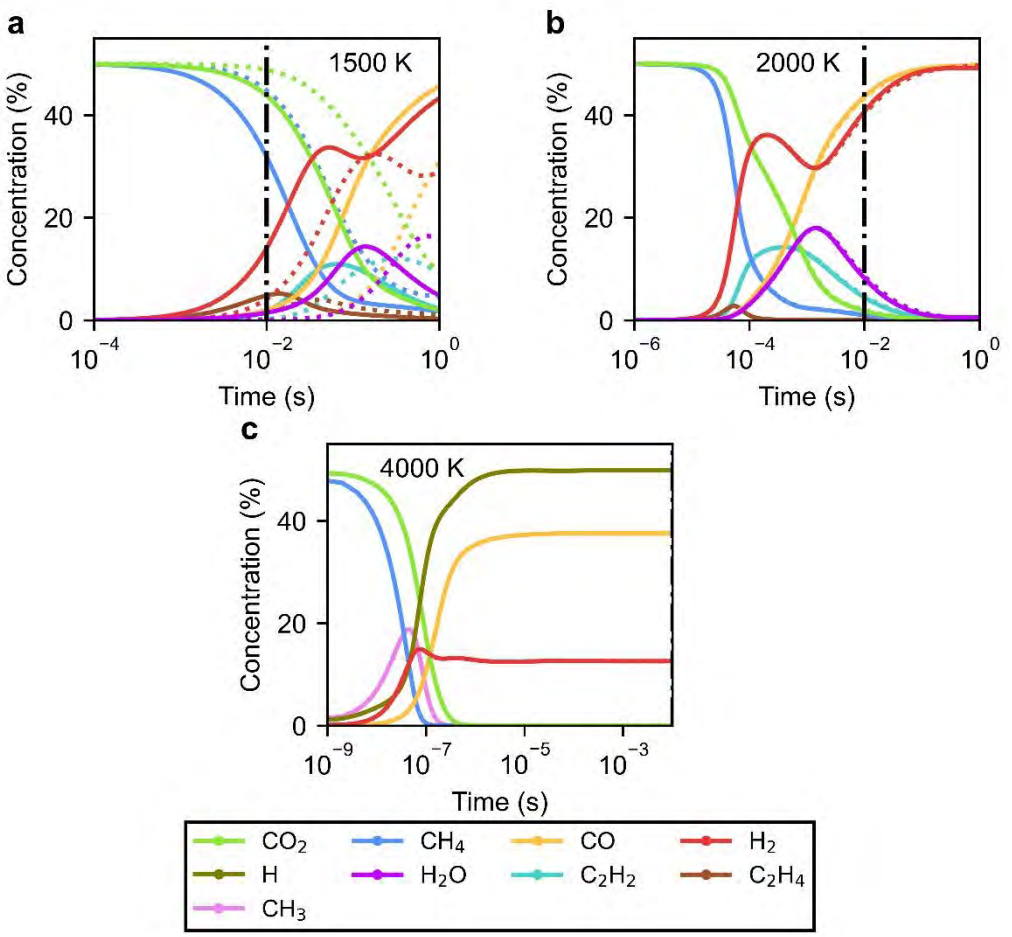

Figure 4.5 Concentration of the main plasma species as a function of residence time for a 50/50 mixture, at 1500 K (a), 2000 K (b) and 4000 K (c), for both thermal (dotted lines) and 1000 W/cm^3 plasma calculations (solid lines). For panels (a) and (b) an extended timescale is shown, with a vertical dash-dotted line marking the reference residence time of 10 ms. Panel (c) only shows up to 10 ms, because steady state is already reached much earlier in time. Also, note that at 4000 K (panel (c)) H and CH_3 are major species, instead of H_2O, C_2H_2 and C_2H_4, which are formed less than 1%.

Both Figures 4.5(a) and 4.5(b) indicate that the reaction pathways can be summarized as the conversion of CH_4 being the first step, yielding the formation of H_2 and C_2-hydrocarbons (C_2H_2 and C_2H_4). The conversion of CO_2 is slightly slower than for CH_4 and results in the formation of CO and H_2O, the latter being obtained through the reverse water gas shift reaction (R4.1). This explains the temporary drop in H_2 concentration.

$$CO_2 + H_2 \rightarrow CO + H_2O \qquad \text{(R4.1)}$$

Before reaching steady state, the created H_2O and C_2 species react further into CO and H_2. Hence, our calculations suggest that the conversion process can be tuned by the temperature and residence time, to more specifically target these valuable C_2 species. Indeed, C_2H_2 reaches its maximum at 66 ms at 1500 K (Figure 4.5(a)) and at 0.40 ms at 2000 K (Figure 4.5(b)), while C_2H_4 (which is even more valuable) reaches its maximum at 14 ms and 54 μs, at 1500 and 2000 K, respectively. However, these maximum concentrations are still lower than for H_2, so post-plasma separation will be necessary, and even post-plasma catalysis[101], to valorize them. In general, it should be noted that further reactions in the post-plasma afterglow can also have an impact on the obtained species distribution, which is not considered in this work.

The chemical pathways clearly change upon higher temperatures, as presented in Figure 4.5(c) for 4000 K. The conversion does not proceed via H_2O, C_2H_2 or C_2H_4, like at 1500 and 2000 K, but instead, CH_3 and H radicals are formed in major concentrations, due to faster thermal CH_4 dissociation. The CH_3 radicals react further towards products (H_2, CO), hence the drop in their concentration, while the H radicals build up more towards steady state, although finally they will recombine in the afterglow (not simulated here). As shown in Figures 4.2 - 4.4, at this temperature the effect of plasma is negligible, and the (thermal) kinetics is even faster, with the simulation reaching steady state well before the reference residence time of 10 ms.

It should also be noted that the time dependence in Figure 4.5 looks similar in shape to the temperature dependence in Figure 4.2. This can be explained by acceleration of the kinetics at higher temperature, resulting in the simulations reaching a further point in the reaction process. For the same reason, the formation of C_2H_2, C_2H_4 and H_2O shown in Figure 4.2(b) results from different

points along the reaction path. The 10 ms timepoint at 1500 K (Figure 4.5(a)) is early in the reaction pathway, where the conversion just started. In contrast, the 2000 K case (Figure 4.5(a)) is already more towards the end of the pathway, closer to reaching steady state. Hence, the maximum concentrations for C_2H_2, C_2H_4 and H_2O were already reached and both species are reacting away at the 10 ms timepoint, explaining why their concentrations are lower in Figure 4.2(b) at 2000 K than at 1700-1800 K.

From this analysis of the time dependence, we conclude that the plasma kinetics accelerates the conversion process, rather than changing the product distributions, but the effect is only significant for temperatures below 2000 K. Higher temperatures, on the other hand, lead to a change in reaction pathway, with radical formation being more significant due to efficient thermal dissociation. At lower temperatures, radicals are also formed, even by electron impact dissociation, but their concentrations remain below 1.5%.

4.3.3 Mechanisms of CO_2 and CH_4 conversion

The kinetic differences and similarities between the thermal and plasma conditions can also directly be explained from the (time-integrated) reaction rates. The relative contributions of the main loss reactions for CO_2 and CH_4 in a 50/50 CO_2/CH_4 mixture are presented as a function of temperature in Figure 4.6. The conversion as a function of temperature is also plotted, for comparison. It is clear from Figure 4.6(a) that the CO_2 conversion is driven by electron impact dissociation up to 1500 K. The largest contributions are from direct electron impact dissociation (78% at 1000 K) and dissociative attachment (21% at 1000 K). However, the CO_2 conversion itself is still below 4% in this temperature range. It only starts to rise dramatically above 1500 K, driven upon reaction with a H radical (starting from 1400 K), which is obtained from the CH_4 conversion. Above 1700-1800 K, the contribution of electron impact dissociation becomes negligible.

The CH_4 conversion occurs through heavy species reactions (see Figure 4.6(b)). At 1000 K the main dissociation reactions are with O and OH, contributing for 41 and 42%, respectively, but decreasing with temperature. For temperatures below 1500 K, the O radicals originate from electron impact CO_2 dissociation, and OH is the product of CH_4 dissociation upon collision with O radicals (first

reaction in the legend of Figure 4.6(b)). This means that one dissociated CO_2 molecule can dissociate two CH_4 molecules, by these two reactions. This effect, together with the lower C-H bond dissociation energy, explains the much higher conversion of CH_4 compared to CO_2, for temperatures below 1500 K (i.e., 30% vs 4% at 1500 K; cf. Figure 4.6).

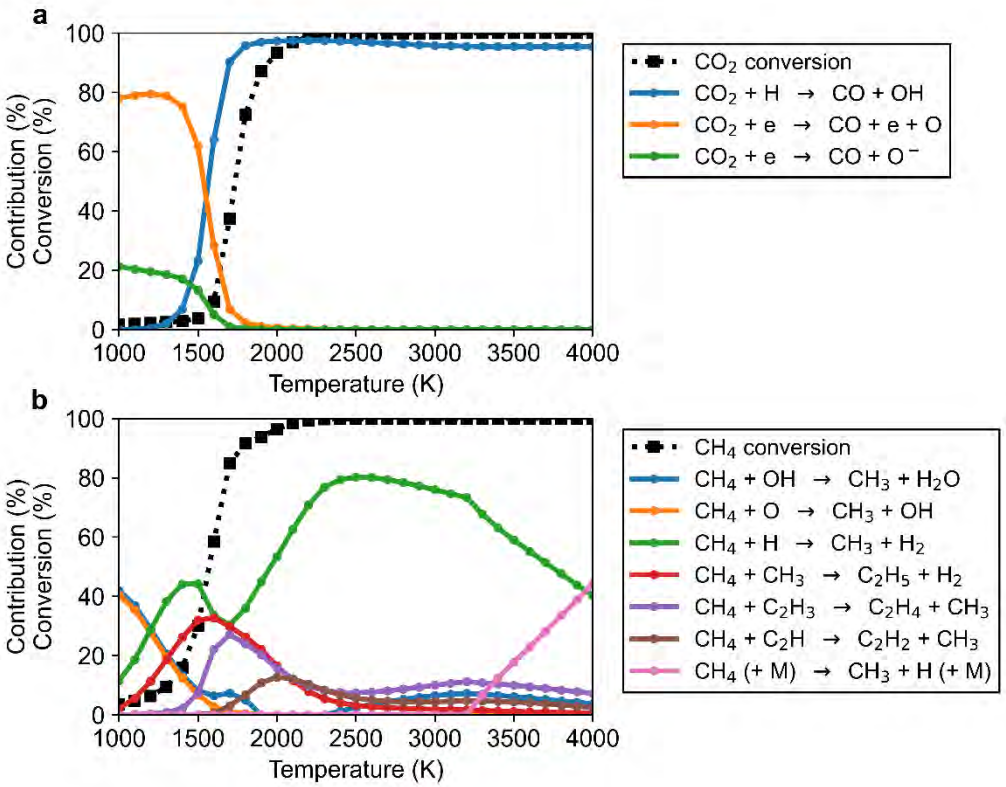

Figure 4.6 CO_2 (a) and CH_4 (b) conversion (dotted black lines), as well as the relative contributions of the main loss reactions (> 5%) based on the time-integrated net reaction rates (see legends), as a function of temperature, for plasma simulations with a power density of 1000 W/cm^3 and for a 50/50 ratio of CO_2/CH_4 at a residence time of 10 ms.

Above 1500 K, reactions with H, CH_3 and C_2H_3 take over as the main loss reactions for CH_4. The reactions with CH_3 and C_2H_3 have a maximum contribution of 33% at 1600 K and 27% at 1700 K, respectively. The highest contribution is obtained for the reaction with H radicals: it reaches a maximum of 44% at 1500 K, then drops to 30% at 1700 K and subsequently increases again to almost 80% at 2500 K and above. The drop at 1700 K is due to the strong

formation of H_2O, effectively capturing H radicals, and thus lowering their contribution to CH_4 dissociation.

For temperatures above 2500 K, the CH_3 and C_2 radicals formed in the above dissociation reactions (see legend in Figure 4.6(b)) quickly convert further into CO and H_2, allowing less of them to react with CH_4, and thus reducing their contribution to the dissociation. On the other hand, the thermal dissociation of H_2 does allow H radicals to be still present and their contribution to the CH_4 dissociation is dominant in almost the entire temperature range, even up to 4000 K. The reaction with C_2H radicals has a minor contribution to the overall CH_4 dissociation throughout the entire temperature range, with a maximum of 13% at 2000 K. Above 3500 K, thermal dissociation of CH_4 into H and CH_3 upon collision with any neutral molecule (M) also becomes important, and its contribution rises with temperature to reach 44% at 4000 K. These dissociation pathways agree with the work presented by Liu et al.[49] in which the reaction with H is the main dissociation reaction for both CO_2 and CH_4 at a gas temperature of 2500 K.

Our model indicates that direct dissociation of CH_4 through electron impact reactions is not important within the given parameter space. However, below 1500 K the importance of O and OH radicals links the dissociation of CH_4 to electron impact dissociation reactions of CO_2. Therefore, the DRM reaction pathways are really a coupled process between CO_2 and CH_4, both requiring the other species for the chemical reactions.

As the main CO_2 dissociation pathway for gas temperatures below 1700 K is through electron impact reactions, we also present the electron density and electron temperature, to further explain these findings (Figure 4.7). Firstly, this figure shows that the electron density steadily increases from around 2×10^{11} to 2×10^{13} cm^{-3} within the studied gas temperature range. This indicates that a high electron density is not the main driver behind the electron impact dissociation of CO_2 below 1700 K (Figure 4.6). On the other hand, the electron temperature (around 17000 K) is significantly higher for these lower gas temperatures, resulting in a larger fraction of electrons with sufficient energy to dissociate CO_2. This in turn leads to higher reaction rates for electron impact dissociation reactions, increasing their contributions in Figure 4.6. While it is logical that the electron temperature decreases upon rising electron density, the sharp

decrease indicates other effects are responsible. It should also be noted that this coincides with a strong increase in conversion and the formation of CO, H_2, C_2H_2 and H_2O (Figure 4.2). Therefore, we relate this lower electron temperature above 1700 K to these species. They have larger elastic collisional cross sections, compared to CO_2 and CH_4, and combined with their higher concentrations, this results in more electron energy loss, i.e., a lower electron temperature.

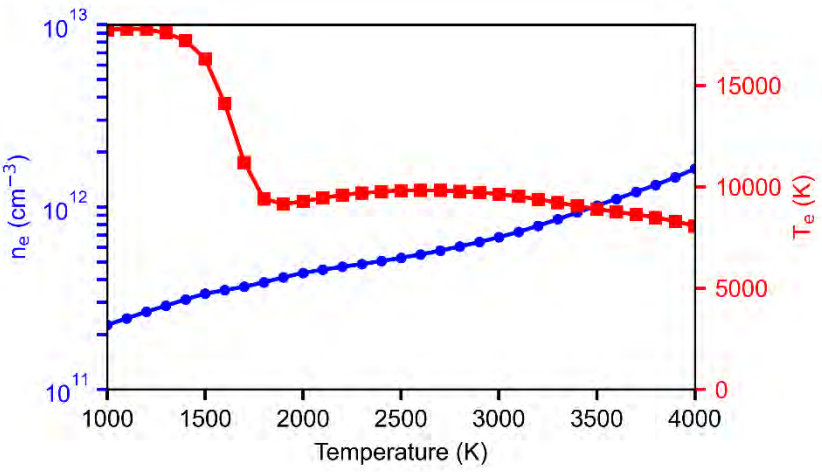

Figure 4.7 Calculated electron density (blue line) and electron temperature (red line) for the gas temperature range of 1000 to 4000 K and a 50/50 CO_2/CH_4 ratio and 1000 W/cm^3 plasma condition, at a residence time of 10 ms.

In general, we can conclude that thermal kinetics dominates the dissociation process above 2000 K, while electron impact reactions are the main mechanism for CO_2 dissociation below 1500 K. Figure 4.4 and Figure B-2 (in the Appendix) indicate that a variation in power density within a range typical for warm plasmas does not significantly alter the temperature at which thermal kinetics starts to dominate.

Electron impact dissociation occurs through excitation to high electronically excited states, which requires more energy than direct thermal dissociation.[12,13] This explains why warm plasmas, for which the conversion is largely thermal, are more energy efficient than cold (or non-thermal) plasmas, which operate near room temperature and have a large contribution of electron impact dissociation, because thermal chemistry is negligible. In addition, cold plasmas require a higher power density to improve the conversion, due to their dependence on electron impact reactions. This is consistent with experimental

findings from literature, which illustrate a much lower energy cost for DRM in warm plasmas (such as GA, MW, APGD and NPD) than in non-thermal plasmas (such as DBD).[13,31–34,37,102,103]

4.3.4 Effect of gas mixing ratio

In previous section (4.3.2) we only considered the stoichiometric gas mixture (50/50). In this section we extend the analysis to mixtures with excess CO_2 or CH_4. First, we can make the same general conclusions as for the 50/50 ratio. Below 2000 K, we again observe the acceleration effect of the plasma kinetics, which becomes negligible towards 2000 K. Furthermore, thermodynamic equilibrium is also reached within the simulation timescale of 10 ms. Hence, the effects of the plasma are the same, but the product distribution is significantly altered, because of the deviation from the stoichiometric mixture. Competing side reactions cause the products to deviate from the DRM reaction as presented in R1.1 in the Introduction.

4.3.4.1 Mixtures with excess CO_2

For mixtures with excess CO_2 (i.e., 90/10 and 70/30 CO_2/CH_4 ratio) the concentrations of the major species are plotted as a function of temperature in Figure 4.8. First of all, as expected, we note a significantly higher CO_2 concentration at 1000 K (in line with the mixing ratio), as there is no conversion yet, and a clear drop in CO_2 concentration upon increasing temperature. Furthermore, unlike the 50/50 ratio, where complete conversion was achieved above 2000 K, mixtures with excess CO_2 require higher temperatures to reach full conversion. At 2000 K, the CO_2 concentration is still about 10% and even about 50%, for the 70/30 and 90/10 CO_2/CH_4 ratios, respectively. These values agree with the concentrations at thermodynamic equilibrium, presented in the Appendix (Figure B-1(a,b)). Hence, the CO_2 conversion for these mixtures is strongly limited by the thermodynamic equilibrium above 2000 K. Nevertheless, upon increasing temperature, the CO_2 concentration drops further, to 0.6% and 2.1% at 4000 K, for the 70/30 and 90/10 mixtures, respectively, because CO_2 becomes less thermodynamically favored. At these high temperatures, O and OH radicals are formed in large amounts, but they can react back to CO_2 in the afterglow. Hence, for mixtures containing an excess of CO_2 (70/30 and 90/10

CO_2/CH_4), the CO_2 conversion is strongly limited by the thermodynamic equilibrium, while a complete conversion of CH_4 can be achieved below 2000 K.

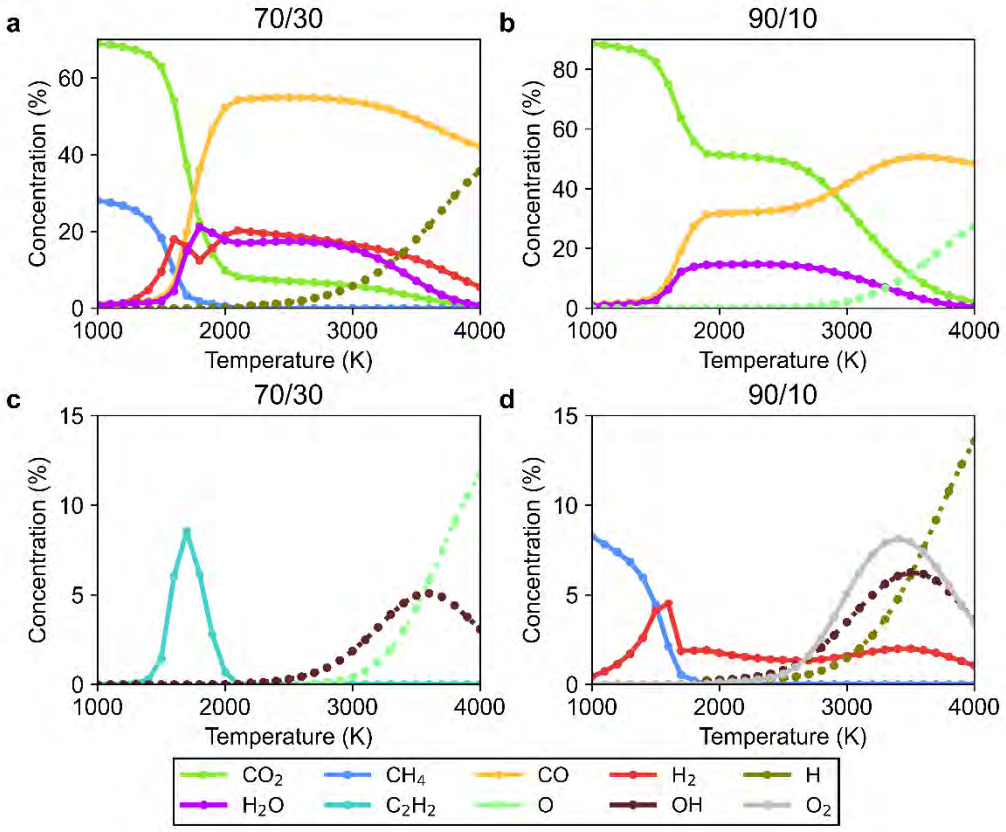

Figure 4.8 Calculated concentrations of the main plasma species (> 4%) as a function of temperature, for a 70/30 and 90/10 CO_2/CH_4 ratio, at a residence time of 10 ms for the 1000 W/cm^3 plasma conditions. The species are split over 2 panels according to their concentration: the top panels (a and b) plot the largest concentration species for the 70/30 and 90/10 mixtures, respectively, while the lower concentration species are illustrated in the bottom panels (c and d), for the 70/30 and 90/10 mixtures, respectively. The stable molecules and radicals are depicted with solid and dotted lines, respectively, for easy recognition.

It is also clear from Figure 4.8 that CO is the major product in case of excess CO_2, with a maximum concentration of 55% at 2600 K and 51% at 3600 K, for the 70/30 and 90/10 CO_2/CH_4 ratios, respectively. On the other hand, the excess of O atoms, originating from CO_2, strongly reduces the formation of H_2, and instead favors the formation of H_2O. This is also indicated by the thermodynamic equilibrium concentrations (Figure B-1, in the Appendix). This is in contrast with the 50/50 CO_2/CH_4 ratio, where H_2O was only an intermediate

species in the reaction pathway towards H_2 and CO (cf. Figure 4.5). The H_2 concentration reaches a maximum of 20% at 2100 K and 4.5% at 1600 K, for the 70/30 and 90/10 ratios, respectively. In contrast, the H_2O concentration reaches similar values to H_2 for the 70/30 ratio (max. 21% at 1800 K), while it is significantly higher for the 90/10 ratio (max. 15% at 2300 K). We observe the competition of reaction R4.2 as a side reaction, which is the combination of the DRM (R1.1) and twice the reverse water gas shift reaction (R4.1).

$$3\ CO_2 + CH_4 \rightarrow 4\ CO + 2\ H_2O \qquad \text{(R4.2)}$$

Above 2500 K, H, OH and O radicals are also formed in significant amounts, due to thermal decomposition of H_2, H_2O and CO_2. However, these radicals will react away in the post-plasma afterglow. For instance, the O radicals can recombine with CO into CO_2, reducing its conversion. Indeed, this back-reaction plays an important role in the afterglow of pure CO_2 plasmas [54,56,57,60], and is thus expected to be significant in DRM as well, especially at large CO_2 fractions. Finally, below 2000 K, we also see the formation of C_2H_2, but only with a maximum concentration of 8.6 and 2.5%, for the 70/30 and 90/10 ratios, respectively, while the C_2H_4 concentration is even lower.

The change in gas mixture influences the dissociation mechanisms of CO_2 and CH_4 compared to the 50/50 ratio presented in Figure 4.6. Figure 4.9 depicts the relative contributions of the main loss reactions for CO_2 and CH_4 in a 90/10 CO_2/CH_4 mixture as a function of temperature. The same trends are observed for the 70/30 mixture, which is presented in the Appendix (Figure B-4).

Electron impact dissociation is the main loss reaction for CO_2 below 1500 K, but still contributes for around 6.5% between 2000 and 3000 K, in contrast to the 50/50 CO_2/CH_4 mixture, where electron impact dissociation became negligible above 2000 K (Figure 4.6). Figure 4.4 indeed shows a slight difference between the plasma and thermal calculations in this temperature range for the 90/10 CO_2/CH_4 mixture (maximum *wMAD* of 0.71% at 2500 K). This is attributed to the large amount of CO_2 (around 50%) still present in the mixture, while electron impact dissociation of CO_2 is still notable in this temperature range. This effect is however minor and does not significantly change the overall product concentrations. Indeed, between 1500 and 3000 K, most CO_2 is converted upon reaction with H radicals (see Figure 4.9(a)), similar to the 50/50 ratio. Finally, for

gas temperatures approaching 3000 K, the reactions with OH and O radicals become increasingly important, and the conversion further increases to nearly 100% at 4000 K, with a negligible contribution of electron impact dissociation.

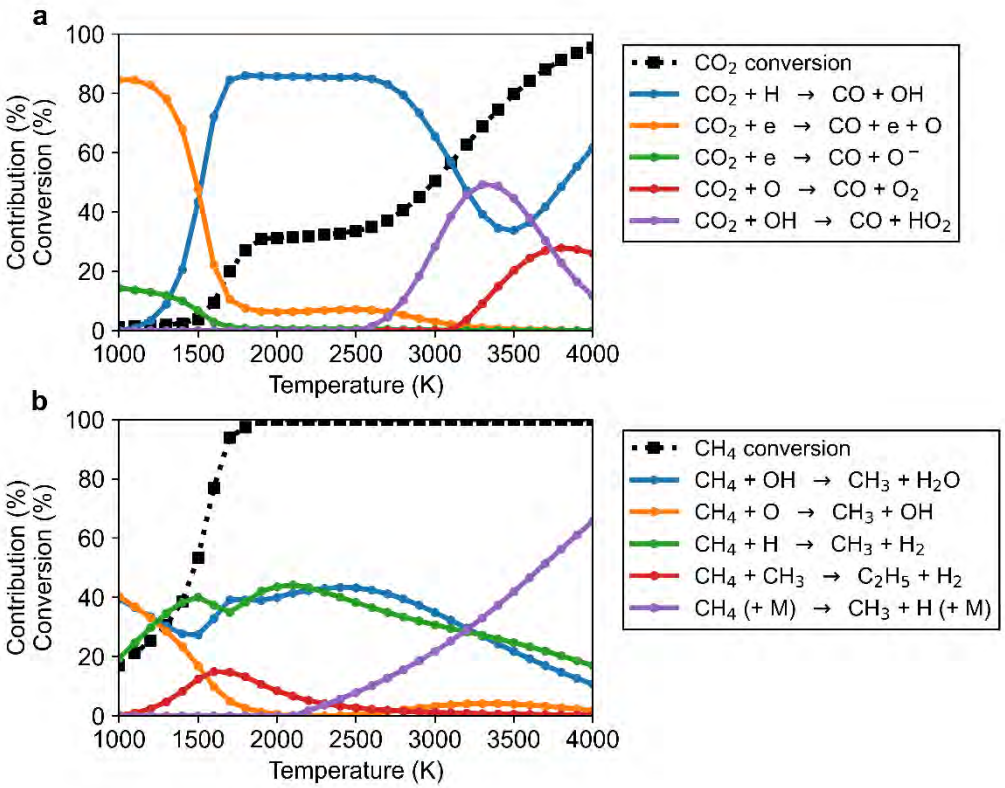

Figure 4.9 CO_2 (a) and CH_4 (b) conversion (dotted black lines), as well as the relative contributions of the main loss reactions (> 5%) based on the time-integrated net reaction rates (see legends), as a function of temperature, for plasma simulations with a power density of 1000 W/cm^3 and for a 90/10 ratio of CO_2/CH_4 at a residence time of 10 ms.

For CH_4 dissociation (Figure 4.9(b)), largely the same reactions and temperature dependence is observed as for the 50/50 ratio of CO_2/CH_4 (Figure 4.6). However, reactions involving CH_4 dissociation products (H, CH_3, C_2H and C_2H_3) do contribute less, which is logical, as the excess of CO_2 reduces their overall concentration. The contribution of C_2H and C_2H_3 are reduced to less than 5% over the studied temperature range (1000 – 4000 K) and therefore not shown in Figure 4.9(b). The reaction with OH increases significantly up to 43%, and is therefore comparable with the reaction upon collision with H radicals (which was dominant at the 50/50 ratio of CO_2/CH_4; Figure 4.6). Finally, also thermal

decomposition is increasingly more important above 2200 K, with a contribution of 66% at 4000 K.

Again, our model shows similar findings to the work of Liu et al.[49] for the same CO_2/CH_4 ratio at 2500 K, where the reaction with H is again the largest contributor to CO_2 dissociation, while for CH_4 dissociation, H and OH have the highest contribution in our results, but we find a lower contribution of the reaction with any neutral species (M) compared to Liu et al.[49] This is likely related to differences in the modelling approach and kinetic schemes.

4.3.4.2 Mixtures with excess CH_4

Figure 4.10 shows the species concentrations as a function of temperature, for mixtures with excess CH_4 (i.e., 30/70 and 10/90 ratio). The corresponding thermodynamic equilibrium concentrations are plotted in the Appendix (Figure B-1(c,d)). The much lower O atom concentration in the mixture limits the oxidation of CH_4 into CO. Consequently, the CO concentration only reaches a maximum of 30% at 2200 K for the 30/70 ratio and 10% at 2100 K for the 10/90 ratio. CH_4 is still fully converted above 2000 K, although not to CO, but to H_2 and C_2H_2. H_2 is by far the most abundant product, reaching concentrations of 60% at 2200 K and nearly 70% at 2100 K, for the 30/70 and 10/90 ratios, respectively. C_2H_2 is the third major product (after H_2 and CO) for the 30/70 ratio, with a maximum concentration of 17% at 1700 K, and it is even the second major project after H_2, reaching 22% at 1800 K, for the 10/90 ratio. However, these values are obtained below 2000 K, where steady state is not fully reached yet at 10 ms residence time, so the concentration is expected to drop again upon longer residence time. Similarly, a maximum concentration of 11% and 3.5% is observed for H_2O at 1800 K, for the 70/30 and 10/90 CO_2/CH_4 mixtures, respectively. As inferred from Figure 4.5, H_2O is formed as an intermediate species, which is present at those conditions because the conversion process is still ongoing. Finally, H atoms are the main radicals formed at high temperature, upon thermal decomposition of H_2, and they become even the dominant species above 3500 K, with also small amounts (up to 7%) of C_2H.

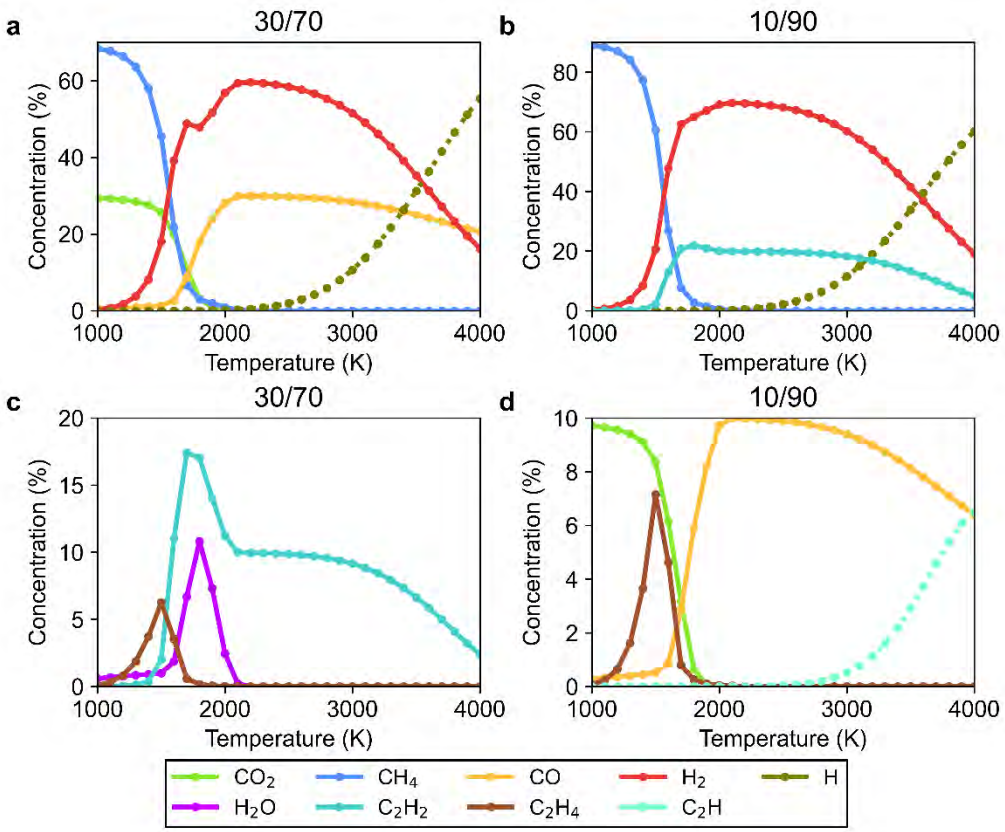

Figure 4.10 Calculated concentrations of the main plasma species (> 4%) as a function of temperature, for the 30/70 and 10/90 CO_2/CH_4 ratio, at a residence time of 10 ms for the 1000 W/cm^3 plasma conditions. The species are split over 2 panels according to their concentration: the top panels (a and b) plot the large concentration species for the 30/70 and 10/90 mixtures, respectively, while the lower concentration species are illustrated in the bottom panels (c and d) for the 30/70 and 10/90 mixtures, respectively. The stable molecules and radicals are depicted with solid and dotted lines, respectively, for easy recognition.

We confirm that the lower O atom concentration, due to the limited CO_2 concentration in the mixture, allows reaction R4.3 to be more important, producing C_2H_2 as a final product. Furthermore, we observe several other benefits for these mixing ratios, such as full conversion of both reactants and H_2/CO ratios above 1, which are preferred for the downstream processing of syngas into desired products, as discussed in depth in section 4.3.5. However, mixtures with excess CH_4 are more difficult to handle in practice, due to excessive solid carbon formation,[34–38] which is not taken into account yet in our model. On the other hand, our model does show significant formation of C_2H_2,

which might be overestimated as this is an important precursor species for the formation of solid carbon,[81,104,105] which is not yet accounted for in our model.

$$2\ CH_4 \rightarrow C_2H_2 + 3\ H_2 \qquad \text{(R4.3)}$$

The relative contributions of the main loss reactions for CO_2 and CH_4 in a 10/90 CO_2/CH_4 mixture as a function of temperature are presented in Figure 4.11. The same trends are observed for the 30/70 mixture, which is presented in the Appendix (Figure B-5).

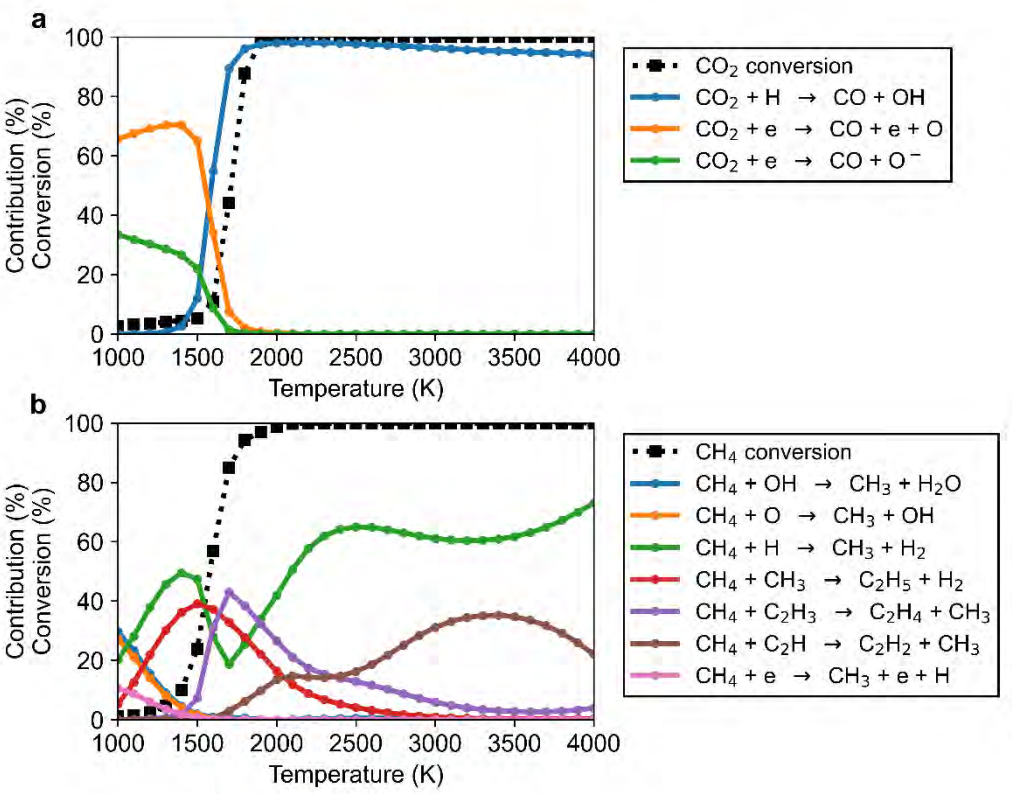

Figure 4.11 CO_2 (a) and CH_4 (b) conversion (dotted black lines), as well as the relative contributions of the main loss reactions (> 5%) based on the time-integrated net reaction rates (see legends), as a function of temperature, for plasma simulations with a power density of 1000 W/cm^3 and for a 10/90 ratio of CO_2/CH_4 at a residence time of 10 ms.

The reaction mechanism for dissociation of CO_2 (Figure 4.11(a)) is very similar to that for the 50/50 CO_2/CH_4 mixture (Figure 4.6(a)). Below 1500 K electron impact reactions are the main dissociation mechanism, and above 1500 K the reaction with H is the most significant. However, for CH_4 (Figure 4.11(b)) there

are more significant changes in the dissociation reactions. Firstly, electron impact dissociation now has a non-negligible contribution in the lower temperature range (< 1500 K) with a maximum of 11% at 1000 K. The higher concentrations of CH_4 dissociation products further increase their contribution to the dissociation process of CH_4. Therefore, reactions with CH_3 and C_2H_3 become more important, and their maximum contributions rise to 39% at 1500 K and 43% at 1700 K, respectively, followed by a drop towards 3000 K. The reaction with H takes over the dissociation of CH_4, similar to the 50/50 ratio, however with a lower contribution, as the rate of the reaction with C_2H has increased between 2000 – 4000 K. These reactions are the two most important up to 4000 K. On the other hand, the thermal dissociation of CH_4 remains below 5% and is therefore not shown in Figure 4.11(b). This is caused by the much higher concentration of CH_4 dissociation products in the mixture.

4.3.5 Optimization of the syngas ratio

The main product of DRM is syngas and the obtained syngas ratio (H_2/CO ratio) is important to evaluate the performance of DRM, with regard to further post-processing. For the Fischer-Tropsch process and methanol synthesis from syngas, a syngas ratio around 2 is desired.[24] The CO_2/CH_4 ratio is important for controlling the syngas ratio, as illustrated in Figure 4.12, which depicts the syngas ratio as a function of temperature at 10 ms for the five gas mixtures.

Near 1000 K, all gas mixtures result in syngas ratios below 1, even though at these conditions more CH_4 is converted than CO_2. Indeed, the syngas ratio remains low due to the formation of side products, like H_2O, C_2H_2 and C_2H_4, which compete with H_2 formation. Raising the temperature to about 1500 K strongly enhances the syngas ratio, as the CH_4 conversion and H_2 formation strongly increase compared to the CO_2 conversion and CO production. This is attributed to the faster reaction kinetics at higher temperatures, with the CO_2 conversion typically lagging behind on the CH_4 conversion, and the fact that steady state is not yet reached within 10 ms at this temperature (cf. Figure 4.5). The difference between the CH_4 and CO_2 conversion reaches a maximum around 1500 K, leading to the highest syngas ratios (see Figure 4.12). For the most extreme cases (i.e., 10/90 and 90/10 CO_2/CH_4 ratios) syngas ratios of 54 and 1.0 are reached, respectively. The other CO_2/CH_4 ratios provide syngas

ratios (well) above 3 at this temperature, and thus, neither of the conditions seem desirable. Raising the temperature further up to 2000 K, the CO_2 conversion rises further, and the CH_4 approaches the steady state limit, leading to a drop in syngas ratio. At 2000 K, the syngas ratio decreases to 0.93 for the stoichiometric mixture, while we obtain lower syngas ratios for mixtures with excess CO_2, i.e., 0.36 and 0.056 for 70/30 and 90/10 CO_2/CH_4, respectively. On the other hand, for mixtures with excess CH_4, the syngas ratio remains above 1, i.e., 2.0 and 7.1 for 30/70 and 10/90, respectively. These results are logical, considering the competing side reactions discussed in section 4.3.4, allowing for more H_2 formation through reaction R4.3. Finally, the syngas ratio slightly decreases upon higher temperatures, as the formation of H radicals becomes significant, resulting in less H_2. However, in practice, this will not be a problem, because after the plasma, the H radicals can recombine back into H_2, which is not simulated by our model.

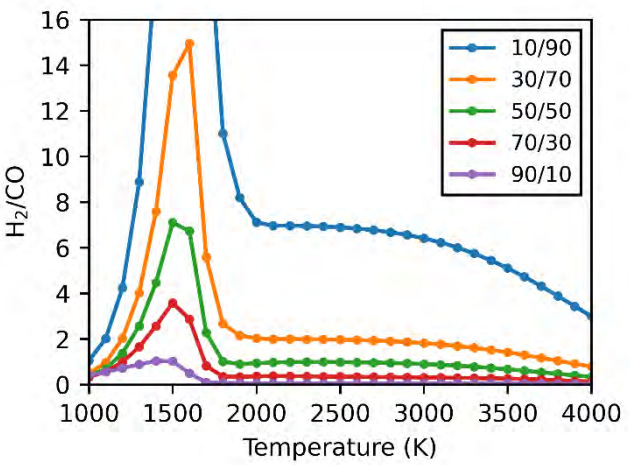

Figure 4.12 Syngas ratio (H_2/CO) obtained at a residence time of 10 ms, as a function of temperature, for five different CO_2/CH_4 ratios (90/10, 70/30, 50/50, 30/70, 10/90). For the 10/90 mixture, the peak in syngas ratio is 54 (outside of the y-axis scale).

Hence our model predicts that syngas ratios of 2 (and above) are achievable for all gas mixing ratios, except for 90/10 CO_2/CH_4, at a temperature around 1500 K, due to kinetic effects, because the CH_4 conversion initially rises faster than that of CO_2. As such, high syngas ratios can be achieved by limiting the conversion, even for mixtures with excess CO_2. However, due to the limited conversion, the corresponding syngas yield will be low. Moreover, the strong

time and temperature dependences make it difficult to target these specific conditions. We believe it is better to target the temperature region above 2000 K, when steady state and maximum conversion are reached. Obviously, a syngas ratio of 2 can be obtained from the 30/70 CO_2/CH_4 ratio, at high conversion and thus also high syngas yield.

4.3.6 Final considerations: Limitations of our model and of DRM

Note that experimental setups are inherently more inhomogeneous than our idealized batch reactor model, due to temperature gradients, transport of species, residence time distributions, as well as the afterglow region, in which back-reactions can occur. Together these effects can introduce deviations from our model predictions, but we believe that our model is valuable to gain deeper insights in the underlying mechanism, and to search for optimized reactor conditions.

Note that our model predicts a variety of products being formed at all conditions investigated, and this is also experimentally observed, although syngas is typically the major product, in line with our calculations. Moreover, in reality the CO_2 and CH_4 conversion will be typically below 100%, due to post-plasma recombination of the reaction products back into CO_2 and CH_4,[54,56,57,59,60] and because not all gas will pass through the active plasma region, and thus, being subject to conversion.[26,28,31,106] The unconverted reactants (CO_2 and CH_4), as well as the side products (like C_2H_2 and H_2O) next to syngas require an extra separation step before further processing. Unfortunately, this cannot be avoided when considering only a binary mixture of CO_2 and CH_4, because there exists no mixing ratio that allows complete conversion, in combination with the optimal syngas ratio of 2, and no side products. Therefore, it might be interesting to explore other mixtures, such as $CO_2/CH_4/H_2O$ (so-called bi-reforming of methane). Indeed, theoretically, this mixture, in a ratio of 1/3/2, can stoichiometrically produce pure syngas with a ratio of 2 at full conversion without side products.[107,108] This may be interesting to investigate in future work.

4.4 Conclusion

We studied the chemical kinetics of plasma-based DRM by means of batch reactor simulations, in a temperature range between 1000 and 4000 K relevant for warm plasma conditions and a wide range of CO_2/CH_4 ratios, and we compared with pure thermal conversion, as well as thermodynamic equilibrium calculations. This computational study provides a broad view of the influence of plasma parameters on conversion and product distribution, and insights into possible improvements to the process. Importantly, we provided an update of the chemical kinetics scheme compared to earlier models by our group PLASMANT. We were able to verify and validate the thermal chemistry in our model at steady state, by reproducing thermodynamic equilibrium concentrations.

Furthermore, we used the model to compare plasma-based DRM to purely thermal gas-phase DRM, thereby isolating the influence of electron and ion reactions and thus revealing the contribution of the plasma-specific chemistry. Our simulations show that plasma can significantly improve the conversion below 2000 K, compared to the pure thermal chemistry. This is attributed to electron impact dissociation of CO_2, which creates O atoms, that give rise to CH_4 conversion. This electron impact reaction can occur at low gas temperatures, allowing the first step in the conversion process to proceed. On the other hand, the purely thermal conversion, without electrons, must rely on molecular collisions to dissociate CO_2 and CH_4 which in this temperature range (below 2000 K) are much slower and cannot obtain significant dissociation. Note that this acceleration does not significantly alter the product distribution, but only the timescale at which they are formed, as the further reactions to product species are through radical reactions, which are the same in both the plasma and thermal process. Consequently, the residence time is an important parameter to target certain products, because for this temperature range (below 2000 K) steady state is not yet reached for residence times in the ms-range.

When increasing the temperature above 2000 K, thermal reactions start to dominate the kinetics in the plasma, even when varying the power density between 500 and 1500 W/cm^3 (i.e., the typical range characteristic for warm

plasmas). Hence the kinetics of warm plasmas, which typically operate above 2000 K, can be described by thermal chemistry. The importance of thermal conversion at these high temperatures explains why warm plasmas are typically more energy-efficient than non-thermal (cold) plasmas, where the conversion occurs by electron impact dissociation, requiring more energy than strictly needed for bond breaking.

Furthermore, we studied the effect of the CO_2/CH_4 ratio on the conversion, product distribution and syngas ratio. Mixtures containing excess CO_2 lead to the formation of H_2O, at the expense of H_2 production. Moreover, at temperatures where steady state is reached, the CO_2 conversion is limited by thermodynamic equilibrium. As a result, full conversion can only be achieved at extremely high temperatures above 4000 K, through dissociation into radicals. Yet, such large concentrations of radicals can recombine back into CO_2 in the afterglow, which will lower the final conversion. From this we conclude that mixtures with excess CO_2 have several disadvantages; mainly the limited conversion combined with the low H_2, and high H_2O production are unfavorable for further processing. On the other hand, for gas mixtures with an excess of CH_4, full conversion can be achieved, as this is thermodynamically favored at temperatures for which steady state is reached (above approximately 2100 K). Due to the increased H content in the mixture, a high concentration of H_2 can be obtained, while C_2H_2 becomes a major carbon product, competing with CO.

Finally, our model predicts that high syngas ratios can be achieved in the temperature range between 1000 and 2000 K, by carefully exploring the kinetics (i.e., selecting the right residence time and temperature), due to the faster destruction of CH_4 compared to CO_2 at these conditions. However, this also limits the conversion and consequently the syngas yield. At higher temperatures, where steady state is reached, high syngas ratios can be obtained by using gas mixtures with an excess of CH_4. We found a mixture of 30/70 CO_2/CH_4 to be optimal for obtaining a syngas ratio of 2, which is important for further processing using the Fischer-Tropsch process and methanol synthesis.

Altogether, we believe our model predictions are useful to gain deeper insights in the underlying chemical kinetics of DRM, for a broad range of conditions, independent of actual reactor designs. This knowledge can be further employed in designing and optimizing experimental reactors to improve the DRM process.

5 Afterglow quenching in plasma-driven DRM: a detailed analysis of the post-plasma chemistry via kinetic modelling

The results presented in this chapter are submitted for publication in:

- Slaets, J.; Morais, E.; Bogaerts, A. Afterglow quenching in plasma-based dry reforming of methane: a detailed analysis of the post-plasma chemistry via kinetic modelling. Submitted to Fuel.

5.1 Introduction

While the gas conversion in warm plasmas is typically driven by thermal chemistry, as discussed in chapter 4, the downstream gas temperature (i.e., the afterglow or post-plasma region, outside of the plasma zone) may still be sufficiently high to enable reaction pathways that can influence reactor performance in different manners, as previously discussed in section 1.4 of chapter 1. The conversion can decrease due to reverse reactions, the product distribution can change, or the conversion can increase leading to a higher product yield. Different experimental methods of quenching and their effect on the DRM performance were discussed in section 1.4. In this chapter, we explore the effects of these post-plasma quenching methods on the chemical kinetics for DRM, and elucidate the mechanisms involved in the observed conversion and selectivity trends. Our model incorporates two distinct approaches to post-plasma quenching: (i) heat removal from the system (emulating the introduction of a cooled rod, hence conductive cooling), and (ii) the mixing of cold gas in the post-plasma region (emulating the introduction of a nozzle, or simply adding cold gas in the afterglow). In the interest of model versatility and relevance, we do not limit our work to specific reactor designs or operating conditions; instead we focus on general warm plasma conditions. To this end, we study a wide range of conditions, with plasma temperatures between 2000 – 4000 K and three different CO_2/CH_4 ratios, i.e., stoichiometric (50/50), excess CH_4 (30/70) and excess CO_2 (70/30). We compare different degrees of gas

cooling, achieved with both methods, and evaluate the effects of the ensuing temperature decrease on conversion, selectivity and energy cost. Our primary objective is to obtain a better understanding of the post-plasma kinetics upon gas cooling. These insights can help experimentalists towards potential improvements and new reactor designs for further advancement of plasma-based DRM technologies.

5.2 Computational details

5.2.1 Simulation details

This in-depth (yet general) study of multiple conditions and approaches is again conducted using the 0D chemical kinetics model described in section 2.1. A schematic overview of the simulation domain is given in Figure 5.1(a), illustrating the plasma zone with a constant temperature, followed by the afterglow in which the gas temperature decreases, as the hot gas is quenched. The plasma conditions are consistent with those in chapter 4, i.e., the gas temperatures between 2000 – 4000 K (typical temperature range for many warm plasmas[13]) and the residence time in the plasma zone of 10 ms (reasonable assumption following the works of Van Alphen et al.[81] and Dahl et al.[98]). To demonstrate the effects in the post-plasma region, we present the important parameters (conversion and selectivity) at points A and/or B (indicated in Figure 5.1), as a function of the plasma temperature.

Two quenching approaches are tested within the post-plasma region, which divides this study into two main parts: (i) in the first approach, we model an afterglow system which is cooled through conductive heat loss (from point A to point B in Figure 5.1), aiming to study the effects of temperature decrease on the reaction kinetics. This conductive cooling is enhanced with a factor, *c,* (1, 10 and 100) with more details given in section 5.2.3. (ii) In the second approach, the cooling stems from mixing room-temperature gas with the hot afterglow, introducing 'fresh' and 'cold' gas molecules which will reduce the overall gas temperature. In this study, the cold gas mixture introduced post-plasma is identical to the unconverted gas mixture. The freshly added CO_2 and CH_4 molecules will be dissociated by the relatively high temperatures in the afterglow, resulting in altered kinetic pathways and extra overall conversion.

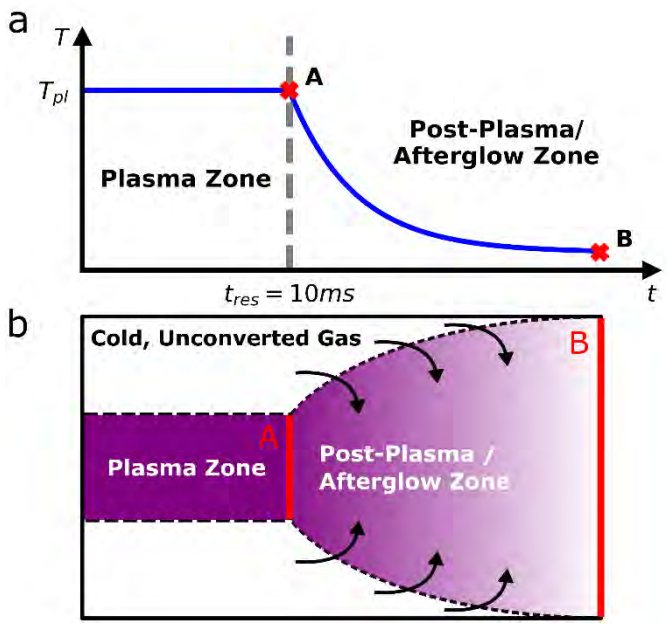

Figure 5.1 (a) Schematic overview of the simulation domain, showing the plasma and post-plasma/afterglow zones, plasma temperature (T_{pl}) and residence time (t_{res}, which is typically around 10 ms)[81,98]*. (b) Schematic overview of the enhanced mixing approach, indicating the plasma and post-plasma/afterglow zones. The cold unconverted gas is only added after the plasma, either from a peripheral region around the plasma zone or from a secondary inlet. The important points in the simulations are compared in the results and discussion section. (A) corresponds to the end of the plasma zone (at the plasma temperature, immediately before the temperature drop), and (B) to the end of the afterglow after all quenching has taken place.*

Since this mixing approach does not consider conductive heat loss to the reactor walls, i.e., the post-plasma region is assumed to be perfectly thermally insulated, the addition of cold gas is the only factor that influences the gas temperature and in turn the kinetics. Hence, without other means to decrease the gas temperature, optimal conditions are created to attain the highest possible conversion of the added gas. This is due to the redistribution of the available energy over more gas molecules, since this quenching method does not remove heat from the system. Thus, to guarantee a realistic cooling and a temperature drop sufficient to stop all reactions, a large amount of cold gas must be added. In our case, we found that adding a cold gas stream nine times larger than the initial flow (i.e., diluting the fraction that travelled through the plasma to 10%) meets this criterion. We change the mixing time between 1, 10 and 100 ms to modulate the cooling strength, which is further explained in

section 5.2.3. This results in temperature gradients in the afterglow similar to the conductive cooling approach.

By studying these two quenching approaches in our model, i.e., the enhanced thermal conductivity (or fast conductive cooling) and enhanced post-plasma mixing, we aim to provide insights into the reaction kinetics in post-plasma DRM processes. We note that these approaches are not directly comparable to experimental conditions, thus the trends and general findings resulting from the model are more relevant than the absolute values.

5.2.2 Chemistry

The species and reaction scheme used in this chapter are the same as in chapter 4. However, we demonstrated in chapter 4 that within the studied temperature range, the kinetics is dominated by thermal chemistry. Therefore, the DRM thermal kinetics suffices to describe the plasma region, hence electrons and ions and their respective reactions can be neglected, simplifying the simulations. In terms of applicability, this approach broadens the potential of our results, since the gained insights can be expanded beyond plasma-specific conditions. This amounts to a total of 40 species and 728 reactions. These species are listed in Table 5.1, and a list of the reactions with the corresponding rate coefficients and respective references is provided in the Appendix (Table D-1).

Table 5.1 Species included in the chemical kinetics set.

C
O, O_2, O_3
H, H_2
CO, CO_2
CH, CH_2, CH_3, CH_4, C_2H, C_2H_2, C_2H_3, C_2H_4, C_2H_5, C_2H_6
OH, H_2O, HO_2, H_2O_2
CH_2CH_2OH, CH_2CO, CH_2OH, CH_3CH_2O, CH_3CH_2OH, CH_3CHO, CH_3CHOH, CH_3CO, CH_3COOH, HCCO, CH_3O, CH_3OH, CH_3OO, CH_3OOH, COOH, HCHO, HCO, HCOOH

5.2.3 Equations in the model

The calculations are again performed using the ZDPlasKin[63] code, which solves the mass conservation equation as described in section 2.1. In this chapter the standard mass conservation expression is expanded with two other terms to include an additional source term to facilitate the mixing method of quenching and a term to correct for gas expansion. The former is used to introduce new species in the system upon mixing with unconverted gas (as explained in section 5.2.1) based on a rate (R_{mix}) and the fraction added of each species in the model ($x_{mix,s}$). These species are limited to CO_2 and CH_4, and their fractions are defined by the CO_2/CH_4 gas mixing ratio, i.e., 30/70, 50/50 and 70/30. The mixing rate (R_{mix}) is defined as a source term that represents species transport from the surrounding cold unconverted gas flow into the modelled plasma effluent volume (as shown in Figure 5.1(b)). This is given in Eq. 5.1, where n_{mix} is the total number density of gas that is added during the mixing process, τ_{mix} is the characteristic mixing time, t_{AG} is the time in the afterglow and α is the gas expansion factor. The dilution of 10% (i.e., flow of unconverted mixing gas being nine times higher than the plasma effluent) is used in all conditions, which results in $n_{mix} = 2.25 \times 10^{20}$ cm^{-3}, equal to nine times the initial number density at 293.15 K and 1 atm. Because the mixing is given by an exponential function, it only tends to zero asymptotically (never actually becoming zero). For reference, 99% of the mixing has occurred at 4.61, 46.1 and 461 ms in the afterglow for the characteristic times of 1, 10 and 100 ms. Since this is not the focus of our study, these values are arbitrarily chosen to modulate the mixing, and more important is the effect of the cooling rate on the kinetics.

$$R_{mix} = \alpha \frac{n_{mix}}{\tau_{mix}} e^{-\frac{t_{AG}}{\tau_{mix}}} \quad (5.1)$$

All simulations are conducted at a constant pressure of 1 atmosphere, and this is directly linked to the absolute number densities for each species in the model. There are two factors that influence the total number density in the system: temperature and chemical reactions. As chemical reactions take place, and the gas temperature changes, the gas needs to expand or contract accordingly if the number density changes, to maintain a constant pressure. To account for this reactive expansion and thermal expansion, the $R_{expansion}$ term is added to mass conservation equation. This correction parameter is given in Eq. 5.2, in which n_s

is the number density of the species s for which the mass balance is solved, n_j the number density of all species in the model j, $a^R_{j,i}$ and $a^L_{j,i}$ the coefficients of j in reaction i, R_i the rate of reaction i, R_{mix} the rate of gas mixing (when applicable), dT/dt the temperature change with respect to time, k_B the Boltzmann constant, P_0 the pressure (1 atm) and T the gas temperature.

$$\mathrm{R_{expansion}} = -\frac{\mathrm{n_s}}{\sum_j \mathrm{n_j}}\left(\sum_j \sum_{i=1}^{j}\left[\left(\mathrm{a^R_{j,i}} - \mathrm{a^L_{j,i}}\right)\cdot \mathrm{R_i}\right] + \mathrm{R_{mix}}\right) - \frac{\mathrm{n_s}}{\sum_j \mathrm{n_j}}\frac{\mathrm{dT}}{\mathrm{dt}}\frac{\mathrm{P_0}}{\mathrm{k_B T^2}} \qquad (5.2)$$

The gas expansion is still monitored throughout the simulation using Eq. 2.13, given in section 2.1.

While the temperature is kept constant in the plasma portion of the simulation, in the post-plasma portion the heat balance equation is solved to calculate the temperature self-consistently. ZDPlasKin normally considers a system at constant volume by using the ratio of specific heats to describe the isochoric heat capacity. However, in this model we consider a system at constant pressure, and therefore the isobaric heat capacity is included instead, thus accounting for volumetric expansion. This heat balance equation is given in Eq. 5.3, in which R_{gas} is the universal gas constant, $c_{p,mix}$ is the heat capacity of the mixture, dT/dt represents the change in temperature with respect to time, $Q_{reaction}$ is the heat gained or lost as a result of reactions, while $Q_{conductive}$ and Q_{mixing} represent the conductive heat losses and the heat losses resulting from post-plasma mixing, respectively.

$$\frac{\mathrm{c_{p,mix}(T)}}{\mathrm{R_{gas}}}\frac{\mathrm{dT}}{\mathrm{dt}} = \mathrm{Q_{reaction}} + \mathrm{Q_{conductive}} + \mathrm{Q_{mixing}} \qquad (5.3)$$

The isobaric heat capacity of the gas mixture $c_{p,mix}$ is given in Eq. 5.4. This is calculated as the sum of the heat capacity $c_{p,i}$ of the individual species i (obtained from McBride et al.[67] and Burcat et al.[68]) weighted to the number density n_i of the species i over the total number density n_{tot}.

$$\mathrm{c_{p,mix}(T)} = \sum_i \mathrm{c_{p,i}(T)}\frac{\mathrm{n_i}}{\mathrm{n_{tot}}} \qquad (5.4)$$

The heat exchange due to reactions ($Q_{reaction}$) is calculated using Eq. 5.5, with N_g the total number density of the heavy species in the simulation, R_i the reaction rate of reaction i and ε_i the reaction enthalpy of reaction i.

$$Q_{reaction} = -\frac{1}{N_g\, R_{gas}} \sum_i [\epsilon_i(T)\, R_i] \tag{5.5}$$

The temperature-dependent reaction enthalpy ε is calculated for reaction i using Eq. 5.6, in which $a^R_{s,i}$ and $a^L_{s,i}$ are the coefficients of species s in reaction i at the right and left side of the reaction, respectively, and H^f_s the temperature-dependent enthalpy of formation of species s (obtained from McBride et al.[67] and Burcat et al.[68]).

$$\epsilon_i(T) = \sum_s [a_s^R - a_s^L]\, H_s^f(T) \tag{5.6}$$

The conductive heat loss is calculated using Eq. 5.7, in which T is the gas temperature, T_0 is the reference wall temperature (293.15 K), k_B the Boltzmann constant, r the radius of the plasma (chosen as 1 cm), λ_{mix} the thermal conductivity of the gas mixture and c an additional factor to artificially increase the external cooling (varied between 1, 10 and 100). This additional c-factor is similar to the one used by Vermeiren et al.[54] The equation assumes a parabolic temperature profile with T being the radially average temperature and T_0 the temperature at the wall.[109] This provides a basic approximation of the temperature in the afterglow. The exact and precise value, however, is not the main focus of our study, as the most important effect here is the cooling rate on the kinetics. For the simulations that investigate post-plasma mixing, this conductive cooling term is set to zero. This is done to emulate a perfectly insulated system, which will isolate the effects of mixing by eliminating competition with conductive cooling. This also creates the optimal conditions for conversion of the freshly mixed gas.

$$Q_{conductive} = -c\, \frac{8\, \lambda_{mix}(T)}{N_g\, k_B\, r^2} [T - T_0] \tag{5.7}$$

The thermal conductivity, used in Eq. 5.7, is calculated as the mixture-averaged conductivity using the Mason Saxena equation (Eq. 5.8),[110] in which i and k are the species in the model, λ_i is their temperature-dependent thermal conductivity (obtained from the polynomials provided by McBride et al.[111]), x_i and x_k are their molar fractions and G_{ik} is a factor calculated using Eq. 5.9.

$$\lambda_{mix}(T) = \sum_i \lambda_i(T) \left[1 + \sum_k G_{ik} \frac{x_k}{x_i}\right]^{-1} \tag{5.8}$$

The factor G_{ik} for species *i* respective to species *k* is given in Eq. 5.9, in which *M* is the molar mass and μ the viscosity (obtained from the polynomials provided by McBride et al.[111]).

$$G_{ik} = \frac{1.065}{2\sqrt{2}}\left(1+\frac{M_i}{M_k}\right)^{-\frac{1}{2}}\left[1+\left(\frac{\mu_i M_k}{\mu_{kMi}}\right)^{\frac{1}{2}}\left(\frac{M_i}{M_k}\right)^{\frac{1}{4}}\right] \quad (5.9)$$

Finally, when applying post-plasma mixing, additional species are added to the afterglow without the removal of other species, which effectively increases the size of the system. Besides, since these new species do not have the same temperature, an amount of energy is required to equalise the temperature of these species to the rest of the system, which affects the heat balance. This is accounted for in the mixing heat term (Q_{mixing}) defined by Eq. 5.10, in which R_{mix} is the mixing rate, $x_{mix,s}$ is the fraction of species *s* in the mixed gas, H_s^f is the temperature-dependent enthalpy of species *s* (obtained from McBride et al.[67] and Burcat et al.[68]), *T* is the gas temperature and T_0 is the temperature of the mixing gas (293.15 K). In the first set of conditions, where enhanced conductive cooling is used to quench the afterglow, no mixing is used and therefore this Q_{mixing} term is zero.

$$Q_{mixing} = \frac{R_{mix}}{N_g R_{gas}} \sum_s x_{mix,s}\left[H_s^f(T_0) - H_s^f(T)\right] \quad (5.10)$$

The reactant conversion and product selectivity are calculated using the equations explained in section 2.2. However, to simplify the understandability and presentation of the results, we display only one value for each product, prioritising the base-atoms in the following order: first carbon (C), then hydrogen (H), and finally oxygen (O). In some cases, product selectivities for different base-atoms are shown in the same figure, thus it is important to keep in mind that the sum of the selectivity can be above 100%. Once again, the results will focus on the individual products and general trends, but not the total sum.

Another important evaluated metric is the energy cost of the process. To this end, we calculated energy cost of conversion, as the ratio between the energy input and the obtained conversion (as defined in Eq. 2.20 in section 2.2). In practice, the lower the energy cost, the more energy efficient the process is. In our case, because we set a constant plasma temperature, no energy input is

defined. Therefore, we utilise a minimum energy input (*MEI*), which is defined as the enthalpy difference between the initial state (CO_2 and CH_4 at 293.15 K) and the state in the plasma (at the fixed temperature). This represents the minimum possible energy required to obtain this state. It is calculated using Eq. 5.11, in which H_s^f is the formation enthalpy of species *s*, n_s is the species density, α is the gas expansion factor and N_A is Avogadro's constant. The formation enthalpy is determined from the thermodynamic data from McBride et al.[67] and Burcat et al.[68]. We use this MEI concept to define the minimum energy cost of conversion (*MEC*) (Eq. 5.12), which represents the minimum energy cost achievable for these conditions. χ_{tot} is the weighted average of the CO_2 and CH_4 conversion relative to their initial concentrations. Even though this cannot be compared to experimental data (as the calculations do not consider energy loss processes), this parameter allows us to compare between our different operating conditions and evaluate their potential.

$$\mathrm{MEI} = \frac{1}{\mathrm{N_A}} \sum_s \left[\mathrm{H_s^f(T)\ n_s\ \alpha - H_s^f(T_0)\ n_s^0} \right] \tag{5.11}$$

$$\mathrm{MEC} = \frac{\mathrm{MEI}}{\chi_{\mathrm{tot}}} \tag{5.12}$$

For the simulations with post-plasma mixing, we also calculate the additional conversion ($\chi_{additional}$), which represents the relative increase in conversion between the end of the plasma and the end of the post-plasma region. This is determined using Eq. 5.13, in which χ_{end} and χ_{plasma} are the conversion at the end of the simulation and at the end of the plasma region, respectively, and *D* is the dilution degree from mixing (10%, as explained above). Note that when the conversion does not change in the afterglow, $\chi_{additional}$ will be 0%; and in the case of recombination, $\chi_{additional}$ will be negative. Finally, this equation does not distinguish between further conversion of gas treated by the plasma or conversion of mixed gas in the hot afterglow.

$$\chi_{\mathrm{additional}} = \left(\frac{\chi_{\mathrm{end}} - \mathrm{D}\ \chi_{\mathrm{plasma}}}{\mathrm{D}\ \chi_{\mathrm{plasma}}} \right) 100\% \tag{5.13}$$

5.3 Results and discussion

5.3.1 Post-plasma cooling

We first analyse the results from simulations where conductive cooling is applied post-plasma. The extent of cooling (and thus quenching) is modulated by the factor c, as described in the previous section. For the three investigated CO_2/CH_4 ratios (30/70, 50/50, 70/30) and the three different c-factors (1, 10, 100), the resulting gas cooling can be observed in the temperature profiles shown in Figures C-1 – C-3 in the Appendix. In turn, this gives rise to cooling rates in the order of $10^5 – 10^8$ K/s (see panels b, d and f in the abovementioned figures) at the start of the afterglow. This magnitude of cooling rate has been proven to be beneficial for the conversion of CO_2,[59,60] which bodes well for this theoretical study of DRM.

The differences observed in the temperature profiles across the three CO_2/CH_4 ratios are ascribed to the lesser and greater proportion of CO_2 or CH_4 in the mixture, which affects the thermal conductivity and heat capacity (leading to changes in the temperature profiles). When slower cooling is considered (c-factor = 1), exothermic radical recombination occurs at high temperature, rendering undisturbed temperature profiles and resulting in a smooth decrease. In the case of faster conductive cooling (i.e., larger c-factors), these exothermic reactions are forced to occur at lower temperatures, deaccelerating the temperature drop at certain points in the afterglow. We do not focus on these absolute temperature profiles in the afterglow for comparing the kinetics, conversion or selectivity results, instead we focus on the overall trends, which provide a more qualitative comparison.

Note that for plasma temperatures near 2000 K, a steady state has not yet been fully reached within the simulated plasma residence time. Therefore, unreacted CO_2 and CH_4 and intermediate species from incomplete conversion can still be present.

5.3.1.1 50/50 ratio CO_2/CH_4

The results from simulations with 50/50 CO_2/CH_4 mixtures and c = 1 are shown in Figure 5.2. For low plasma temperatures, small fractions of C_2H_2 and H_2O are present, with the highest selectivity registered at 2000 K – 15 and 16%, respectively. At this temperature the conversion of CH_4 and CO_2 reaches 93 and 96%, respectively. At higher plasma temperatures, the simulations reach a steady state in the plasma and the selectivity towards C_2H_2 and H_2O is lower, with less than 1% above 2400 K. As the plasma temperature is increased, more H radicals are found in the plasma, with a selectivity of 66% at 4000 K. However, in the afterglow these radicals recombine exclusively to H_2, which occurs through a two-reaction pathway involving CO, according to our kinetics scheme. Our simulations show that the measured conversion for this mixture is preserved in the post-plasma region, with syngas ratio (i.e., H_2/CO) of 1, which corresponds to the theoretical product distribution from the DRM reaction.

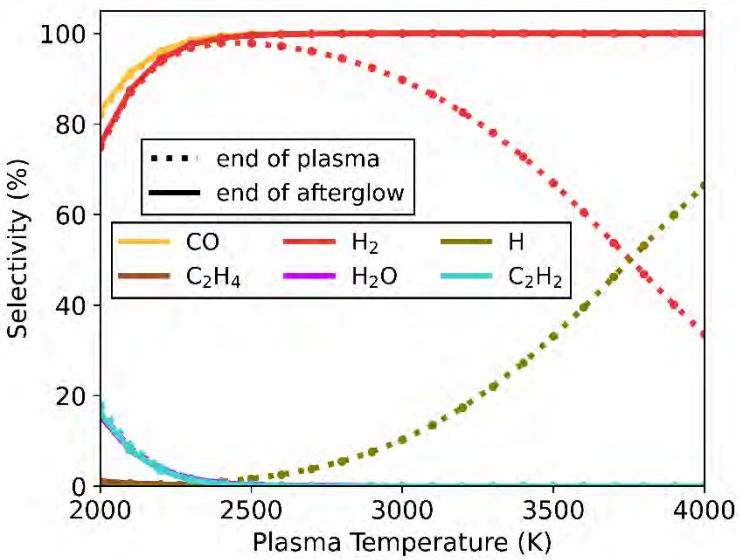

Figure 5.2 Selectivity of the main species (above 5%) as a function of the plasma temperature, for the 50/50 CO_2/CH_4 ratio and c-factor of 1 (no enhanced cooling), at the end of the plasma zone (point A in Figure 5.1; dotted lines) and end of the afterglow (point B in Figure 5.1; solid lines). The CO curves (both at the end of the plasma and afterglow) and H_2 curves at the end of the afterglow largely overlap. Also, the H_2O and C_2H_2 selectivity curves overlap both at the end of the plasma and afterglow. Near full conversion of CO_2 and CH_4 is observed under all conditions, at the end of the plasma, and maintained till the end of the afterglow.

When the cooling degree is increased by a ten- or hundred-fold (c = 10, 100), we observe the same behaviour (see Figure C-4), with only negligible alterations in minor product species (H_2O, C_2H_2 and CH_4). In summary, our model suggests that for a 50/50 CO_2/CH_4 mixture, quenching is not required to maintain the conversion reached in the afterglow, while the main products are consistently CO and H_2.

5.3.1.2 30/70 ratio CO_2/CH_4

For the gas mixture with an excess of CH_4 (30/70) (Figure 5.3), both CO_2 and CH_4 are fully dissociated in the plasma region, with conversion above 99% for both gases. This is the case for all plasma temperatures, except 2000 K where the conversion process is not fully completed, with CH_4 and CO_2 conversion reaching 97 and 98%, respectively. Also, at 2000 K a H_2O selectivity of 3.5% is observed (from the incomplete conversion process), though this falls below 0.4% for all higher temperatures. Similar to the previous mixture (50/50), the presence of H radicals at the end of the plasma is clearly identifiable. However, with an excess of CH_4, also C_2H radicals are formed with a maximum concentration of 20% at 4000 K (see Figure 5.3), and to a lesser extent, C radicals with a maximum of 5.5% at 4000 K (see Figure 5.3). The recombination of these radicals in the afterglow forms a large concentration of H_2 (85%) and C_2H_2 (37%) seen in Figure 5.3, and small fractions of C_2H_4 (2.5%), which is displayed in Figure C-5. Overall, the temperature in the plasma has a negligible effect on the final product distribution. It should also be noted that for this gas mixture the resulting syngas ratio is 2, which is ideal for further Fischer-Tropsch processing or methanol synthesis.[24]

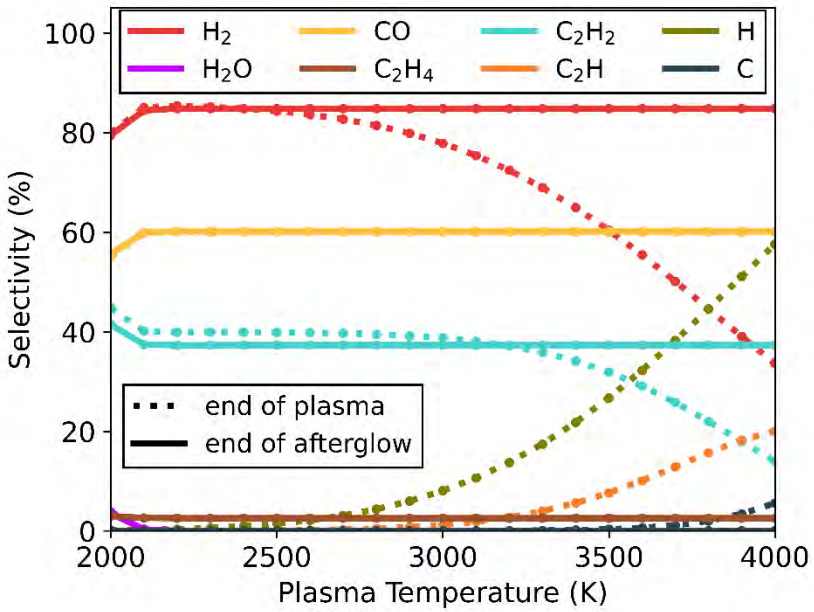

Figure 5.3 Selectivity of the main species (above 5%) as a function of the plasma temperature, for the 30/70 CO_2/CH_4 ratio and c-factor of 1 (no enhanced cooling), at the end of the plasma zone (point A in Figure 5.1; dotted lines) and end of the afterglow (point B in Figure 5.1; solid lines). Full conversion of CO_2 and CH_4 is observed under all conditions (except for 2000 K, as explained in the text).

When the cooling rate for this mixture is increased, the main products predicted by the model continue to be H_2, CO and C_2H_2, without any new products being formed (see Figure C-5). However, the C_2H_4 selectivity is reduced to 1.3% for both c-factors 10 and 100 (compared to 2.5% at c=1). In conclusion, for 30/70 CO_2/CH_4 mixtures, these results also reveal that quenching of the afterglow is not beneficial for conversion and has a negligible effect on the species distribution.

5.3.1.3 70/30 ratio CO_2/CH_4

Lastly, we consider a CO_2/CH_4 mixture at a 70/30 ratio (with excess CO_2). Akin to the previously discussed mixtures, the afterglow has a negligible effect in the lower end of the plasma temperature range (< 2300 K, see Figure 5.4). At these temperatures, the concentration of radical species is insignificant, resulting in unobservable effects from recombination reactions in the afterglow. On the other hand, more interesting effects are observed at higher plasma temperatures. Despite reaching a steady state, complete conversion of CO_2 in

the plasma zone is not achieved at a 70/30 CO_2/CH_4 ratio, which is an important factor to consider in this case. Also, various radical species (such as H, OH and O) are present at the end of the plasma zone, along with the primary products: H_2, CO and H_2O. As a result, we encounter more complex kinetics in this afterglow compared to the two previous mixtures.

In the lower range of plasma temperatures (< 3000 K), radical concentrations are rather low (only small fractions of H and OH are present). Despite radical recombination being limited, there is a notable shift in product distribution – with the formation of H_2 and CO_2 being favoured over that of CO and H_2O, through the occurrence of the water gas shift (WGS) reaction (R5.1). For instance, at 2500 K the conversion of CO_2 decreases from 84 to 75% due to WGS, while simultaneously the H_2 selectivity increases from 51 to 62% and the H_2O selectivity decreases from 47 to 38%.

$$CO + H_2O \rightarrow CO_2 + H_2 \qquad \text{(R5.1)}$$

For higher plasma temperatures, higher CO_2 conversions can be achieved in the plasma, up to 98% at 4000 K. This is accompanied by considerable formation of H, OH and O radicals, instead of H_2O and H_2. At this temperature, the low H_2O concentrations limit the occurrence of WGS. However, between 2300 and 4000 K, we observe approximately the same product distribution at the end of the afterglow, regardless of the initial plasma temperature. This indicates that different chemical pathways are triggered, with radical recombination reactions favouring CO_2 and H_2 over CO and H_2O. Also noteworthy is that all extra CO_2 conversion originating from the higher plasma temperatures is lost again in the afterglow upon gas cooling. This negates the supposed benefits of high plasma temperatures for CO_2 conversion, as in this case this effect alone is counteracted in the afterglow region. This is aligned with results for pure CO_2 conversion without quenching of Vermeiren et al.[54] where significant recombination is demonstrated to reduce the conversion to similar levels, regardless the gas temperature obtained in the plasma.

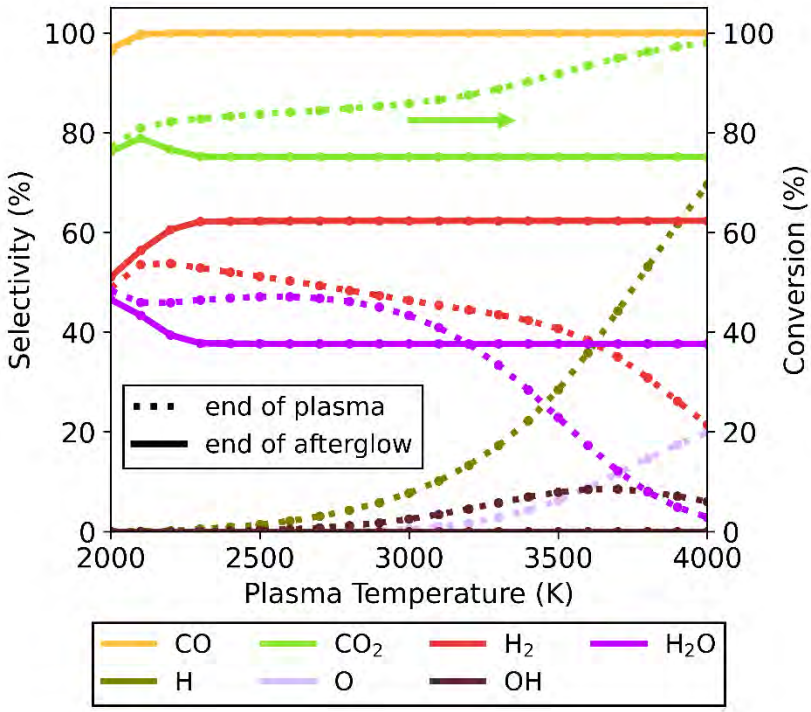

Figure 5.4 Selectivity of the main species (above 5%) as a function of the plasma temperature, for the 30/70 CO_2/CH_4 ratio and c-factor of 1 (no enhance cooling), at the end of the plasma zone (point A in Figure 5.1; dotted lines) and end of the afterglow (point B in Figure 5.1; solid lines). Full conversion of CH_4 is observed under all conditions, but not for CO_2, and therefore the CO_2 conversion is also plotted (right y-axis).

These recombination reactions and pathways are further explored by analysing the evolution of key species over time in the afterglow for the 4000 K plasma temperature case (Figure 5.5). Owing to the presence of O, OH and H radicals produced in the plasma for the 70/30 CO_2/CH_4 ratio, multiple recombination processes can occur. The two most straightforward processes are the O + CO reaction to CO_2 and H + H to H_2. Aside from these, a reaction of minor importance occurs between O and H to form OH, with the OH selectivity peaking at 8.5% around 1.8 ms. Subsequently, these OH radicals are important to further produce H_2O, which has a maximum selectivity of 46% at 9.9 ms. This is again reduced by ~ 9% due to the WGS reaction (R5.1), before it plateaus at 38%. The CO selectivity is constant at 100%, and as this is the only main C-containing species, the C-based selectivity remains constant. However, the absolute amount of CO does decrease (not shown in the figure) as the CO_2 conversion drops due to WGS.

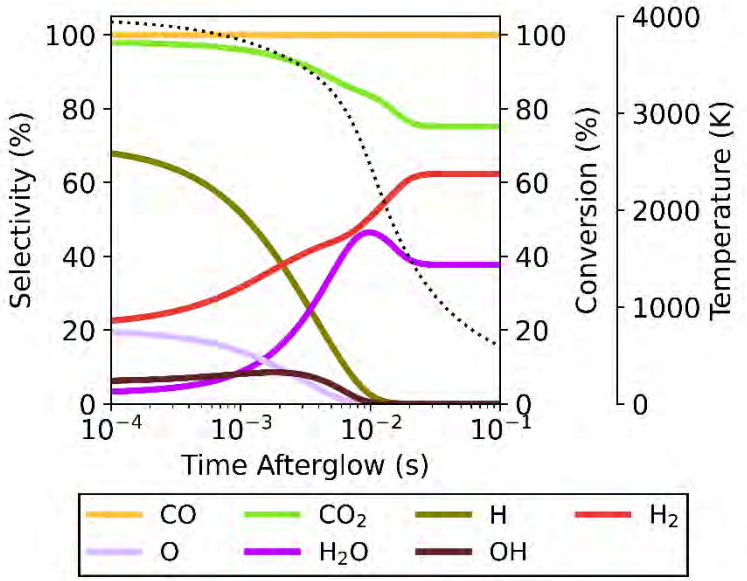

Figure 5.5 Evolution of the selectivity of the main species in the afterglow, starting from a plasma temperature of 4000 K for the 70/30 CO_2/CH_4 ratio and c-factor of 1. The evolution of the CO_2 conversion and of the gas temperature (dotted line) are also plotted, and shown on the right axis.

Upon increasing the cooling factor to 10 and 100, radical recombination towards CO_2 continues to be observed in the afterglow in all cases for this mixture (see Figure C-6). The lower end of the plasma temperature range (T < 2100 K) remains largely unaffected by the magnitude of cooling. This is also where the highest CO_2 conversions are attained upon cooling implementation (see Figure 5.6) – with 79, 80 and 81% conversion for c-factors of 1, 10 and 100, and at 2100, 2100 and 2200 K, respectively. These conversions lie slightly below those found in the plasma, signalling only a small amount of CO + O recombination. This can be attributed to the small amount of radicals present, combined with the relatively low plasma temperatures, which upon quenching in the afterglow will drastically limit recombination reactions. Therefore, at these temperatures the effect of the WGS reaction is small, which in turn preserves the higher CO_2 conversions obtained in the plasma (alongside the CO and H_2O products).

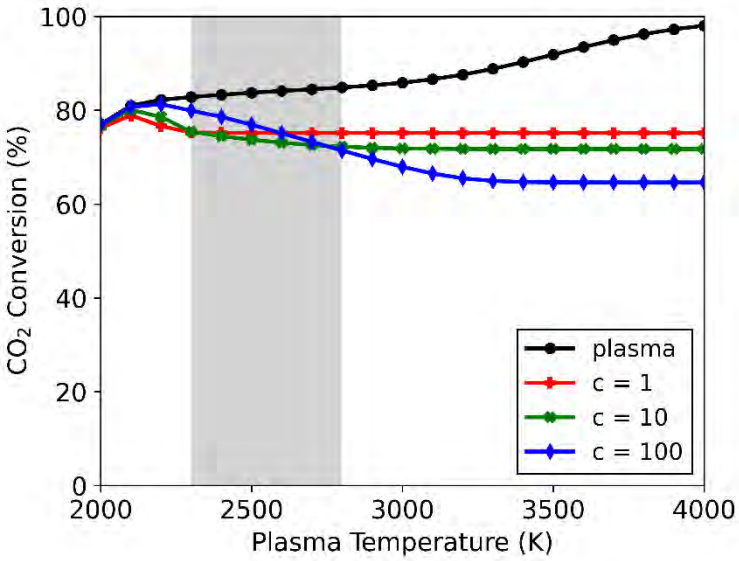

Figure 5.6 CO_2 conversion in the plasma and in the afterglow (for three different c-factors: 1, 10 and 100) as a function of the plasma temperature, for the CO_2/CH_4 ratio of 70/30. The range of plasma temperatures where the transition between the two afterglow effects occurs is indicated with a grey rectangle.

At plasma temperatures exceeding 2800 K, the opposite effect is observed. A shift in the afterglow reaction mechanisms promotes the formation of CO_2 and H_2 over that of H_2O. As shown in Figure 5.6, the CO_2 conversion drops with increasing cooling, only reaching 72 and 65% (for c-factors of 10 and 100, respectively) at a plasma temperature of 4000 K, compared to 75% for c = 1. Consequently, this allows for more H_2 to be produced – with a selectivity of 66 and 74% for c-factors of 10 and 100, respectively, compared to 62% for c = 1 (see Figure C-6). This enhanced H_2 formation, combined with lower CO_2 conversions, improves the syngas ratio, from 0.45 to 0.59. The product selectivities and chemical pathways are consistent with those observed at a c-factor of 1 (Figure 5.5). However, the faster decrease in temperature in the afterglow (at c = 10 and c = 100) forces radical recombination to occur predominantly at lower temperatures (see Figure C-7), which favours the recombination of O with CO to CO_2, over the reaction with H to OH, which subsequently forms H_2O. In the second stage (in the 1800 K to 1000 K range), where the WGS reaction applies, the H_2O concentration drops, whilst more CO_2 is formed. For plasma temperatures between 2300 and 2800 K, there is effectively a transition zone (see Figure 5.6), where these opposing effects (as

discussed above) compete. In this zone, the overall CO_2 conversion is dependent on the combined influences of cooling and plasma temperature.

In conclusion, the mixture with excess CO_2 (70/30) clearly exhibits distinct behaviour compared to the other mixtures (50/50 and 30/70), as the CO_2 conversion is shown to decrease drastically in the afterglow upon cooling. The drop in conversion is worsened by increasing the cooling rate to quench the hot gas in the afterglow. The lower CO_2 conversions coincide with changes in product distribution, with CO and H_2O being favoured at the lower end of the plasma temperature range, while CO_2 and H_2 are dominant at the higher end.

The latter effect is similar to the observations noted by Kwon et al.[37] from their quenching rod experiment. They also reported higher selectivity towards H_2 (instead of H_2O) alongside a lower CO_2 conversion. Even though they attributed this result to the suppression of RWGS (i.e., further limiting conversion of CO_2 with H_2 in the afterglow), our model suggests a different mechanism could be responsible for the observed shift. Their experiments presumably have plasma temperatures above 2800 K, where the CO_2 conversion decreases as a result of quenching the post-plasma region (as seen in Figure 5.6). Under these conditions, our calculations show significant radical recombination towards CO_2 regardless of quenching, however by accelerating the temperature drop (i.e., stronger cooling) different species are favoured, as illustrated in Figure 5.5 and Figure C-7. While we trust these modelled results, we are aware that other experimental factors (which cannot be captured by our 0D model) may influence the reaction kinetics.

Targeting this effect to synthesise higher H_2 concentrations (over H_2O) at higher plasma temperatures is certainly beneficial, as H_2O is an unwanted side product. A H_2-richer product mixture improves the overall value of the effluent. The ensuing lower CO_2 conversion is an unfortunate side effect, but not a major issue as the remaining CO_2 requires post-processing in a separation step in either case (as complete conversion cannot be achieved). However, a detailed process optimisation study and an in-depth economic analysis are necessary to determine the more cost-effective targets.

Another important consideration is the role of the afterglow in further converting CO_2 and CH_4 when a steady state is not achieved in the plasma (due

to a shorter residence time, for example). This is a plausible scenario for the lower end of the temperature range, in which case quenching of the hot gas can suppress further dissociations in the afterglow, also lowering the conversion.

5.3.1.4 Effect on energy cost

We calculated the difference in enthalpy between the initial system (at the start of the simulation, i.e., a mixture of CO_2 and CH_4 at 293.15 K) and at the end of the plasma zone (mixture of unconverted CO_2 and CH_4, as well as products and radical species at the plasma temperature). This enthalpy difference represents the minimum energy required to drive the system to the final chemical state (at the end of the plasma), which includes the chemical changes, as well as the temperature increase that occurs in the plasma. Note that this calculation does not include thermal losses; therefore, these results cannot be directly compared to experimental data. However, they give an indication of the minimum values of an idealised system. The energy input (see Figure 5.7) ranges between 7.5 and 37 kJ/L depending on gas mixture (CO_2/CH_4 ratio) and plasma temperatures, i.e., higher temperature values correspond to higher energy inputs, since more energy is required to reach higher temperatures, leading to greater dissociation into radicals.

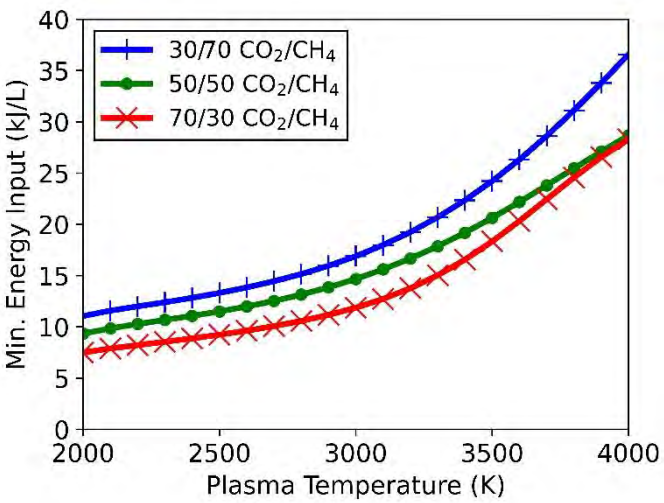

Figure 5.7 Minimum energy input required to achieve the final species distribution at the end of the plasma as a function of plasma temperature for the three different CO_2/CH_4 ratios (70/30, 50/50, 30/70).

From this minimum energy input, we calculated the minimum energy cost for CO_2 and CH_4 conversion, based on the total conversion reached at the end of the afterglow for the different cooling strengths (c-factors) (see Figure 5.8). This energy cost is approximately equal to the energy input, which is logical as the conversion of both CO_2 and CH_4 in the plasma zone is approximately 100% in all cases. The exception is the 70/30 CO_2/CH_4 ratio (where the CO_2 conversion is lower than 100%, as shown in Figure 5.6) which has a total conversion between 75 and 87% depending on plasma temperature and cooling strength. In this specific case, the minimum energy cost increases with the cooling strength, however, the overall difference is less than 3.4 kJ/L.

Our results clearly suggest it is best to maintain a plasma temperature as low as possible (while still being sufficiently high to fully convert the reactants) to obtain the lowest minimum energy costs. Also, an interesting analysis is the comparison of our results to the target energy cost of 4.27 eV/molecule (17.1 kJ/L), which was proposed by Snoeckx and Bogaerts[13] for competitiveness with existing technologies. This would suggest that plasma temperatures above 3000 K should be avoided, as such systems could not meet this energy target, while temperatures below 3000 K could meet this target.

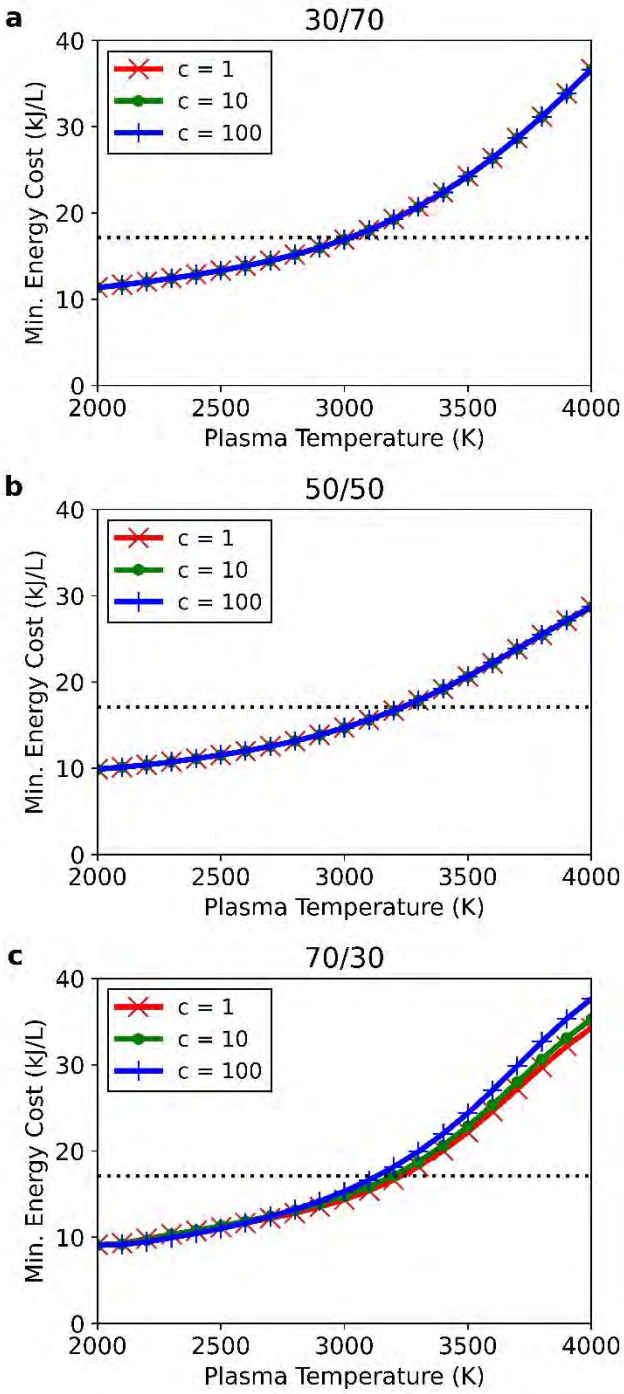

Figure 5.8 Minimum energy cost of conversion for c-factors of 1, 10 and 100 as a function of plasma temperature for CO_2/CH_4 ratios of 30/70 (a), 50/50 (b) and 70/30 (c). The horizontal dotted black line indicates the target energy cost value of 17.1 kJ/L (4.27 eV/molecule) proposed by Snoeckx and Bogaerts for plasma-based DRM to be competitive with existing technologies.[13]

However, it must be noted that these insights should be nuanced when comparing this idealised system to experimental conditions. Firstly, our calculations only consider the minimum energy input, and not the total energy input of the process or reactor setup, which in reality is higher since energy loss channels are present (such as heat loss from the plasma) and the efficiency of the power supply is not 100%. Under experimental conditions, these factors will contribute to a higher energy cost. Secondly, this approach only accounts for the gas that is interacting with the plasma, i.e., it assumes that 100% of the gas flow is treated by the plasma. However, experimentally, the power deposition in the reactor is localised and non-uniform, which results in only a fraction of the gas flow to be treated by the plasma. This also results in a temperature gradient across the plasma, of which parts can operate at more ideal conditions with respect to energy cost. On the other hand, this could also create regions with less ideal conditions, by either operating at a too high temperature (above 3000 K, as discussed above) or too low to achieve considerable conversion at the periphery of the plasma, and both effects would increase the energy cost again. Ultimately, the above experimental intricacies will probably lead to a higher energy input requirement, which according to our results will not be reflected in an enhanced overall conversion; on the contrary, it will probably result in an increased energy cost.

5.3.2 Post-plasma mixing

While for the above study of quenching via fast cooling, we assumed all gas passes through the plasma discharge, this is unlikely since experimental setups are not completely and homogeneously filled with plasma.[26,112,113] Instead, what is most likely is the existence of a peripheral colder zone surrounding the plasma, where reactant conversion is significantly lower. When these two zones remain separated, the results of the previous section apply specifically to the plasma and its effluent only, albeit the overall conversion will be significantly lower than those predicted by the model. On the other hand, this colder surrounding gas flow can mix with the plasma effluent in the hot afterglow, which will lead to additional thermal conversion, improving the overall output of the reactor. This effect is targeted in some reactors by introducing a nozzle to force these two distinct layers of gas to mix.[57–59]

In this section, we apply our model to explore this effect theoretically, by adding unconverted cold gas in the hot afterglow of a DRM plasma. To this end, we consider a perfectly insulated system, which makes gas mixing the only factor influencing the temperature. This represents the ideal and best-case scenario to target maximum additional conversion of the added gas. The plasma effluent is diluted to 10%, which corresponds to adding nine times the amount of initial gas during the afterglow region. As this dilution lowers the temperature to below 1000 K (at the end of the mixing stage), thermal reactions are effectively halted. We investigate three different mixing rates, modulated through the mixing time (τ_{mix}) set to 1, 10 or 100 ms. Further explanation regarding the implementation of the mixing is given in the model description (section 5.2.3). The plasma zone assumed before the mixing has been described in the previous section, with temperatures ranging from 2000 to 4000 K and three distinct CO_2/CH_4 ratios.

An overview of the temperatures and cooling rates throughout the afterglow for different gas mixtures, plasma temperatures and characteristic mixing times, is shown in Figures C-8 - C-10 in the Appendix, demonstrating that the highest cooling rates vary between 10^5 and 10^8 K/s, depending on the specific conditions. This is a similar range to that observed in the previous section.

5.3.2.1 Additional conversion

In this section we compare the conversions obtained in the post-plasma region for a characteristic mixing time of 10 ms (Figure 5.9), calculated as the relative increase in conversion between the end of the plasma and the final conversion at the end of the afterglow (accounting for the dilution effect as shown in Eq. 5.13).

For the plasma temperature of 2000 K, the overall change in the afterglow is negligible. As the plasma temperature is increased, the extra conversion for both CO_2 and CH_4 also rises, with a maximum additional conversion, relative to the conversion in the plasma, of 258% for CO_2 (at 4000 K and a 30/70 CO_2/CH_4 ratio) and 301% for CH_4 (at 4000 K and a 70/30 ratio). This increasing trend is logical, as the initial higher afterglow temperatures allow the newly added CO_2 and CH_4 to experience a longer residence time at elevated temperatures, in turn converting a larger fraction of the mixed gas. In all three gas mixtures, the

principal radical in the afterglow is H, which also plays a crucial role in the initial dissociation processes within the plasma. Expectedly, the additional conversion is driven upon reaction of these H radicals with CO_2 and CH_4 via reactions R5.2 and R5.3, respectively. This can also be correlated to the plasma temperature: as the temperature is raised, higher concentrations of H radicals are available in the afterglow, thereby increasing the conversion.

$$CO_2 + H \rightarrow CO + OH \quad \text{(R5.2)}$$

$$CH_4 + H \rightarrow CH_3 + H_2 \quad \text{(R5.3)}$$

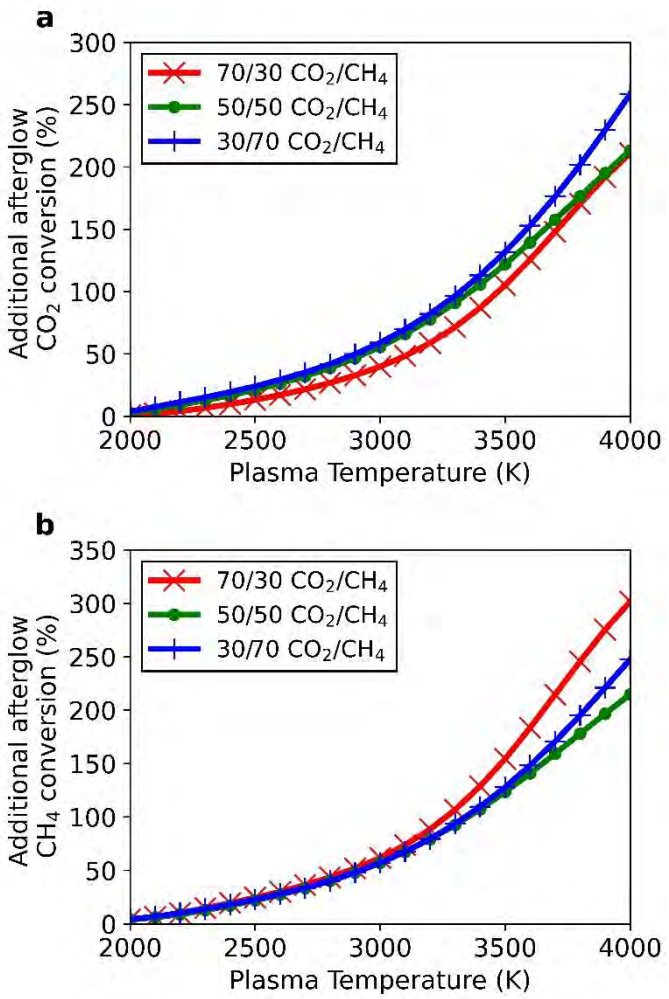

Figure 5.9 Additional CO_2 (a) and CH_4 (b) conversion obtained in the afterglow relative to the conversion obtained in the plasma, as a function of plasma temperature, for three different CO_2/CH_4 ratios (70/30, 50/50, 30/70) at τ_{mix} = 10 ms.

The most notable effect is seen for the 70/30 CO_2/CH_4 ratio, which also undergoes the greatest extent of recombination to CO_2, decreasing the overall conversion when quenching with fast cooling was considered (see Figure 5.6 in section 5.3.1.3). This detrimental effect is circumvented with the post-plasma mixing, by shifting the reaction pathways towards dissociation instead of recombination. The increase in CO_2 density acts to reduce the net recombination reaction of CO and O, and instead CO_2 conversion is further enhanced by reaction with H radicals (R5.2).

Regarding the other mixing rates (i.e., τ_{mix} = 1 and 100 ms), the same trends discussed above are observed, however the additional conversion is closely linked to the mixing rate. At the largest mixing rate (τ_{mix} = 1 ms), the system achieves the lowest additional conversion, with maximum values of 202 and 252% for CO_2 and CH_4, respectively, while at the lowest mixing rate (τ_{mix} = 100 ms), the additional conversion rises to 258 and 301% for CO_2 and CH_4, respectively. These results are again logical and are in line with the explanation given above for the effect of plasma temperature. With stronger mixing, the temperature experiences a faster decrease, thus the reactants have a shorter residence time at sufficiently high temperature to be converted.

These results demonstrate that post-plasma mixing can indeed be beneficial, especially upon coupling of high plasma temperatures with slow mixing. This mixing effect should be nuanced with respect to common experimental conditions, where perfect insulation described in our model is unattainable. As a consequence, heat loss to the reactor walls will increase the overall cooling in the afterglow, thereby diminishing the overall benefit. Nevertheless, the above results provide qualitative insights into how post-plasma mixing can improve the conversion.

5.3.2.2 Effect on product distribution

While an enhancement in conversion is certainly beneficial, changes in product distribution must also be considered. In this section, we present the selectivity of different products, noting that the selectivity was determined with respect to a base atom (as explained in section 2.2). Accordingly, carbon has been prioritised over hydrogen and hydrogen over oxygen.

For the stoichiometric CO_2/CH_4 ratio of 50/50, syngas is still the main component of the product stream (see Figure 5.10). The lowest selectivity is observed at 2000 K and the slowest mixing (τ_{mix} = 100 ms), with 74 and 81% for H_2 and CO, respectively. This can be ascribed to incomplete reactant conversion, forming H_2O and C_2H_2 with 16 and 17% selectivity, respectively. These results are similar to those discussed in the previous section, without post-plasma mixing. The selectivity of the latter species is reduced with increasing plasma temperature, as 'more complete' conversion can occur in the plasma. This increases the selectivity towards syngas, reaching a maximum at 2300 K – with H_2 and CO exhibiting 87 and 93% selectivity, respectively. This corresponds to a C_2H_2 and H_2O selectivity of 6.4 and 7.2%, which again increases for higher plasma temperatures, and this can be explained as follows. Since H_2O and C_2H_2 are intermediate species in the DRM process (occurring at temperatures between 1500 K and 2500 K) (see chapter 4), these species can be formed in the post-plasma region of higher plasma temperatures when mixing is implemented. As the plasma temperature drops in the afterglow (due to mixing), it reaches the above-mentioned optimum range for C_2H_2 and H_2O formation, forming these intermediates. However, as the mixing continues, the temperature decreases further, inhibiting the pathways that convert H_2O and C_2H_2 to H_2 and CO. Hence the former species remain as final products.

The effect of the mixing rate on the product distribution is directly related to the plasma temperature (Figure 5.10). For plasma temperatures below 2700 K, increasing the mixing rate favours the formation of syngas. The acceleration of the temperature drop simply results in less influence of the already small additional conversion to H_2O and C_2H_2. Above 3000 K, the opposite effect is seen, with the product selectivity shifting towards H_2O and C_2H_2 (in detriment of syngas). This can be ascribed to the exponential mixing rate, rendering a stronger temperature decrease in the early part of the afterglow (closer to the plasma zone) than that experienced in the later part. As such, the relative contribution of H_2O and C_2H_2 at the tail end of the temperature profile becomes larger, increasing their selectivity.

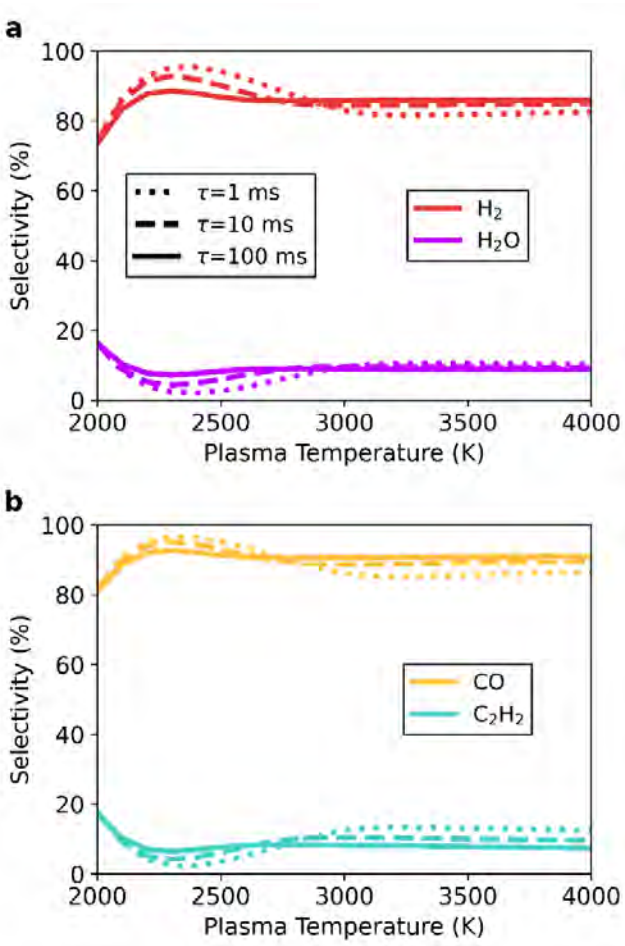

Figure 5.10 Selectivity towards the main product species as a function of the plasma temperature, for the 50/50 CO_2/CH_4 ratio, at the end of the afterglow at τ_{mix} = 1 (dotted line), 10 (dashed line) and 100 (solid line) ms. The hydrogen-based H_2 and H_2O selectivity is shown in panel a, and the carbon-based CO and C_2H_2 selectivity in panel b.

The formation of these products can be further explained by the species selectivity profiles throughout the afterglow in Figure 5.11 for the plasma temperature of 4000 K and τ_{mix} = 100 ms. In the early afterglow, the remaining H radicals (formed in the plasma zone) are consumed in the direct conversion of the added CO_2 and CH_4 to CO and H_2. As outlined above in reactions R5.2 and R5.3 (see section 5.3.2.1), these H radicals react with both CO_2 and CH_4 – being the main driving force for the additional conversion. This also causes a shift in the selectivity from H to H_2. The secondary product species (C_2H_2 and H_2O) only emerge later in the afterglow, coinciding with a drop in H_2 and CO selectivity. The selectivity towards H_2O remains below 1% until 15.9 ms in the afterglow,

and at this point the original flow is diluted to 43% and the temperature has dropped from 4000 K to 2675 K. As the temperature decreases further, the H_2O selectivity increases up to a maximum of 8.7%, while simultaneously C_2H_2 is also formed (with 7.4% selectivity). This is when steady state is reached, and the temperature has dropped to approximately 1550 K. Continuing dilution from this point onwards only decreases the gas temperature further, as all reactions are halted; and thus the H_2O and C_2H_2 species will be seen in the final products. For the lower plasma temperatures or faster mixing, the same processes occur, but to a smaller extent due to the reduced residence time in the afterglow, which allows for a lesser extent of chemical reactions.

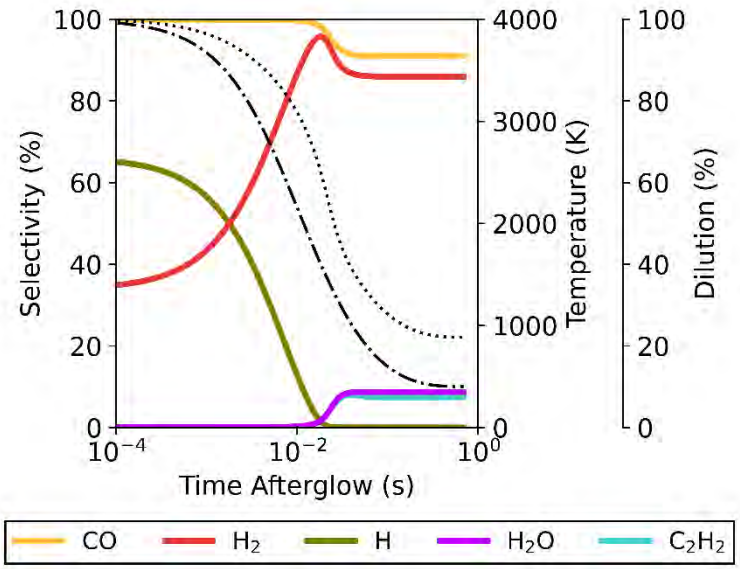

Figure 5.11 Temporal evolution of the main species' selectivity in the afterglow, starting from a plasma temperature of 4000 K, for the 50/50 CO_2/CH_4 ratio at τ_{mix} = 100 ms. The temperature (dotted line) and mixing progress (dash-dotted line) are also plotted, and shown on the right axes.

The work of Sun et al.[48] discusses mixing between the plasma effluent and a surrounding gas stream, using a reactor network model for a microwave plasma setup for DRM with a 1/1 ratio of CO_2/CH_4 and compared to their experimental findings. The difference in model description and higher plasma temperature (5000 – 5900 K) make a direct comparison difficult. However, they reported similar product distributions, mainly syngas production with smaller fractions of H_2O and C_2H_2.

The gas mixtures with different ratios exhibit the same overall effect, with the intermediate species (H_2O, C_2H_2 and C_2H_4) emerging as final products because the abrupt temperature drop in the afterglow slows down the kinetics, resulting in incomplete conversion pathways.

For the 30/70 CO_2/CH_4 ratio (see Figure 5.12), the products shift more towards C_2H_2 (at the expense of CO), because of the higher CH_4 fraction compared to the 50/50 ratio. H_2 is the main product with selectivity between 78 and 85%, while the selectivity of CO is slightly lower (between 54 and 59%), and C_2H_2 becomes a significant product – with selectivity between 32 and 44%. The remaining products are H_2O and C_2H_4, with selectivity ranging from 0.19 to 4.2% and from 0.70 to 10%, respectively.

Akin to the 50/50 CO_2/CH_4 ratio, the highest selectivity towards H_2 and CO is observed at 2100 K and faster mixing. However, at the 30/70 CO_2/CH_4 ratio, C_2H_4 formation does not follow this trend, since it exhibits the highest selectivity at the lowest mixing rate and highest plasma temperature. A transition from C_2H_2 to C_2H_4 can be noticed in the afterglow when the temperature drops from 1775 to 1230 K for a plasma temperature of 4000 K and τ_{mix} = 100 ms (see Figure C-11). This occurs through reactions with H_2 (R5.4) or with H and CH_4 with C_2H_3 as an intermediate (R5.5, R5.6).

$$C_2H_2 + H_2\ (+M) \rightarrow C_2H_4\ (+M) \quad \text{(R5.4)}$$

$$C_2H_2 + H\ (+M) \rightarrow C_2H_3\ (+M) \quad \text{(R5.5)}$$

$$C_2H_2 + CH_4 \rightarrow C_2H_3 + CH_3 \quad \text{(R5.6)}$$

This transition to C_2H_4 proceeds at lower temperatures than the other afterglow processes (e.g., the additional CO_2 and CH_4 conversion and the formation of C_2H_2 and H_2O), and therefore much later in the post-plasma region. This can be ascribed to a combination of longer residence times (due to slower mixing) with high C_2H_2 concentrations (achieved at high CH_4 ratios), driving the reactions towards C_2H_4. When optimising the process, C_2H_2 and especially C_2H_4 are worth considering, as they are also valuable products.

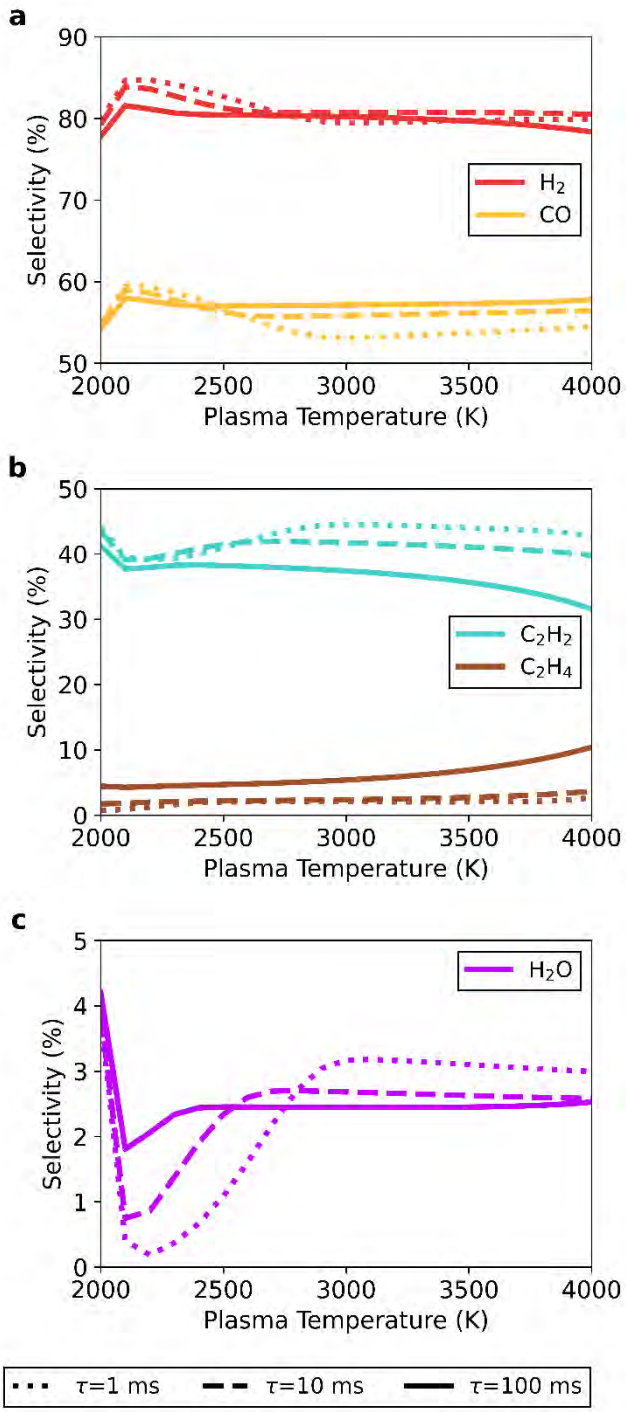

Figure 5.12 Selectivity at the end of the afterglow towards the main product species (H_2 and CO in panel a, C_2H_2 and C_2H_4 in panel b, and H_2O in panel c) as a function of the plasma temperature, at the 30/70 CO_2/CH_4 ratio and τ_{mix} = 1 (dotted line), 10 (dashed line) and 100 (solid line) ms.

Finally, we consider the 70/30 CO_2/CH_4 ratio (see Figure 5.13) whose selectivity trends are the least affected by the plasma temperature and mixing speed. The main product is CO, reaching a selectivity between 95 and 100%, while H_2 and H_2O range from 49 to 53% and from 45 to 48%, respectively.

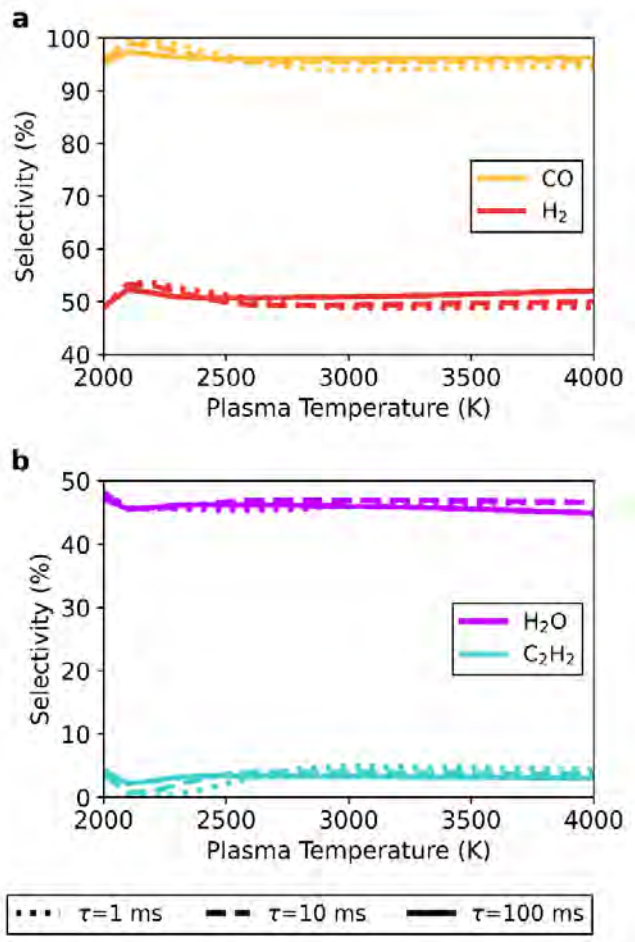

Figure 5.13 Selectivity at the end of the afterglow towards the main product species (H_2 and CO in panel a, and C_2H_2 and H_2O in panel b) as a function of the plasma temperature, at the 70/30 CO_2/CH_4 ratio and τ_{mix} = 1 (dotted line), 10 (dashed line) and 100 (solid line) ms.

In this mixture, C_2H_2 is formed as a minor product with selectivity between 0.063 and 4.9%. For the lower plasma temperatures (below 2500 K), increasing the mixing speed (accelerating the temperature drop) favours the formation of syngas. However, the product selectivity shifts towards H_2O and C_2H_2 above 2500 K. Again, this can be ascribed to the exponential mixing rate, which causes a stronger temperature decrease in the early afterglow and limits H_2 and CO

formation. In the later afterglow, the relative formation of H_2O and C_2H_2 is increased as the tail end of the temperature profile becomes larger, resulting in higher H_2O and C_2H_2 selectivity.

To summarise, the selectivity results for the three CO_2/CH_4 ratios suggest that post-plasma mixing does not yield drastic changes to the product distribution in DRM plasmas. Across the studied range of plasma temperatures and mixing rates, the selectivity of the products varies by less than 10%. The main products across all mixtures are still syngas (H_2 and CO), with also high fractions of H_2O or C_2H_2 being observed for mixtures with excess CO_2 or CH_4, respectively. Additionally, incomplete conversion of the freshly added gas in the afterglow leads to the formation of small quantities of C_2H_y and/or H_2O depending on the gas mixture (C_2H_2 and H_2O for the 50/50 ratio, C_2H_2 for excess CO_2, and H_2O and C_2H_4 for excess CH_4).

From these simulation results, we can postulate that the optimal condition to maximise selectivity towards syngas is using a plasma with a temperature of ~2200 K coupled to a fast mixing rate (τ_{mix} = 1 ms) of fresh gas in the afterglow. However, at this temperature, the model suggests the effect of quenching is negligible (see section 5.3.1), while also the additional CO_2 and CH_4 conversion because of mixing is predicted to be less than 1%, (as discussed in section 5.3.2.1). The temperature is too low under these conditions (~2200 K and τ_{mix} = 1 ms) to benefit from the heat recovery approach. On the other hand, at elevated temperatures our results suggest the additional conversion of the mixed gas is directly coupled to a partial selectivity shift from syngas towards secondary products (H_2O, C_2H_2 and C_2H_4). For these temperatures the slowest mixing (τ_{mix} = 100 ms) shows the highest syngas selectivity. Also worthy of note, despite this shift in the product distribution, the overall syngas yield is still significantly improved by the much higher additional conversion gained at elevated plasma temperatures, which can be industrially more interesting than a slightly higher syngas selectivity. Hence, overall we would recommend elevated plasma temperatures (4000 K or even higher) combined with slow mixing, to maximize the (additional) CO_2 and CH_4 conversion and reach a high syngas yield.

Considering the non-uniformity of the plasma, there will likely be deviations from an ideal condition. For instance, inevitable temperature gradients will also

alter the overall selectivity, as the conversion process occurs across a range of different temperatures. In addition, it is important to recognize the possible formation of solid carbon (and ensuing operational challenges) for gas mixtures with excess CH_4,[34–38] which can result from C_2H_2 and C_2H_4 formation, as these are important precursor species.[81,104,105] This phenomenon has not been accounted for in our study. Nonetheless, the aforementioned results offer qualitative insights into the influence of post-plasma mixing on product selectivities.

5.3.2.3 Effect on energy cost

In this section we discuss the implications of the post-plasma mixing on the minimum energy cost of conversion. In this case, only 10% of the total gas flow is treated directly with plasma (instead of the complete gas flow), hence the minimum energy input is ten times lower compared to the previous conditions in section 5.3.1.4 (Figure 5.7). The minimum energy input ranges between 0.75 and 3.7 kJ/L, increasing with targeted plasma temperature and depending on the CO_2/CH_4 ratio.

The calculated minimum energy cost of conversion for the three different gas mixtures is shown in Figure 5.14, with the optimal results achieved for the slowest mixing (τ_{mix} = 100 ms). The energy cost slightly decreases with rising plasma temperature for all gas mixtures. The 30/70 CO_2/CH_4 ratio has the highest overall minimum energy cost. It decreases from 10.9 to 10.4 kJ/L when the plasma temperature is raised from 2000 to 4000 K. The stoichiometric (50/50) and 70/30 ratios have slightly lower values which follow the same trend, decreasing from 9.6 to 9.1 kJ/L and from 8.8 to 8.4 kJ/L, respectively. Increasing the mixing rate tempers the additional conversion, increasing the minimum energy cost (see Figure 5.14). At 2000 K, the difference in energy cost between τ_{mix} = 100 ms and 1 ms is less than 0.5 kJ/L, for all mixtures, because the impact of mixing is very minor. For higher plasma temperatures the effects of mixing are more significant. Indeed, as the faster mixing limits the additional conversion, the minimum energy cost rises, which increases the energy cost disparity between τ_{mix} = 100 ms and 1 ms to 1.4 – 1.5 kJ/L at 2900 K, depending on the gas mixture.

These results contrast those discussed in section 5.3.1.4 (in the absence of mixing), where the energy cost always increased with plasma temperature. The higher temperatures reached in those results are unfavourable due to overheating of the gas, not having the option to be reused effectively. However, by applying mixing, additional conversion can be achieved, creating a use for this excess heat. For a plasma temperature of 4000 K, the mixing allows a reduction in energy cost of between 19 and 29 kJ/L (depending on the CO_2/CH_4 ratio) compared to the results discussed in section 5.3.1.4, which corresponds to a relative drop in energy cost of 68 to 78%. Note that when a high fraction of gas is treated in the reactor, one can argue that it is equally useful to increase the flow rate through the plasma to decrease the specific energy input, thereby operating at a lower temperature, which can still achieve the same conversion, instead of using post-plasma mixing. However, for reactors in which the treated gas fraction is limited, increasing the mixing with the surrounding unconverted gas does have a benefit on the overall performance (for the same energy input).

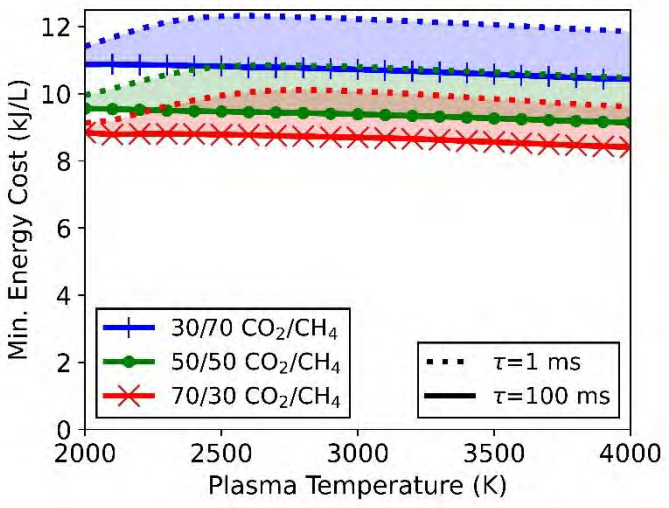

Figure 5.14 Minimum energy cost of conversion as a function of plasma temperature, for three different CO_2/CH_4 ratios (70/30, 50/50, 30/70). The range between the slowest mixing (τ_{mix} = 100 ms, solid lines) and the fastest mixing (τ_{mix} = 1 ms, dotted lines) is indicated.

The nuances previously discussed should also be applied here. As our results are derived from an idealised setup, the actual energy cost in the experiments will be higher because of various thermal losses and non-uniformity of the plasma. Also, our modelling approach considers a discrete temperature difference between the high temperature plasma zone and the cold

surrounding gas, which are eventually mixed in the post-plasma region. In plasma reactors, a temperature gradient will exist on the interface between the two zones. On the one hand, this will increase the overall energy input assuming the same plasma fraction and temperature. However, on the other hand, partial conversion can also occur in this gradient zone as temperatures will approach that of the plasma. Although uncaptured by the model, this effect will also influence the overall effect of mixing in the post-plasma region. This aspect of mixing is subject to further research, possibly using higher dimensional modelling that allows for more detailed studies of heat transport phenomena.

Moreover, since a certain degree of post-plasma mixing will already be present in experimental setups, this effect is intrinsically always in place. As a result, further enhancing this mixing will be less beneficial than predicted by our model (since the model assumes no prior mixing). This is supported by Sun et al.[48], who determined in their reactor network model for a DRM microwave setup that the heat loss to the wall is on a longer timescale than the mixing and subsequent reactions. Consequently, mixing plays an integral role in the reforming process within their system. These observations reinforce the importance of accounting for this effect.

Nevertheless, mixing the hot plasma effluent with cold new gas has the potential to greatly improve the system's energy efficiency. This strategy represents an effective implementation of a heat recovery system, reusing the energy applied in the plasma by harnessing the generated heat post-plasma, which would otherwise just be dissipated and lost. Furthermore, this strategy could also be combined with a complete heat recovery system, reusing the energy for preheating the plasma, so that the applied plasma power can effectively (all) be used for the chemical conversion. This can both be thought as an optimisation method, particularly well-suited for setups with localised, high temperature plasmas. Therefore, post-plasma mixing is an important consideration in the design and optimisation of reactors for DRM processes and further development of plasma technology in general.

5.4 Conclusion

In this chapter, we studied the post-plasma DRM kinetics for warm plasmas, in a wide range of plasma temperatures, and for different CO_2/CH_4 ratios and cooling/mixing methods.

Firstly, we evaluated enhanced conductive cooling to decrease the afterglow temperature, thereby gaining insights into the effect of heat quenching on the DRM chemistry. For gas mixtures with stoichiometric CO_2/CH_4 ratio (50/50), the model shows CO and H_2 are the main product species, and are negligibly affected by the quenching rate and initial plasma temperature. This also applies for mixtures with excess CH_4 (30/70), which besides syngas also form a significant amount of C_2H_2. For both mixtures, we obtained nearly 100% conversion in the plasma region, which is maintained throughout the afterglow. However, for mixtures with excess CO_2 (70/30), 100% conversion could only be achieved in the plasma region at temperatures of 4000 K. Our model indicates that the conversion diminishes throughout the afterglow, due to the occurrence of radical recombination towards CO_2, and due to the water gas shift reaction. Indeed, large fractions of H_2O are formed, which is the third main species (besides syngas) for this gas mixture. These reaction pathways are affected by increasing the quenching rate in the afterglow, influencing the kinetics to favour CO and H_2O formation below 2300 K, while H_2 and CO_2 are preferred with faster quenching above 2800 K. Though the latter effect seems detrimental in terms of conversion, in that case the syngas ratio (H_2/CO) is enhanced, while the concentration of unwanted H_2O is lowered, thus producing a more valuable effluent. Overall, this may be beneficial in terms of energy use towards production of these desired species. In general, however, we can conclude that heat quenching in the afterglow of DRM plasmas only has a significant impact for mixtures with excess CO_2.

In the second part of this study, we evaluated the effects of post-plasma mixing of the hot plasma effluent with a cold fresh mixture of CO_2 and CH_4. The aim of this approach is two-fold: the fresh gas not only provides cooling of the hot afterglow (quenching), but it can also further react to syngas, boosting the conversion. Essentially, this allows to recover energy from the plasma and effectively use it to improve the overall performance. For plasma temperatures

near 2000 K, the improvement was negligible however, with less than 5% increase in conversion relative to the plasma. Within our investigated conditions, this gain rises strongly with the plasma temperature, reaching a maximum additional conversion, relative to the conversion in the plasma, of 258 and 301% for CO_2 and CH_4, respectively, for plasma temperatures of 4000 K. The model also shows that stronger mixing limits the additional conversion, which is logical since the faster the mixing, the shorter the residence times at sufficiently elevated temperature (which is the main conversion driver).

Besides conversion, the post-plasma mixing also leads to minor changes in product selectivity, still favouring mainly H_2 and CO, while H_2O and C_2H_2 are also still important side-products in mixtures with excess CO_2 and CH_4, respectively. Additionally, upon the temperature drop, brought forth by the mixing, the additional conversion stops, and the reaction pathways are interrupted as revealed by the time-dependent analysis with our model. This consequently leads to the small selectivities towards intermediate species (H_2O and C_2H_4 for the 30/70 ratio, H_2O and C_2H_2 for the 50/50 ratio and C_2H_2 for the 70/30 ratio).

Furthermore, we also discussed the implications of these effects on the minimum energy cost of conversion. In the case of quenching the afterglow solely by conductive cooling, the energy cost strictly increases with plasma temperature. As the effects on conversion are less significant than the higher energy requirements (to obtain these higher plasma temperatures), our calculations suggest it is best to keep the plasma temperature as low as possible, around 2000 K (considering the assumption of a homogeneous plasma at a constant temperature). However, when uniform heating is not possible, post-plasma mixing can be used to harness the plasma heat to boost CO_2 and CH_4 conversion, considerably lowering the energy costs. Our model reveals that significant reductions in energy cost are theoretically possible (up to 78%). However, under experimental conditions, heat transfer from the gas to the reactor wall can reduce the overall benefit by limiting the additional conversion compared to our idealised conditions. Nonetheless, our study demonstrates that post-plasma mixing can add an opportunity to optimise DRM in warm plasmas.

6 Overall conclusions and future outlook

This thesis covers the chemical kinetics of plasma-based DRM for a wide range of operating conditions of warm plasmas. Different aspects of the conversion process are investigated through chemical kinetics modelling across the different chapters.

In chapter 3, we studied the influence of N_2 in the gas mixture on plasma-based DRM in a GAP, and we found it does not hinder the DRM process. Because N_2 is largely unconverted throughout the plasma process, the major product remains syngas (CO and H_2). The kinetic model further indicates C_2H_2 and H_2O are likely also formed, however in much smaller quantities. A fellow PhD student's modelling showed that adding N_2 to the mixture increases the temperature, and using this as input in the kinetics model translates to higher reaction rates. Because of this, a higher conversion can be reached. Experimentally the required power to maintain a constant current decreased with increasing N_2 content, thereby reducing the SEI. Hence, the higher absolute conversion combined with the lower SEI for increasing N_2 fractions is beneficial for the energy cost and energy efficiency. However, diluting the CO_2-CH_4 mixture reduces the effective CO_2 and CH_4 conversion. Altogether, the advantages of adding N_2 outweigh the dilution effect for a N_2 fraction of around 20%, improving the energy efficiency with respect to pure CO_2-CH_4 mixtures, by 21%, i.e., from 37 to 58%, and reducing the energy cost from 2.9 to 2.2 eV/molec (or from 11.5 to 8.7 kJ/L). This suggests that small fractions (~20%) of N_2 in the DRM gas stream do not impede the DRM process and may even enhance its energy efficiency slightly.

Furthermore, to gain a better understanding of the DRM chemistry over a wide range of warm plasma conditions, we performed an in-depth analysis of the DRM kinetics in chapter 4. An extensive range of gas temperatures, plasma power density, and most importantly, a full range of CO_2/CH_4 gas mixtures was considered. To our knowledge, this is one of the most complete analyses of this kinetics conduced, which revealed several key insights in the DRM conversion process.

Through a comparison of plasma conditions to thermal-only conversion, the influence of electron and ion reactions is illustrated. The electron impact reactions in the plasma conditions are shown to initiate the conversion process, by electron impact dissociation of CO_2. This creates O atoms, which further contribute to the CH_4 conversion mechanisms. Therefore, these electron processes are shown to be especially important in contributing to the conversion process below 2000 K. In contrast, purely thermal conversion, without the involvement of electrons, must rely on molecular collisions to dissociate CO_2 and CH_4. However, at this temperature range (below 2000 K), these collisions are much slower, making significant dissociation unachievable. The influence of the electron impact reactions is however only limited to this first step of the process, and the further reactions towards the product species are through radical reactions, which are the same regardless of the plasma or thermal conditions. Moreover, this also means the product distribution does not change. For temperatures above 2000 K, thermal reactions start to dominate the dissociation in the plasma conditions. Hence the kinetics of warm plasmas, which typically operate above 2000 K, can be described by thermal chemistry.

The use of different CO_2/CH_4 ratios showed changes in conversion and product distribution. For a 50/50 ratio of CO_2 to CH_4 (the stoichiometric ratio of the DRM reaction) the main products are CO and H_2, while at increasing gas temperature, more H radials are present (instead of H_2). The follow-up study on post-plasma quenching (chapter 5) showed these radicals recombine almost exclusively to H_2 in the afterglow region, resulting in the main output for this gas mixture being syngas. Mixtures with an excess of CH_4 largely exhibit the same behaviour, with full conversion achieved in the plasma, forming syngas, together with mainly C_2H_2 as a side product. The radicals present for higher temperatures are H and C_2H, which in the post-plasma region also recombine to mainly H_2 and C_2H_2. However, future research should also consider the formation of solid carbon particles for CH_4-rich mixtures, as this has been demonstrated to be experimentally significant[34–38], which is lacking from this study. Finally, mixtures with excess CO_2 have several drawbacks; they lead to higher H_2O production at the expense of H_2, and the CO_2 conversion in the plasma is thermodynamically limited, requiring extremely high temperatures (above 4000 K) for full

conversion. However, the follow-up study on post-plasma quenching (chapter 5) revealed this complete conversion cannot be sustained in the afterglow due to radical recombination into CO_2 and the water gas shift reaction, resulting in significant H_2O formation. The quenching rates influence these reactions, with slower quenching below 2300 K, favouring CO and H_2O formation, while faster quenching above 2800 K enhances the syngas ratio (H_2/CO) and reduces unwanted H_2O. Overall, this may be beneficial in terms of energy use towards production of these desired species.

While for CO_2 splitting quenching is almost essential to obtain significant and efficient conversion, for DRM this is not the case, as shown in chapter 5. This demonstrates the fundamental differences between the two processes and illustrates the need to develop and optimize distinct strategies tailored to each individual plasma process. Integrating this plasma process into a comprehensive techno-economic analysis can help identify the most promising optimization routes, considering factors such as gas separation and subsequent chemical processes (e.g. Fischer-Tropsch), such as performed for catalytic-DRM[114,115]. Research should explore various options for a comprehensive and fundamental understanding, but further optimizations must be context-driven to obtain a competitive plasma-based conversion process.

Another post-plasma effect that was considered in chapter 5, next to cooling (or enhanced quenching), is the mixing with cold gas. The conversion can be significantly improved, by up to 258 and 301%, relative to the conversion in the plasma, for CO_2 and CH_4, respectively, compared to when this effect is fully absent, in an idealised environment. The longer the high temperature can be maintained, the more conversion reactions can occur. However, this is limited by thermal losses or faster mixing, which increase the cooling rate. At a certain point the extra conversion stops, which also gives rise to small fractions of intermediate species, depending on the gas mixture. This mixing effect essentially allows to recover energy from the plasma and effectively use it to improve the overall performance, by increasing the conversion and thus lowering the energy costs.

Further research should focus on more advanced simulations of this mixing effect, which is needed to determine to what extent this effect is already present in existing setups. However, within this thesis, this was found to have

the most influence from a kinetic point of view. The nozzle designs and quenching rods are good examples of this.[37,55–58,61] While they are already being explored, these designs are mostly not optimized. This is where modelling can provide great value. As the DRM kinetics is reasonably well understood, computational research can shift more towards higher dimensional modelling, with a reduced chemistry set, based on the findings in this thesis. This can further bridge the gap between experiments and modelling and investigate the effects of physical processes (e.g. fluid dynamics, heat transfer) on the DRM kinetics and coupling between them.[116] Thus moving closer to a more comprehensive optimization of the plasma-based DRM process as an integrated and cohesive system.

This thesis provides broad general knowledge on the kinetics of DRM, to be further used in more advanced and more specific (higher dimensional) modelling work. This can help guide further reactor design and process optimisation of different warm plasma setups. Hopefully this can lead to practical large-scale applications of DRM in the future.

References

(1) Calvin, K.; Dasgupta, D.; Krinner, G.; Mukherji, A.; Thorne, P. W.; Trisos, C.; Romero, J.; Aldunce, P.; et al. *IPCC, 2023: Climate Change 2023: Synthesis Report. Contribution of Working Groups I, II and III to the Sixth Assessment Report of the Intergovernmental Panel on Climate Change.*; Geneva, Switzerland, 2023. https://doi.org/10.59327/IPCC/AR6-9789291691647.

(2) Olivier, J. G. J. *Trends in Global CO2 and Total Greenhouse Gas Emissions: 2021 Summary Report*; 2022; Vol. 5.

(3) Reisinger, A.; Meinshausen, M.; Manning, M.; Bodeker, G. Uncertainties of Global Warming Metrics: CO2 and CH4. *Geophys. Res. Lett.* **2010**, *37*. https://doi.org/10.1029/2010GL043803.

(4) Trenberth, K. E.; Dai, A.; van der Schrier, G.; Jones, P. D.; Barichivich, J.; Briffa, K. R.; Sheffield, J. Global Warming and Changes in Drought. *Nat. Clim. Chang.* **2014**, *4*, 17–22. https://doi.org/10.1038/nclimate2067.

(5) Parmesan, C.; Yohe, G. A Globally Coherent Fingerprint of Climate Change Impacts across Natural Systems. *Nature* **2003**, *421*, 37–42. https://doi.org/10.1038/nature01286.

(6) Clark, P. U.; Shakun, J. D.; Marcott, S. A.; Mix, A. C.; Eby, M.; Kulp, S.; Levermann, A.; Milne, G. A.; et al. Consequences of Twenty-First-Century Policy for Multi-Millennial Climate and Sea-Level Change. *Nat. Clim. Chang.* **2016**, *6*, 360–369. https://doi.org/10.1038/nclimate2923.

(7) Rummukainen, M. Changes in Climate and Weather Extremes in the 21st Century. *WIREs Clim. Chang.* **2012**, *3*, 115–129. https://doi.org/10.1002/wcc.160.

(8) Cuéllar-Franca, R. M.; Azapagic, A. Carbon Capture, Storage and Utilisation Technologies: A Critical Analysis and Comparison of Their Life Cycle Environmental Impacts. *J. CO2 Util.* **2015**, *9*, 82–102. https://doi.org/10.1016/j.jcou.2014.12.001.

(9) McDonough, W.; Braungart, M.; Anastas, P. T.; Zimmerman, J. B. Peer Reviewed: Applying the Principles of Green Engineering to Cradle-to-Cradle Design. *Environ. Sci. Technol.* **2003**, *37*, 434A-441A. https://doi.org/10.1021/es0326322.

(10) Wich, T.; Lueke, W.; Deerberg, G.; Oles, M. Carbon2Chem®-CCU as a Step

Toward a Circular Economy. *Front. Energy Res.* **2020**, *7*. https://doi.org/10.3389/fenrg.2019.00162.

(11) Bogaerts, A.; Neyts, E.; Gijbels, R.; van der Mullen, J. Gas Discharge Plasmas and Their Applications. *Spectrochim. Acta Part B At. Spectrosc.* **2002**, *57*, 609–658. https://doi.org/10.1016/S0584-8547(01)00406-2.

(12) Fridman, A. *Plasma Chemistry*; Cambridge University Press, 2008. https://doi.org/10.1017/CBO9780511546075.

(13) Snoeckx, R.; Bogaerts, A. Plasma Technology – a Novel Solution for CO2 Conversion? *Chem. Soc. Rev.* **2017**, *46*, 5805–5863. https://doi.org/10.1039/C6CS00066E.

(14) Schultz, T.; Nagel, M.; Engenhorst, T.; Nymand-Andersen, A.; Kunze, E.; Stenner, P.; Lang, J. E. Electrifying Chemistry: A Company Strategy Perspective. *Curr. Opin. Chem. Eng.* **2023**, *40*. https://doi.org/10.1016/j.coche.2023.100916.

(15) Kogelschatz, U. Dielectric-Barrier Discharges: Their History, Discharge Physics, and Industrial Applications. *Plasma Chem. Plasma Process.* **2003**, *23*, 1–46. https://doi.org/10.1023/A:1022470901385.

(16) Bogaerts, A.; Centi, G. Plasma Technology for CO2 Conversion: A Personal Perspective on Prospects and Gaps. *Front. Energy Res.* **2020**, *8*, 1–23. https://doi.org/10.3389/fenrg.2020.00111.

(17) Mallapragada, D. S.; Dvorkin, Y.; Modestino, M. A.; Esposito, D. V.; Smith, W. A.; Hodge, B.-M.; Harold, M. P.; Donnelly, V. M.; et al. Decarbonization of the Chemical Industry through Electrification: Barriers and Opportunities. *Joule* **2023**, *7*, 23–41. https://doi.org/10.1016/j.joule.2022.12.008.

(18) Fridman, A.; Chirokov, A.; Gutsol, A. Non-Thermal Atmospheric Pressure Discharges. *J. Phys. D. Appl. Phys.* **2005**, *38*, R1–R24. https://doi.org/10.1088/0022-3727/38/2/R01.

(19) Nunnally, T.; Gutsol, K.; Rabinovich, A.; Fridman, A.; Gutsol, A.; Kemoun, A. Dissociation of CO2 in a Low Current Gliding Arc Plasmatron. *J. Phys. D. Appl. Phys.* **2011**, *44*. https://doi.org/10.1088/0022-3727/44/27/274009.

(20) Gallagher, M. J.; Geiger, R.; Polevich, A.; Rabinovich, A.; Gutsol, A.; Fridman, A. On-Board Plasma-Assisted Conversion of Heavy Hydrocarbons into Synthesis Gas. *Fuel* **2010**, *89*, 1187–1192.

https://doi.org/10.1016/j.fuel.2009.11.039.

(21) Centi, G.; Quadrelli, E. A.; Perathoner, S. Catalysis for CO2 Conversion: A Key Technology for Rapid Introduction of Renewable Energy in the Value Chain of Chemical Industries. *Energy Environ. Sci.* **2013**, *6*, 1711. https://doi.org/10.1039/c3ee00056g.

(22) Pakhare, D.; Spivey, J. A Review of Dry (CO2) Reforming of Methane over Noble Metal Catalysts. *Chem. Soc. Rev.* **2014**, *43*, 7813–7837. https://doi.org/10.1039/C3CS60395D.

(23) Leckel, D. Diesel Production from Fischer−Tropsch: The Past, the Present, and New Concepts. *Energy & Fuels* **2009**, *23*, 2342–2358. https://doi.org/10.1021/ef900064c.

(24) Spath, P. L.; Dayton, D. C. *Preliminary Screening -- Technical and Economic Assessment of Synthesis Gas to Fuels and Chemicals with Emphasis on the Potential for Biomass-Derived Syngas*; Golden, CO (United States), 2003. https://doi.org/10.2172/15006100.

(25) Scapinello, M.; Martini, L. M.; Dilecce, G.; Tosi, P. Conversion of CH4/CO2 by a Nanosecond Repetitively Pulsed Discharge. *J. Phys. D. Appl. Phys.* **2016**, *49*. https://doi.org/10.1088/0022-3727/49/7/075602.

(26) Ramakers, M.; Trenchev, G.; Heijkers, S.; Wang, W.; Bogaerts, A. Gliding Arc Plasmatron: Providing an Alternative Method for Carbon Dioxide Conversion. *ChemSusChem* **2017**, *10*, 2642–2652. https://doi.org/10.1002/cssc.201700589.

(27) Zhang, H.; Wang, W.; Li, X.; Han, L.; Yan, M.; Zhong, Y.; Tu, X. Plasma Activation of Methane for Hydrogen Production in a N2 Rotating Gliding Arc Warm Plasma: A Chemical Kinetics Study. *Chem. Eng. J.* **2018**, *345*, 67–78. https://doi.org/10.1016/j.cej.2018.03.123.

(28) Trenchev, G.; Nikiforov, A.; Wang, W.; Kolev, S.; Bogaerts, A. Atmospheric Pressure Glow Discharge for CO2 Conversion: Model-Based Exploration of the Optimum Reactor Configuration. *Chem. Eng. J.* **2019**, *362*, 830–841. https://doi.org/10.1016/j.cej.2019.01.091.

(29) Martin-del-Campo, J.; Coulombe, S.; Kopyscinski, J. Influence of Operating Parameters on Plasma-Assisted Dry Reforming of Methane in a Rotating Gliding Arc Reactor. *Plasma Chem. Plasma Process.* **2020**, *40*, 857–881. https://doi.org/10.1007/s11090-020-10074-2.

(30) Devid, E.; Zhang, D.; Wang, D.; Ronda-Lloret, M.; Huang, Q.; Rothenberg,

G.; Shiju, N. R.; Kleyn, A. W. Dry Reforming of Methane under Mild Conditions Using Radio Frequency Plasma. *Energy Technol.* **2020**, *8*. https://doi.org/10.1002/ente.201900886.

(31) Cleiren, E.; Heijkers, S.; Ramakers, M.; Bogaerts, A. Dry Reforming of Methane in a Gliding Arc Plasmatron: Towards a Better Understanding of the Plasma Chemistry. *ChemSusChem* **2017**, *10*, 4025–4036. https://doi.org/10.1002/cssc.201701274.

(32) Slaets, J.; Aghaei, M.; Ceulemans, S.; Van Alphen, S.; Bogaerts, A. CO2 and CH4 Conversion in "Real" Gas Mixtures in a Gliding Arc Plasmatron: How Do N2 and O2 Affect the Performance? *Green Chem.* **2020**, *22*, 1366–1377. https://doi.org/10.1039/C9GC03743H.

(33) Wanten, B.; Maerivoet, S.; Vantomme, C.; Slaets, J.; Trenchev, G.; Bogaerts, A. Dry Reforming of Methane in an Atmospheric Pressure Glow Discharge: Confining the Plasma to Expand the Performance. *J. CO2 Util.* **2022**, *56*. https://doi.org/10.1016/j.jcou.2021.101869.

(34) Kelly, S.; Mercer, E.; De Meyer, R.; Ciocarlan, R.-G.; Bals, S.; Bogaerts, A. Microwave Plasma-Based Dry Reforming of Methane: Reaction Performance and Carbon Formation. *J. CO2 Util.* **2023**, *75*. https://doi.org/10.1016/j.jcou.2023.102564.

(35) Lu, N.; Sun, D.; Xia, Y.; Shang, K.; Wang, B.; Jiang, N.; Li, J.; Wu, Y. Dry Reforming of CH4–CO2 in AC Rotating Gliding Arc Discharge: Effect of Electrode Structure and Gas Parameters. *Int. J. Hydrogen Energy* **2018**, *43*, 13098–13109. https://doi.org/10.1016/j.ijhydene.2018.05.053.

(36) Raja, R. B.; Sarathi, R.; Vinu, R. Selective Production of Hydrogen and Solid Carbon via Methane Pyrolysis Using a Swirl-Induced Point–Plane Non-Thermal Plasma Reactor. *Energy & Fuels* **2022**, *36*, 826–836. https://doi.org/10.1021/acs.energyfuels.1c03383.

(37) Kwon, H.; Kim, T.; Song, S. Dry Reforming of Methane in a Rotating Gliding Arc Plasma: Improving Efficiency and Syngas Cost by Quenching Product Gas. *J. CO2 Util.* **2023**, *70*. https://doi.org/10.1016/j.jcou.2023.102448.

(38) Raja, R. B.; Halageri, A. C.; Sankar, R.; Sarathi, R.; Vinu, R. Dry Reforming of Methane Using a Swirl-Induced Plasma Discharge Reactor. *Energies* **2023**, *16*. https://doi.org/10.3390/en16041823.

(39) Khoja, A. H.; Tahir, M.; Amin, N. A. S. Dry Reforming of Methane Using

Different Dielectric Materials and DBD Plasma Reactor Configurations. *Energy Convers. Manag.* **2017**, *144*, 262–274. https://doi.org/10.1016/j.enconman.2017.04.057.

(40) Tu, X.; Whitehead, J. C. Plasma-Catalytic Dry Reforming of Methane in an Atmospheric Dielectric Barrier Discharge: Understanding the Synergistic Effect at Low Temperature. *Appl. Catal. B Environ.* **2012**, *125*, 439–448. https://doi.org/10.1016/j.apcatb.2012.06.006.

(41) Uytdenhouwen, Y.; Hereijgers, J.; Breugelmans, T.; Cool, P.; Bogaerts, A. How Gas Flow Design Can Influence the Performance of a DBD Plasma Reactor for Dry Reforming of Methane. *Chem. Eng. J.* **2021**, *405*. https://doi.org/10.1016/j.cej.2020.126618.

(42) Uytdenhouwen, Y.; Bal, K. M.; Neyts, E. C.; Meynen, V.; Cool, P.; Bogaerts, A. On the Kinetics and Equilibria of Plasma-Based Dry Reforming of Methane. *Chem. Eng. J.* **2021**, *405*, 126630. https://doi.org/10.1016/j.cej.2020.126630.

(43) Michielsen, I.; Uytdenhouwen, Y.; Bogaerts, A.; Meynen, V. Altering Conversion and Product Selectivity of Dry Reforming of Methane in a Dielectric Barrier Discharge by Changing the Dielectric Packing Material. *Catalysts* **2019**, *9*. https://doi.org/10.3390/catal9010051.

(44) Wang, A.; Harrhy, J. H.; Meng, S.; He, P.; Liu, L.; Song, H. Nonthermal Plasma-Catalytic Conversion of Biogas to Liquid Chemicals with Low Coke Formation. *Energy Convers. Manag.* **2019**, *191*, 93–101. https://doi.org/10.1016/j.enconman.2019.04.026.

(45) Li, D.; Rohani, V.; Fabry, F.; Parakkulam Ramaswamy, A.; Sennour, M.; Fulcheri, L. Direct Conversion of CO2 and CH4 into Liquid Chemicals by Plasma-Catalysis. *Appl. Catal. B Environ.* **2020**, *261*. https://doi.org/10.1016/j.apcatb.2019.118228.

(46) LI, D.; LI, X.; BAI, M.; TAO, X.; SHANG, S.; DAI, X.; YIN, Y. CO2 Reforming of CH4 by Atmospheric Pressure Glow Discharge Plasma: A High Conversion Ability☆. *Int. J. Hydrogen Energy* **2009**, *34*, 308–313. https://doi.org/10.1016/j.ijhydene.2008.10.053.

(47) Chun, S. M.; Hong, Y. C.; Choi, D. H. Reforming of Methane to Syngas in a Microwave Plasma Torch at Atmospheric Pressure. *J. CO2 Util.* **2017**, *19*, 221–229. https://doi.org/10.1016/j.jcou.2017.03.016.

(48) Sun, H.; Lee, J.; Bak, M. S. Experiments and Modeling of Atmospheric

Pressure Microwave Plasma Reforming of a Methane-Carbon Dioxide Mixture. *J. CO2 Util.* **2021**, *46*. https://doi.org/10.1016/j.jcou.2021.101464.

(49) Liu, J.; Xue, Z.; Zhang, Z.; Sun, B.; Zhu, A. Mechanism Study on Gliding Arc (GA) Plasma Reforming: Unraveling the Decisive Role of CH4/CO2 Ratio in the Dry Reforming Reaction. *Plasma Process. Polym.* **2023**, *20*. https://doi.org/10.1002/ppap.202200175.

(50) Wang, W.; Snoeckx, R.; Zhang, X.; Cha, M. S.; Bogaerts, A. Modeling Plasma-Based CO2 and CH4 Conversion in Mixtures with N2, O2, and H2O: The Bigger Plasma Chemistry Picture. *J. Phys. Chem. C* **2018**, *122*, 8704–8723. https://doi.org/10.1021/acs.jpcc.7b10619.

(51) Snoeckx, R.; Aerts, R.; Tu, X.; Bogaerts, A. Plasma-Based Dry Reforming: A Computational Study Ranging from the Nanoseconds to Seconds Time Scale. *J. Phys. Chem. C* **2013**, *117*, 4957–4970. https://doi.org/10.1021/jp311912b.

(52) De Bie, C.; van Dijk, J.; Bogaerts, A. The Dominant Pathways for the Conversion of Methane into Oxygenates and Syngas in an Atmospheric Pressure Dielectric Barrier Discharge. *J. Phys. Chem. C* **2015**, *119*, 22331–22350. https://doi.org/10.1021/acs.jpcc.5b06515.

(53) Wolf, A. J.; Peeters, F. J. J.; Groen, P. W. C.; Bongers, W. A.; van de Sanden, M. C. M. CO2 Conversion in Nonuniform Discharges: Disentangling Dissociation and Recombination Mechanisms. *J. Phys. Chem. C* **2020**, *124*, 16806–16819. https://doi.org/10.1021/acs.jpcc.0c03637.

(54) Vermeiren, V.; Bogaerts, A. Plasma-Based CO2 Conversion: To Quench or Not to Quench? *J. Phys. Chem. C* **2020**, *124*, 18401–18415. https://doi.org/10.1021/acs.jpcc.0c04257.

(55) Kim, H.; Song, S.; Tom, C. P.; Xie, F. Carbon Dioxide Conversion in an Atmospheric Pressure Microwave Plasma Reactor: Improving Efficiencies by Enhancing Afterglow Quenching. *J. CO2 Util.* **2020**, *37*, 240–247. https://doi.org/10.1016/j.jcou.2019.12.011.

(56) Mercer, E. R.; Van Alphen, S.; van Deursen, C. F. A. M.; Righart, T. W. H.; Bongers, W. A.; Snyders, R.; Bogaerts, A.; van de Sanden, M. C. M.; Peeters, F. J. J. Post-Plasma Quenching to Improve Conversion and Energy Efficiency in a CO2 Microwave Plasma. *Fuel* **2023**, *334*. https://doi.org/10.1016/j.fuel.2022.126734.

(57) Li, J.; Zhang, X.; Shen, J.; Ran, T.; Chen, P.; Yin, Y. Dissociation of CO2 by Thermal Plasma with Contracting Nozzle Quenching. *J. CO2 Util.* **2017**, *21*, 72–76. https://doi.org/10.1016/j.jcou.2017.04.003.

(58) Hecimovic, A.; D'Isa, F. A.; Carbone, E.; Fantz, U. Enhancement of CO2 Conversion in Microwave Plasmas Using a Nozzle in the Effluent. *J. CO2 Util.* **2022**, *57*. https://doi.org/10.1016/j.jcou.2021.101870.

(59) Yang, T.; Shen, J.; Ran, T.; Li, J.; Chen, P.; Yin, Y. Understanding CO2 Decomposition by Thermal Plasma with Supersonic Expansion Quench. *Plasma Sci. Technol.* **2018**, *20*. https://doi.org/10.1088/2058-6272/aaa969.

(60) Van Alphen, S.; Hecimovic, A.; Kiefer, C. K.; Fantz, U.; Snyders, R.; Bogaerts, A. Modelling Post-Plasma Quenching Nozzles for Improving the Performance of CO2 Microwave Plasmas. *Chem. Eng. J.* **2023**, *462*. https://doi.org/10.1016/j.cej.2023.142217.

(61) Wang, K.; Ceulemans, S.; Zhang, H.; Tsonev, I.; Zhang, Y.; Long, Y.; Fang, M.; Li, X.; et al. Inhibiting Recombination to Improve the Performance of Plasma-Based CO2 Conversion. *Chem. Eng. J.* **2024**, *481*. https://doi.org/10.1016/j.cej.2024.148684.

(62) Hyun Cho, C.; Kim, J. H.; Yang, J. K.; Park, I. S.; Choi, Y.-S.; Kang, I. J. Dry Reforming Process Using Microwave Plasma Generator with High Carbon Dioxide Conversion Efficiency for Syngas Production. *Fuel* **2024**, *361*. https://doi.org/10.1016/j.fuel.2023.130707.

(63) Pancheshnyi, S.; Eismann, B.; Hagelaar, G. J. M.; Pitchford, L. C. *Computer code ZDPlasKin, http://www.zdplaskin.laplace.univ-tlse.fr (University of Toulouse, LAPLACE, CNRS-UPSINP, Toulouse, France, 2008)*. http://www.zdplaskin.laplace.univ-tlse.fr.

(64) Hagelaar, G. J. M.; Pitchford, L. C. Solving the Boltzmann Equation to Obtain Electron Transport Coefficients and Rate Coefficients for Fluid Models. *Plasma Sources Sci. Technol.* **2005**, *14*, 722–733. https://doi.org/10.1088/0963-0252/14/4/011.

(65) Baulch, D. L.; Bowman, C. T.; Cobos, C. J.; Cox, R. A.; Just, T.; Kerr, J. A.; Pilling, M. J.; Stocker, D.; et al. Evaluated Kinetic Data for Combustion Modeling: Supplement II. *J. Phys. Chem. Ref. Data* **2005**, *34*, 757–1397. https://doi.org/10.1063/1.1748524.

(66) Gilbert, R. G.; Luther, K.; Troe, J. Theory of Thermal Unimolecular

Reactions in the Fall-off Range. II. Weak Collision Rate Constants. *Berichte der Bunsengesellschaft für Phys. Chemie* **1983**, *87*, 169–177. https://doi.org/10.1002/bbpc.19830870218.

(67) McBride, B. J.; Zehe, M. J.; Gordon, S. *NASA Glenn Coefficients for Calculating Thermodynamic Properties of Individual Species: National Aeronautics and Space Administration*; 2002. https://ntrs.nasa.gov/search.jsp?R=20020085330 2020-05-03T03:42:36+00:00Z.

(68) Burcat, A.; Ruscic, B.; Chemistry. *Third Millenium Ideal Gas and Condensed Phase Thermochemical Database for Combustion (with Update from Active Thermochemical Tables).*; Argonne, IL, 2005. https://doi.org/10.2172/925269.

(69) Turner, M. M. Uncertainty and Error in Complex Plasma Chemistry Models. *Plasma Sources Sci. Technol.* **2015**, *24*. https://doi.org/10.1088/0963-0252/24/3/035027.

(70) Turner, M. M. Uncertainty and Sensitivity Analysis in Complex Plasma Chemistry Models. *Plasma Sources Sci. Technol.* **2016**, *25*. https://doi.org/10.1088/0963-0252/25/1/015003.

(71) Berthelot, A.; Bogaerts, A. Modeling of CO2 Plasma: Effect of Uncertainties in the Plasma Chemistry. *Plasma Sources Sci. Technol.* **2017**, *26*. https://doi.org/10.1088/1361-6595/aa8ffb.

(72) Wang, W.; Berthelot, A.; Zhang, Q.; Bogaerts, A. Modelling of Plasma-Based Dry Reforming: How Do Uncertainties in the Input Data Affect the Calculation Results? *J. Phys. D. Appl. Phys.* **2018**, *51*. https://doi.org/10.1088/1361-6463/aab97a.

(73) Cleiren, E.; Heijkers, S.; Ramakers, M.; Bogaerts, A. Dry Reforming of Methane in a Gliding Arc Plasmatron: Towards a Better Understanding of the Plasma Chemistry. *ChemSusChem* **2017**, *10*, 3864–3864. https://doi.org/10.1002/cssc.201701891.

(74) Wanten, B.; Vertongen, R.; De Meyer, R.; Bogaerts, A. Plasma-Based CO2 Conversion: How to Correctly Analyze the Performance? *J. Energy Chem.* **2023**, *86*, 180–196. https://doi.org/10.1016/j.jechem.2023.07.005.

(75) Snoeckx, R.; Heijkers, S.; Van Wesenbeeck, K.; Lenaerts, S.; Bogaerts, A. CO2 Conversion in a Dielectric Barrier Discharge Plasma: N2 in the Mix as a Helping Hand or Problematic Impurity? *Energy Environ. Sci.* **2016**, *9*,

999–1011. https://doi.org/10.1039/c5ee03304g.

(76) Heijkers, S.; Snoeckx, R.; Kozák, T.; Silva, T.; Godfroid, T.; Britun, N.; Snyders, R.; Bogaerts, A. CO2 Conversion in a Microwave Plasma Reactor in the Presence of N2: Elucidating the Role of Vibrational Levels. *J. Phys. Chem. C* **2015**, *119*, 12815–12828. https://doi.org/10.1021/acs.jpcc.5b01466.

(77) Ramakers, M.; Heijkers, S.; Tytgat, T.; Lenaerts, S.; Bogaerts, A. Combining CO2 Conversion and N2 Fixation in a Gliding Arc Plasmatron. *J. CO2 Util.* **2019**, *33*, 121–130. https://doi.org/10.1016/j.jcou.2019.05.015.

(78) Snoeckx, R.; Van Wesenbeeck, K.; Lenaerts, S.; Cha, M. S.; Bogaerts, A. Suppressing the Formation of NOX and N2O in CO2/N2 Dielectric Barrier Discharge Plasma by Adding CH4: Scavenger Chemistry at Work. *Sustain. Energy Fuels* **2019**, *3*, 1388–1395. https://doi.org/10.1039/c8se00584b.

(79) Yeo, Z. Y.; Chew, T. L.; Zhu, P. W.; Mohamed, A. R.; Chai, S. P. Conventional Processes and Membrane Technology for Carbon Dioxide Removal from Natural Gas: A Review. *J. Nat. Gas Chem.* **2012**, *21*, 282–298. https://doi.org/10.1016/S1003-9953(11)60366-6.

(80) Aresta, M.; Dibenedetto, A.; Angelini, A. Catalysis for the Valorization of Exhaust Carbon: From CO2 to Chemicals, Materials, and Fuels. Technological Use of CO2. *Chem. Rev.* **2014**, *114*, 1709–1742. https://doi.org/10.1021/cr4002758.

(81) Van Alphen, S.; Jardali, F.; Creel, J.; Trenchev, G.; Snyders, R.; Bogaerts, A. Sustainable Gas Conversion by Gliding Arc Plasmas: A New Modelling Approach for Reactor Design Improvement. *Sustain. Energy Fuels* **2021**, *5*, 1786–1800. https://doi.org/10.1039/D0SE01782E.

(82) Pinhão, N.; Moura, A.; Branco, J. B.; Neves, J. Influence of Gas Expansion on Process Parameters in Non-Thermal Plasma Plug-Flow Reactors: A Study Applied to Dry Reforming of Methane. *Int. J. Hydrogen Energy* **2016**, *41*, 9245–9255. https://doi.org/10.1016/j.ijhydene.2016.04.148.

(83) Snoeckx, R.; Setareh, M.; Aerts, R.; Simon, P.; Maghari, A.; Bogaerts, A. Influence of N2 Concentration in a CH4/N2 Dielectric Barrier Discharge Used for CH4 Conversion into H2. *Int. J. Hydrogen Energy* **2013**, *38*, 16098–16120. https://doi.org/10.1016/j.ijhydene.2013.09.136.

(84) Kozàk, T.; Bogaerts, A. Splitting of CO2 by Vibrational Excitation in Non-

Equilibrium Plasmas: A Reaction Kinetics Model. *Plasma Sources Sci. Technol.* **2014**, *23*. https://doi.org/10.1088/0963-0252/23/4/045004.

(85) Jardali, F.; Van Alphen, S.; Creel, J.; Ahmadi Eshtehardi, H.; Axelsson, M.; Ingels, R.; Snyders, R.; Bogaerts, A. NO x Production in a Rotating Gliding Arc Plasma: Potential Avenue for Sustainable Nitrogen Fixation. *Green Chem.* **2021**, *23*, 1748–1757. https://doi.org/10.1039/D0GC03521A.

(86) Snoeckx, R.; Ozkan, A.; Reniers, F.; Bogaerts, A. The Quest for Value-Added Products from Carbon Dioxide and Water in a Dielectric Barrier Discharge: A Chemical Kinetics Study. *ChemSusChem* **2017**, *10*, 409–424. https://doi.org/10.1002/cssc.201601234.

(87) De Bie, C.; Verheyde, B.; Martens, T.; van Dijk, J.; Paulussen, S.; Bogaerts, A. Fluid Modeling of the Conversion of Methane into Higher Hydrocarbons in an Atmospheric Pressure Dielectric Barrier Discharge. *Plasma Process. Polym.* **2011**, *8*, 1033–1058. https://doi.org/10.1002/ppap.201100027.

(88) Aerts, R.; Snoeckx, R.; Bogaerts, A. In-Situ Chemical Trapping of Oxygen in the Splitting of Carbon Dioxide by Plasma. *Plasma Process. Polym.* **2014**, *11*, 985–992. https://doi.org/10.1002/ppap.201400091.

(89) van de Steeg, A. W.; Butterworth, T.; van den Bekerom, D. C. M.; Silva, A. F.; van de Sanden, M. C. M.; van Rooij, G. J. Plasma Activation of N2, CH4 and CO2: An Assessment of the Vibrational Non-Equilibrium Time Window. *Plasma Sources Sci. Technol.* **2020**, *29*. https://doi.org/10.1088/1361-6595/abbae4.

(90) Park, C.; Howe, J. T.; Jaffe, R. L.; Candler, G. V. Review of Chemical-Kinetic Problems of Future NASA Missions. II - Mars Entries. *J. Thermophys. Heat Transf.* **1994**, *8*, 9–23. https://doi.org/10.2514/3.496.

(91) Vialetto, L.; van de Steeg, A. W.; Viegas, P.; Longo, S.; van Rooij, G. J.; van de Sanden, M. C. M.; van Dijk, J.; Diomede, P. Charged Particle Kinetics and Gas Heating in CO2 Microwave Plasma Contraction: Comparisons of Simulations and Experiments. *Plasma Sources Sci. Technol.* **2022**, *31*. https://doi.org/10.1088/1361-6595/ac56c5.

(92) Kossyi, I. A.; Kostinsky, A. Y.; Matveyev, A. A.; Silakov, V. P. Kinetic Scheme of the Non-Equilibrium Discharge in Nitrogen-Oxygen Mixtures. *Plasma Sources Sci. Technol.* **1992**, *1*, 207–220. https://doi.org/10.1088/0963-0252/1/3/011.

(93) Dinh, D. K.; Trenchev, G.; Lee, D. H.; Bogaerts, A. Arc Plasma Reactor Modification for Enhancing Performance of Dry Reforming of Methane. *J. CO2 Util.* **2020**, *42*. https://doi.org/10.1016/j.jcou.2020.101352.

(94) Green, K. M.; Borras, M. C.; Woskov, P. P.; Flores, G. J.; Hadidi, K.; Thomas, P. Electronic Excitation Temperature Profiles in an Air Microwave Plasma Torch. *IEEE Trans. Plasma Sci.* **2001**, *29*, 399–406. https://doi.org/10.1109/27.922753.

(95) Heijkers, S.; Aghaei, M.; Bogaerts, A. Plasma-Based CH4 Conversion into Higher Hydrocarbons and H2: Modeling to Reveal the Reaction Mechanisms of Different Plasma Sources. *J. Phys. Chem. C* **2020**, *124*, 7016–7030. https://doi.org/10.1021/acs.jpcc.0c00082.

(96) Liu, J.-L.; Park, H.-W.; Chung, W.-J.; Ahn, W.-S.; Park, D.-W. Simulated Biogas Oxidative Reforming in AC-Pulsed Gliding Arc Discharge. *Chem. Eng. J.* **2016**, *285*, 243–251. https://doi.org/10.1016/j.cej.2015.09.100.

(97) Moon, S. Y.; Choe, W. Parametric Study of Atmospheric Pressure Microwave-Induced Ar/O2 Plasmas and the Ambient Air Effect on the Plasma. *Phys. Plasmas* **2006**, *13*. https://doi.org/10.1063/1.2357722.

(98) Dahl, J. K.; Weimer, A. W.; Lewandowski, A.; Bingham, C.; Bruetsch, F.; Steinfeld, A. Dry Reforming of Methane Using a Solar-Thermal Aerosol Flow Reactor. *Ind. Eng. Chem. Res.* **2004**, *43*, 5489–5495. https://doi.org/10.1021/ie030307h.

(99) Biondo, O.; Hughes, A.; van de Steeg, A.; Maerivoet, S.; Loenders, B.; van Rooij, G.; Bogaerts, A. Power Concentration Determined by Thermodynamic Properties in Complex Gas Mixtures: The Case of Plasma-Based Dry Reforming of Methane. *Plasma Sources Sci. Technol.* **2023**, *32*. https://doi.org/10.1088/1361-6595/acc6ec.

(100) *CRC Handbook of Chemistry and Physics*; Haynes, W. M., Lide, D. R., Bruno, T. J., Eds.; CRC Press, 2016. https://doi.org/10.1201/9781315380476.

(101) Delikonstantis, E.; Scapinello, M.; Stefanidis, G. D. Low Energy Cost Conversion of Methane to Ethylene in a Hybrid Plasma-Catalytic Reactor System. *Fuel Process. Technol.* **2018**, *176*, 33–42. https://doi.org/10.1016/j.fuproc.2018.03.011.

(102) Abiev, R. S.; Sladkovskiy, D. A.; Semikin, K. V.; Murzin, D. Y.; Rebrov, E. V. Non-Thermal Plasma for Process and Energy Intensification in Dry

Reforming of Methane. *Catalysts* **2020**, *10*. https://doi.org/10.3390/catal10111358.

(103) Vadikkeettil, Y.; Subramaniam, Y.; Murugan, R.; Ananthapadmanabhan, P. V.; Mostaghimi, J.; Pershin, L.; Batiot-Dupeyrat, C.; Kobayashi, Y. Plasma Assisted Decomposition and Reforming of Greenhouse Gases: A Review of Current Status and Emerging Trends. *Renew. Sustain. Energy Rev.* **2022**, *161*. https://doi.org/10.1016/j.rser.2022.112343.

(104) De Bleecker, K.; Bogaerts, A.; Goedheer, W. Aromatic Ring Generation as a Dust Precursor in Acetylene Discharges. *Appl. Phys. Lett.* **2006**, *88*. https://doi.org/10.1063/1.2193796.

(105) De Bleecker, K.; Bogaerts, A.; Goedheer, W. Detailed Modeling of Hydrocarbon Nanoparticle Nucleation in Acetylene Discharges. *Phys. Rev. E* **2006**, *73*. https://doi.org/10.1103/PhysRevE.73.026405.

(106) Heijkers, S.; Bogaerts, A. CO2 Conversion in a Gliding Arc Plasmatron: Elucidating the Chemistry through Kinetic Modeling. *J. Phys. Chem. C* **2017**, *121*, 22644–22655. https://doi.org/10.1021/acs.jpcc.7b06524.

(107) Kumar, N.; Shojaee, M.; Spivey, J. Catalytic Bi-Reforming of Methane: From Greenhouse Gases to Syngas. *Curr. Opin. Chem. Eng.* **2015**, *9*, 8–15. https://doi.org/10.1016/j.coche.2015.07.003.

(108) Mohanty, U. S.; Ali, M.; Azhar, M. R.; Al-Yaseri, A.; Keshavarz, A.; Iglauer, S. Current Advances in Syngas (CO + H2) Production through Bi-Reforming of Methane Using Various Catalysts: A Review. *Int. J. Hydrogen Energy* **2021**, *46*, 32809–32845. https://doi.org/10.1016/j.ijhydene.2021.07.097.

(109) Guerra, V.; Tatarova, E.; Dias, F. M.; Ferreira, C. M. On the Self-Consistent Modeling of a Traveling Wave Sustained Nitrogen Discharge. *J. Appl. Phys.* **2002**, *91*, 2648–2661. https://doi.org/10.1063/1.1446229.

(110) Mason, E. A.; Saxena, S. C. Approximate Formula for the Thermal Conductivity of Gas Mixtures. *Phys. Fluids* **1958**, *1*, 361–369. https://doi.org/10.1063/1.1724352.

(111) McBride, B. J.; Gordon, S.; Reno, M. A. *Coefficients for Calculating Thermodynamic and Transport Properties of Individual Species*; 1993.

(112) Vertongen, R.; Bogaerts, A. How Important Is Reactor Design for CO2 Conversion in Warm Plasmas? *J. CO2 Util.* **2023**, *72*. https://doi.org/10.1016/j.jcou.2023.102510.

(113) Tsonev, I.; Ahmadi Eshtehardi, H.; Delplancke, M.-P.; Bogaerts, A. Importance of Geometric Effects in Scaling up Energy-Efficient Plasma-Based Nitrogen Fixation. *Sustain. Energy Fuels* **2024**, *8*, 2191–2209. https://doi.org/10.1039/D3SE01615C.

(114) Godini, H. R.; Xiao, S.; Jašo, S.; Stünkel, S.; Salerno, D.; Son, N. X.; Song, S.; Wozny, G. Techno-Economic Analysis of Integrating the Methane Oxidative Coupling and Methane Reforming Processes. *Fuel Process. Technol.* **2013**, *106*, 684–694. https://doi.org/10.1016/j.fuproc.2012.10.002.

(115) Osat, M.; Shojaati, F. Techno-Economic-Environmental Evaluation of a Combined Tri and Dry Reforming of Methane for Methanol Synthesis with a High Efficiency CO2 Utilization. *Int. J. Hydrogen Energy* **2022**, *47*, 9058–9070. https://doi.org/10.1016/j.ijhydene.2021.12.207.

(116) Maerivoet, S.; Tsonev, I.; Slaets, J.; Reniers, F.; Bogaerts, A. Coupled Multi-Dimensional Modelling of Warm Plasmas: Application and Validation for an Atmospheric Pressure Glow Discharge in CO2/CH4/O2. *Chem. Eng. J.* **2024**, *492*. https://doi.org/10.1016/j.cej.2024.152006.

Appendix

A. Supplementary tables and figures: chapter 3

Table A-1 Species included in the chemical kinetics model, sorted by type.

Molecules	**Ions**	**Radicals**	**Excited species**
	electrons		
C_3H_8, C_3H_6		C_3H_7, C_3H_5	
C_2H_6, C_2H_4, C_2H_2	$C_2H_6^+$, $C_2H_5^+$, $C_2H_4^+$, $C_2H_3^+$, $C_2H_2^+$, C_2H^+	C_2H_5, C_2H_3, C_2H	
CH_4	CH_5^+, CH_4^+, CH_3^+, CH_2^+, CH^+	CH_3, CH_2, CH	
H_2	H_2^+		$H_2(V_1\text{-}V_{14})$
	H^+, H^-, H_3^+	H	
N_2	N_2^+		$N_2(V_1\text{-}V_{24})$, $N_2(A^3\Sigma_u^+)$, $N_2(B^3\Pi_g)$, $N_2(a^1\Sigma_u^-)$, $N_2(C^3\Pi_u)$
	N^+, N_3^+, N_4^+	N	N(2D), N(2P)
N_2O	NO^+, N_2O^+, NO_2^+, NO^-, N_2O^-, NO_2^-, NO_3^-	NO, NO_2, NO_3	
		CN, NCN	
		NCO	
CO_2	CO_2^+		$CO_2(V_a\text{-}V_d)$, $CO_2(V_1\text{-}V_{21})$, $CO_2(E_1)$
CO	CO^+, CO_3^-, CO_4^-		$CO(V_1\text{-}V_{10})$, $CO(E_1\text{-}E_4)$
O_2	O^-, O_2^-	O	$O_2(V_1\text{-}V_4)$, $O_2(E_1\text{-}E_2)$
CH_2O, CH_3OH		CHO, CH_2OH	
CH_3OOH		CH_3O, CH_3O_2	
		C_2HO, CH_3CO	
CH_3CHO, CH_2CO			
H_2O, H_2O_2	H_2O^+, H_3O^+, OH^-, OH^+	HO_2, OH	
NH_3 N_2H_4		NH, NH_2, N_2H_3	
HNO			

B. Supplementary tables and figures: chapter 4

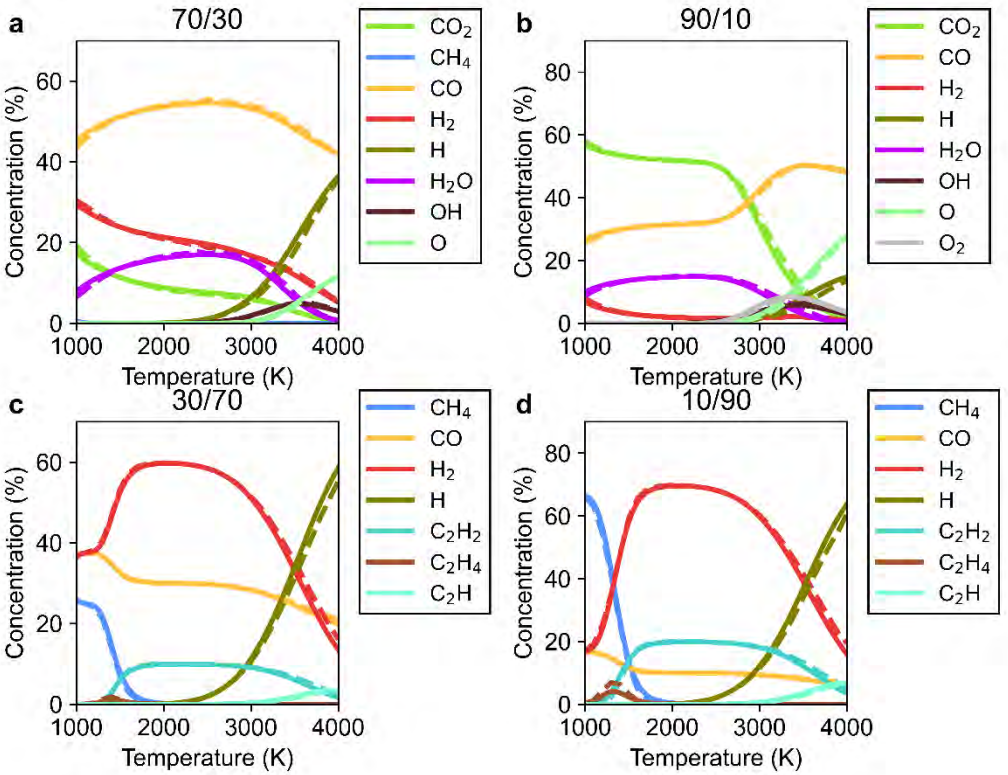

Figure B-1 Calculated species concentrations of the thermal kinetics simulations (for t = 10^{10} s) (dashed) and corresponding thermodynamic equilibrium concentrations (solid), in the temperature range of 1000 to 4000 K, for four different CO_2/CH_4 ratios (70/30 (a), 90/10 (b), 30/70 (c), 10/90 (d)).

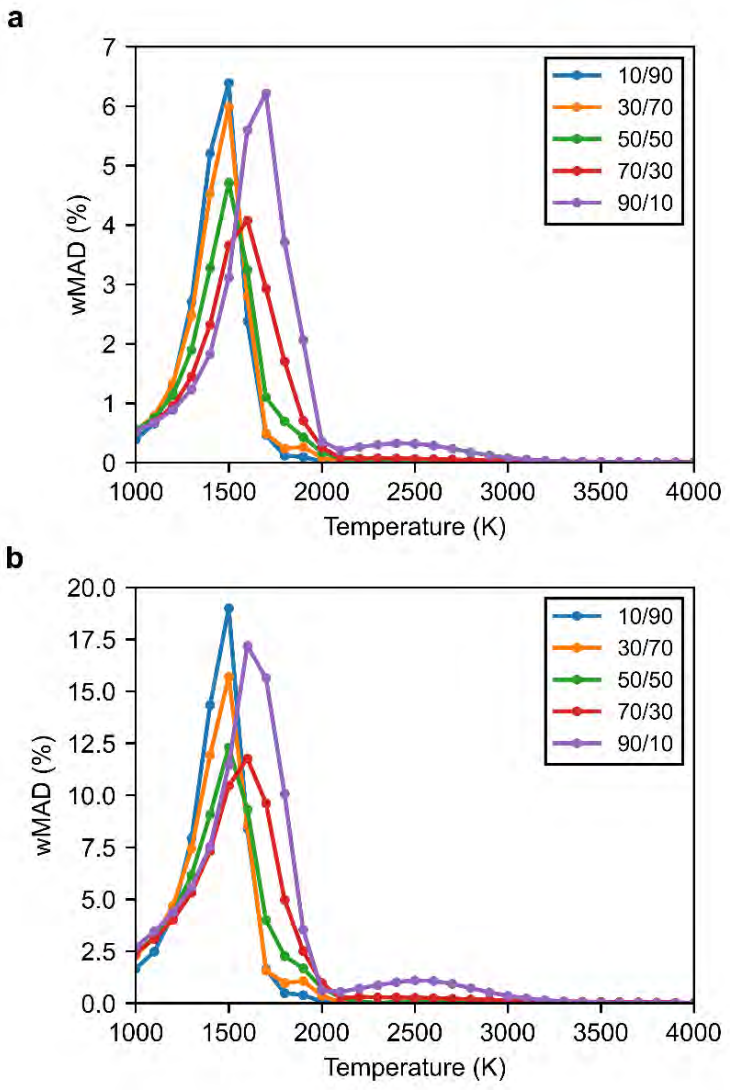

Figure B-2 Weighted mean absolute deviation (wMAD) between the calculated species concentrations at thermal and plasma conditions at 500 W cm^{-3} (a) and 1500 W cm^{-3} (b), at a residence time of 10 ms, in the temperature range of 1000 to 4000 K, for five different CO_2/CH_4 ratios (90/10, 70/30, 50/50, 30/70, 10/90).

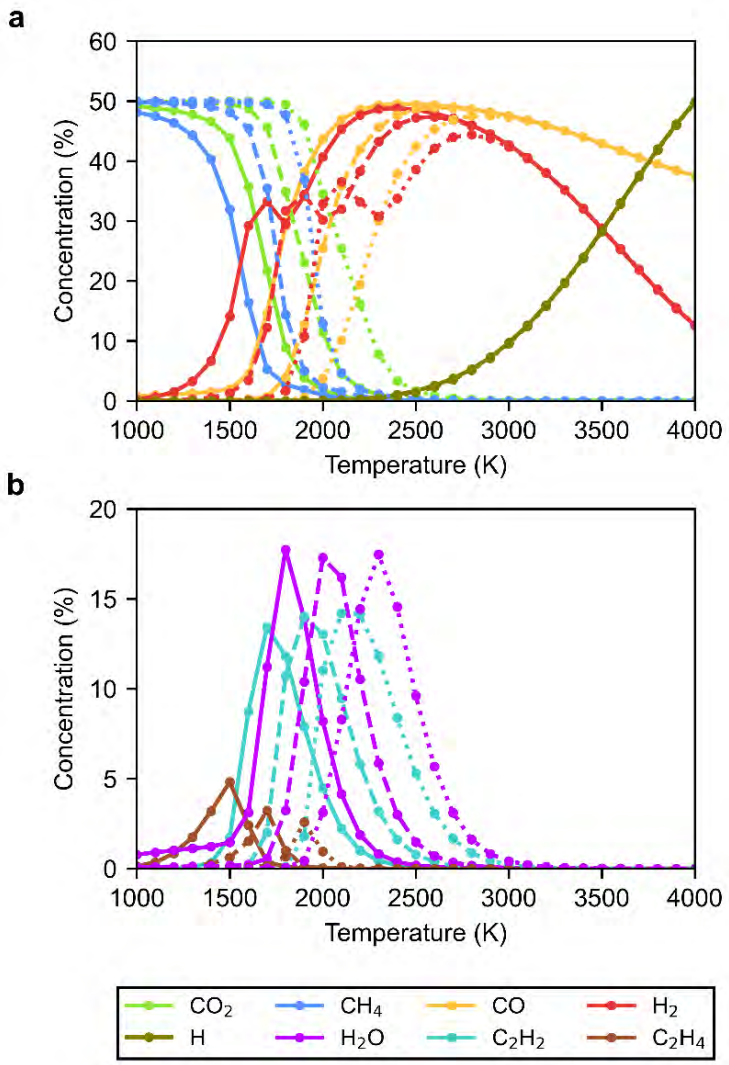

Figure B-3 Calculated concentrations of the main plasma species for the temperature range of 1000 to 4000 K and a 50/50 CO_2/CH_4 ratio and 1000 W cm^{-3} plasma condition, at a residence time of 10 ms (solid lines), 1 ms (dashed lines) and 0.1 ms (dotted lines).

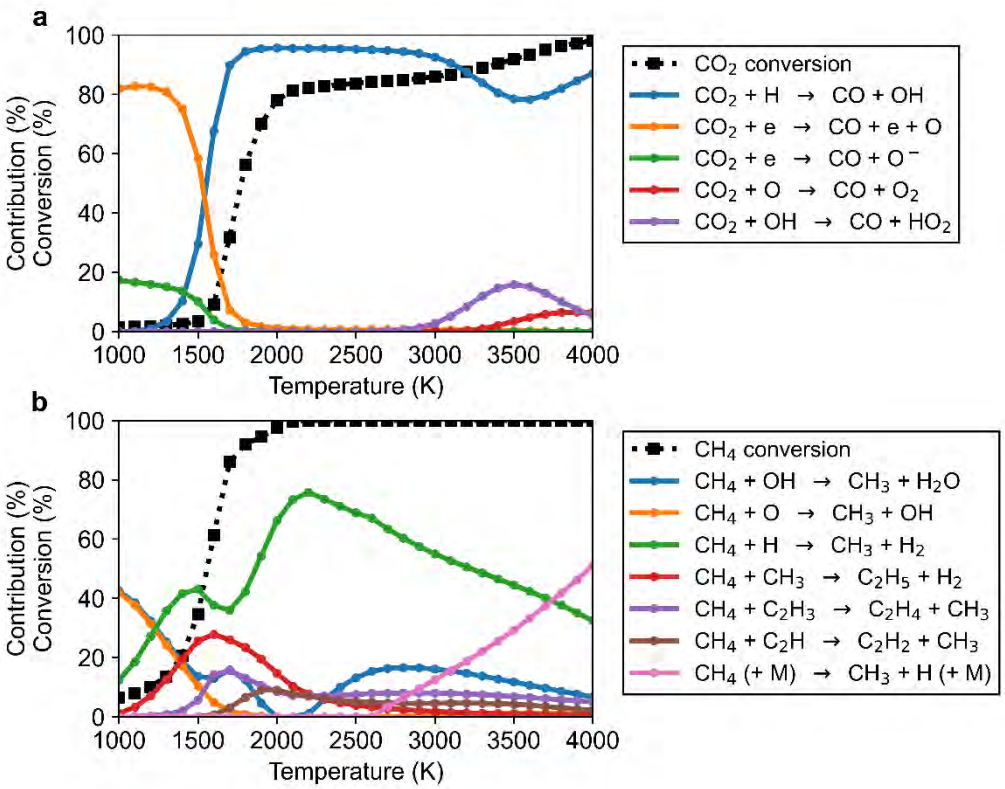

Figure B-4 CO_2 (a) and CH_4 (b) conversion (dotted black lines), as well as the relative contributions of the main loss reactions (>5%) based on the time-integrated net reaction rates (see legends), as a function of temperature, for plasma simulations with a power density of 1000 W cm^{-3} and for a 70/30 ratio of CO_2/CH_4 at a residence time of 10 ms.

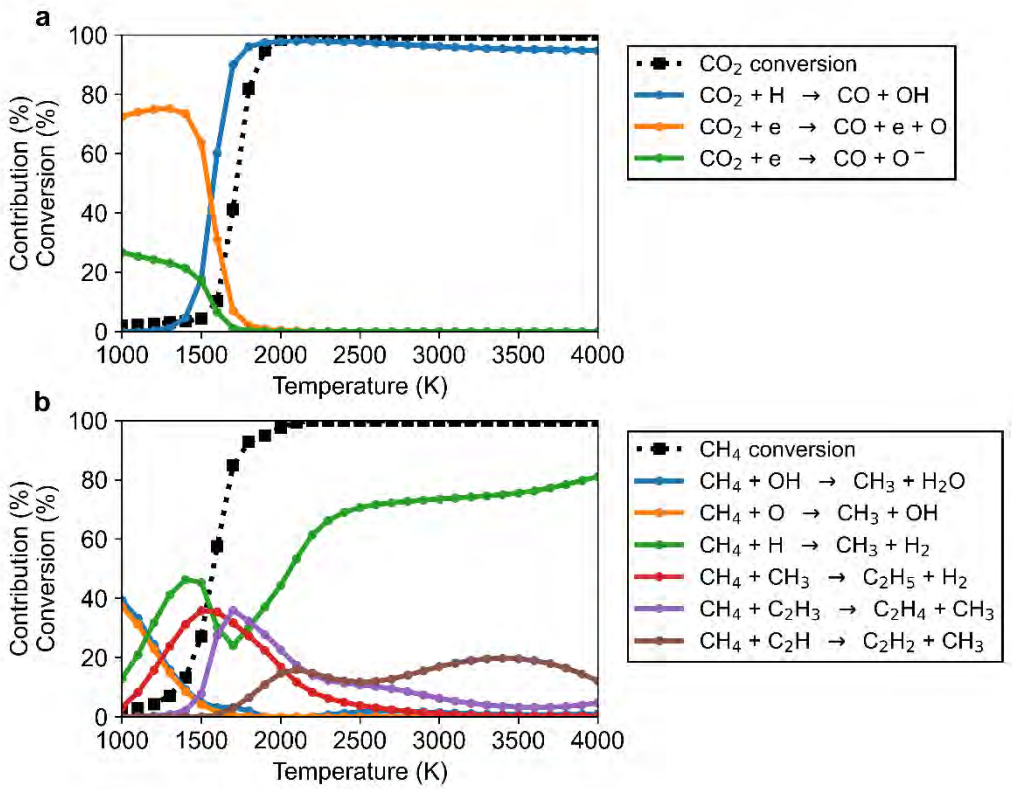

Figure B-5 CO_2 (a) and CH_4 (b) conversion (dotted black lines), as well as the relative contributions of the main loss reactions (>5%) based on the time-integrated net reaction rates (see legends), as a function of temperature, for plasma simulations with a power density of 1000 W cm^{-3} and for a 30/70 ratio of CO_2/CH_4 at a residence time of 10 ms CO_2 (a) and CH_4 (b) conversion (dotted black lines), as well as the relative contributions of the main loss reactions (>5%) based on the time-integrated net reaction rates (see legends), as a function of temperature, for plasma simulations with a power density of 1000 W cm^{-3} and for a 30/70 ratio of CO_2/CH_4 at a residence time of 10 ms.

C. Supplementary tables and figures: chapter 5

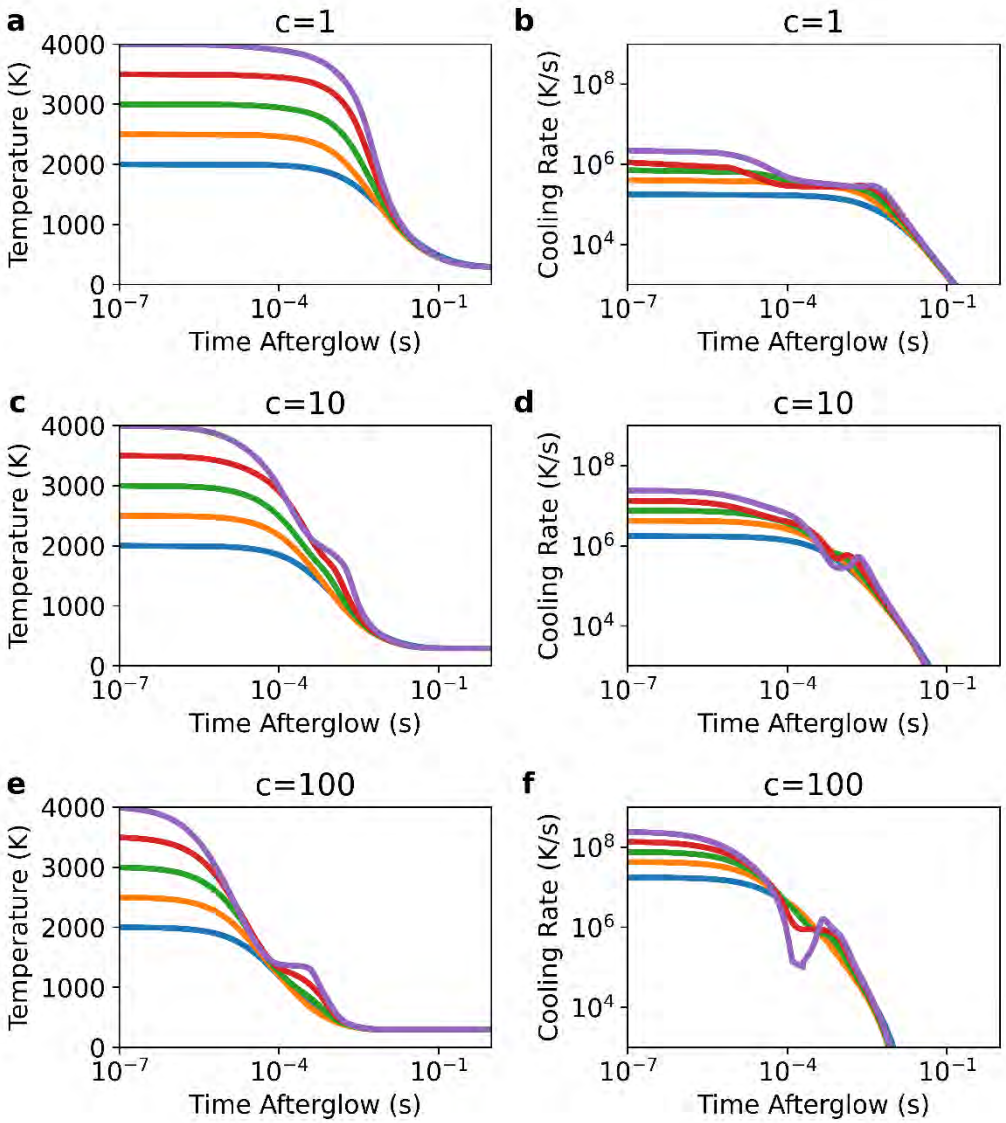

Figure C-1 Gas temperature profiles (left panels a, c, e) and cooling rates (right panels b, d, f) as a function of time in the afterglow for the 50/50 CO_2/CH_4 gas mixture, starting from plasma temperatures of 2000, 2500, 3000, 3500 and 4000 K, for quenching with c-factors of 1 (a, b), 10 (c, d) and 100 (e, f).

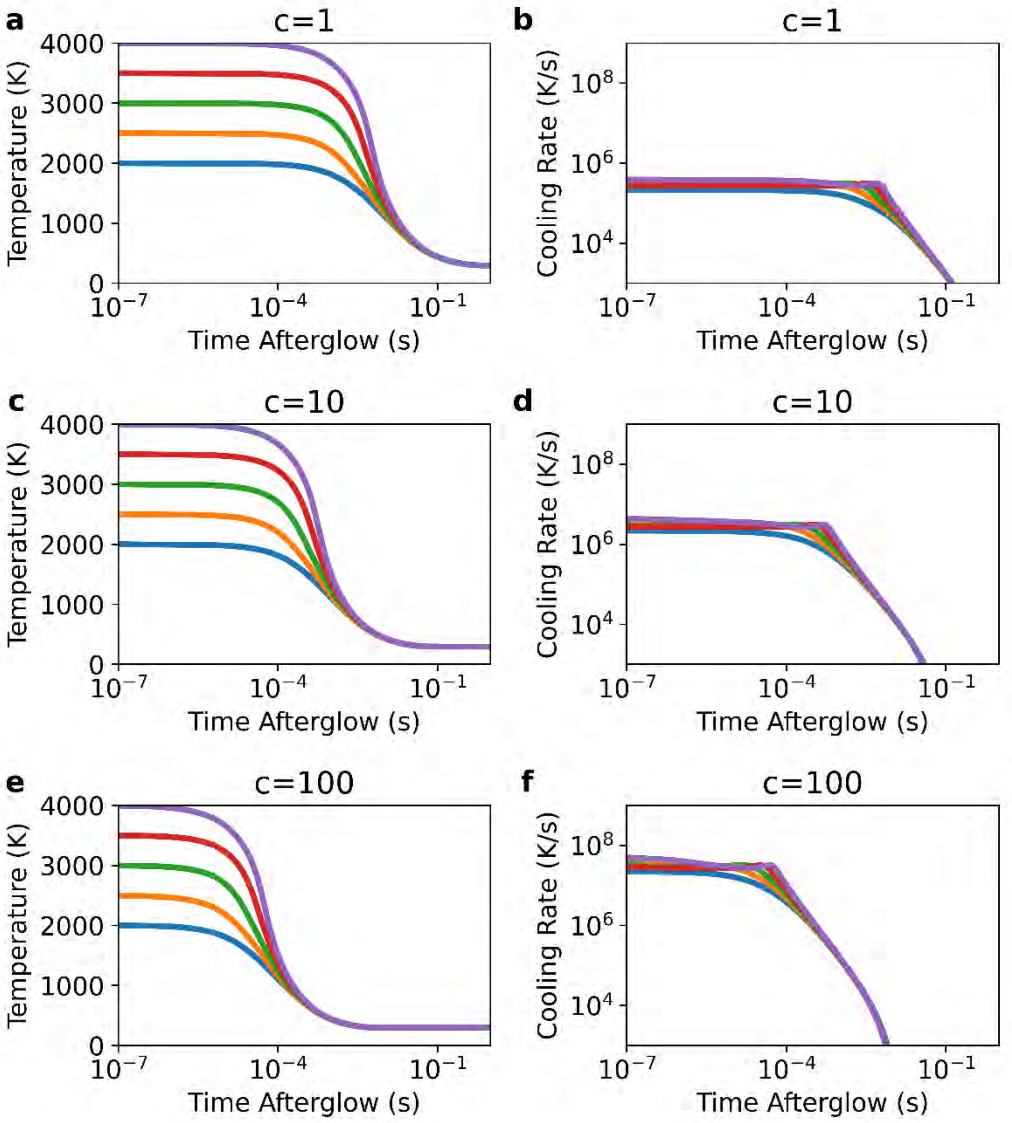

Figure C-2 Gas temperature profiles (left panels a, c, e) and cooling rates (right panels b, d, f) as a function of time in the afterglow for the 30/70 CO_2/CH_4 gas mixture, starting from plasma temperatures of 2000, 2500, 3000, 3500 and 4000 K, for quenching with c-factors of 1 (a, b), 10 (c, d) and 100 (e, f).

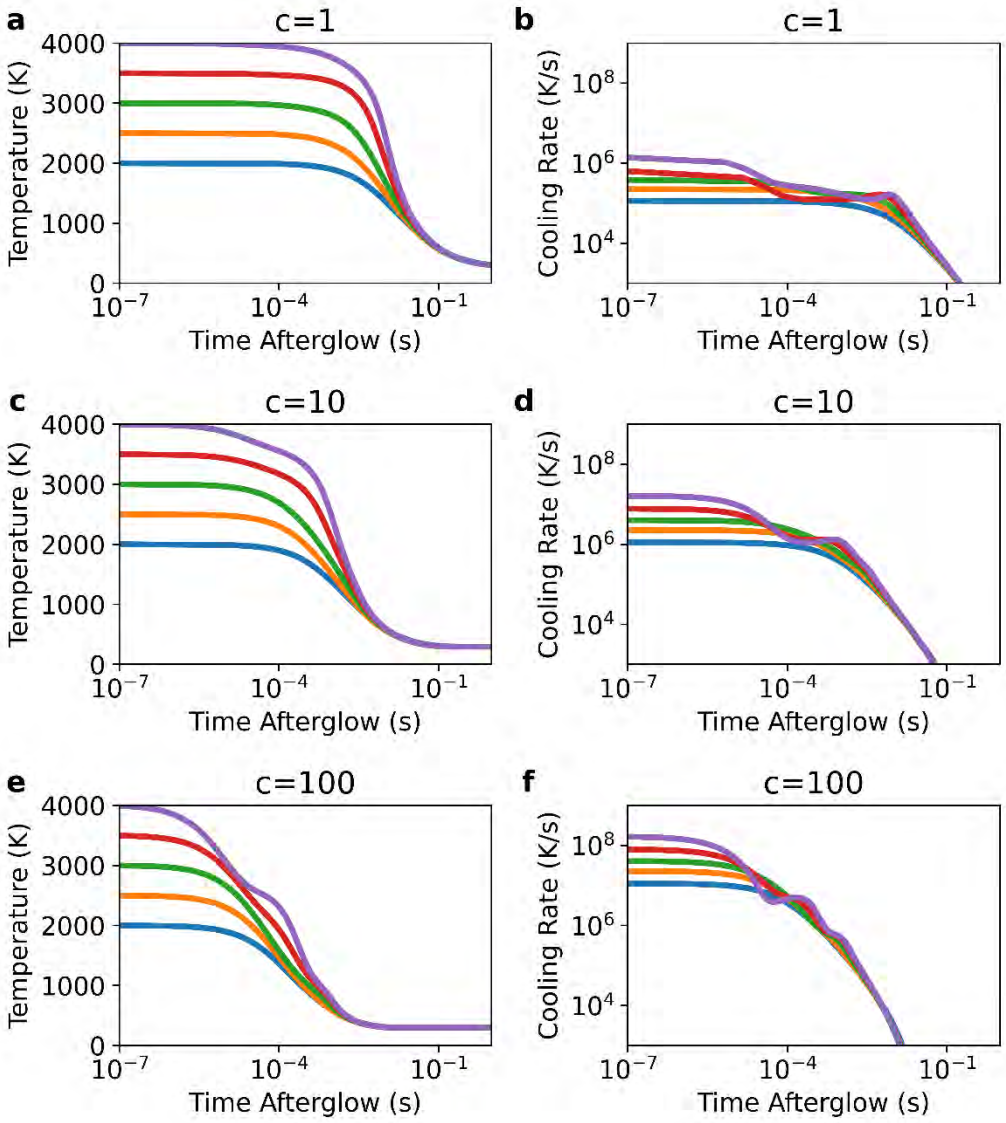

Figure C-3 Gas temperature profiles (left panels a, c, e) and cooling rates (right panels b, d, f) as a function of time in the afterglow for the 70/30 CO_2/CH_4 gas mixture, starting from plasma temperatures of 2000, 2500, 3000, 3500 and 4000 K, for quenching with c-factors of 1 (a, b), 10 (c, d) and 100 (e, f).

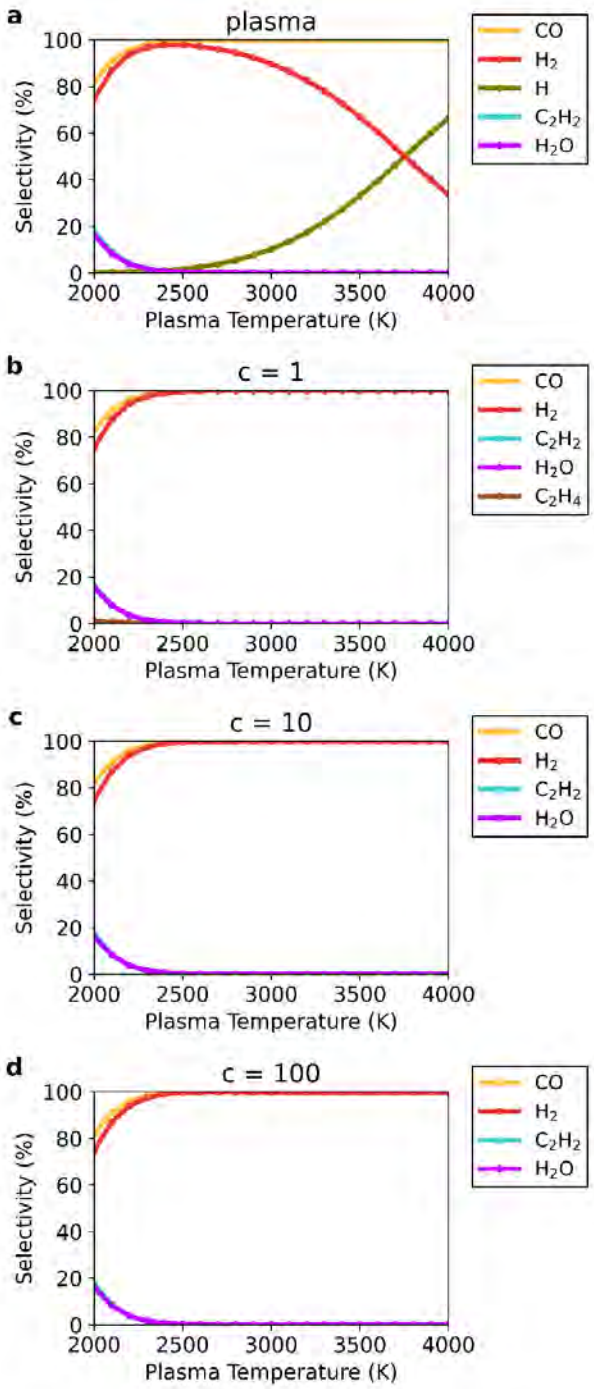

Figure C-4 Selectivity of the main species (above 1%), as a function of the plasma temperature for the 50/50 CO_2/CH_4 ratio, at the end of the plasma (a), and at the end of the afterglow (b, c, d), for c-factors of 1 (b), 10 (c) and 100 (d). The H_2 and CO selectivity curves and the H_2O and C_2H_2 selectivity curves overlap.

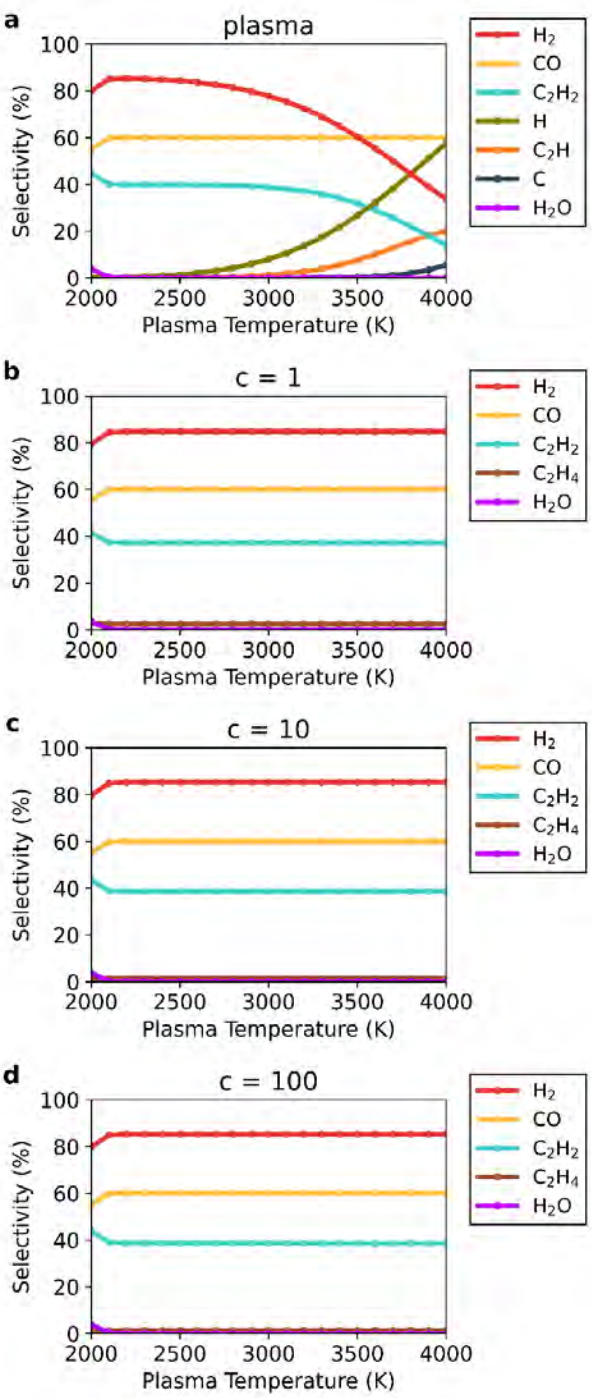

Figure C-5 Selectivity of the main species (above 1%), as a function of the plasma temperature for the 30/70 CO_2/CH_4 ratio, at the end of the plasma (a), and at the end of the afterglow (b, c, d), for c-factors of 1 (b), 10 (c) and 100 (d). The H_2O and C_2H_4 selectivity curves overlap.

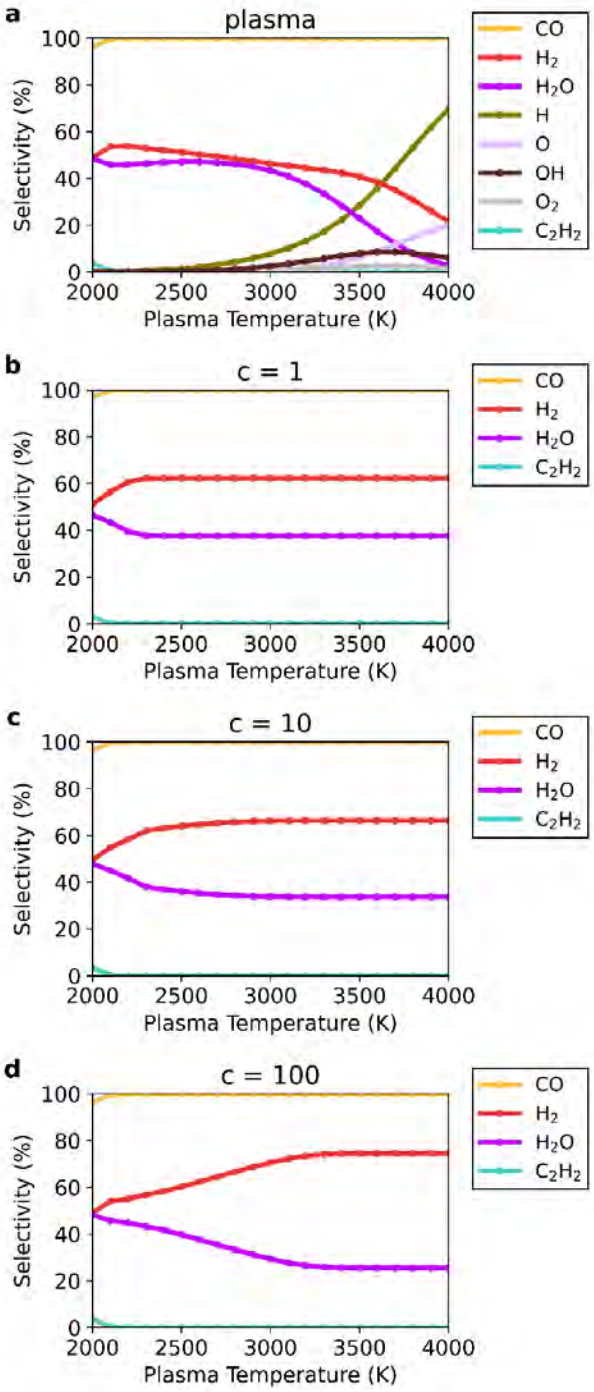

Figure C-6 Selectivity of the main species (above 1%), as a function of the plasma temperature for the 70/30 CO_2/CH_4 ratio, at the end of the plasma (a), and at the end of the afterglow (b, c, d), for c-factors of 1 (b), 10 (c) and 100 (d).

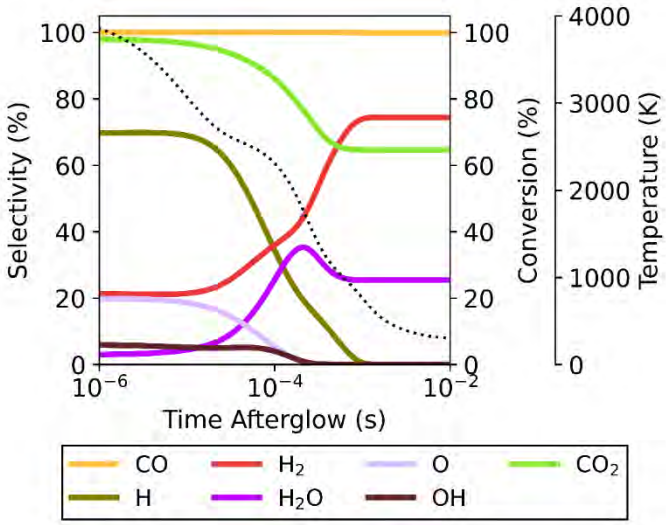

Figure C-7 Time-evolution of the selectivity of the main species in the afterglow, starting from a plasma temperature of 4000 K for the 70/30 CO_2/CH_4 ratio and c-factor = 100. The evolution of the CO_2 conversion (lime green curve) and the gas temperature (dotted line) are also plotted, and shown on the right axis.

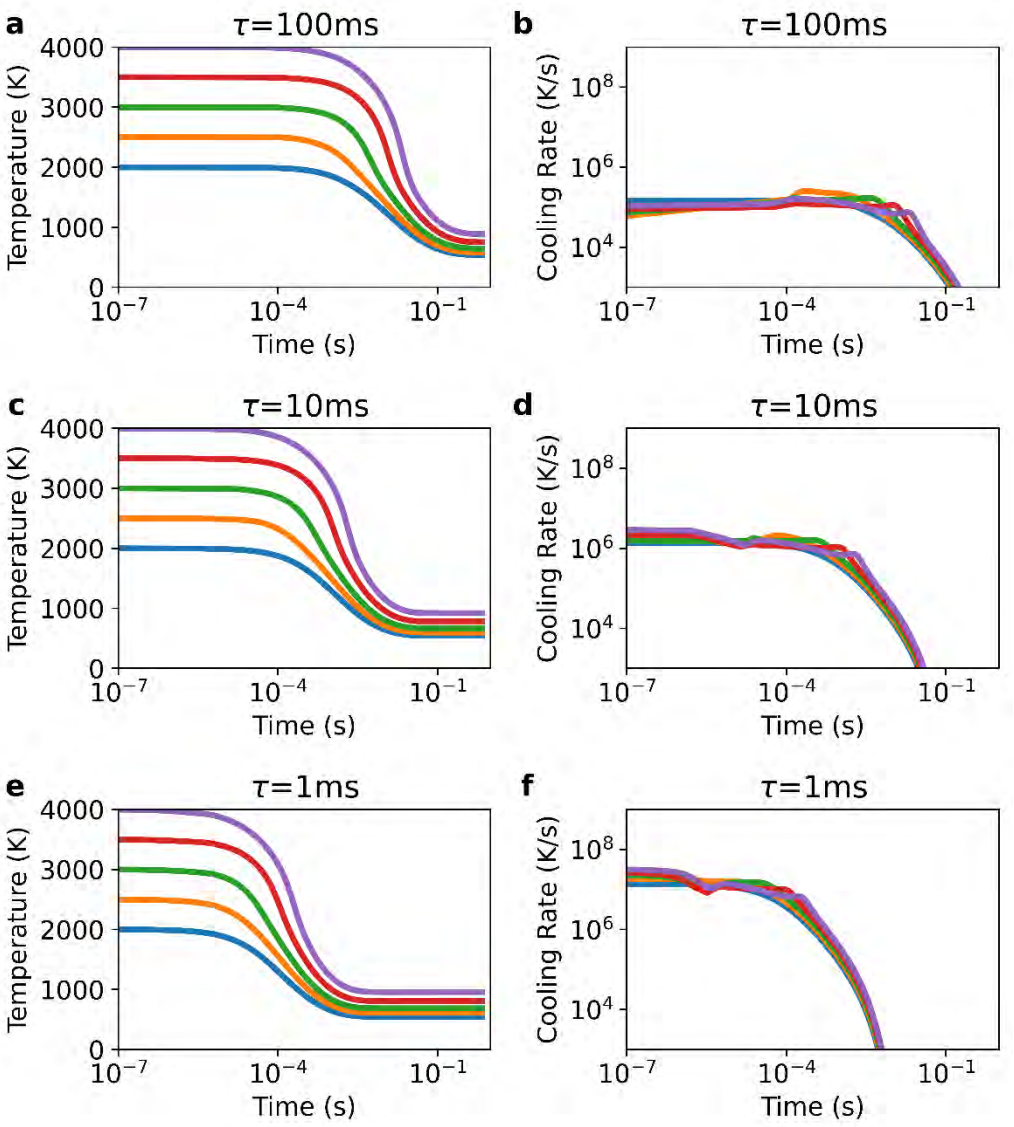

Figure C-8 Gas temperature profiles (left panels a, c, e) and cooling rates (right panels b, d, f) as a function of time in the afterglow for the 50/50 CO_2/CH_4 gas mixture, starting from plasma temperatures of 2000, 2500, 3000, 3500 and 4000 K, for characteristic mixing times of τ_{mix} = 100 ms (a, b), 10 ms (c, d) and 1 ms (e, f).

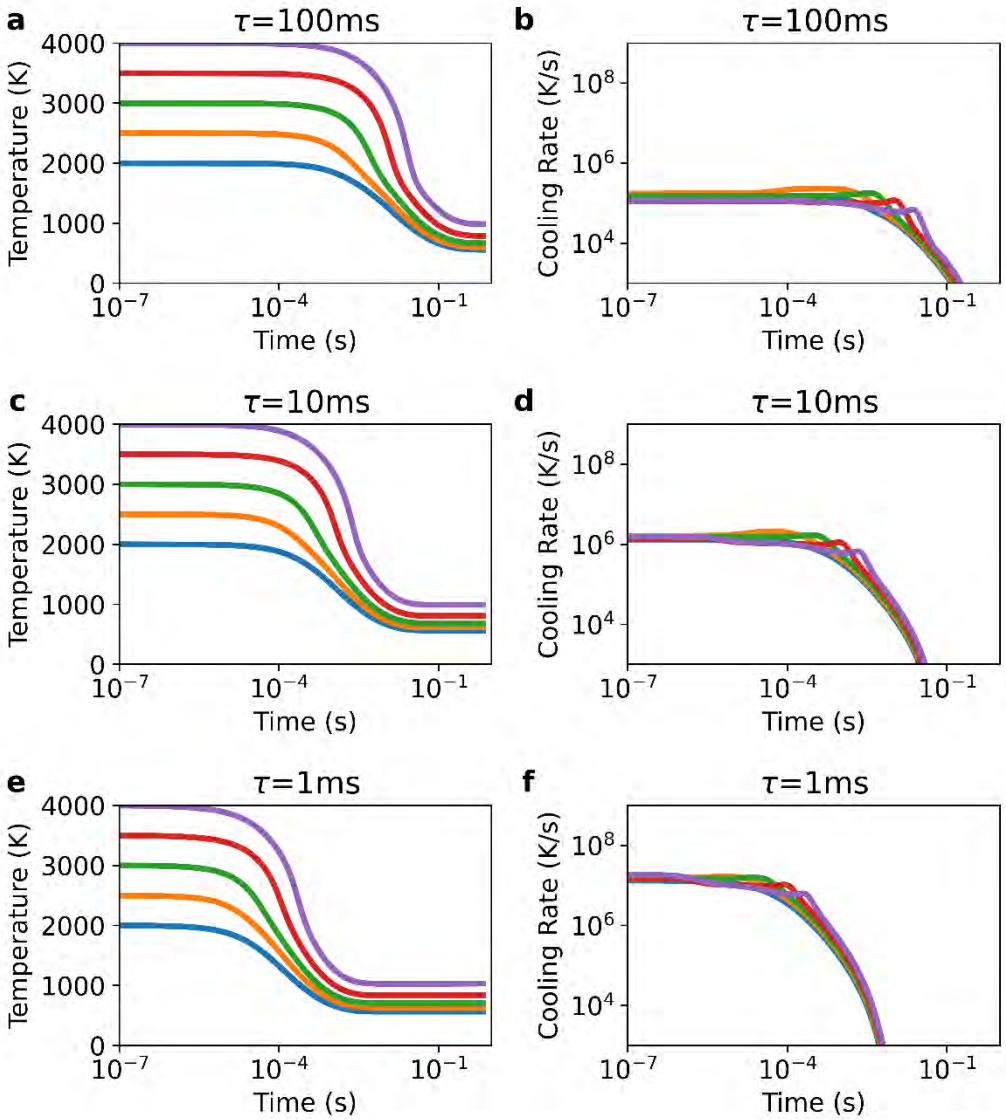

Figure C-9 Gas temperature profiles (left panels a, c, e) and cooling rates (right panels b, d, f) as a function of time in the afterglow for the 30/70 CO_2/CH_4 gas mixture, starting from plasma temperatures of 2000, 2500, 3000, 3500 and 4000 K, for characteristic mixing times of τ_{mix} = 100 ms (a, b), 10 ms (c, d) and 1 ms (e, f).

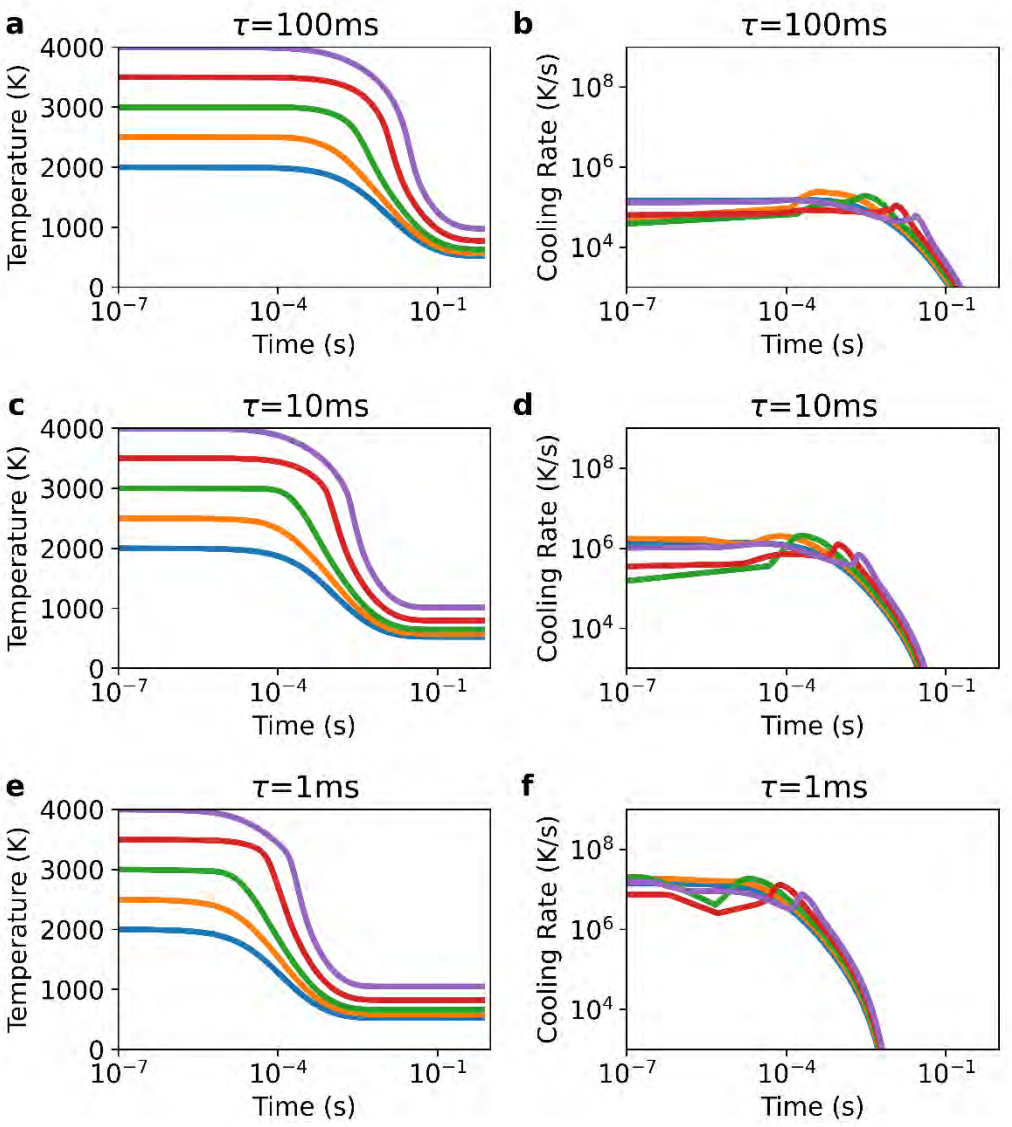

Figure C-10 Gas temperature profiles (left panels a, c, e) and cooling rates (right panels b, d, f) as a function of time in the afterglow for the 70/30 CO_2/CH_4 gas mixture, starting from plasma temperatures of 2000, 2500, 3000, 3500 and 4000 K, for characteristic mixing times of τ_{mix} = 100 ms (a, b), 10 ms (c, d) and 1 ms (e, f).

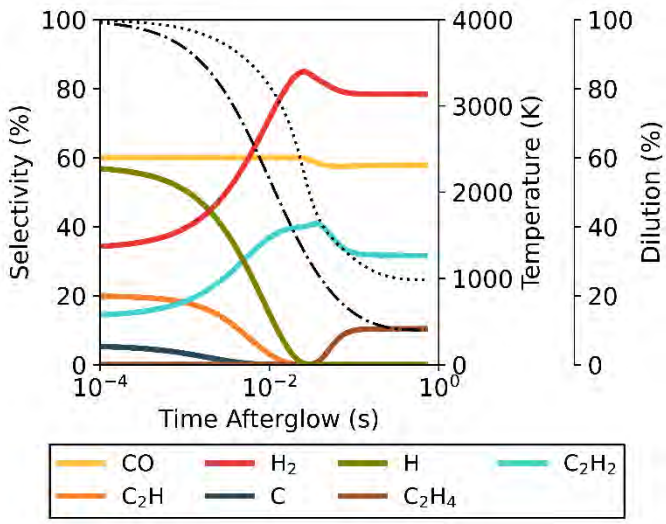

Figure C-11 Temporal evolution of the main species' selectivity in the afterglow, starting from a plasma temperature of 4000 K, for the 30/70 CO_2/CH_4 ratio at τ_{mix} = 100 ms. The temperature (dotted line) and mixing progress (dash-dotted line) are also plotted, and shown on the right axes. The timespan in which the shift from C_2H_2 to C_2H_4 occurs is indicated with a grey rectangle.

D. Chemical kinetics set

Table D-1 Reactions reference list with the rate coefficients (third column) expressed in $cm^3\ s^{-1}$ for two-body reactions, and in $cm^6\ s^{-1}$ for three-body reactions. In the rate equations, N_A is Avogadro's constant, k_B is the Boltzmann constant, R is the ideal gas constant, T_g is the gas temperature in K and n_M is the total number density of neutral species in cm^{-3}.

#	Reaction / Rate equation	Ref.
1	$C + H^- \rightarrow CH + e$ 1×10^{-9}	[1]
2	$C + H_3^+ \rightarrow CH^+ + H_2$ 2×10^{-9}	[1]
3	$C + H_2^+ \rightarrow CH^+ + H$ 2.4×10^{-9}	[1]
4	$C^+ + H^- \rightarrow C + H$ $7.51 \times 10^{-8} \cdot \left(\frac{T_g}{3 \times 10^2}\right)^{-0.5}$	[2, 3]
5	$CH_4 + H \rightarrow CH_3 + H_2$ $6.4 \times 10^{-18} \cdot T_g^{2.11} \cdot exp\left(\frac{-3.9 \times 10^3}{T_g}\right)$	[4]
6	$CH_3 + H_2 \rightarrow CH_4 + H$ $6.62 \times 10^{-20} \cdot T_g^{2.24} \cdot exp\left(\frac{-3.22 \times 10^3}{T_g}\right)$	[4]
7	$CH_3 + H \rightarrow CH_2 + H_2$ $2.1 \times 10^{-8} \cdot T_g^{-0.56} \cdot exp\left(\frac{-8.0 \times 10^3}{T_g}\right)$	[5]
8	$CH_3 + H \rightarrow CH_4$ $k_0 = 1.7 \times 10^{-24} \cdot T_g^{-1.8}$ $k_\infty = 3.5 \times 10^{-10}$ $F_c = 0.63 \cdot exp\left(\frac{-T_g}{3.3150 \times 10^3}\right)$ $+0.37 \cdot exp\left(\frac{-T_g}{6.10 \times 10^1}\right)$	[5][a]
9	$CH_2 + H_2 \rightarrow CH_3 + H$ $7.32 \times 10^{-19} \cdot T_g^{2.3} \cdot exp\left(\frac{-3.6990 \times 10^3}{T_g}\right)$	[6]
10	$CH_2 + H \rightarrow CH + H_2$ 2×10^{-10}	[5]
11	$CH + H_2 \rightarrow CH_2 + H$ $2.9 \times 10^{-10} \cdot exp\left(\frac{-1.670 \times 10^3}{T_g}\right)$	[5]

#	Reaction / Rate equation	Ref.
12	$CH + H_2 \rightarrow CH_3$ $k_0 = 4.7 \times 10^{-26} \cdot T_g^{-1.6}$ $k_\infty = 8.5 \times 10^{-11} \cdot T_g^{0.15}$ $F_c = 0.48$ $+0.25 \cdot exp\left(\frac{-T_g}{3.0 \times 10^2}\right)$	[5][a]
13	$CH + H \rightarrow C + H_2$ 2×10^{-10}	[5]
14	$CH_4 + H^+ \rightarrow CH_4^+ + H$ 1.5×10^{-9}	[1]
15	$CH_4 + H^+ \rightarrow CH_3^+ + H_2$ 2.3×10^{-9}	[1]
16	$CH_3 + H^+ \rightarrow CH_3^+ + H$ 3.4×10^{-9}	[1]
17	$CH_2 + H^+ \rightarrow CH_2^+ + H$ 1.4×10^{-9}	[1]
18	$CH_2 + H^+ \rightarrow CH^+ + H_2$ 1.4×10^{-9}	[1]
19	$CH + H^+ \rightarrow CH^+ + H$ 1.9×10^{-9}	[1]
20	$CH_4 + H_2^+ \rightarrow CH_5^+ + H$ 1.14×10^{-10}	[7]
21	$CH_4 + H_2^+ \rightarrow CH_4^+ + H_2$ 1.406×10^{-9}	[7]
22	$CH_4 + H_2^+ \rightarrow CH_3^+ + H + H_2$ 2.28×10^{-9}	[7]
23	$CH_2 + H_2^+ \rightarrow CH_3^+ + H$ 1×10^{-9}	[1]
24	$CH_2 + H_2^+ \rightarrow CH_2^+ + H_2$ 1×10^{-9}	[1]
25	$CH + H_2^+ \rightarrow CH_2^+ + H$ 7.1×10^{-10}	[1]
26	$CH + H_2^+ \rightarrow CH^+ + H_2$ 7.1×10^{-10}	[1]
27	$CH_4 + H_3^+ \rightarrow CH_5^+ + H_2$ 2.4×10^{-9}	[1]
28	$CH_3 + H_3^+ \rightarrow CH_4^+ + H_2$ 2.1×10^{-9}	[1]
29	$CH_2 + H_3^+ \rightarrow CH_3^+ + H_2$ 1.7×10^{-9}	[1]
30	$CH + H_3^+ \rightarrow CH_2^+ + H_2$ 1.2×10^{-9}	[1]

#	Reaction / Rate equation	Ref.
31	$CH_3 + H^- \rightarrow CH_4 + e$ 1×10^{-9}	[1]
32	$CH_2 + H^- \rightarrow CH_3 + e$ 1×10^{-9}	[1]
33	$CH + H^- \rightarrow CH_2 + e$ 1×10^{-10}	[1]
34	$CH_5^+ + H \rightarrow CH_4^+ + H_2$ 1.5×10^{-10}	[8]
35	$CH_4^+ + H_2 \rightarrow CH_5^+ + H$ 3.3×10^{-11}	[9]
36	$CH_4^+ + H \rightarrow CH_3^+ + H_2$ 2×10^{-10}	[1]
37	$CH_2^+ + H_2 \rightarrow CH_3^+ + H$ 1.6×10^{-9}	[9]
38	$CH^+ + H_2 \rightarrow CH_2^+ + H$ 1.2×10^{-9}	[8]
39	$CH_3^+ + H^- \rightarrow CH_3 + H$ $7.51 \times 10^{-8} \cdot \left(\frac{T_g}{3 \times 10^2}\right)^{-0.5}$	[2, 3]
40	$C + CH_4 \rightarrow C_2H_4$ 5×10^{-15}	[10]
41	$C + CH_3 \rightarrow C_2H_2 + H$ 8.3×10^{-11}	[11]
42	$C + CH_2 \rightarrow C_2H + H$ 8.3×10^{-11}	[11]
43	$CH_4 + C^+ \rightarrow C_2H_3^+ + H$ 1×10^{-9}	[12]
44	$CH_4 + C^+ \rightarrow C_2H_2^+ + H_2$ 3.89×10^{-10}	[12]
45	$CH_3 + C^+ \rightarrow C_2H_2^+ + H$ 1.3×10^{-9}	[1]
46	$CH_3 + C^+ \rightarrow C_2H^+ + H_2$ 1×10^{-9}	[13]
47	$CH_2 + C^+ \rightarrow C + CH_2^+$ 5.2×10^{-10}	[1]
48	$CH_2 + C^+ \rightarrow C_2H^+ + H$ 5.2×10^{-10}	[1]
49	$CH + C^+ \rightarrow C + CH^+$ 3.8×10^{-10}	[1]
50	$C + CH_5^+ \rightarrow CH_4 + CH^+$ 1.2×10^{-9}	[1]

#	Reaction / Rate equation	Ref.
51	$C + CH_3^+ \rightarrow C_2H^+ + H_2$ 1.2×10^{-9}	[1]
52	$C + CH_2^+ \rightarrow C_2H^+ + H$ 1.2×10^{-9}	[1]
53	$CH_3 + CH_4 \rightarrow C_2H_6 + H$ $\frac{8 \times 10^{13}}{N_A} \cdot exp\left(\frac{-1.6736 \times 10^5}{R \cdot T_g}\right)$	[14]
54	$CH_3 + CH_4 \rightarrow C_2H_5 + H_2$ $\frac{1 \times 10^{13}}{N_A} \cdot exp\left(\frac{-9.6232 \times 10^4}{R \cdot T_g}\right)$	[14]
55	$CH_2 + CH_4 \rightarrow CH_3 + CH_3$ $7.14 \times 10^{-12} \cdot exp\left(\frac{-4.199 \times 10^4}{R \cdot T_g}\right)$	[15]
56	$CH + CH_4 \rightarrow C_2H_4 + H$ $2.2 \times 10^{-8} \cdot T_g^{-0.94} \cdot exp\left(\frac{-2.9 \times 10^1}{T_g}\right)$	[5]
57	$CH_3 + CH_3 \rightarrow C_2H_6$ $k_0 = 3.5 \times 10^{-7} \cdot T_g^{-7} \cdot exp\left(\frac{-1.39 \times 10^3}{T_g}\right)$ $k_\infty = 6 \times 10^{-11}$ $F_c = 0.38 \cdot exp\left(\frac{-T_g}{7.3 \times 10^1}\right)$ $+0.62 \cdot exp\left(\frac{-T_g}{1.18 \times 10^3}\right)$	[5][a]
58	$CH_3 + CH_3 \rightarrow C_2H_5 + H$ $9 \times 10^{-11} \cdot exp\left(\frac{-8.08 \times 10^3}{T_g}\right)$	[5]
59	$CH_3 + CH_3 \rightarrow CH_2 + CH_4$ $5.6 \times 10^{-17} \cdot T_g^{1.34} \cdot exp\left(\frac{-6.791 \times 10^4}{R \cdot T_g}\right)$	[16]
60	$CH_2 + CH_3 \rightarrow C_2H_4 + H$ 1.2×10^{-10}	[5]
61	$CH_2 + CH_2 \rightarrow C_2H_2 + H_2$ $\frac{10^{1.52 \times 10^1}}{N_A} \cdot exp\left(\frac{-5 \times 10^4}{R \cdot T_g}\right)$	[17]
62	$CH + CH \rightarrow C_2H_2$ $\frac{1.2 \times 10^{14}}{N_A}$	[18]
63	$CH_2 + CH_5^+ \rightarrow CH_3^+ + CH_4$ 9.6×10^{-10}	[1]
64	$CH + CH_5^+ \rightarrow CH_2^+ + CH_4$ 6.9×10^{-10}	[1]
65	$CH_4 + CH_4^+ \rightarrow CH_3 + CH_5^+$ 1.5×10^{-9}	[9]

#	Reaction / Rate equation	Ref.
66	$CH_3^+ + CH_4 \rightarrow CH_3 + CH_4^+$ 1.36×10^{-10}	[19]
67	$CH_3^+ + CH_4 \rightarrow C_2H_5^+ + H_2$ 1.2×10^{-9}	[20]
68	$CH_2 + CH_3^+ \rightarrow C_2H_3^+ + H_2$ 9.9×10^{-10}	[1]
69	$CH + CH_3^+ \rightarrow C_2H_2^+ + H_2$ 7.1×10^{-10}	[1]
70	$CH_2^+ + CH_4 \rightarrow CH_3 + CH_3^+$ 1.38×10^{-10}	[21]
71	$CH_2^+ + CH_4 \rightarrow C_2H_5^+ + H$ 3.6×10^{-10}	[9]
72	$CH_2^+ + CH_4 \rightarrow C_2H_4^+ + H_2$ 8.4×10^{-10}	[9]
73	$CH_2^+ + CH_4 \rightarrow C_2H_3^+ + H + H_2$ 2.31×10^{-10}	[21]
74	$CH_2^+ + CH_4 \rightarrow C_2H_2^+ + H_2 + H_2$ 3.97×10^{-10}	[21]
75	$CH_4 + CH^+ \rightarrow C_2H_4^+ + H$ 6.5×10^{-11}	[9]
76	$CH_4 + CH^+ \rightarrow C_2H_3^+ + H_2$ 1.09×10^{-9}	[9]
77	$CH_4 + CH^+ \rightarrow C_2H_2^+ + H + H_2$ 1.43×10^{-10}	[9]
78	$CH_2 + CH^+ \rightarrow C_2H^+ + H_2$ 1×10^{-9}	[1]
79	$CH_4 + e \rightarrow CH_4^+ + e + e$ $f(\sigma)$	[22, 23]
80	$CH_3 + e \rightarrow CH_3^+ + e + e$ $f(\sigma)$	[22, 23]
81	$CH_2 + e \rightarrow CH_2^+ + e + e$ $f(\sigma)$	[22, 23]
82	$CH + e \rightarrow CH^+ + e + e$ $f(\sigma)$	[22, 23]
83	$CH_4 + e \rightarrow CH_3^+ + e + e + H$ $f(\sigma)$	[22, 23]
84	$CH_4 + e \rightarrow CH_2^+ + e + e + H_2$ $f(\sigma)$	[22, 23]
85	$CH_4 + e \rightarrow CH_2^+ + e + e + H + H$ $f(\sigma)$	[22, 23]
86	$CH_4 + e \rightarrow CH^+ + e + e + H + H_2$ $f(\sigma)$	[22, 23]

#	Reaction / Rate equation	Ref.
87	$CH_3 + e \rightarrow CH_2^+ + e + e + H$ $f(\sigma)$	[22, 23]
88	$CH_3 + e \rightarrow CH^+ + e + e + H_2$ $f(\sigma)$	[22, 23]
89	$CH_3 + e \rightarrow CH^+ + e + e + H + H$ $f(\sigma)$	[22, 23]
90	$CH_3 + e \rightarrow C^+ + e + e + H + H_2$ $f(\sigma)$	[22, 23]
91	$CH_3 + e \rightarrow CH_2 + e + e + H^+$ $f(\sigma)$	[22, 23]
92	$CH_2 + e \rightarrow CH^+ + e + e + H$ $f(\sigma)$	[22, 23]
93	$CH_2 + e \rightarrow C^+ + e + e + H_2$ $f(\sigma)$	[22, 23]
94	$CH_2 + e \rightarrow C^+ + e + e + H + H$ $f(\sigma)$	[22, 23]
95	$CH_2 + e \rightarrow CH + e + e + H^+$ $f(\sigma)$	[22, 23]
96	$CH_2 + e \rightarrow C + e + e + H_2^+$ $f(\sigma)$	[22, 23]
97	$CH + e \rightarrow C^+ + e + e + H$ $f(\sigma)$	[22, 23]
98	$CH + e \rightarrow C + e + e + H^+$ $f(\sigma)$	[22, 23]
99	$CH_4 + e \rightarrow CH_3 + e + H$ $f(\sigma)$	[22, 23]
100	$CH_4 + e \rightarrow CH + e + H + H_2$ $f(\sigma)$	[22, 23]
101	$CH_4 + e \rightarrow C + e + H + H + H_2$ $f(\sigma)$	[22, 23]
102	$CH_4 + e \rightarrow C + e + H_2 + H_2$ $f(\sigma)$	[22, 23]
103	$CH_4 + e \rightarrow CH_2 + e + H_2$ $f(\sigma)$	[22, 23]
104	$CH_4 + e \rightarrow CH_2 + e + H + H$ $f(\sigma)$	[22, 23]
105	$CH_3 + e \rightarrow CH + e + H_2$ $f(\sigma)$	[22, 23]
106	$CH_3 + e \rightarrow C + e + H + H_2$ $f(\sigma)$	[22, 23]
107	$CH_3 + e \rightarrow CH + e + H + H$ $f(\sigma)$	[22, 23]

#	Reaction / Rate equation	Ref.
108	$CH_3 + e \rightarrow CH_2 + e + H$ $f(\sigma)$	[22, 23]
109	$CH_2 + e \rightarrow C + e + H_2$ $f(\sigma)$	[22, 23]
110	$CH_2 + e \rightarrow CH + e + H$ $f(\sigma)$	[22, 23]
111	$CH_2 + e \rightarrow C + e + H + H$ $f(\sigma)$	[22, 23]
112	$CH + e \rightarrow C + e + H$ $f(\sigma)$	[22, 23]
113	$CH_4^+ + e \rightarrow CH_3^+ + e + e + H^+$ $f(\sigma)$	[22, 23]
114	$CH_4^+ + e \rightarrow CH_3^+ + e + H$ $f(\sigma)$	[22, 23]
115	$CH_4^+ + e \rightarrow CH_2^+ + e + H_2$ $f(\sigma)$	[22, 23]
116	$CH_4^+ + e \rightarrow CH_2^+ + e + H + H$ $f(\sigma)$	[22, 23]
117	$CH_4^+ + e \rightarrow CH^+ + e + H + H_2$ $f(\sigma)$	[22, 23]
118	$CH_4^+ + e \rightarrow CH^+ + e + H + H + H$ $f(\sigma)$	[22, 23]
119	$CH_4^+ + e \rightarrow C^+ + e + H_2 + H_2$ $f(\sigma)$	[22, 23]
120	$CH_4^+ + e \rightarrow C^+ + e + H + H + H_2$ $f(\sigma)$	[22, 23]
121	$CH_4^+ + e \rightarrow C^+ + e + H + H + H + H$ $f(\sigma)$	[22, 23]
122	$CH_4^+ + e \rightarrow CH + e + H_3^+$ $f(\sigma)$	[22, 23]
123	$CH_4^+ + e \rightarrow C + e + H_2 + H_2^+$ $f(\sigma)$	[22, 23]
124	$CH_4^+ + e \rightarrow CH + e + H + H_2^+$ $f(\sigma)$	[22, 23]
125	$CH_4^+ + e \rightarrow CH_2 + e + H_2^+$ $f(\sigma)$	[22, 23]
126	$CH_4^+ + e \rightarrow C + e + H + H + H_2^+$ $f(\sigma)$	[22, 23]
127	$CH_4^+ + e \rightarrow CH_2 + e + H + H^+$ $f(\sigma)$	[22, 23]
128	$CH_4^+ + e \rightarrow CH_3 + e + H^+$ $f(\sigma)$	[22, 23]

#	Reaction / Rate equation	Ref.
129	$CH_4^+ + e \rightarrow CH + e + H_2 + H^+$ $f(\sigma)$	[22, 23]
130	$CH_3^+ + e \rightarrow CH_2^+ + e + H$ $f(\sigma)$	[22, 23]
131	$CH_3^+ + e \rightarrow CH^+ + e + H_2$ $f(\sigma)$	[22, 23]
132	$CH_3^+ + e \rightarrow CH^+ + e + H + H$ $f(\sigma)$	[22, 23]
133	$CH_3^+ + e \rightarrow C^+ + e + H + H_2$ $f(\sigma)$	[22, 23]
134	$CH_3^+ + e \rightarrow C^+ + e + H + H + H$ $f(\sigma)$	[22, 23]
135	$CH_3^+ + e \rightarrow C + e + H + H_2^+$ $f(\sigma)$	[22, 23]
136	$CH_3^+ + e \rightarrow CH + e + H_2^+$ $f(\sigma)$	[22, 23]
137	$CH_3^+ + e \rightarrow C + e + H_2 + H^+$ $f(\sigma)$	[22, 23]
138	$CH_3^+ + e \rightarrow CH_2 + e + H^+$ $f(\sigma)$	[22, 23]
139	$CH_3^+ + e \rightarrow CH + e + H + H^+$ $f(\sigma)$	[22, 23]
140	$CH_2^+ + e \rightarrow CH^+ + e + H$ $f(\sigma)$	[22, 23]
141	$CH_2^+ + e \rightarrow C^+ + e + H_2$ $f(\sigma)$	[22, 23]
142	$CH_2^+ + e \rightarrow C^+ + e + H + H$ $f(\sigma)$	[22, 23]
143	$CH_2^+ + e \rightarrow C + e + H_2^+$ $f(\sigma)$	[22, 23]
144	$CH_2^+ + e \rightarrow CH + e + H^+$ $f(\sigma)$	[22, 23]
145	$CH_2^+ + e \rightarrow C + e + H + H^+$ $f(\sigma)$	[22, 23]
146	$CH^+ + e \rightarrow C + e + H^+$ $f(\sigma)$	[22, 23]
147	$CH^+ + e \rightarrow C^+ + e + H$ $f(\sigma)$	[22, 23]
148	$CH_4^+ + e \rightarrow CH_3 + H$ $f(\sigma)$	[22, 23]
149	$CH_4^+ + e \rightarrow CH + H + H_2$ $f(\sigma)$	[22, 23]

#	Reaction / Rate equation	Ref.
150	$CH_4^+ + e \rightarrow C + H_2 + H_2$ $f(\sigma)$	[22, 23]
151	$CH_4^+ + e \rightarrow CH_2 + H_2$ $f(\sigma)$	[22, 23]
152	$CH_4^+ + e \rightarrow CH_2 + H + H$ $f(\sigma)$	[22, 23]
153	$CH_3^+ + e \rightarrow CH + H_2$ $f(\sigma)$	[22, 23]
154	$CH_3^+ + e \rightarrow C + H + H_2$ $f(\sigma)$	[22, 23]
155	$CH_3^+ + e \rightarrow CH + H + H$ $f(\sigma)$	[22, 23]
156	$CH_3^+ + e \rightarrow CH_2 + H$ $f(\sigma)$	[22, 23]
157	$CH_2^+ + e \rightarrow C + H_2$ $f(\sigma)$	[22, 23]
158	$CH_2^+ + e \rightarrow CH + H$ $f(\sigma)$	[22, 23]
159	$CH_2^+ + e \rightarrow C + H + H$ $f(\sigma)$	[22, 23]
160	$CH^+ + e \rightarrow C + H$ $f(\sigma)$	[22, 23]
161	$CH_4 + e \rightarrow CH_3 + H^-$ $f(\sigma)$	[24]
162	$CH_4 \rightarrow CH_3 + H$ $k_0 = 7.5 \times 10^{-7} \cdot exp\left(\frac{-4.570 \times 10^4}{T_g}\right)$ $k_\infty = 2.4 \times 10^{16} \cdot exp\left(\frac{-5.280 \times 10^4}{T_g}\right)$ $F_c = exp\left(\frac{-T_g}{1.350 \times 10^3}\right)$ $+exp\left(\frac{-7.8340 \times 10^3}{T_g}\right)$	[5][a]
163	$CH_3 \rightarrow CH + H_2$ $1.1 \times 10^{-8} \cdot exp\left(\frac{-4.280 \times 10^4}{T_g}\right) \cdot n_M$	[5]
164	$CH_3 \rightarrow CH_2 + H$ $1.7 \times 10^{-8} \cdot exp\left(\frac{-4.560 \times 10^4}{T_g}\right) \cdot n_M$	[5]
165	$CH_2 \rightarrow CH + H$ $1.56 \times 10^{-8} \cdot exp\left(\frac{-4.488 \times 10^4}{T_g}\right) \cdot n_M$	[5]

#	Reaction / Rate equation	Ref.
166	$CH_2 \rightarrow C + H_2$ $5 \times 10^{-10} \cdot exp\left(\frac{-3.26 \times 10^4}{T_g}\right) \cdot n_M$	[5]
167	$CH \rightarrow C + H$ $\frac{1.9 \times 10^{14}}{N_A} \cdot exp\left(\frac{-3.37 \times 10^4}{T_g}\right) \cdot n_M$	[11]
168	$C_2H_6 + H \rightarrow C_2H_5 + H_2$ $1.63 \times 10^{-10} \cdot exp\left(\frac{-4.640 \times 10^3}{T_g}\right)$	[5]
169	$C_2H_5 + H_2 \rightarrow C_2H_6 + H$ $5.1 \times 10^{-24} \cdot T_g^{3.6} \cdot exp\left(\frac{-4.253 \times 10^3}{T_g}\right)$	[5]
170	$C_2H_5 + H \rightarrow CH_3 + CH_3$ 7×10^{-11}	[5]
171	$C_2H_5 + H \rightarrow C_2H_6$ $\frac{6 \times 10^{-11}}{1 + 10^{-1.915+2.69\times10^{-3}\cdot T_g - 2.35\times10^{-7}\cdot T_g^2}}$	[25]
172	$C_2H_5 + H \rightarrow C_2H_4 + H_2$ 3×10^{-12}	[25]
173	$C_2H_4 + H_2 \rightarrow C_2H_5 + H$ $1.7 \times 10^{-11} \cdot exp\left(\frac{-3.43 \times 10^4}{T_g}\right)$	[25]
174	$C_2H_4 + H \rightarrow C_2H_3 + H_2$ $3.9 \times 10^{-22} \cdot T_g^{3.62} \cdot exp\left(\frac{-5.67 \times 10^3}{T_g}\right)$	[5]
175	$C_2H_4 + H \rightarrow C_2H_5$ $k_0 = 1.3 \times 10^{-29} \cdot exp\left(\frac{-3.8 \times 10^2}{T_g}\right)$ $k_\infty = 6.6 \times 10^{-15} \cdot T_g^{1.28} \cdot exp\left(\frac{-6.5 \times 10^2}{T_g}\right)$ $F_c = 0.24 \cdot exp\left(\frac{-T_g}{4 \times 10^1}\right)$ $+0.76 \cdot exp\left(\frac{-T_g}{1.025 \times 10^3}\right)$	[5]a
176	$C_2H_3 + H_2 \rightarrow C_2H_4 + H$ $1.57 \times 10^{-20} \cdot T_g^{2.56} \cdot exp\left(\frac{-2.529 \times 10^3}{T_g}\right)$	[26]
177	$C_2H_3 + H \rightarrow C_2H_2 + H_2$ 7×10^{-11}	[5]
178	$C_2H_3 + H \rightarrow C_2H_4$ $k_0 = 3.5 \times 10^{-27}$ $k_\infty = 1.6 \times 10^{-10}$ $F_c = 0.5$	[5]a
179	$C_2H_2 + H_2 \rightarrow C_2H_3 + H$ $4 \times 10^{-12} \cdot exp\left(\frac{-3.27 \times 10^4}{T_g}\right)$	[25]

#	Reaction / Rate equation	Ref.
180	$C_2H_2 + H_2 \rightarrow C_2H_4$ $5 \times 10^{-13} \cdot exp\left(\frac{-1.96 \times 10^4}{T_g}\right)$	[25]
181	$C_2H_2 + H \rightarrow C_2H_3$ $k_0 = 1 \times 10^{-20} \cdot T_g^{-3.38} \cdot exp\left(\frac{-4.26 \times 10^2}{T_g}\right)$ $k_\infty = 9.2 \times 10^{-16} \cdot T_g^{1.64} \cdot exp\left(\frac{-1.055 \times 10^3}{T_g}\right)$ $F_c = 7.37 \times 10^{-4} \cdot T_g^{0.8}$	[5][a]
182	$C_2H_2 + H \rightarrow C_2H + H_2$ $1.67 \times 10^{-14} \cdot T_g^{1.64} \cdot exp\left(\frac{-1.525 \times 10^4}{T_g}\right)$	[5]
183	$C_2H + H_2 \rightarrow C_2H_2 + H$ $3.5 \times 10^{-18} \cdot T_g^{2.32} \cdot exp\left(\frac{-4.44 \times 10^2}{T_g}\right)$	[5]
184	$C_2H + H \rightarrow C_2H_2$ 3×10^{-10}	[25]
185	$C_2H_6^+ + H \rightarrow C_2H_5^+ + H_2$ 1×10^{-10}	[27]
186	$C_2H_5^+ + H \rightarrow C_2H_4^+ + H_2$ 1×10^{-11}	[8]
187	$C_2H_4^+ + H \rightarrow C_2H_3^+ + H_2$ 3×10^{-10}	[8]
188	$C_2H_3^+ + H \rightarrow C_2H_2^+ + H_2$ 6.8×10^{-11}	[8]
189	$C_2H_2^+ + H_2 \rightarrow C_2H_3^+ + H$ 1×10^{-11}	[8]
190	$C_2H^+ + H_2 \rightarrow C_2H_2^+ + H$ 1.1×10^{-9}	[8]
191	$C_2H_6 + H^+ \rightarrow C_2H_5^+ + H_2$ 1.287×10^{-9}	[28]
192	$C_2H_6 + H^+ \rightarrow C_2H_4^+ + H + H_2$ 1.287×10^{-9}	[28]
193	$C_2H_6 + H^+ \rightarrow C_2H_3^+ + H_2 + H_2$ 1.287×10^{-9}	[28]
194	$C_2H_4 + H^+ \rightarrow C_2H_4^+ + H$ 9.8×10^{-10}	[29]
195	$C_2H_4 + H^+ \rightarrow C_2H_3^+ + H_2$ 2.94×10^{-9}	[29]
196	$C_2H_4 + H^+ \rightarrow C_2H_2^+ + H + H_2$ 9.8×10^{-10}	[29]
197	$C_2H_3 + H^+ \rightarrow C_2H_3^+ + H$ 2×10^{-9}	[13]

#	Reaction / Rate equation	Ref.
198	$C_2H_3 + H^+ \rightarrow C_2H_2^+ + H_2$ 2×10^{-9}	[13]
199	$C_2H_2 + H^+ \rightarrow C_2H_2^+ + H$ 5.4×10^{-10}	[29]
200	$C_2H + H^+ \rightarrow C_2H^+ + H$ 1.5×10^{-9}	[1]
201	$C_2H_6 + H_2^+ \rightarrow C_2H_6^+ + H_2$ 2.94×10^{-10}	[7]
202	$C_2H_6 + H_2^+ \rightarrow C_2H_5^+ + H + H_2$ 1.372×10^{-9}	[7]
203	$C_2H_6 + H_2^+ \rightarrow C_2H_4^+ + H_2 + H_2$ 2.352×10^{-9}	[7]
204	$C_2H_6 + H_2^+ \rightarrow C_2H_3^+ + H + H_2 + H_2$ 6.86×10^{-10}	[7]
205	$C_2H_6 + H_2^+ \rightarrow C_2H_2^+ + H_2 + H_2 + H_2$ 1.96×10^{-10}	[7]
206	$C_2H_4 + H_2^+ \rightarrow C_2H_4^+ + H_2$ 2.205×10^{-9}	[7]
207	$C_2H_4 + H_2^+ \rightarrow C_2H_3^+ + H + H_2$ 1.813×10^{-9}	[7]
208	$C_2H_4 + H_2^+ \rightarrow C_2H_2^+ + H_2 + H_2$ 8.82×10^{-10}	[7]
209	$C_2H_2 + H_2^+ \rightarrow C_2H_3^+ + H$ 4.77×10^{-10}	[7]
210	$C_2H_2 + H_2^+ \rightarrow C_2H_2^+ + H_2$ 4.823×10^{-9}	[7]
211	$C_2H + H_2^+ \rightarrow C_2H_2^+ + H$ 1×10^{-9}	[1]
212	$C_2H + H_2^+ \rightarrow C_2H^+ + H_2$ 1×10^{-9}	[1]
213	$C_2H_6 + H_3^+ \rightarrow C_2H_5^+ + H_2 + H_2$ 3.4×10^{-9}	[30, 31]
214	$C_2H_4 + H_3^+ \rightarrow C_2H_5^+ + H_2$ 1.44×10^{-9}	[30, 31]
215	$C_2H_4 + H_3^+ \rightarrow C_2H_3^+ + H_2 + H_2$ 2.16×10^{-9}	[30, 31]
216	$C_2H_2 + H_3^+ \rightarrow C_2H_3^+ + H_2$ 3.5×10^{-9}	[30, 31]
217	$C_2H + H_3^+ \rightarrow C_2H_2^+ + H_2$ 1.7×10^{-9}	[1]
218	$C_2H + H^- \rightarrow C_2H_2 + e$ 1×10^{-9}	[1]

#	Reaction / Rate equation	Ref.
219	$C_2H_2^+ + H^- \rightarrow C_2H_2 + H$ $7.51 \times 10^{-8} \cdot \left(\frac{T_g}{3 \times 10^2}\right)^{-0.5}$	[2, 3]
220	$C_2H_3^+ + H^- \rightarrow C_2H_3 + H$ $7.51 \times 10^{-8} \cdot \left(\frac{T_g}{3 \times 10^2}\right)^{-0.5}$	[2, 3]
221	$C + C_2H_4 \rightarrow C_2H_2 + CH_2$ 1.239×10^{-11}	[32, 33]
222	$C_2H_6 + CH_3 \rightarrow C_2H_5 + CH_4$ $9.3 \times 10^{-14} \cdot exp\left(\frac{-4.740 \times 10^3}{T_g}\right)$ $+1.4 \times 10^{-9} \cdot exp\left(\frac{-1.120 \times 10^4}{T_g}\right)$	[5]
223	$C_2H_6 + CH_2 \rightarrow C_2H_5 + CH_3$ $\frac{6.5 \times 10^{12}}{N_A} \cdot exp\left(\frac{-3.31 \times 10^4}{R \cdot T_g}\right)$	[15]
224	$C_2H_6 + CH \rightarrow C_2H_4 + CH_3$ 1.3×10^{-10}	[34]
225	$C_2H_5 + CH_4 \rightarrow C_2H_6 + CH_3$ $1.43 \times 10^{-25} \cdot T_g^{4.14} \cdot exp\left(\frac{-6.322 \times 10^3}{T_g}\right)$	[25]
226	$C_2H_5 + CH_3 \rightarrow C_2H_4 + CH_4$ 1.5×10^{-12}	[5]
227	$C_2H_5 + CH_3 \rightarrow C_2H_6 + CH_2$ $3 \times 10^{-44} \cdot T_g^{9.0956}$	[35]
228	$C_2H_5 + CH_2 \rightarrow C_2H_4 + CH_3$ 3×10^{-11}	[25]
229	$C_2H_4 + CH_3 \rightarrow C_2H_3 + CH_4$ $1 \times 10^{-16} \cdot T_g^{1.56} \cdot exp\left(\frac{-8.37 \times 10^3}{T_g}\right)$	[5]
230	$C_2H_3 + CH_4 \rightarrow C_2H_4 + CH_3$ $2.4 \times 10^{-24} \cdot T_g^{4.02} \cdot exp\left(\frac{-2.754 \times 10^3}{T_g}\right)$	[25]
231	$C_2H_3 + CH_3 \rightarrow C_2H_2 + CH_4$ $1.5 \times 10^{-11} \cdot exp\left(\frac{3.850 \times 10^2}{T_g}\right)$	[36]
232	$C_2H_3 + CH_2 \rightarrow C_2H_2 + CH_3$ 3×10^{-11}	[25]
233	$C_2H_2 + CH_3 \rightarrow C_2H + CH_4$ $3 \times 10^{-13} \cdot exp\left(\frac{-8.7 \times 10^3}{T_g}\right)$	[25]
234	$C_2H + CH_4 \rightarrow C_2H_2 + CH_3$ $3.6 \times 10^{-14} \cdot T_g^{0.94} \cdot exp\left(\frac{-3.28 \times 10^2}{T_g}\right)$	[5]

#	Reaction / Rate equation	Ref.
235	$C_2H + CH_2 \rightarrow C_2H_2 + CH$ 3×10^{-11}	[25]
236	$C_2H_6 + CH_5^+ \rightarrow C_2H_5^+ + CH_4 + H_2$ 2.25×10^{-10}	[28]
237	$C_2H_4 + CH_5^+ \rightarrow C_2H_5^+ + CH_4$ 1.5×10^{-8}	[37]
238	$C_2H_2 + CH_5^+ \rightarrow C_2H_3^+ + CH_4$ 1.56×10^{-9}	[38]
239	$C_2H + CH_5^+ \rightarrow C_2H_2^+ + CH_4$ 9×10^{-10}	[1]
240	$C_2H_6 + CH_4^+ \rightarrow C_2H_4^+ + CH_4 + H_2$ 1.91×10^{-9}	[39]
241	$C_2H_4 + CH_4^+ \rightarrow C_2H_4^+ + CH_4$ 1.38×10^{-9}	[39]
242	$C_2H_4 + CH_4^+ \rightarrow C_2H_5^+ + CH_3$ 4.232×10^{-10}	[39]
243	$C_2H_2 + CH_4^+ \rightarrow C_2H_2^+ + CH_4$ 1.134×10^{-9}	[39]
244	$C_2H_2 + CH_4^+ \rightarrow C_2H_3^+ + CH_3$ 1.2348×10^{-9}	[39]
245	$C_2H_6 + CH_3^+ \rightarrow C_2H_5^+ + CH_4$ 1.479×10^{-9}	[39]
246	$C_2H_4 + CH_3^+ \rightarrow C_2H_3^+ + CH_4$ 3.496×10^{-10}	[39]
247	$C_2H_2^+ + CH_4 \rightarrow C_2H_3^+ + CH_3$ 4.1×10^{-9}	[21]
248	$C_2H^+ + CH_4 \rightarrow C_2H_2^+ + CH_3$ 3.74×10^{-10}	[9]
249	$C_2H_3 + C_2H_6 \rightarrow C_2H_4 + C_2H_5$ $1 \times 10^{-21} \cdot T_g^{3.3} \cdot exp\left(\frac{-5.285 \times 10^3}{T_g}\right)$	[25]
250	$C_2H + C_2H_6 \rightarrow C_2H_2 + C_2H_5$ $6.75 \times 10^{-12} \cdot T_g^{0.28} \cdot exp\left(\frac{6.2 \times 10^1}{T_g}\right)$	[5]
251	$C_2H_5 + C_2H_5 \rightarrow C_2H_4 + C_2H_6$ 2.3×10^{-12}	[5]
252	$C_2H_4 + C_2H_5 \rightarrow C_2H_3 + C_2H_6$ $8.1 \times 10^{-31} \cdot T_g^{5.82} \cdot exp\left(\frac{-6 \times 10^3}{T_g}\right)$	[5]
253	$C_2H_3 + C_2H_5 \rightarrow C_2H_2 + C_2H_6$ 2.3985×10^{-11}	[40, 41]
254	$C_2H_3 + C_2H_5 \rightarrow C_2H_4 + C_2H_4$ 4.42×10^{-11}	[40, 41]

#	Reaction / Rate equation	Ref.
255	$C_2H_2 + C_2H_5 \rightarrow C_2H + C_2H_6$ $4.5 \times 10^{-13} \cdot exp\left(\frac{-1.18 \times 10^4}{T_g}\right)$	[25]
256	$C_2H + C_2H_5 \rightarrow C_2H_2 + C_2H_4$ 3×10^{-12}	[25]
257	$C_2H_4 + C_2H_4 \rightarrow C_2H_3 + C_2H_5$ $8 \times 10^{-10} \cdot exp\left(\frac{-3.6 \times 10^4}{T_g}\right)$	[25]
258	$C_2H_2 + C_2H_4 \rightarrow C_2H_3 + C_2H_3$ $4 \times 10^{-11} \cdot exp\left(\frac{-3.44 \times 10^4}{T_g}\right)$	[25]
259	$C_2H + C_2H_4 \rightarrow C_2H_2 + C_2H_3$ $3.35 \times 10^{-18} \cdot T_g^{2.24}$	[42]
260	$C_2H_3 + C_2H_3 \rightarrow C_2H_2 + C_2H_4$ 1.6×10^{-12}	[25]
261	$C_2H + C_2H_3 \rightarrow C_2H_2 + C_2H_2$ 1.6×10^{-12}	[25]
262	$C_2H_2 + C_2H_2 \rightarrow C_2H + C_2H_3$ $1.6 \times 10^{-11} \cdot exp\left(\frac{-4.25 \times 10^4}{T_g}\right)$	[25]
263	$C_2H_4 + C_2H_6^+ \rightarrow C_2H_4^+ + C_2H_6$ 1.15×10^{-9}	[39]
264	$C_2H_2 + C_2H_6^+ \rightarrow C_2H_3 + C_2H_5^+$ 2.223×10^{-10}	[39]
265	$C_2H_3^+ + C_2H_6 \rightarrow C_2H_4 + C_2H_5^+$ 2.914×10^{-10}	[39]
266	$C_2H_3^+ + C_2H_4 \rightarrow C_2H_2 + C_2H_5^+$ 9.3×10^{-10}	[39]
267	$C_2H_2^+ + C_2H_6 \rightarrow C_2H_3 + C_2H_5^+$ 1.314×10^{-10}	[39]
268	$C_2H_2^+ + C_2H_6 \rightarrow C_2H_4 + C_2H_4^+$ 2.628×10^{-10}	[39]
269	$C_2H_2^+ + C_2H_4 \rightarrow C_2H_2 + C_2H_4^+$ 4.012×10^{-10}	[39]
270	$C_2H + e \rightarrow C_2H^+ + e + e$ $f(\sigma)$	[23, 43]
271	$C_2H_2 + e \rightarrow C_2H_2^+ + e + e$ $f(\sigma)$	[23, 43]
272	$C_2H_3 + e \rightarrow C_2H_3^+ + e + e$ $f(\sigma)$	[23, 43]
273	$C_2H_4 + e \rightarrow C_2H_4^+ + e + e$ $f(\sigma)$	[23, 43]

#	Reaction / Rate equation	Ref.
274	$C_2H_5 + e \rightarrow C_2H_5^+ + e + e$ $f(\sigma)$	[23, 43]
275	$C_2H_6 + e \rightarrow C_2H_6^+ + e + e$ $f(\sigma)$	[23, 43]
276	$C_2H + e \rightarrow C + CH^+ + e + e$ $f(\sigma)$	[23, 43]
277	$C_2H + e \rightarrow CH + C^+ + e + e$ $f(\sigma)$	[23, 43]
278	$C_2H_2 + e \rightarrow C_2H^+ + e + e + H$ $f(\sigma)$	[23, 43]
279	$C_2H_2 + e \rightarrow C_2H + e + e + H^+$ $f(\sigma)$	[23, 43]
280	$C_2H_3 + e \rightarrow C_2H_2^+ + e + e + H$ $f(\sigma)$	[23, 43]
281	$C_2H_3 + e \rightarrow C_2H^+ + e + e + H_2$ $f(\sigma)$	[23, 43]
282	$C_2H_3 + e \rightarrow C_2H^+ + e + e + H + H$ $f(\sigma)$	[23, 43]
283	$C_2H_3 + e \rightarrow CH + CH_2^+ + e + e$ $f(\sigma)$	[23, 43]
284	$C_2H_3 + e \rightarrow CH_2 + CH^+ + e + e$ $f(\sigma)$	[23, 43]
285	$C_2H_3 + e \rightarrow CH_3 + C^+ + e + e$ $f(\sigma)$	[23, 43]
286	$C_2H_3 + e \rightarrow C_2H_2 + e + e + H^+$ $f(\sigma)$	[23, 43]
287	$C_2H_4 + e \rightarrow C_2H_3^+ + e + e + H$ $f(\sigma)$	[23, 43]
288	$C_2H_4 + e \rightarrow C_2H_2^+ + e + e + H_2$ $f(\sigma)$	[23, 43]
289	$C_2H_4 + e \rightarrow C_2H_2^+ + e + e + H + H$ $f(\sigma)$	[23, 43]
290	$C_2H_4 + e \rightarrow C_2H^+ + e + e + H + H + H$ $f(\sigma)$	[23, 43]
291	$C_2H_4 + e \rightarrow CH + CH_3^+ + e + e$ $f(\sigma)$	[23, 43]
292	$C_2H_4 + e \rightarrow CH_2 + CH_2^+ + e + e$ $f(\sigma)$	[23, 43]
293	$C_2H_4 + e \rightarrow CH_3 + CH^+ + e + e$ $f(\sigma)$	[23, 43]
294	$C_2H_4 + e \rightarrow CH_4 + C^+ + e + e$ $f(\sigma)$	[23, 43]

#	Reaction / Rate equation	Ref.
295	$C_2H_5 + e \rightarrow C_2H_4^+ + e + e + H$ $f(\sigma)$	[23, 43]
296	$C_2H_5 + e \rightarrow C_2H_3^+ + e + e + H_2$ $f(\sigma)$	[23, 43]
297	$C_2H_5 + e \rightarrow C_2H_3^+ + e + e + H + H$ $f(\sigma)$	[23, 43]
298	$C_2H_5 + e \rightarrow C_2H_2^+ + e + e + H + H_2$ $f(\sigma)$	[23, 43]
299	$C_2H_5 + e \rightarrow C_2H^+ + e + e + H_2 + H_2$ $f(\sigma)$	[23, 43]
300	$C_2H_5 + e \rightarrow CH_2 + CH_3^+ + e + e$ $f(\sigma)$	[23, 43]
301	$C_2H_5 + e \rightarrow CH_2^+ + CH_3 + e + e$ $f(\sigma)$	[23, 43]
302	$C_2H_5 + e \rightarrow CH_4 + CH^+ + e + e$ $f(\sigma)$	[23, 43]
303	$C_2H_5 + e \rightarrow CH_4 + C^+ + e + e + H$ $f(\sigma)$	[23, 43]
304	$C_2H_5 + e \rightarrow CH_3 + C^+ + e + e + H_2$ $f(\sigma)$	[23, 43]
305	$C_2H_6 + e \rightarrow C_2H_5^+ + e + e + H$ $f(\sigma)$	[23, 43]
306	$C_2H_6 + e \rightarrow C_2H_4^+ + e + e + H_2$ $f(\sigma)$	[23, 43]
307	$C_2H_6 + e \rightarrow C_2H_3^+ + e + e + H + H_2$ $f(\sigma)$	[23, 43]
308	$C_2H_6 + e \rightarrow C_2H_2^+ + e + e + H_2 + H_2$ $f(\sigma)$	[23, 43]
309	$C_2H_6 + e \rightarrow C_2H_2^+ + e + e + H + H + H_2$ $f(\sigma)$	[23, 43]
310	$C_2H_6 + e \rightarrow CH_3 + CH_3^+ + e + e$ $f(\sigma)$	[23, 43]
311	$C_2H_6 + e \rightarrow C_2H_4 + e + e + H_2^+$ $f(\sigma)$	[23, 43]
312	$C_2H_6 + e \rightarrow C_2H_2 + e + H_2 + H_2$ $f(\sigma)$	[23, 43]
313	$C_2H_6 + e \rightarrow C_2H_5 + e + H$ $f(\sigma)$	[23, 43]
314	$C_2H_6 + e \rightarrow CH_2 + CH_4 + e$ $f(\sigma)$	[23, 43]
315	$C_2H_6 + e \rightarrow C_2H_4 + e + H_2$ $f(\sigma)$	[23, 43]

#	Reaction / Rate equation	Ref.
316	$C_2H_6 + e \rightarrow C_2H_3 + e + H + H_2$ $f(\sigma)$	[23, 43]
317	$C_2H_6 + e \rightarrow CH_3 + CH_3 + e$ $f(\sigma)$	[23, 43]
318	$C_2H_5 + e \rightarrow CH_2 + CH_3 + e$ $f(\sigma)$	[23, 43]
319	$C_2H_5 + e \rightarrow C_2H_3 + e + H_2$ $f(\sigma)$	[23, 43]
320	$C_2H_5 + e \rightarrow C_2H_4 + e + H$ $f(\sigma)$	[23, 43]
321	$C_2H_5 + e \rightarrow C_2H + e + H_2 + H_2$ $f(\sigma)$	[23, 43]
322	$C_2H_5 + e \rightarrow C_2H_2 + e + H + H_2$ $f(\sigma)$	[23, 43]
323	$C_2H_5 + e \rightarrow CH + CH_4 + e$ $f(\sigma)$	[23, 43]
324	$C_2H_5 + e \rightarrow C_2H_3 + e + H + H$ $f(\sigma)$	[23, 43]
325	$C_2H_4 + e \rightarrow C + CH_4 + e$ $f(\sigma)$	[23, 43]
326	$C_2H_4 + e \rightarrow C_2H_2 + e + H + H$ $f(\sigma)$	[23, 43]
327	$C_2H_4 + e \rightarrow C_2H_2 + e + H_2$ $f(\sigma)$	[23, 43]
328	$C_2H_4 + e \rightarrow C_2H + e + H + H_2$ $f(\sigma)$	[23, 43]
329	$C_2H_4 + e \rightarrow CH + CH_3 + e$ $f(\sigma)$	[23, 43]
330	$C_2H_4 + e \rightarrow CH_2 + CH_2 + e$ $f(\sigma)$	[23, 43]
331	$C_2H_4 + e \rightarrow C_2H_3 + e + H$ $f(\sigma)$	[23, 43]
332	$C_2H_3 + e \rightarrow C_2H + e + H_2$ $f(\sigma)$	[23, 43]
333	$C_2H_3 + e \rightarrow CH + CH_2 + e$ $f(\sigma)$	[23, 43]
334	$C_2H_3 + e \rightarrow C_2H_2 + e + H$ $f(\sigma)$	[23, 43]
335	$C_2H_3 + e \rightarrow C + CH_3 + e$ $f(\sigma)$	[23, 43]
336	$C_2H_3 + e \rightarrow C_2H + e + H + H$ $f(\sigma)$	[23, 43]

#	Reaction / Rate equation	Ref.
337	$C_2H_2 + e \rightarrow C + CH_2 + e$ $f(\sigma)$	[23, 43]
338	$C_2H_2 + e \rightarrow C_2H + e + H$ $f(\sigma)$	[23, 43]
339	$C_2H_2 + e \rightarrow CH + CH + e$ $f(\sigma)$	[23, 43]
340	$C_2H + e \rightarrow C + CH + e$ $f(\sigma)$	[23, 43]
341	$C_2H^+ + e \rightarrow C + CH^+ + e$ $f(\sigma)$	[23, 43]
342	$C_2H^+ + e \rightarrow CH + C^+ + e$ $f(\sigma)$	[23, 43]
343	$C_2H_2^+ + e \rightarrow C_2H^+ + e + H$ $f(\sigma)$	[23, 43]
344	$C_2H_2^+ + e \rightarrow C_2H + e + H^+$ $f(\sigma)$	[23, 43]
345	$C_2H_2^+ + e \rightarrow CH_2 + C^+ + e$ $f(\sigma)$	[23, 43]
346	$C_2H_2^+ + e \rightarrow CH + CH^+ + e$ $f(\sigma)$	[23, 43]
347	$C_2H_2^+ + e \rightarrow C + CH_2^+ + e$ $f(\sigma)$	[23, 43]
348	$C_2H_3^+ + e \rightarrow CH_2 + CH^+ + e$ $f(\sigma)$	[23, 43]
349	$C_2H_3^+ + e \rightarrow C_2H_2 + e + H^+$ $f(\sigma)$	[23, 43]
350	$C_2H_3^+ + e \rightarrow C_2H + e + H_2^+$ $f(\sigma)$	[23, 43]
351	$C_2H_3^+ + e \rightarrow C_2H^+ + e + H_2$ $f(\sigma)$	[23, 43]
352	$C_2H_3^+ + e \rightarrow C + CH_3^+ + e$ $f(\sigma)$	[23, 43]
353	$C_2H_3^+ + e \rightarrow C_2H_2^+ + e + H$ $f(\sigma)$	[23, 43]
354	$C_2H_3^+ + e \rightarrow CH + CH_2^+ + e$ $f(\sigma)$	[23, 43]
355	$C_2H_3^+ + e \rightarrow CH_3 + C^+ + e$ $f(\sigma)$	[23, 43]
356	$C_2H_4^+ + e \rightarrow CH + CH_3^+ + e$ $f(\sigma)$	[23, 43]
357	$C_2H_4^+ + e \rightarrow CH_2 + CH_2^+ + e$ $f(\sigma)$	[23, 43]

#	Reaction / Rate equation	Ref.
358	$C_2H_4^+ + e \rightarrow CH_3 + CH^+ + e$ $f(\sigma)$	[23, 43]
359	$C_2H_4^+ + e \rightarrow CH_4 + C^+ + e$ $f(\sigma)$	[23, 43]
360	$C_2H_4^+ + e \rightarrow C_2H_2 + e + H_2^+$ $f(\sigma)$	[23, 43]
361	$C_2H_4^+ + e \rightarrow C_2H_2^+ + e + H_2$ $f(\sigma)$	[23, 43]
362	$C_2H_4^+ + e \rightarrow C_2H_3^+ + e + H$ $f(\sigma)$	[23, 43]
363	$C_2H_5^+ + e \rightarrow C_2H_3^+ + e + H + H$ $f(\sigma)$	[23, 43]
364	$C_2H_5^+ + e \rightarrow CH_2^+ + CH_3 + e$ $f(\sigma)$	[23, 43]
365	$C_2H_5^+ + e \rightarrow C_2H_3^+ + e + H_2$ $f(\sigma)$	[23, 43]
366	$C_2H_5^+ + e \rightarrow C_2H_4^+ + e + H$ $f(\sigma)$	[23, 43]
367	$C_2H_5^+ + e \rightarrow CH_2 + CH_3^+ + e$ $f(\sigma)$	[23, 43]
368	$C_2H_6^+ + e \rightarrow CH_3 + CH_3^+ + e$ $f(\sigma)$	[23, 43]
369	$C_2H_6^+ + e \rightarrow C_2H_4^+ + e + H_2$ $f(\sigma)$	[23, 43]
370	$C_2H_6^+ + e \rightarrow C_2H_5^+ + e + H$ $f(\sigma)$	[23, 43]
371	$C_2H_6^+ + e \rightarrow C_2H_5 + H$ $f(\sigma)$	[23, 43]
372	$C_2H_6^+ + e \rightarrow CH_2 + CH_2 + H_2$ $f(\sigma)$	[23, 43]
373	$C_2H_6^+ + e \rightarrow C_2H_4 + H + H$ $f(\sigma)$	[23, 43]
374	$C_2H_6^+ + e \rightarrow CH_2 + CH_3 + H$ $f(\sigma)$	[23, 43]
375	$C_2H_6^+ + e \rightarrow CH_2 + CH_4$ $f(\sigma)$	[23, 43]
376	$C_2H_6^+ + e \rightarrow C_2H_4 + H_2$ $f(\sigma)$	[23, 43]
377	$C_2H_6^+ + e \rightarrow C_2H_3 + H + H_2$ $f(\sigma)$	[23, 43]
378	$C_2H_6^+ + e \rightarrow CH_3 + CH_3$ $f(\sigma)$	[23, 43]

#	Reaction / Rate equation	Ref.
379	$C_2H_5^+ + e \rightarrow C_2H_2 + H + H + H$ $f(\sigma)$	[23, 43]
380	$C_2H_5^+ + e \rightarrow C_2H_3 + H_2$ $f(\sigma)$	[23, 43]
381	$C_2H_5^+ + e \rightarrow CH_2 + CH_3$ $f(\sigma)$	[23, 43]
382	$C_2H_5^+ + e \rightarrow C_2H_4 + H$ $f(\sigma)$	[23, 43]
383	$C_2H_5^+ + e \rightarrow C_2H_2 + H + H_2$ $f(\sigma)$	[23, 43]
384	$C_2H_5^+ + e \rightarrow CH + CH_4$ $f(\sigma)$	[23, 43]
385	$C_2H_5^+ + e \rightarrow C_2H_3 + H + H$ $f(\sigma)$	[23, 43]
386	$C_2H_4^+ + e \rightarrow CH + CH_3$ $f(\sigma)$	[23, 43]
387	$C_2H_4^+ + e \rightarrow C_2H_2 + H + H$ $f(\sigma)$	[23, 43]
388	$C_2H_4^+ + e \rightarrow C + CH_4$ $f(\sigma)$	[23, 43]
389	$C_2H_4^+ + e \rightarrow C_2H_2 + H_2$ $f(\sigma)$	[23, 43]
390	$C_2H_4^+ + e \rightarrow C_2H + H + H_2$ $f(\sigma)$	[23, 43]
391	$C_2H_4^+ + e \rightarrow CH_2 + CH_2$ $f(\sigma)$	[23, 43]
392	$C_2H_4^+ + e \rightarrow C_2H_3 + H$ $f(\sigma)$	[23, 43]
393	$C_2H_3^+ + e \rightarrow C_2H + H_2$ $f(\sigma)$	[23, 43]
394	$C_2H_3^+ + e \rightarrow C + CH_3$ $f(\sigma)$	[23, 43]
395	$C_2H_3^+ + e \rightarrow CH + CH_2$ $f(\sigma)$	[23, 43]
396	$C_2H_3^+ + e \rightarrow C_2H_2 + H$ $f(\sigma)$	[23, 43]
397	$C_2H_3^+ + e \rightarrow C_2H + H + H$ $f(\sigma)$	[23, 43]
398	$C_2H_2^+ + e \rightarrow C_2H + H$ $f(\sigma)$	[23, 43]
399	$C_2H_2^+ + e \rightarrow CH + CH$ $f(\sigma)$	[23, 43]

#	Reaction / Rate equation	Ref.
400	$C_2H_2^+ + e \rightarrow C + CH_2$ $f(\sigma)$	[23, 43]
401	$C_2H^+ + e \rightarrow C + CH$ $f(\sigma)$	[23, 43]
402	$C_2H^+ + e \rightarrow C + C + H$ $f(\sigma)$	[23, 43]
403	$C_2H_6 \rightarrow CH_3 + CH_3$ $k_0 = 2.6 \times 10^{25} \cdot T_g^{-8.37} \cdot exp\left(\frac{-4.729 \times 10^4}{T_g}\right)$ $k_\infty = 4.5 \times 10^{21} \cdot T_g^{-1.37} \cdot exp\left(\frac{-4.59 \times 10^4}{T_g}\right)$ $F_c = 0.38 \cdot exp\left(\frac{-T_g}{7.3 \times 10^1}\right)$ $+0.62 \cdot exp\left(\frac{-T_g}{1.18 \times 10^3}\right)$	[5]a
404	$C_2H_6 \rightarrow C_2H_5 + H$ $k_0 = \frac{10^{4.2839 \times 10^1}}{n_M} \cdot T_g^{-6.431} \cdot exp\left(\frac{-5.3938 \times 10^4}{T_g}\right)$ $k_\infty = 10^{2.0947 \times 10^1} \cdot T_g^{-1.228} \cdot exp\left(\frac{-5.1439 \times 10^4}{T_g}\right)$ $F_c = 4.761 \times 10^1 \cdot exp\left(\frac{-1.6182 \times 10^4}{T_g}\right)$ $+exp\left(\frac{-T_g}{3.371 \times 10^3}\right)$	[44]a
405	$C_2H_5 \rightarrow C_2H_4 + H$ $k_0 = 1.7 \times 10^{-6} \cdot exp\left(\frac{-1.68 \times 10^4}{T_g}\right)$ $k_\infty = 8.2 \times 10^{13} \cdot exp\left(\frac{-2.007 \times 10^4}{T_g}\right)$ $F_c = 0.25 \cdot exp\left(\frac{-T_g}{9.7 \times 10^1}\right)$ $+0.75 \cdot exp\left(\frac{-T_g}{1.379 \times 10^3}\right)$	[5]a
406	$C_2H_4 \rightarrow C_2H_3 + H$ $10^{1.63 \times 10^1} \cdot exp\left(\frac{-4.6 \times 10^5}{R \cdot T_g}\right)$	[45]
407	$C_2H_4 \rightarrow C_2H_2 + H_2$ $10^{1.29 \times 10^1} \cdot T_g^{0.44} \cdot exp\left(\frac{-4.467 \times 10^4}{T_g}\right)$	[25]
408	$C_2H_3 \rightarrow C_2H_2 + H$ $k_0 = 4.3 \times 10^3 \cdot T_g^{-3.4} \cdot exp\left(\frac{-1.802 \times 10^4}{T_g}\right)$ $k_\infty = 3.9 \times 10^8 \cdot T_g^{1.62} \cdot exp\left(\frac{-1.865 \times 10^4}{T_g}\right)$ $F_c = 7.37 \times 10^{-4} \cdot T_g^{0.8}$	[5]a

#	Reaction / Rate equation	Ref.
409	$C_2H_2 \rightarrow C_2H + H$ $10^{1.542\times10^{1}} \cdot exp\left(\frac{-6.2445\times10^{4}}{T_g}\right)$	[25]
410	$e + H_2O \rightarrow e + e + H_2O^+$ $f(\sigma)$	[46, 47]
411	$e + H_2O \rightarrow H_2 + O^-$ $f(\sigma)$	[46, 48]
412	$e + H_2O \rightarrow H^- + OH$ $f(\sigma)$	[46, 48]
413	$e + H_2O \rightarrow e + H + OH$ $f(\sigma)$	[48]
414	$e + H_2O \rightarrow e + e + H^+ + OH$ $f(\sigma)$	[46, 47]
415	$e + H_2O \rightarrow e + e + H + OH^+$ $f(\sigma)$	[46, 47]
416	$e + H_2O \rightarrow e + e + H_2 + O^+$ $f(\sigma)$	[46, 47]
417	$e + H_2O \rightarrow e + e + H_2^+ + O$ $f(\sigma)$	[46, 47]
418	$e + H_2O \rightarrow H + OH^-$ $f(\sigma)$	[46, 47]
419	$e + H_2O_2 \rightarrow H_2O + O^-$ $f(\sigma)$	[49]
420	$e + H_2O_2 \rightarrow OH + OH^-$ $f(\sigma)$	[49]
421	$e + OH^- \rightarrow e + e + OH$ $f(\sigma)$	[46]
422	$e + OH \rightarrow e + H + O$ $2.55\times10^{-4} \cdot T_e^{-0.76} \cdot exp\left(\frac{-8.01074\times10^{4}}{T_e}\right)$	[50]
423	$e + OH \rightarrow e + e + OH^+$ $1.16\times10^{-17} \cdot T_e^{1.78} \cdot exp\left(\frac{-1.602671\times10^{5}}{T_e}\right)$	[50]
424	$M + e + OH \rightarrow M + OH^-$ 3×10^{-31}	[51]
425	$e + OH^+ \rightarrow H + O$ $3.19\times10^{4} \cdot T_e^{-2.04} \cdot exp\left(\frac{-1.754618\times10^{5}}{T_e}\right)$	[50]
426	$e + H_2O^+ \rightarrow H_2 + O$ $3.9\times10^{-8} \cdot \left(\frac{T_e}{3.0\times10^{2}}\right)^{-0.5}$	[3]
427	$e + H_2O^+ \rightarrow H + H + O$ $3.05\times10^{-7} \cdot \left(\frac{T_e}{3.0\times10^{2}}\right)^{-0.5}$	[3]

#	Reaction / Rate equation	Ref.
428	$e + H_2O^+ \rightarrow H + OH$ $8.6 \times 10^{-8} \cdot \left(\frac{T_e}{3.0 \times 10^2}\right)^{-0.5}$	[3]
429	$e + H_3O^+ \rightarrow H + H + OH$ $3.05 \times 10^{-7} \cdot \left(\frac{T_e}{3.0 \times 10^2}\right)^{-0.5}$	[3]
430	$e + H_3O^+ \rightarrow H + H_2O$ $7.09 \times 10^{-8} \cdot \left(\frac{T_e}{3.0 \times 10^2}\right)^{-0.5}$	[3]
431	$e + H_3O^+ \rightarrow H + H_2 + O$ $5.6 \times 10^{-9} \cdot \left(\frac{T_e}{3.0 \times 10^2}\right)^{-0.5}$	[3]
432	$e + H_3O^+ \rightarrow H_2 + OH$ $5.37 \times 10^{-8} \cdot \left(\frac{T_e}{3.0 \times 10^2}\right)^{-0.5}$	[3]
433	$O_2^- + OH \rightarrow O_2 + OH^-$ 1×10^{-10}	[51]
434	$OH + O^+ \rightarrow O + OH^+$ 3.6×10^{-10}	[1]
435	$OH + O^+ \rightarrow H + O_2^+$ 3.6×10^{-10}	[1]
436	$H_2^+ + OH \rightarrow H_2 + OH^+$ 7.6×10^{-10}	[1]
437	$H_2^+ + OH \rightarrow H + H_2O^+$ 7.6×10^{-10}	[1]
438	$H^+ + OH \rightarrow H + OH^+$ 2.1×10^{-9}	[1]
439	$O + OH \rightarrow H + O_2$ $4.33 \times 10^{-11} \cdot \left(\frac{T_g}{3.0 \times 10^2}\right)^{-0.5} \cdot exp\left(\frac{-3.0 \times 10^1}{T_g}\right)$	[25]
440	$H + OH \rightarrow H_2 + O$ $4.1 \times 10^{-12} \cdot \frac{T_g}{3.0 \times 10^2} \cdot exp\left(\frac{-3.50 \times 10^3}{T_g}\right)$	[52]
441	$OH + OH \rightarrow H_2O + O$ $1.02 \times 10^{-12} \cdot \left(\frac{T_g}{3.0 \times 10^2}\right)^{1.4} \cdot exp\left(\frac{2.0 \times 10^2}{T_g}\right)$	[25]
442	$OH + OH \rightarrow H + HO_2$ $2 \times 10^{-11} \cdot exp\left(\frac{-2.020 \times 10^4}{T_g}\right)$	[52]
443	$OH + OH \rightarrow H_2 + O_2$ $1.82 \times 10^{-13} \cdot T_g^{0.51} \cdot exp\left(\frac{-2.54 \times 10^4}{T_g}\right)$	[53]

#	Reaction / Rate equation	Ref.
444	$M + OH \rightarrow M + H + O$ $4.7 \times 10^{-8} \cdot \left(\frac{T_g}{3.0 \times 10^2}\right)^{-1.0} \cdot exp\left(\frac{-5.0830 \times 10^4}{T_g}\right)$	[52]
445	$H_2 + OH \rightarrow H + H_2O$ $3.6 \times 10^{-16} \cdot T_g^{1.52} \cdot exp\left(\frac{-1.74 \times 10^3}{T_g}\right)$	[5]
446	$O_2 + OH \rightarrow H + O_3$ $2.7 \times 10^{-13} \cdot \left(\frac{T_g}{3.0 \times 10^2}\right)^{1.44} \cdot exp\left(\frac{-3.860 \times 10^4}{T_g}\right)$	[52]
447	$O_2 + OH \rightarrow HO_2 + O$ $2.2 \times 10^{-11} \cdot exp\left(\frac{-2.820 \times 10^4}{T_g}\right)$	[52]
448	$O_3 + OH \rightarrow HO_2 + O_2$ $1.69 \times 10^{-12} \cdot exp\left(\frac{-9.410 \times 10^2}{T_g}\right)$	[54]
449	$H_2O + OH \rightarrow H + H_2O_2$ $4 \times 10^{-10} \cdot exp\left(\frac{-4.050 \times 10^4}{T_g}\right)$	[52]
450	$HO_2 + OH \rightarrow H_2O + O_2$ $8.05 \times 10^{-11} \cdot \left(\frac{T_g}{3.0 \times 10^2}\right)^{-1.0}$	[25]
451	$HO_2 + OH \rightarrow H_2O_2 + O$ $1.5 \times 10^{-12} \cdot \left(\frac{T_g}{3.0 \times 10^2}\right)^{0.5} \cdot exp\left(\frac{-1.060 \times 10^4}{T_g}\right)$	[52]
452	$H_2O_2 + OH \rightarrow H_2O + HO_2$ $2.9 \times 10^{-12} \cdot exp\left(\frac{-1.60 \times 10^2}{T_g}\right)$	[25]
453	$O + OH^+ \rightarrow H + O_2^+$ 7.1×10^{-10}	[1]
454	$O_2 + OH^+ \rightarrow O_2^+ + OH$ 3.8×10^{-10}	[27]
455	$H_2O + OH^+ \rightarrow H_2O^+ + OH$ 1.5895×10^{-9}	[27]
456	$H_2O + OH^+ \rightarrow H_3O^+ + O$ 1.3005×10^{-9}	[27]
457	$M + OH^- \rightarrow M + e + OH$ $2 \times 10^{-10} \cdot \left(\frac{T_g}{3 \times 10^2}\right)^{0.5}$	c
458	$H + OH^- \rightarrow e + H_2O$ 1.8×10^{-9}	[55]
459	$O + OH^- \rightarrow e + HO_2$ 2×10^{-10}	[56]

#	Reaction / Rate equation	Ref.
460	$O_2 + OH^- \rightarrow O_2^- + OH$ $8.7 \times 10^{-10} \cdot exp\left(\frac{-1.663 \times 10^4}{T_g}\right)$	[51]
461	$O_3 + OH^- \rightarrow O_3^- + OH$ 9×10^{-10}	[56]
462	$O_3 + OH^- \rightarrow HO_2 + O_2^-$ 1.08×10^{-11}	[57]
463	$OH^- + OH^+ \rightarrow H + H + O + O$ 1×10^{-7}	[57]
464	$M + OH^- + OH^+ \rightarrow M + OH + OH$ $2 \times 10^{-25} \cdot \left(\frac{T_g}{3.0 \times 10^2}\right)^{-2.5}$	[57]
465	$OH^- + OH^+ \rightarrow H + O + OH$ 1×10^{-7}	[57]
466	$OH^- + O^+ \rightarrow H + O + O$ 1×10^{-7}	[57]
467	$OH^- + O^+ \rightarrow O + OH$ $2 \times 10^{-7} \cdot \left(\frac{T_g}{3.0 \times 10^2}\right)^{-0.5}$	[57]
468	$M + OH^- + O^+ \rightarrow M + HO_2$ $2 \times 10^{-25} \cdot \left(\frac{T_g}{3.0 \times 10^2}\right)^{-2.5}$	[57]
469	$O_2^+ + OH^- \rightarrow H + O + O_2$ 1×10^{-7}	[57]
470	$O_2^+ + OH^- \rightarrow O_2 + OH$ 2×10^{-7}	[57]
471	$O_2^+ + OH^- \rightarrow O + O + OH$ 1×10^{-7}	[57]
472	$M + O_2^+ + OH^- \rightarrow M + O_2 + OH$ $2 \times 10^{-25} \cdot \left(\frac{T_g}{3.0 \times 10^2}\right)^{-2.5}$	[57]
473	$M + H_2O^+ + OH^- \rightarrow M + H_2O + OH$ $2 \times 10^{-25} \cdot \left(\frac{T_g}{3.0 \times 10^2}\right)^{-2.5}$	[57]
474	$H^+ + OH^- \rightarrow H + OH$ $7.51 \times 10^{-8} \cdot \left(\frac{T_g}{3 \times 10^2}\right)^{-0.5}$	[2, 3]
475	$H_3^+ + OH^- \rightarrow H + H_2 + OH$ $7.51 \times 10^{-8} \cdot \left(\frac{T_g}{3 \times 10^2}\right)^{-0.5}$	[2, 3]
476	$H_3O^+ + OH^- \rightarrow H + H_2O + OH$ $7.51 \times 10^{-8} \cdot \left(\frac{T_g}{3 \times 10^2}\right)^{-0.5}$	[2, 3]

#	Reaction / Rate equation	Ref.
477	$H + HO_2 \rightarrow H_2 + O_2$ $1.1 \times 10^{-10} \cdot exp\left(\frac{-1.070 \times 10^3}{T_g}\right)$	[25]
478	$H + HO_2 \rightarrow OH + OH$ $2.8 \times 10^{-10} \cdot exp\left(\frac{-4.40 \times 10^2}{T_g}\right)$	[25]
479	$H + HO_2 \rightarrow H_2O + O$ $5 \times 10^{-11} \cdot exp\left(\frac{-8.660 \times 10^2}{T_g}\right)$	[58]
480	$H_2O + HO_2 \rightarrow H_2O_2 + OH$ $3 \times 10^{-11} \cdot exp\left(\frac{-1.510 \times 10^4}{T_g}\right)$	[52]
481	$H_2 + HO_2 \rightarrow H_2O + OH$ $1.1 \times 10^{-12} \cdot exp\left(\frac{-9.40 \times 10^3}{T_g}\right)$	[52]
482	$H_2 + HO_2 \rightarrow H + H_2O_2$ $1 \times 10^{-12} \cdot exp\left(\frac{-9.30 \times 10^3}{T_g}\right)$	[52]
483	$HO_2 + HO_2 \rightarrow H_2O_2 + O_2$ $2.2 \times 10^{-13} \cdot exp\left(\frac{6.0 \times 10^2}{T_g}\right)$	[59]
484	$HO_2 + O \rightarrow O_2 + OH$ $2.9 \times 10^{-11} \cdot exp\left(\frac{2.0 \times 10^2}{T_g}\right)$	[25]
485	$HO_2 + O_2 \rightarrow O_3 + OH$ 1.5×10^{-15}	[52]
486	$H + H_2O_2 \rightarrow H_2 + HO_2$ $8 \times 10^{-11} \cdot exp\left(\frac{-4.0 \times 10^3}{T_g}\right)$	[25]
487	$H + H_2O_2 \rightarrow H_2O + OH$ $4 \times 10^{-11} \cdot exp\left(\frac{-2.0 \times 10^3}{T_g}\right)$	[25]
488	$H_2O_2 + O \rightarrow HO_2 + OH$ $1.44 \times 10^{-12} \cdot \left(\frac{T_g}{3.0 \times 10^2}\right)^{2.0} \cdot exp\left(\frac{-2.0 \times 10^3}{T_g}\right)$	[25]
489	$H_2O_2 \rightarrow OH + OH$ $k_0 = 3.8 \times 10^{-8} \cdot exp\left(\frac{-2.196 \times 10^4}{T_g}\right)$ $k_\infty = 3 \times 10^{14} \cdot exp\left(\frac{-2.44 \times 10^4}{T_g}\right)$ $F_c = 0.5$	[5][a]
490	$H_2O_2 + O_2 \rightarrow HO_2 + HO_2$ $5 \times 10^{-11} \cdot exp\left(\frac{-2.160 \times 10^4}{T_g}\right)$	[52]

#	Reaction / Rate equation	Ref.
491	$H_2O + O^- \rightarrow OH + OH^-$ 3×10^{-13}	[56]
492	$H_2O + O^- \rightarrow e + H_2O_2$ 3×10^{-13}	[56]
493	$H_2O + H^- \rightarrow H_2 + OH^-$ 3.7×10^{-9}	[56]
494	$H_2O + O^+ \rightarrow H_2O^+ + O$ 2.2×10^{-9}	[29]
495	$H_2O + H_2O^+ \rightarrow H_3O^+ + OH$ 1.67×10^{-9}	[56, 60]
496	$H_2O + H^+ \rightarrow H + H_2O^+$ 6.9×10^{-9}	[29]
497	$H_2O + O \rightarrow OH + OH$ $7.6 \times 10^{-15} \cdot T_g^{1.3} \cdot exp\left(\frac{-8.6 \times 10^3}{T_g}\right)$	[25]
498	$M + H_2O \rightarrow M + H + OH$ $5.9 \times 10^{-7} \cdot \left(\frac{T_g}{3.0 \times 10^2}\right)^{-2.2} \cdot exp\left(\frac{-5.90 \times 10^4}{T_g}\right)$	[52]
499	$H + H_2O \rightarrow H_2 + OH$ $7.5 \times 10^{-16} \cdot T_g^{1.6} \cdot exp\left(\frac{-9.03 \times 10^3}{T_g}\right)$	[5]
500	$H_2O + OH \rightarrow H_2 + HO_2$ $1.4 \times 10^{-13} \cdot exp\left(\frac{-3.610 \times 10^4}{T_g}\right)$	[52]
501	$H_2O + O \rightarrow H + HO_2$ $2.8 \times 10^{-12} \cdot \left(\frac{T_g}{3.0 \times 10^2}\right)^{0.37} \cdot exp\left(\frac{-2.87430 \times 10^4}{T_g}\right)$	[52]
502	$H_2O + O_2 \rightarrow H_2O_2 + O$ $9.8 \times 10^{-8} \cdot \left(\frac{T_g}{3.0 \times 10^2}\right)^{0.5} \cdot exp\left(\frac{-4.480 \times 10^4}{T_g}\right)$	[52]
503	$H_2O + O_2 \rightarrow HO_2 + OH$ $4.3 \times 10^{-12} \cdot \left(\frac{T_g}{3.0 \times 10^2}\right)^{0.5} \cdot exp\left(\frac{-3.660 \times 10^4}{T_g}\right)$	[52]
504	$H_2 + H_2O^+ \rightarrow H + H_3O^+$ 6.4×10^{-10}	[61]
505	$H_2O^+ + O_2 \rightarrow H_2O + O_2^+$ 2×10^{-10}	[56]
506	$H_2O^+ + O^- \rightarrow H_2O + O$ $2 \times 10^{-7} \cdot \left(\frac{T_g}{3.0 \times 10^2}\right)^{-0.5}$	[57]
507	$H_2O^+ + O_2^- \rightarrow H_2O + O_2$ $2 \times 10^{-7} \cdot \left(\frac{T_g}{3.0 \times 10^2}\right)^{-0.5}$	[57]

#	Reaction / Rate equation	Ref.
508	$H_2O^+ + O_3^- \rightarrow H_2O + O_3$ $2 \times 10^{-7} \cdot \left(\frac{T_g}{3.0 \times 10^2}\right)^{-0.5}$	[57]
509	$M + H_2O^+ + O^- \rightarrow M + H_2O + O$ $2 \times 10^{-25} \cdot \left(\frac{T_g}{3.0 \times 10^2}\right)^{-2.5}$	[57]
510	$M + H_2O^+ + O^- \rightarrow M + H_2O_2$ $2 \times 10^{-25} \cdot \left(\frac{T_g}{3.0 \times 10^2}\right)^{-2.5}$	[57]
511	$M + H_2O^+ + O_3^- \rightarrow M + H_2O + O_3$ $2 \times 10^{-25} \cdot \left(\frac{T_g}{3.0 \times 10^2}\right)^{-2.5}$	[57]
512	$H + H_3O^+ \rightarrow H_2 + H_2O^+$ $6.1 \times 10^{-10} \cdot exp\left(\frac{-2.05 \times 10^4}{T_g}\right)$	[62]
513	$H_3O^+ + O^- \rightarrow H + H_2O + O$ $7.51 \times 10^{-8} \cdot \left(\frac{T_g}{3 \times 10^2}\right)^{-0.5}$	[2, 3]
514	$H_3O^+ + O_2^- \rightarrow H + H_2O + O_2$ $7.51 \times 10^{-8} \cdot \left(\frac{T_g}{3 \times 10^2}\right)^{-0.5}$	[2, 3]
515	$H_3O^+ + O_2^- \rightarrow H + H_2O + O + O$ 1×10^{-7}	[57]
516	$H + O^- \rightarrow e + OH$ 5×10^{-10}	[1]
517	$H + O_2^- \rightarrow e + HO_2$ 7×10^{-10}	[56]
518	$H + O_2^- \rightarrow H^- + O_2$ 7×10^{-10}	[56]
519	$H + O^+ \rightarrow H^+ + O$ 7×10^{-10}	[1]
520	$M + H + O \rightarrow M + OH$ $4.33 \times 10^{-32} \cdot \left(\frac{T_g}{3 \times 10^2}\right)^{-1}$	[25]
521	$H + O_2 \rightarrow O + OH$ $1.62 \times 10^{-10} \cdot exp\left(\frac{-7.4740 \times 10^3}{T_g}\right)$	[58]
522	$M + H + O_2 \rightarrow M + HO_2$ $3.33 \times 10^{-31} \cdot \left(\frac{T_g}{3.0 \times 10^2}\right)^{-1}$	[5]
523	$H + O_3 \rightarrow HO_2 + O$ 7.76×10^{-13}	[63]
524	$H + O_3 \rightarrow O_2 + OH$ 2.36×10^{-11}	[63]

#	Reaction / Rate equation	Ref.
525	$H^- + O_2 \rightarrow e + HO_2$ 1.2×10^{-9}	[56]
526	$H^- + O \rightarrow e + OH$ 1×10^{-9}	[1]
527	$H^- + OH \rightarrow e + H_2O$ 1×10^{-10}	[1]
528	$M + H^- + O_2^+ \rightarrow M + HO_2$ $2 \times 10^{-25} \cdot \left(\frac{T_g}{3.0 \times 10^2}\right)^{-2.5}$	[57]
529	$H^- + O^+ \rightarrow H + O$ $7.51 \times 10^{-8} \cdot \left(\frac{T_g}{3 \times 10^2}\right)^{-0.5}$	[2, 3]
530	$H_3O^+ + H^- \rightarrow H + H + H_2O$ $7.51 \times 10^{-8} \cdot \left(\frac{T_g}{3 \times 10^2}\right)^{-0.5}$	[2, 3]
531	$H^+ + O \rightarrow H + O^+$ $6.86 \times 10^{-10} \cdot \left(\frac{T_g}{3.0 \times 10^2}\right)^{0.26} \cdot exp\left(\frac{2.243 \times 10^2}{T_g}\right)$	[3]
532	$H^+ + O_2 \rightarrow H + O_2^+$ 2×10^{-9}	[29]
533	$H^+ + O^- \rightarrow H + O$ $7.51 \times 10^{-8} \cdot \left(\frac{T_g}{3 \times 10^2}\right)^{-0.5}$	[2, 3]
534	$H^+ + O_2^- \rightarrow H + O_2$ $7.51 \times 10^{-8} \cdot \left(\frac{T_g}{3 \times 10^2}\right)^{-0.5}$	[2, 3]
535	$H_2 + O^- \rightarrow H + OH^-$ 3.1×10^{-11}	[56]
536	$H_2 + O^- \rightarrow e + H_2O$ 5.98×10^{-10}	[56]
537	$H_2 + O_2^- \rightarrow OH + OH^-$ 5×10^{-13}	[56, 57]
538	$H_2 + O_2^- \rightarrow HO_2 + H^-$ 5×10^{-13}	[56, 57]
539	$H_2 + O^+ \rightarrow H + OH^+$ 1.7×10^{-9}	[56]
540	$H_2 + O_3 \rightarrow HO_2 + OH$ $1 \times 10^{-13} \cdot exp\left(\frac{-1.0 \times 10^4}{T_g}\right)$	[52]
541	$H_2 + O_2 \rightarrow H + HO_2$ $3.2 \times 10^{-11} \cdot exp\left(\frac{-2.410 \times 10^4}{T_g}\right)$	[52]

#	Reaction / Rate equation	Ref.
542	$H_2 + O \rightarrow H + OH$ $9 \times 10^{-12} \cdot \frac{T_g}{3.0 \times 10^2} \cdot exp\left(\frac{-4.480 \times 10^3}{T_g}\right)$	[52]
543	$H_2^+ + O_2 \rightarrow H_2 + O_2^+$ 7.8×10^{-10}	[7]
544	$H_2^+ + O_2 \rightarrow H + HO_2^+$ 1.9×10^{-9}	[64]
545	$H_3^+ + O \rightarrow H + H_2O^+$ $8.87 \times 10^{-10} \cdot \left(\frac{T_g}{3.0 \times 10^2}\right)^{-0.32}$	[65]
546	$H_3^+ + O \rightarrow H_2 + OH^+$ $5.26 \times 10^{-11} \cdot \left(\frac{T_g}{3.0 \times 10^2}\right)^{-0.32}$	[65]
547	$H_3^+ + O^- \rightarrow H + H_2 + O$ $7.51 \times 10^{-8} \cdot \left(\frac{T_g}{3 \times 10^2}\right)^{-0.5}$	[2, 3]
548	$H_3^+ + O_2^- \rightarrow H + H_2 + O_2$ $7.51 \times 10^{-8} \cdot \left(\frac{T_g}{3 \times 10^2}\right)^{-0.5}$	[2, 3]
549	$H + O \rightarrow e + OH^+$ $\frac{1.12 \times 10^{13}}{N_A} \cdot exp\left(\frac{-8.06 \times 10^4}{T_g}\right)$	d
550	$H + OH \rightarrow e + H_2O^+$ $\frac{1.12 \times 10^{13}}{N_A} \cdot exp\left(\frac{-8.06 \times 10^4}{T_g}\right)$	d
551	$H_2 + O \rightarrow e + H_2O^+$ $\frac{1.12 \times 10^{13}}{N_A} \cdot exp\left(\frac{-8.06 \times 10^4}{T_g}\right)$	d
552	$C + OH \rightarrow CO + H$ $\frac{5 \times 10^{13}}{N_A}$	[66]
553	$C + OH^+ \rightarrow CH^+ + O$ 1.2×10^{-9}	[1]
554	$C + H_2O^+ \rightarrow CH^+ + OH$ 1.1×10^{-9}	[1]
555	$C + H_3O^+ \rightarrow H_2 + HCO^+$ 1×10^{-11}	[1]
556	$C + HO_2^+ \rightarrow CH^+ + O_2$ 1×10^{-9}	[1]
557	$C + OH^- \rightarrow e + HCO$ 5×10^{-10}	[1]
558	$C^+ + OH \rightarrow CO^+ + H$ 7.7×10^{-10}	[1]

#	Reaction / Rate equation	Ref.
559	$C^+ + H_2O \rightarrow H + HCO^+$ 2.7×10^{-9}	[67]
560	$C^+ + OH^- \rightarrow C + OH$ $7.51 \times 10^{-8} \cdot \left(\frac{T_g}{3 \times 10^2}\right)^{-0.5}$	[2, 3]
561	$CO_2 + H \rightarrow CO + OH$ $4.7 \times 10^{-10} \cdot exp\left(\frac{-1.3915 \times 10^4}{T_g}\right)$	[5]
562	$CO + H \rightarrow HCO$ $2 \times 10^{-35} \cdot T_g^{0.2} \cdot n_M$	[5]
563	$CO_2 + H^+ \rightarrow HCO^+ + O$ 3.5×10^{-9}	[29]
564	$CO + H_2^+ \rightarrow CO^+ + H_2$ 6.44×10^{-10}	[7]
565	$CO + H_2^+ \rightarrow H + HCO^+$ 2.16×10^{-9}	[7]
566	$CO + H_3^+ \rightarrow H_2 + HCO^+$ $1.36 \times 10^{-9} \cdot \left(\frac{T_g}{3 \times 10^2}\right)^{-0.142} \cdot exp\left(\frac{3.41}{T_g}\right)$	[68]
567	$CO + H^- \rightarrow e + HCO$ 2×10^{-11}	[69]
568	$CO_2^+ + H \rightarrow HCO^+ + O$ 2.9×10^{-10}	[70]
569	$CO^+ + H \rightarrow CO + H^+$ 7.5×10^{-10}	[71]
570	$CO^+ + H_2 \rightarrow H + HCO^+$ 1.5×10^{-9}	[72]
571	$CO + OH \rightarrow CO_2 + H$ $\frac{3.3 \times 10^6}{N_A} \cdot T_g^{1.55} \cdot exp\left(\frac{4.02 \times 10^2}{T_g}\right)$	[73]
572	$CO + HO_2 \rightarrow CO_2 + OH$ $\frac{5.8 \times 10^{13}}{N_A} \cdot exp\left(\frac{-2.293 \times 10^4 \cdot 4.184}{R \cdot T_g}\right)$	[74]
573	$CO + H_2O_2 \rightarrow COOH + OH$ $\frac{3.6 \times 10^4}{N_A} \cdot T_g^{2.5} \cdot exp\left(\frac{-1.4425 \times 10^4}{T_g}\right)$	[75]
574	$CO_2 + OH^+ \rightarrow HCO^+ + O_2$ 5.4×10^{-10}	[1]
575	$CO + OH^+ \rightarrow HCO^+ + O$ 1.05×10^{-9}	[76]
576	$CO + H_2O^+ \rightarrow HCO^+ + OH$ 5×10^{-10}	[76]

#	Reaction / Rate equation	Ref.
577	$CO + HO_2^+ \rightarrow HCO^+ + O_2$ 8.4×10^{-10}	[1]
578	$CO_2^+ + H_2O \rightarrow CO_2 + H_2O^+$ 2.044×10^{-9}	[77]
579	$CO^+ + OH \rightarrow CO + OH^+$ 3.1×10^{-10}	[1]
580	$CO^+ + OH \rightarrow HCO^+ + O$ 3.1×10^{-10}	[1]
581	$CO^+ + H_2O \rightarrow CO + H_2O^+$ 1.7×10^{-9}	[78]
582	$CO^+ + H_2O \rightarrow HCO^+ + OH$ 9×10^{-10}	[78]
583	$CH_4 + O \rightarrow CH_3 + OH$ $7.3 \times 10^{-19} \cdot T_g^{2.5} \cdot exp\left(\frac{-3.31 \times 10^3}{T_g}\right)$	[5]
584	$CH_4 + O_2 \rightarrow CH_3 + HO_2$ $8.1 \times 10^{-19} \cdot T_g^{2.5} \cdot exp\left(\frac{-2.637 \times 10^4}{T_g}\right)$	[5]
585	$CH_4 + O_2 \rightarrow CH_3OO + H$ $\frac{4.3 \times 10^{13}}{N_A} \cdot \left(\frac{T_g}{1 \times 10^3}\right)^{1.96} \cdot exp\left(\frac{-8.73 \times 10^1 \cdot 4.184 \times 10^3}{R \cdot T_g}\right)$	[79]
586	$CH_3 + O \rightarrow H + HCHO$ 1.12×10^{-10}	[5]
587	$CH_3 + O_2 \rightarrow HCHO + OH$ $3.7 \times 10^{-12} \cdot exp\left(\frac{-1.114 \times 10^4}{T_g}\right)$	[5]
588	$CH_3 + O_2 \rightarrow CH_3O + O$ $3.5 \times 10^{-11} \cdot exp\left(\frac{-1.634 \times 10^4}{T_g}\right)$	[5]
589	$CH_3 + O_2 \rightarrow CH_3OO$ $1.3 \times 10^{-15} \cdot T_g^{1.2}$	[5]
590	$CH_2 + O \rightarrow CO + H_2$ $0.4 \cdot 3.4 \times 10^{-10} \cdot exp\left(\frac{-2.7 \times 10^2}{T_g}\right)$	[5]
591	$CH_2 + O_2 \rightarrow HCHO + O$ $\frac{4 \times 10^{10}}{N_A}$	[80]
592	$CH_2 + O_2 \rightarrow CO + H_2O$ 4.2×10^{-13}	[25]
593	$CH + O \rightarrow CO + H$ 6.6×10^{-11}	[5]
594	$CH + O \rightarrow e + HCO^+$ $4.2 \times 10^{-13} \cdot exp\left(\frac{-8.5 \times 10^2}{T_g}\right)$	[5]

#	Reaction / Rate equation	Ref.
595	$CH + O_2 \rightarrow CO_2 + H$ 4.2×10^{-11}	[5]
596	$CH + O_2 \rightarrow CO + OH$ 2.8×10^{-11}	[5]
597	$CH + O_2 \rightarrow HCO + O$ 2.8×10^{-11}	[5]
598	$CH_4 + O^+ \rightarrow CH_3^+ + OH$ 1.1×10^{-10}	[27]
599	$CH_4 + O^+ \rightarrow CH_4^+ + O$ 8.9×10^{-10}	[27]
600	$CH_4 + O^- \rightarrow CH_3 + OH^-$ 1×10^{-10}	[1]
601	$CH_2 + O^+ \rightarrow CH_2^+ + O$ 9.7×10^{-10}	[1]
602	$CH_2 + O_2^+ \rightarrow CH_2^+ + O_2$ 4.3×10^{-10}	[1]
603	$CH_2 + O^- \rightarrow e + HCHO$ 5×10^{-10}	[1]
604	$CH + O^+ \rightarrow CH^+ + O$ 3.5×10^{-10}	[1]
605	$CH + O^+ \rightarrow CO^+ + H$ 3.5×10^{-10}	[1]
606	$CH + O_2^+ \rightarrow CH^+ + O_2$ 3.1×10^{-10}	[1]
607	$CH + O_2^+ \rightarrow HCO^+ + O$ 3.1×10^{-10}	[1]
608	$CH + O^- \rightarrow e + HCO$ 5×10^{-10}	[1]
609	$CH_5^+ + O \rightarrow CH_2 + H_3O^+$ 2.156×10^{-10}	[81]
610	$CH_4^+ + O_2 \rightarrow CH_4 + O_2^+$ 3.9×10^{-10}	[27]
611	$CH_3^+ + O \rightarrow H_2 + HCO^+$ 3.08×10^{-10}	[82]
612	$CH_3^+ + O \rightarrow CO + H_3^+$ 8.8×10^{-11}	[82]
613	$CH_3^+ + O_2 \rightarrow H_2O + HCO^+$ 4.3×10^{-11}	[27]
614	$CH_3^+ + O^- \rightarrow CH_3 + O$ $7.51 \times 10^{-8} \cdot \left(\frac{T_g}{3 \times 10^2}\right)^{-0.5}$	[2, 3]

#	Reaction / Rate equation	Ref.
615	$CH_3^+ + O_2^- \rightarrow CH_3 + O_2$ $7.51 \times 10^{-8} \cdot \left(\frac{T_g}{3 \times 10^2}\right)^{-0.5}$	[2, 3]
616	$CH_2^+ + O \rightarrow H + HCO^+$ 7.5×10^{-10}	[1]
617	$CH_2^+ + O_2 \rightarrow HCO^+ + OH$ 4.55×10^{-10}	[27]
618	$CH^+ + O \rightarrow CO^+ + H$ 1.75×10^{-10}	[81]
619	$CH^+ + O \rightarrow CO + H^+$ 1.75×10^{-10}	[81]
620	$CH^+ + O_2 \rightarrow HCO + O^+$ 9.7×10^{-10}	[27]
621	$CH^+ + O_2 \rightarrow CO_2^+ + H$ 4.8×10^{-10}	[1]
622	$CH_3 + CO \rightarrow CH_3CO$ $k_0 = 1.6 \times 10^{-37} \cdot T_g^{1.05} \cdot exp\left(\frac{-1.3 \times 10^3}{T_g}\right)$ $k_\infty = 3.1 \times 10^{-16} \cdot T_g^{1.05} \cdot exp\left(\frac{-2.85 \times 10^3}{T_g}\right)$ $F_c = 0.5$	[5][a]
623	$CH_2 + CO_2 \rightarrow CO + HCHO$ 3.9×10^{-14}	[25]
624	$CH_2 + CO \rightarrow CH_2CO$ 1×10^{-15}	[25]
625	$CH + CO_2 \rightarrow CO + HCO$ $0.5 \cdot 1.06 \times 10^{-16} \cdot T_g^{1.51} \cdot exp\left(\frac{3.6 \times 10^2}{T_g}\right)$	[5]
626	$CH + CO \rightarrow HCCO$ $k_0 = 6.3 \times 10^{-24} \cdot T_g^{-2.5}$ $k_\infty = 1.7 \times 10^{-9} \cdot T_g^{-0.4}$ $F_c = 0.6$	[5][a]
627	$CH_4 + CO_2^+ \rightarrow CH_4^+ + CO_2$ 5.5×10^{-10}	[83]
628	$CH_4 + CO^+ \rightarrow CH_4^+ + CO$ 8.978×10^{-10}	[27]
629	$CH_4 + CO^+ \rightarrow CH_3 + HCO^+$ 3.752×10^{-10}	[27]
630	$CH_2 + CO^+ \rightarrow CH_2^+ + CO$ 4.3×10^{-10}	[1]
631	$CH_2 + CO^+ \rightarrow CH + HCO^+$ 4.3×10^{-10}	[1]

#	Reaction / Rate equation	Ref.
632	$CH + CO^+ \rightarrow CH^+ + CO$ 3.2×10^{-10}	[1]
633	$CH + CO^+ \rightarrow C + HCO^+$ 3.2×10^{-10}	[1]
634	$CH_5^+ + CO \rightarrow CH_4 + HCO^+$ 9.9×10^{-10}	[27]
635	$CH_4^+ + CO \rightarrow CH_3 + HCO^+$ 1.0368×10^{-9}	[27]
636	$CH^+ + CO_2 \rightarrow CO + HCO^+$ 1.6×10^{-9}	[27]
637	$CH^+ + CO \rightarrow C + HCO^+$ 7×10^{-12}	[27]
638	$CH_4 + OH \rightarrow CH_3 + H_2O$ $1.66 \times 10^{-18} \cdot T_g^{2.182} \cdot exp\left(\frac{-1.231 \times 10^3}{T_g}\right)$	[84]
639	$CH_4 + HO_2 \rightarrow CH_3 + H_2O_2$ $7.8 \times 10^{-20} \cdot T_g^{2.5} \cdot exp\left(\frac{-1.057 \times 10^4}{T_g}\right)$	[5]
640	$CH_3 + OH \rightarrow CH_3OH$ $k_0 = 1.06 \times 10^{-10} \cdot T_g^{-6.21} \cdot exp\left(\frac{-6.71 \times 10^2}{T_g}\right)$ $k_\infty = 7.2 \times 10^{-9} \cdot T_g^{-0.79}$ $F_c = 0.75 \cdot exp\left(\frac{-T_g}{2.1 \times 10^2}\right)$ $+0.25 \cdot exp\left(\frac{-T_g}{1.434 \times 10^3}\right)$	[5]a
641	$CH_3 + OH \rightarrow CH_2 + H_2O$ $\frac{k}{n_M}$ $k_0 = 1.8 \times 10^{-8} \cdot T_g^{-0.91} \cdot exp\left(\frac{-2.75 \times 10^2}{T_g}\right)$ $k_\infty = 6.4 \times 10^{-8} \cdot T_g^{5.8} \cdot exp\left(\frac{4.85 \times 10^2}{T_g}\right)$ $F_c = 0.664 \cdot exp\left(\frac{-T_g}{3.569 \times 10^3}\right)$ $+0.336 \cdot exp\left(\frac{-T_g}{1.08 \times 10^2}\right)$ $+exp\left(\frac{-3.24 \times 10^3}{T_g}\right)$	[5]a
642	$CH_3 + OH \rightarrow CH_2OH + H$ $1.2 \times 10^{-12} \cdot exp\left(\frac{-2.76 \times 10^3}{T_g}\right)$	[5]
643	$CH_3 + OH \rightarrow CH_3O + H$ $2 \times 10^{-14} \cdot exp\left(\frac{-6.99 \times 10^3}{T_g}\right)$	[5]

#	Reaction / Rate equation	Ref.
644	$CH_3 + OH \rightarrow H_2 + HCHO$ $5.3 \times 10^{-15} \cdot exp\left(\frac{-2.53 \times 10^3}{T_g}\right)$	[5]
645	$CH_3 + OH \rightarrow CH_4 + O$ $1.16 \times 10^{-19} \cdot T_g^{2.2} \cdot exp\left(\frac{-2.24 \times 10^3}{T_g}\right)$	[85]
646	$CH_3 + H_2O \rightarrow CH_4 + OH$ $8 \times 10^{-22} \cdot T_g^{2.9} \cdot exp\left(\frac{-7.48 \times 10^3}{T_g}\right)$	[86]
647	$CH_3 + HO_2 \rightarrow CH_3O + OH$ 3×10^{-11}	[5]
648	$CH_3 + HO_2 \rightarrow CH_4 + O_2$ 6×10^{-12}	[25]
649	$CH_3 + H_2O_2 \rightarrow CH_4 + HO_2$ $2 \times 10^{-14} \cdot exp\left(\frac{3.0 \times 10^2}{T_g}\right)$	[25]
650	$CH_2 + OH \rightarrow H + HCHO$ 5×10^{-11}	[25]
651	$CH_2 + H_2O \rightarrow CH_3 + OH$ 1×10^{-16}	[25]
652	$CH_2 + HO_2 \rightarrow HCHO + OH$ 3×10^{-11}	[25]
653	$CH_2 + H_2O_2 \rightarrow CH_3 + HO_2$ 1×10^{-14}	[25]
654	$CH + OH \rightarrow C + H_2O$ $\frac{4 \times 10^7}{N_A} \cdot T_g^2 \cdot exp\left(\frac{-3 \times 10^3 \cdot 4.184}{R \cdot T_g}\right)$	[74]
655	$CH + OH \rightarrow H + HCO$ $\frac{3 \times 10^{13}}{N_A}$	[74]
656	$CH + H_2O \rightarrow H + HCHO$ $\frac{8.5 \times 10^8}{N_A} \cdot T_g^{1.144} \cdot exp\left(\frac{2.051 \times 10^3 \cdot 4.184}{R \cdot T_g}\right)$	[66]
657	$CH_4 + OH^+ \rightarrow CH_5^+ + O$ 1.885×10^{-10}	[27]
658	$CH_4 + OH^+ \rightarrow CH_2 + H_3O^+$ 1.2615×10^{-9}	[27]
659	$CH_4 + H_2O^+ \rightarrow CH_3 + H_3O^+$ 1.12×10^{-9}	[27]
660	$CH_4 + HO_2^+ \rightarrow CH_3^+ + H_2 + O_2$ 8×10^{-11}	[27]
661	$CH_4 + HO_2^+ \rightarrow CH_5^+ + O_2$ 9.2×10^{-10}	[27]

#	Reaction / Rate equation	Ref.
662	$CH_3 + OH^- \rightarrow CH_3OH + e$ 1×10^{-9}	[1]
663	$CH_2 + OH^+ \rightarrow CH_2^+ + OH$ 4.8×10^{-10}	[1]
664	$CH_2 + OH^+ \rightarrow CH_3^+ + O$ 4.8×10^{-10}	[1]
665	$CH_2 + H_2O^+ \rightarrow CH_2^+ + H_2O$ 4.7×10^{-10}	[1]
666	$CH_2 + H_2O^+ \rightarrow CH_3^+ + OH$ 4.7×10^{-10}	[1]
667	$CH_2 + H_3O^+ \rightarrow CH_3^+ + H_2O$ 9.4×10^{-10}	[1]
668	$CH_2 + HO_2^+ \rightarrow CH_3^+ + O_2$ 8.5×10^{-10}	[1]
669	$CH + OH^+ \rightarrow CH^+ + OH$ 3.5×10^{-10}	[1]
670	$CH + OH^+ \rightarrow CH_2^+ + O$ 3.5×10^{-10}	[1]
671	$CH + H_2O^+ \rightarrow CH^+ + H_2O$ 3.4×10^{-10}	[1]
672	$CH + H_2O^+ \rightarrow CH_2^+ + OH$ 3.4×10^{-10}	[1]
673	$CH + H_3O^+ \rightarrow CH_2^+ + H_2O$ 6.8×10^{-10}	[1]
674	$CH + HO_2^+ \rightarrow CH_2^+ + O_2$ 6.2×10^{-10}	[1]
675	$CH + OH^- \rightarrow e + HCHO$ 5×10^{-10}	[1]
676	$CH_5^+ + OH \rightarrow CH_4 + H_2O^+$ 7×10^{-10}	[1]
677	$CH_5^+ + H_2O \rightarrow CH_4 + H_3O^+$ 3.7×10^{-9}	[27]
678	$CH_4^+ + H_2O \rightarrow CH_3 + H_3O^+$ 2.5×10^{-9}	[27]
679	$CH_3^+ + OH^- \rightarrow CH_3 + OH$ $7.51 \times 10^{-8} \cdot \left(\frac{T_g}{3 \times 10^2}\right)^{-0.5}$	[2, 3]
680	$CH^+ + OH \rightarrow CO^+ + H_2$ 7.5×10^{-10}	[1]
681	$CH^+ + H_2O \rightarrow C + H_3O^+$ 1.45×10^{-9}	[27]

#	Reaction / Rate equation	Ref.
682	$C^+ + HCO \rightarrow C + HCO^+$ 4.8×10^{-10}	[1]
683	$C^+ + HCO \rightarrow CH^+ + CO$ 4.8×10^{-10}	[1]
684	$C^+ + HCHO \rightarrow CH_2^+ + CO$ 2.112×10^{-9}	[87]
685	$C^+ + HCHO \rightarrow CH + HCO^+$ 9.24×10^{-10}	[87]
686	$CH_3OH + C^+ \rightarrow CH_3 + HCO^+$ 3.28×10^{-10}	[87]
687	$CH_3OH + C^+ \rightarrow CH_3^+ + HCO$ 1.189×10^{-9}	[87]
688	$C + HCO^+ \rightarrow CH^+ + CO$ 1.1×10^{-9}	[1]
689	$CO + COOH \rightarrow CO_2 + HCO$ 1×10^{-14}	[88]
690	$CH_3O + CO \rightarrow CH_3 + CO_2$ $2.6 \times 10^{-11} \cdot exp\left(\frac{-5.94 \times 10^3}{T_g}\right)$	[25]
691	$CH_3O + CO \rightarrow HCHO + HCO$ 5.23×10^{-15}	[89]
692	$CH_3OO + CO \rightarrow CH_3O + CO_2$ 7×10^{-18}	[90]
693	$CO^+ + HCO \rightarrow CO + HCO^+$ 7.4×10^{-10}	[1]
694	$CO^+ + HCHO \rightarrow HCO + HCO^+$ 1.65×10^{-9}	[91]
695	$H + HCO \rightarrow CO + H_2$ 1.5×10^{-10}	[5]
696	$H + HCO \rightarrow CH_2 + O$ $\frac{3.98107171 \times 10^{13}}{N_A} \cdot exp\left(\frac{-4.29 \times 10^5}{R \cdot T_g}\right)$	[92]
697	$H + HCHO \rightarrow H_2 + HCO$ $3.34 \times 10^{-23} \cdot T_g^{-3.81} \cdot exp\left(\frac{-2.02 \times 10^2}{T_g}\right)$	[5]
698	$H + HCHO \rightarrow CH_3O$ $\frac{2.4 \times 10^{13}}{N_A} \cdot exp\left(\frac{-4.11 \times 10^3 \cdot 4.184}{T_g}\right)$	[93]
699	$CH_3O + H \rightarrow H_2 + HCHO$ 3.3×10^{-11}	[25]
700	$CH_3O + H \rightarrow CH_3OH$ $3.4 \times 10^{-10} \cdot \left(\frac{T_g}{3 \times 10^2}\right)^{0.33}$	[94]

#	Reaction / Rate equation	Ref.
701	$CH_3O + H_2 \rightarrow CH_3OH + H$ $1.7 \times 10^{-15} \cdot \left(\frac{T_g}{3 \times 10^2}\right)^4 \cdot exp\left(\frac{-2.47 \times 10^3}{T_g}\right)$	[95]
702	$CH_2OH + H \rightarrow H_2 + HCHO$ 1×10^{-11}	[96]
703	$CH_2OH + H \rightarrow CH_3 + OH$ 1.6×10^{-10}	[96]
704	$CH_2OH + H_2 \rightarrow CH_3OH + H$ $1.12 \times 10^{-18} \cdot T_g^2 \cdot exp\left(\frac{-6.722 \times 10^3}{T_g}\right)$	[96]
705	$CH_3OH + H \rightarrow CH_2OH + H_2$ $5.7 \times 10^{-15} \cdot T_g^{1.24} \cdot exp\left(\frac{-2.26 \times 10^3}{T_g}\right)$	[5]
706	$CH_3OH + H \rightarrow CH_3 + H_2O$ $\frac{2 \times 10^{12}}{N_A} \cdot exp\left(\frac{-5.3 \cdot 4.184 \times 10^3}{R \cdot T_g}\right)$	[97]
707	$CH_3OO + H \rightarrow CH_4 + O_2$ $\frac{4.02 \times 10^{13}}{N_A} \cdot \left(\frac{T_g}{1 \times 10^3}\right)^{1.02} \cdot exp\left(\frac{-1.66 \times 10^1 \cdot 4.184 \times 10^3}{R \cdot T_g}\right)$	[79]
708	$CH_3OO + H \rightarrow CH_3O + OH$ 1.6×10^{-10}	[25]
709	$CH_3OO + H_2 \rightarrow CH_3OOH + H$ $5 \times 10^{-11} \cdot exp\left(\frac{-1.31 \times 10^4}{T_g}\right)$	[25]
710	$HCO + H^+ \rightarrow H + HCO^+$ 9.4×10^{-10}	[1]
711	$HCO + H^+ \rightarrow CO^+ + H_2$ 9.4×10^{-10}	[1]
712	$HCO + H^+ \rightarrow CO + H_2^+$ 9.4×10^{-10}	[1]
713	$H_2^+ + HCO \rightarrow H_2 + HCO^+$ 1×10^{-9}	[1]
714	$H_2^+ + HCO \rightarrow CO + H_3^+$ 1×10^{-9}	[1]
715	$HCO + H^- \rightarrow e + HCHO$ 1×10^{-9}	[1]
716	$HCHO + H^+ \rightarrow CO^+ + H + H_2$ 1.064×10^{-9}	[98]
717	$HCHO + H^+ \rightarrow H_2 + HCO^+$ 3.572×10^{-9}	[98]
718	$H_2^+ + HCHO \rightarrow H + H_2 + HCO^+$ 1.4×10^{-9}	[1]

#	Reaction / Rate equation	Ref.
719	$H_3^+ + HCOOH \rightarrow CO + H_2 + H_3O^+$ 1.83×10^{-9}	[99]
720	$H_3^+ + HCOOH \rightarrow H_2 + H_2O + HCO^+$ 4.27×10^{-9}	[99]
721	$CH_3OH + H^+ \rightarrow CH_3^+ + H_2O$ 7.4×10^{-10}	[29]
722	$CH_3OH + H^+ \rightarrow H_2 + H_2 + HCO^+$ 1.11×10^{-9}	[29]
723	$CH_3OH + H_3^+ \rightarrow CH_3^+ + H_2 + H_2O$ 3.71×10^{-9}	[100]
724	$CH_3OH + H_3^+ \rightarrow H_2 + H_2 + H_2 + HCO^+$ 1.26×10^{-9}	[100]
725	$HCO^+ + H^- \rightarrow CO + H + H$ $3.76 \times 10^{-8} \cdot \left(\frac{T_g}{3 \times 10^2}\right)^{-0.5}$	[2, 3]
726	$HCO^+ + H^- \rightarrow H + HCO$ $3.76 \times 10^{-8} \cdot \left(\frac{T_g}{3 \times 10^2}\right)^{-0.5}$	[2, 3]
727	$HCO^+ + H^- \rightarrow CO + H_2$ $2.3 \times 10^{-7} \cdot \left(\frac{T_g}{3 \times 10^2}\right)^{-0.5}$	[1]
728	$HCO + OH \rightarrow CO + H_2O$ 1.8×10^{-10}	[5]
729	$H_2O + HCO \rightarrow HCHO + OH$ $3.9 \times 10^{-16} \cdot T_g^{1.35} \cdot exp\left(\frac{-1.3146 \times 10^4}{T_g}\right)$	[25]
730	$H_2O_2 + HCO \rightarrow HCHO + HO_2$ $1.7 \times 10^{-13} \cdot exp\left(\frac{-3.486 \times 10^3}{T_g}\right)$	[25]
731	$HCHO + OH \rightarrow H_2O + HCO$ $2.31 \times 10^{-11} \cdot exp\left(\frac{-3.04 \times 10^2}{T_g}\right)$	[5]
732	$HCHO + OH \rightarrow H + HCOOH$ 2×10^{-13}	[101]
733	$HCHO + HO_2 \rightarrow H_2O_2 + HCO$ $6.8 \times 10^{-20} \cdot T_g^{2.5} \cdot exp\left(\frac{-5.14 \times 10^3}{T_g}\right)$	[5]
734	$HCHO + HO_2 \rightarrow CH_2OH + O_2$ $\frac{3.38844156 \times 10^{12}}{N_A} \cdot exp\left(\frac{-8 \times 10^4}{R \cdot T_g}\right)$	[92]
735	$HCOOH + OH \rightarrow COOH + H_2O$ $\frac{5.93 \times 10^8 \cdot 1 \times 10^3}{N_A} \cdot exp\left(\frac{-1.036 \times 10^3}{T_g}\right)$	[102]

#	Reaction / Rate equation	Ref.
736	$CH_3O + OH \rightarrow H_2O + HCHO$ 3×10^{-11}	[25]
737	$CH_3O + HO_2 \rightarrow H_2O_2 + HCHO$ 5×10^{-13}	[25]
738	$CH_3O + HO_2 \rightarrow CH_3OH + O_2$ 4.7×10^{-11}	[103]
739	$CH_2OH + OH \rightarrow H_2O + HCHO$ 4×10^{-11}	[96]
740	$CH_2OH + H_2O \rightarrow CH_3OH + OH$ $\frac{1.54881662 \times 10^{14}}{N_A} \cdot exp\left(\frac{-1.1 \times 10^5}{R \cdot T_g}\right)$	[92]
741	$CH_2OH + HO_2 \rightarrow H_2O_2 + HCHO$ $\frac{1.3 \times 10^6 \cdot 1 \times 10^3}{N_A} \cdot \left(\frac{T_g}{2.98 \times 10^2}\right)^{5.31} \cdot exp\left(\frac{-6.01 \times 10^4}{R \cdot T_g}\right)$	[104]
742	$CH_2OH + HO_2 \rightarrow CH_3OH + O_2$ $\frac{5.7 \times 10^4 \cdot 1 \times 10^3}{N_A} \cdot \left(\frac{T_g}{2.98 \times 10^2}\right)^{3.2} \cdot exp\left(\frac{-6.8 \times 10^3}{R \cdot T_g}\right)$	[104]
743	$CH_2OH + HO_2 \rightarrow H_2O + HCOOH$ $\frac{3.6 \times 10^9 \cdot 1 \times 10^3}{N_A} \cdot T_g^{0.12} \cdot exp\left(\frac{-1.9 \times 10^3}{R \cdot T_g}\right)$	[104]
744	$CH_2OH + H_2O_2 \rightarrow CH_3OH + HO_2$ $5 \times 10^{-15} \cdot exp\left(\frac{-1.3 \times 10^3}{T_g}\right)$	[96]
745	$CH_3OH + HO_2 \rightarrow CH_2OH + H_2O_2$ $5.41 \times 10^{-11} \cdot exp\left(\frac{-9.2 \times 10^3}{T_g}\right)$	[105]
746	$CH_3OH + HO_2 \rightarrow CH_3O + H_2O_2$ $2.02 \times 10^{-12} \cdot exp\left(\frac{-1.01 \times 10^4}{T_g}\right)$	[105]
747	$CH_3OOH + OH \rightarrow CH_3OO + H_2O$ $1.8 \times 10^{-12} \cdot exp\left(\frac{2.2 \times 10^2}{T_g}\right)$	[5]
748	$CH_3OO + OH \rightarrow CH_3OH + O_2$ 1×10^{-10}	[25]
749	$CH_3OO + HO_2 \rightarrow CH_3OOH + O_2$ $0.9 \cdot 4.2 \times 10^{-13} \cdot exp\left(\frac{7.5 \times 10^2}{T_g}\right)$	[5]
750	$CH_3OO + H_2O_2 \rightarrow CH_3OOH + HO_2$ $4 \times 10^{-12} \cdot exp\left(\frac{-5 \times 10^3}{T_g}\right)$	[25]
751	$HCO + OH^+ \rightarrow HCO^+ + OH$ 2.8×10^{-10}	[1]
752	$HCO + OH^+ \rightarrow CO + H_2O^+$ 2.8×10^{-10}	[1]

#	Reaction / Rate equation	Ref.
753	$H_2O^+ + HCO \rightarrow H_2O + HCO^+$ 2.8×10^{-10}	[1]
754	$H_2O^+ + HCO \rightarrow CO + H_3O^+$ 2.8×10^{-10}	[1]
755	$HCO^+ + OH \rightarrow CO + H_2O^+$ 6.2×10^{-10}	[1]
756	$H_2O + HCO^+ \rightarrow CO + H_3O^+$ 2.5×10^{-9}	[91]
757	$HCO^+ + OH^- \rightarrow CO + H + OH$ $3.76 \times 10^{-8} \cdot \left(\frac{T_g}{3 \times 10^2}\right)^{-0.5}$	[2, 3]
758	$HCO^+ + OH^- \rightarrow HCO + OH$ $3.76 \times 10^{-8} \cdot \left(\frac{T_g}{3 \times 10^2}\right)^{-0.5}$	[2, 3]
759	$HCO + O \rightarrow CO + OH$ 5×10^{-11}	[25]
760	$HCO + O \rightarrow CO_2 + H$ 5×10^{-11}	[25]
761	$HCO + O_2 \rightarrow CO + HO_2$ $4.5 \times 10^{-14} \cdot T_g^{0.68} \cdot exp\left(\frac{2.36 \times 10^2}{T_g}\right)$	[5]
762	$HCHO + O \rightarrow HCO + OH$ $6.9 \times 10^{-13} \cdot T_g^{0.57} \cdot exp\left(\frac{-1.39 \times 10^3}{T_g}\right)$	[5]
763	$HCHO + O_2 \rightarrow HCO + HO_2$ $4.05 \times 10^{-19} \cdot T_g^{2.5} \cdot exp\left(\frac{-1.835 \times 10^4}{T_g}\right)$	[5]
764	$CH_3O + O \rightarrow CH_3 + O_2$ 1.875×10^{-11}	[5]
765	$CH_3O + O \rightarrow HCHO + OH$ 6.25×10^{-12}	[5]
766	$CH_3O + O_2 \rightarrow HCHO + HO_2$ $3.6 \times 10^{-14} \cdot exp\left(\frac{-8.8 \times 10^2}{T_g}\right)$	[5]
767	$CH_2OH + O_2 \rightarrow HCHO + HO_2$ $4.8 \times 10^{-8} \cdot T_g^{-1.5}$ $+1.2 \times 10^{-10} \cdot exp\left(\frac{-1.88 \times 10^3}{T_g}\right)$	[5]
768	$CH_3OH + O \rightarrow CH_2OH + OH$ $4.1 \times 10^{-11} \cdot exp\left(\frac{-2.67 \times 10^3}{T_g}\right)$	[5]
769	$CH_3OH + O_2 \rightarrow CH_2OH + HO_2$ $3.4 \times 10^{-11} \cdot exp\left(\frac{-2.26 \times 10^4}{T_g}\right)$	[96]

#	Reaction / Rate equation	Ref.
770	$CH_3OO + O \rightarrow CH_3O + O_2$ 6×10^{-11}	[25]
771	$HCO + O^+ \rightarrow HCO^+ + O$ 4.3×10^{-10}	[1]
772	$HCO + O^+ \rightarrow CO + OH^+$ 4.3×10^{-10}	[1]
773	$HCO + O_2^+ \rightarrow HCO^+ + O_2$ 3.6×10^{-10}	[1]
774	$HCO + O_2^+ \rightarrow CO + HO_2^+$ 3.6×10^{-10}	[1]
775	$HCHO + O^+ \rightarrow CO + H_2O^+$ 4×10^{-10}	[1]
776	$HCO^+ + O^- \rightarrow CO + H + O$ $3.76 \times 10^{-8} \cdot \left(\frac{T_g}{3 \times 10^2}\right)^{-0.5}$	[2, 3]
777	$HCO^+ + O^- \rightarrow HCO + O$ $3.76 \times 10^{-8} \cdot \left(\frac{T_g}{3 \times 10^2}\right)^{-0.5}$	[2, 3]
778	$HCO^+ + O_2^- \rightarrow CO + H + O_2$ $3.76 \times 10^{-8} \cdot \left(\frac{T_g}{3 \times 10^2}\right)^{-0.5}$	[2, 3]
779	$HCO^+ + O_2^- \rightarrow HCO + O_2$ $3.76 \times 10^{-8} \cdot \left(\frac{T_g}{3 \times 10^2}\right)^{-0.5}$	[2, 3]
780	$CH_4 + HCO \rightarrow CH_3 + HCHO$ $1.21 \times 10^{-20} \cdot T_g^{2.85} \cdot exp\left(\frac{-1.133 \times 10^4}{T_g}\right)$	[25]
781	$CH_3 + HCO \rightarrow CH_4 + CO$ 2×10^{-10}	[25]
782	$CH_3 + HCO \rightarrow CH_3CHO$ 3×10^{-11}	[25]
783	$CH_2 + HCO \rightarrow CH_3 + CO$ 3×10^{-11}	[25]
784	$CH_3 + COOH \rightarrow CH_2CO + H_2O$ $\left(1.52 + 1.95 \times 10^{-4} \cdot T_g\right) \cdot 3.24 \times 10^{-11} \cdot T_g^{0.1024}$	[106]
785	$CH_3 + COOH \rightarrow CH_4 + CO_2$ $3.24 \times 10^{-11} \cdot T_g^{0.1024}$	[106]
786	$CH_3 + HCHO \rightarrow CH_3CH_2O$ $\frac{3 \times 10^{11}}{N_A} \cdot exp\left(\frac{-6.336 \times 10^3 \cdot 4.186}{R \cdot T_g}\right)$	[93]
787	$CH_3 + HCHO \rightarrow CH_4 + HCO$ $5.3 \times 10^{-23} \cdot T_g^{3.36} \cdot exp\left(\frac{-2.17 \times 10^3}{T_g}\right)$	[5]

#	Reaction / Rate equation	Ref.
788	$CH_2 + HCHO \rightarrow CH_3 + HCO$ 1×10^{-14}	[25]
789	$CH + HCHO \rightarrow CH_2CO + H$ $7.62 \times 10^{-10} \cdot T_g^{-0.32} \cdot exp\left(\frac{3.86 \times 10^2}{T_g}\right)$	[107]
790	$CH_3O + CH_4 \rightarrow CH_3 + CH_3OH$ $2.6 \times 10^{-13} \cdot exp\left(\frac{-4.45 \times 10^3}{T_g}\right)$	[25]
791	$CH_3 + CH_3O \rightarrow CH_4 + HCHO$ 4×10^{-11}	[25]
792	$CH_2 + CH_3O \rightarrow CH_3 + HCHO$ 3×10^{-11}	[25]
793	$CH_2OH + CH_4 \rightarrow CH_3 + CH_3OH$ $3.6 \times 10^{-23} \cdot T_g^{3.1} \cdot exp\left(\frac{-8.166 \times 10^3}{T_g}\right)$	[96]
794	$CH_2OH + CH_3 \rightarrow CH_3CH_2OH$ 2×10^{-11}	[96]
795	$CH_2OH + CH_3 \rightarrow CH_4 + HCHO$ 4×10^{-12}	[96]
796	$CH_2 + CH_2OH \rightarrow C_2H_4 + OH$ 4×10^{-11}	[96]
797	$CH_2 + CH_2OH \rightarrow CH_3 + HCHO$ 2×10^{-12}	[96]
798	$CH_3 + CH_3OH \rightarrow CH_2OH + CH_4$ $0.33 \cdot 5 \times 10^{-23} \cdot T_g^{3.45} \cdot exp\left(\frac{-4.02 \times 10^3}{T_g}\right)$	[5]
799	$CH_3 + CH_3OH \rightarrow CH_3O + CH_4$ $0.67 \cdot 5 \times 10^{-23} \cdot T_g^{3.45} \cdot exp\left(\frac{-4.02 \times 10^3}{T_g}\right)$	[5]
800	$CH_2 + CH_3OH \rightarrow CH_2OH + CH_3$ $5.3 \times 10^{-23} \cdot T_g^{3.2} \cdot exp\left(\frac{-3.609 \times 10^3}{T_g}\right)$	[96]
801	$CH_2 + CH_3OH \rightarrow CH_3 + CH_3O$ $2.4 \times 10^{-23} \cdot T_g^{3.1} \cdot exp\left(\frac{-3.49 \times 10^3}{T_g}\right)$	[96]
802	$CH_3OO + CH_4 \rightarrow CH_3 + CH_3OOH$ $3 \times 10^{-13} \cdot exp\left(\frac{-9.3 \times 10^3}{T_g}\right)$	[25]
803	$CH_3 + CH_3OO \rightarrow CH_3O + CH_3O$ 4×10^{-11}	[25]
804	$CH_2 + CH_3OO \rightarrow CH_3O + HCHO$ 3×10^{-11}	[25]
805	$CH_2 + CH_3OO \rightarrow C_2H_5 + O_2$ 3×10^{-11}	[25]

#	Reaction / Rate equation	Ref.
806	$CH_3^+ + HCO \rightarrow CH_3 + HCO^+$ 4.4×10^{-10}	[1]
807	$CH_3^+ + HCO \rightarrow CH_4^+ + CO$ 4.4×10^{-10}	[1]
808	$CH_2^+ + HCO \rightarrow CH_3^+ + CO$ 4.5×10^{-10}	[1]
809	$CH^+ + HCO \rightarrow CH + HCO^+$ 4.6×10^{-10}	[1]
810	$CH^+ + HCO \rightarrow CH_2^+ + CO$ 4.6×10^{-10}	[1]
811	$CH_3^+ + HCHO \rightarrow CH_4 + HCO^+$ 1.6×10^{-9}	[20]
812	$CH_2 + HCO^+ \rightarrow CH_3^+ + CO$ 8.6×10^{-10}	[1]
813	$CH + HCO^+ \rightarrow CH_2^+ + CO$ 6.3×10^{-10}	[1]
814	$HCO + HCO \rightarrow CO + HCHO$ 4.265×10^{-11}	[5]
815	$CH_3O + HCO \rightarrow CH_3OH + CO$ 1.5×10^{-10}	[25]
816	$CH_2OH + HCO \rightarrow CH_3OH + CO$ 2×10^{-10}	[96]
817	$CH_2OH + HCO \rightarrow HCHO + HCHO$ 3×10^{-10}	[96]
818	$CH_3OH + HCO \rightarrow CH_2OH + HCHO$ $1.6 \times 10^{-20} \cdot T_g^{2.9} \cdot exp\left(\frac{-6.596 \times 10^3}{T_g}\right)$	[96]
819	$CH_3OH + HCO \rightarrow CH_3O + HCHO$ $1.6 \times 10^{-22} \cdot T_g^{2.9} \cdot exp\left(\frac{-6.596 \times 10^3}{T_g}\right)$	[96]
820	$CH_3O + HCHO \rightarrow CH_3OH + HCO$ $1.7 \times 10^{-13} \cdot exp\left(\frac{-1.5 \times 10^3}{T_g}\right)$	[25]
821	$CH_2OH + HCHO \rightarrow CH_3OH + HCO$ $9.1 \times 10^{-21} \cdot T_g^{2.8} \cdot exp\left(\frac{-2.95 \times 10^3}{T_g}\right)$	[96]
822	$CH_3O + CH_3O \rightarrow CH_3OH + HCHO$ 1×10^{-10}	[25]
823	$CH_2OH + CH_3O \rightarrow CH_3OH + HCHO$ 4×10^{-11}	[96]
824	$CH_3O + CH_3OH \rightarrow CH_2OH + CH_3OH$ $5 \times 10^{-13} \cdot exp\left(\frac{-2.05 \times 10^3}{T_g}\right)$	[96]

#	Reaction / Rate equation	Ref.
825	$CH_2OH + CH_2OH \rightarrow CH_3OH + HCHO$ 8×10^{-12}	[96]
826	$CH_2OH + CH_3OH \rightarrow CH_3O + CH_3OH$ $1.3 \times 10^{-14} \cdot exp\left(\frac{-6.07 \times 10^3}{T_g}\right)$	[96]
827	$CH_3O + CH_3OO \rightarrow CH_3OOH + HCHO$ 5×10^{-13}	[25]
828	$CH_3OH + CH_3OO \rightarrow CH_2OH + CH_3OOH$ $3.421 \times 10^{-33} \cdot T_g^{6.2} \cdot exp\left(\frac{-2.9826 \times 10^4}{R \cdot T_g}\right)$	[108]
829	$CH_3OH + CH_3OO \rightarrow CH_3O + CH_3OOH$ $1.318 \times 10^{-27} \cdot T_g^{4.71} \cdot exp\left(\frac{-5.6739 \times 10^4}{R \cdot T_g}\right)$	[108]
830	$CH_2OH + CH_3OO \rightarrow CH_3OOH + HCHO$ $1.047 \times 10^{-24} \cdot T_g^{2.69} \cdot exp\left(\frac{1.4344 \times 10^4}{R \cdot T_g}\right)$	[108]
831	$CH_2OH + CH_3OO \rightarrow CH_3OH + HCOOH$ $3.89 \times 10^{-24} \cdot T_g^{2.74} \cdot exp\left(\frac{1.4922 \times 10^4}{R \cdot T_g}\right)$	[108]
832	$CH_3OO + HCHO \rightarrow CH_3OOH + HCO$ $3.3 \times 10^{-12} \cdot exp\left(\frac{-5.87 \times 10^3}{T_g}\right)$	[25]
833	$C_2H_6 + OH \rightarrow C_2H_5 + H_2O$ $1.52 \times 10^{-17} \cdot T_g^2 \cdot exp\left(\frac{-5 \times 10^2}{T_g}\right)$	[5]
834	$C_2H_6 + HO_2 \rightarrow C_2H_5 + H_2O_2$ $1.83 \times 10^{-19} \cdot T_g^{2.5} \cdot exp\left(\frac{-8.48 \times 10^3}{T_g}\right)$	[5]
835	$C_2H_5 + OH \rightarrow C_2H_6 + O$ $1.7 \times 10^{-40} \cdot T_g^{8.8} \cdot exp\left(\frac{-2.5 \times 10^2}{T_g}\right)$	[85]
836	$C_2H_5 + OH \rightarrow C_2H_4 + H_2O$ 4×10^{-11}	[25]
837	$C_2H_5 + H_2O \rightarrow C_2H_6 + OH$ $5.6 \times 10^{-18} \cdot T_g^{1.44} \cdot exp\left(\frac{-1.015 \times 10^4}{T_g}\right)$	[25]
838	$C_2H_5 + HO_2 \rightarrow C_2H_6 + O_2$ 5×10^{-13}	[25]
839	$C_2H_5 + HO_2 \rightarrow C_2H_4 + H_2O_2$ 5×10^{-13}	[25]
840	$C_2H_5 + H_2O_2 \rightarrow C_2H_6 + HO_2$ $1.45 \times 10^{-14} \cdot exp\left(\frac{-4.9 \times 10^2}{T_g}\right)$	[25]

#	Reaction / Rate equation	Ref.
841	$C_2H_4 + OH \rightarrow CH_3 + HCHO$ $\frac{1}{3} \cdot 3.4 \times 10^{-11} \cdot exp\left(\frac{-2.99 \times 10^3}{T_g}\right)$	[5]
842	$C_2H_4 + OH \rightarrow CH_3CHO + H$ $\frac{1}{3} \cdot 3.4 \times 10^{-11} \cdot exp\left(\frac{-2.99 \times 10^3}{T_g}\right)$	[5]
843	$C_2H_4 + OH \rightarrow CH_2CH_2OH$ $1.92 \times 10^{-18} \cdot T_g^{2.03} \cdot exp\left(\frac{7.97 \times 10^3}{R \cdot T_g}\right)$	[109]
844	$C_2H_4 + HO_2 \rightarrow C_2H_5 + O_2$ $1 \times 10^{-13} \cdot T_g^{0.07} \cdot exp\left(\frac{-6.58 \times 10^3}{T_g}\right)$	[5]
845	$C_2H_3 + OH \rightarrow CH_3 + HCO$ $1.09 \times 10^{-5} \cdot T_g^{-1.85} \cdot exp\left(\frac{-5.01 \times 10^2}{T_g}\right)$	[110]
846	$C_2H_3 + OH \rightarrow CH_3CO + H$ $9.42 \times 10^{-9} \cdot T_g^{-1.014} \cdot exp\left(\frac{-1.95 \times 10^2}{T_g}\right)$	[110]
847	$C_2H_3 + OH \rightarrow C_2H_2 + H_2O$ $3.96 \times 10^{-13} \cdot T_g^{0.081} \cdot exp\left(\frac{1.91 \times 10^2}{T_g}\right)$	[110]
848	$C_2H_3 + OH \rightarrow CH_2CO + H_2$ $1.26 \times 10^{-8} \cdot T_g^{-1.517} \cdot exp\left(\frac{-3.63 \times 10^2}{T_g}\right)$	[110]
849	$C_2H_3 + OH \rightarrow CH_4 + CO$ $1.32 \times 10^{-8} \cdot T_g^{-1.328} \cdot exp\left(\frac{-2.98 \times 10^2}{T_g}\right)$	[110]
850	$C_2H_3 + H_2O \rightarrow C_2H_4 + OH$ $8 \times 10^{-22} \cdot T_g^{2.9} \cdot exp\left(\frac{-7.48 \times 10^3}{T_g}\right)$	[25]
851	$C_2H_3 + H_2O_2 \rightarrow C_2H_4 + HO_2$ $2 \times 10^{-14} \cdot exp\left(\frac{3 \times 10^2}{T_g}\right)$	[25]
852	$C_2H_2 + OH \rightarrow CH_2CO + H$ $0.5 \cdot 1.3 \times 10^{-10} \cdot exp\left(\frac{-6.8 \times 10^3}{T_g}\right)$	[5]
853	$C_2H_2 + OH \rightarrow C_2H + H_2O$ $0.5 \cdot 1.3 \times 10^{-10} \cdot exp\left(\frac{-6.8 \times 10^3}{T_g}\right)$	[5]
854	$C_2H_2 + HO_2 \rightarrow C_2H_3 + O_2$ $5.18 \times 10^{-18} \cdot T_g^{1.61} \cdot exp\left(\frac{-7.1309 \times 10^3}{T_g}\right)$	[111]
855	$C_2H + OH \rightarrow C_2H_2 + O$ 3×10^{-11}	[25]
856	$C_2H + OH \rightarrow CH_2 + CO$ 3×10^{-11}	[25]

#	Reaction / Rate equation	Ref.
857	$C_2H + H_2O \rightarrow C_2H_2 + OH$ $2.2 \times 10^{-21} \cdot T_g^{3.05} \cdot exp\left(\frac{-3.76 \times 10^2}{T_g}\right)$	[112]
858	$C_2H + HO_2 \rightarrow C_2H_2 + O_2$ 3×10^{-11}	[25]
859	$C_2H + HO_2 \rightarrow HCCO + OH$ 3×10^{-11}	[25]
860	$C_2H_6 + OH^+ \rightarrow C_2H_4^+ + H_2 + OH$ 1.04×10^{-9}	[28]
861	$C_2H_6 + OH^+ \rightarrow C_2H_5^+ + H_2 + O$ 3.2×10^{-10}	[28]
862	$C_2H_6 + OH^+ \rightarrow C_2H_4 + H_3O^+$ 1.6×10^{-10}	[28]
863	$C_2H_6 + OH^+ \rightarrow C_2H_6^+ + OH$ 4.8×10^{-11}	[28]
864	$C_2H_6 + H_2O^+ \rightarrow C_2H_5 + H_3O^+$ 1.328×10^{-9}	[28]
865	$C_2H_6 + H_2O^+ \rightarrow C_2H_4^+ + H_2 + H_2O$ 1.92×10^{-10}	[28]
866	$C_2H_6 + H_2O^+ \rightarrow C_2H_6^+ + H_2O$ 6.4×10^{-11}	[28]
867	$C_2H_6 + H_2O^+ \rightarrow C_2H_5^+ + H + H_2O$ 1.6×10^{-11}	[28]
868	$C_2H_4 + H_2O^+ \rightarrow C_2H_4^+ + H_2O$ 1.5×10^{-9}	[61]
869	$C_2H_2 + H_2O^+ \rightarrow C_2H_2^+ + H_2O$ 1.9×10^{-9}	[61]
870	$C_2H + OH^+ \rightarrow C_2H^+ + OH$ 4.5×10^{-10}	[1]
871	$C_2H + OH^+ \rightarrow C_2H_2^+ + O$ 4.5×10^{-10}	[1]
872	$C_2H + H_2O^+ \rightarrow C_2H^+ + H_2O$ 4.4×10^{-10}	[1]
873	$C_2H + H_2O^+ \rightarrow C_2H_2^+ + OH$ 4.4×10^{-10}	[1]
874	$C_2H + HO_2^+ \rightarrow C_2H_2^+ + O_2$ 7.6×10^{-10}	[1]
875	$C_2H_6^+ + H_2O \rightarrow C_2H_5 + H_3O^+$ 2.95×10^{-9}	[87]
876	$C_2H_5^+ + H_2O \rightarrow C_2H_4 + H_3O^+$ 1.4×10^{-9}	[113]

#	Reaction / Rate equation	Ref.
877	$C_2H_3^+ + H_2O \rightarrow C_2H_2 + H_3O^+$ 8.5×10^{-10}	[1]
878	$C_2H_3^+ + OH^- \rightarrow C_2H_3 + OH$ $7.51 \times 10^{-8} \cdot \left(\frac{T_g}{3 \times 10^2}\right)^{-0.5}$	[2, 3]
879	$C_2H_2^+ + H_2O \rightarrow C_2H + H_3O^+$ 2.2×10^{-10}	[1]
880	$C_2H_2^+ + OH^- \rightarrow C_2H_2 + OH$ $7.51 \times 10^{-8} \cdot \left(\frac{T_g}{3 \times 10^2}\right)^{-0.5}$	[2, 3]
881	$C_2H_4^+ + OH^- \rightarrow C_2H_3 + H + OH$ $7.51 \times 10^{-8} \cdot \left(\frac{T_g}{3 \times 10^2}\right)^{-0.5}$	[2, 3]
882	$C_2H_6 + O \rightarrow C_2H_5 + OH$ $3 \times 10^{-19} \cdot T_g^{2.8} \cdot exp\left(\frac{-2.92 \times 10^3}{T_g}\right)$	[5]
883	$C_2H_6 + O_2 \rightarrow C_2H_5 + HO_2$ $1.21 \times 10^{-18} \cdot T_g^{2.5} \cdot exp\left(\frac{-2.474 \times 10^4}{T_g}\right)$	[5]
884	$C_2H_5 + O \rightarrow CH_3CHO + H$ 8.8×10^{-11}	[5]
885	$C_2H_5 + O \rightarrow CH_3 + HCHO$ 6.6×10^{-11}	[5]
886	$C_2H_5 + O \rightarrow C_2H_4 + OH$ 4.4×10^{-11}	[5]
887	$C_2H_5 + O_2 \rightarrow C_2H_4 + HO_2$ 1×10^{-13}	[5]
888	$C_2H_4 + O \rightarrow CH_3 + HCO$ $0.6 \cdot 2.25 \times 10^{-17} \cdot T_g^{1.88} \cdot exp\left(\frac{-9.2 \times 10^1}{T_g}\right)$	[5]
889	$C_2H_4 + O \rightarrow CH_2CO + H_2$ $0.05 \cdot 2.25 \times 10^{-17} \cdot T_g^{1.88} \cdot exp\left(\frac{-9.2 \times 10^1}{T_g}\right)$	[5]
890	$C_2H_4 + O_2 \rightarrow C_2H_3 + HO_2$ $7 \times 10^{-11} \cdot exp\left(\frac{-2.9 \times 10^4}{T_g}\right)$	[25]
891	$C_2H_3 + O \rightarrow C_2H_2 + OH$ $1.6666667 \times 10^{-11}$	[5]
892	$C_2H_3 + O \rightarrow CH_3 + CO$ $1.6666667 \times 10^{-11}$	[5]
893	$C_2H_3 + O \rightarrow CH_2 + HCO$ $1.6666667 \times 10^{-11}$	[5]

#	Reaction / Rate equation	Ref.
894	$C_2H_3 + O_2 \rightarrow C_2H_2 + HO_2$ $\frac{6.6 \times 10^{21}}{N_A} \cdot T_g^{-3.3} \cdot exp\left(\frac{-5.41 \times 10^3 \cdot 4.184}{R \cdot T_g}\right)$	[114]
895	$C_2H_3 + O_2 \rightarrow HCHO + HCO$ $\frac{4 \times 10^{21}}{N_A} \cdot T_g^{-3} \cdot exp\left(\frac{-2.4 \times 10^3 \cdot 4.184}{R \cdot T_g}\right)$	[114]
896	$C_2H_2 + O \rightarrow CH_2 + CO$ $0.2 \cdot 1.95 \times 10^{-15} \cdot T_g^{1.4} \cdot exp\left(\frac{-1.11 \times 10^3}{T_g}\right)$	[5]
897	$C_2H_2 + O \rightarrow H + HCCO$ $0.8 \cdot 1.95 \times 10^{-15} \cdot T_g^{1.4} \cdot exp\left(\frac{-1.11 \times 10^3}{T_g}\right)$	[5]
898	$C_2H_2 + O_2 \rightarrow HCO + HCO$ $\frac{6.1 \times 10^{12}}{N_A} \cdot exp\left(\frac{-5.325 \times 10^4 \cdot 4.184}{R \cdot T_g}\right)$	[115]
899	$C_2H + O \rightarrow CH + CO$ 9.9×10^{-11}	[5]
900	$C_2H + O_2 \rightarrow CO + HCO$ $0.45 \cdot 2.7 \times 10^{-10} \cdot T_g^{-0.35}$	[5]
901	$C_2H + O_2 \rightarrow CH + CO_2$ $0.1 \cdot 2.7 \times 10^{-10} \cdot T_g^{-0.35}$	[5]
902	$C_2H_6 + O^+ \rightarrow C_2H_4^+ + H_2O$ 1.33×10^{-9}	[28]
903	$C_2H_6 + O^+ \rightarrow C_2H_5^+ + OH$ 5.7×10^{-10}	[28]
904	$C_2H_4 + O^+ \rightarrow C_2H_4^+ + O$ 7×10^{-11}	[29]
905	$C_2H_4 + O^+ \rightarrow C_2H_2^+ + H_2O$ 1.12×10^{-9}	[29]
906	$C_2H_4 + O^+ \rightarrow C_2H_3^+ + OH$ 2.1×10^{-10}	[29]
907	$C_2H_4 + O_2^+ \rightarrow C_2H_4^+ + O_2$ 6.8×10^{-10}	[116]
908	$C_2H_2 + O^+ \rightarrow C_2H_2^+ + O$ 3.9×10^{-11}	[29]
909	$C_2H_2 + O_2^+ \rightarrow C_2H_2^+ + O_2$ 1.105×10^{-9}	[117]
910	$C_2H_2 + O_2^+ \rightarrow CO + H + HCO^+$ 6.5×10^{-11}	[117]
911	$C_2H + O^+ \rightarrow C_2H^+ + O$ 4.6×10^{-10}	[1]
912	$C_2H + O^+ \rightarrow CH + CO^+$ 4.6×10^{-10}	[1]

#	Reaction / Rate equation	Ref.
913	$C_2H_4^+ + O \rightarrow CH_3^+ + HCO$ 1.08×10^{-10}	[118]
914	$C_2H_4^+ + O \rightarrow CH_3 + HCO^+$ 8.4×10^{-11}	[118]
915	$C_2H_4^+ + O^- \rightarrow C_2H_3 + H + O$ $7.51 \times 10^{-8} \cdot \left(\frac{T_g}{3 \times 10^2}\right)^{-0.5}$	[2, 3]
916	$C_2H_3^+ + O \rightarrow CH_3^+ + CO$ 5×10^{-12}	[118]
917	$C_2H_3^+ + O^- \rightarrow C_2H_3 + O$ $7.51 \times 10^{-8} \cdot \left(\frac{T_g}{3 \times 10^2}\right)^{-0.5}$	[2, 3]
918	$C_2H_3^+ + O^- \rightarrow C_2H + H_2 + O$ $7.51 \times 10^{-8} \cdot \left(\frac{T_g}{3 \times 10^2}\right)^{-0.5}$	[2, 3]
919	$C_2H_3^+ + O_2^- \rightarrow C_2H_3 + O_2$ $7.51 \times 10^{-8} \cdot \left(\frac{T_g}{3 \times 10^2}\right)^{-0.5}$	[2, 3]
920	$C_2H_2^+ + O \rightarrow CH + HCO^+$ 8.5×10^{-11}	[81]
921	$C_2H_2^+ + O^- \rightarrow C_2H_2 + O$ $7.51 \times 10^{-8} \cdot \left(\frac{T_g}{3 \times 10^2}\right)^{-0.5}$	[2, 3]
922	$C_2H_2^+ + O_2^- \rightarrow C_2H_2 + O_2$ $7.51 \times 10^{-8} \cdot \left(\frac{T_g}{3 \times 10^2}\right)^{-0.5}$	[2, 3]
923	$C_2H^+ + O \rightarrow C + HCO^+$ 1×10^{-11}	[1]
924	$C_2H_4 + CO \rightarrow C_2H_3 + HCO$ $2.5 \times 10^{-10} \cdot exp\left(\frac{-4.56 \times 10^4}{T_g}\right)$	[25]
925	$C_2H_2 + CO \rightarrow C_2H + HCO$ $8 \times 10^{-10} \cdot exp\left(\frac{-5.37 \times 10^4}{T_g}\right)$	[25]
926	$C_2H_4 + CO_2^+ \rightarrow C_2H_4^+ + CO_2$ 8.775×10^{-10}	[61]
927	$C_2H_2 + CO_2^+ \rightarrow C_2H_2^+ + CO_2$ 7.3×10^{-10}	[61]
928	$C_2H + CO^+ \rightarrow C_2H^+ + CO$ 3.9×10^{-10}	[1]
929	$C_2H_6 + HCO \rightarrow C_2H_5 + HCHO$ $7.8 \times 10^{-20} \cdot T_g^{2.72} \cdot exp\left(\frac{-9.176 \times 10^3}{T_g}\right)$	[25]

#	Reaction / Rate equation	Ref.
930	$C_2H_6 + CH_3O \rightarrow C_2H_5 + CH_3OH$ $4 \times 10^{-13} \cdot exp\left(\frac{-3.57 \times 10^3}{T_g}\right)$	[25]
931	$C_2H_6 + CH_2OH \rightarrow C_2H_5 + CH_3OH$ $3.3 \times 10^{-22} \cdot T_g^{2.95} \cdot exp\left(\frac{-7.033 \times 10^3}{T_g}\right)$	[96]
932	$C_2H_6 + CH_3OO \rightarrow C_2H_5 + CH_3OOH$ $4.9 \times 10^{-13} \cdot exp\left(\frac{-7.52 \times 10^3}{T_g}\right)$	[25]
933	$C_2H_5 + HCO \rightarrow C_2H_6 + CO$ 2×10^{-10}	[25]
934	$C_2H_5 + HCHO \rightarrow C_2H_6 + HCO$ $9.2 \times 10^{-21} \cdot T_g^{2.81} \cdot exp\left(\frac{-2.95 \times 10^3}{T_g}\right)$	[25]
935	$C_2H_5 + CH_3O \rightarrow C_2H_6 + HCHO$ 4×10^{-11}	[25]
936	$C_2H_5 + CH_2OH \rightarrow C_2H_4 + CH_3OH$ 4×10^{-12}	[96]
937	$C_2H_5 + CH_2OH \rightarrow C_2H_6 + HCHO$ 4×10^{-12}	[96]
938	$C_2H_5 + CH_3OH \rightarrow C_2H_6 + CH_2OH$ $5.3 \times 10^{-23} \cdot T_g^{3.2} \cdot exp\left(\frac{-4.61 \times 10^3}{T_g}\right)$	[96]
939	$C_2H_5 + CH_3OH \rightarrow C_2H_6 + CH_3O$ $2.4 \times 10^{-23} \cdot T_g^{3.1} \cdot exp\left(\frac{-4.5 \times 10^3}{T_g}\right)$	[96]
940	$C_2H_5 + CH_3OO \rightarrow CH_3CH_2O + CH_3O$ 4×10^{-11}	[25]
941	$C_2H_4 + COOH \rightarrow C_2H_5 + CO_2$ 1×10^{-14}	[88]
942	$C_2H_4 + CH_2OH \rightarrow C_2H_5 + HCHO$ $\frac{8 \times 10^{-14} \cdot exp\left(\frac{-3.5 \times 10^3}{T_g}\right) \cdot exp\left(\frac{-2 \times 10^3}{T_g}\right)}{1.0 + exp\left(\frac{-2 \times 10^3}{T_g}\right)}$	[96]
943	$C_2H_3 + HCO \rightarrow C_2H_4 + CO$ 1.5×10^{-10}	[25]
944	$C_2H_3 + HCHO \rightarrow C_2H_4 + HCO$ $9 \times 10^{-21} \cdot T_g^{2.81} \cdot exp\left(\frac{-2.95 \times 10^3}{T_g}\right)$	[25]
945	$C_2H_3 + CH_3O \rightarrow C_2H_4 + HCHO$ 4×10^{-11}	[25]
946	$C_2H_3 + CH_2OH \rightarrow C_2H_4 + HCHO$ 5×10^{-11}	[96]

#	Reaction / Rate equation	Ref.
947	$C_2H_3 + CH_3OH \rightarrow C_2H_4 + CH_2OH$ $5.3 \times 10^{-23} \cdot T_g^{3.2} \cdot exp\left(\frac{-3.609 \times 10^3}{T_g}\right)$	[96]
948	$C_2H_3 + CH_3OH \rightarrow C_2H_4 + CH_3O$ $2.4 \times 10^{-23} \cdot T_g^{3.1} \cdot exp\left(\frac{-3.49 \times 10^3}{T_g}\right)$	[96]
949	$C_2H_2 + COOH \rightarrow C_2H_3 + CO_2$ 3×10^{-14}	[88]
950	$C_2H_2 + CH_2OH \rightarrow C_2H_3 + HCHO$ $1.2 \times 10^{-12} \cdot exp\left(\frac{-4.531 \times 10^3}{T_g}\right)$	[96]
951	$C_2H + HCO \rightarrow C_2H_2 + CO$ 1×10^{-10}	[25]
952	$C_2H + CH_3O \rightarrow C_2H_2 + HCHO$ 4×10^{-11}	[25]
953	$C_2H + CH_2OH \rightarrow C_2H_2 + HCHO$ 6×10^{-11}	[96]
954	$C_2H + CH_3OH \rightarrow C_2H_2 + CH_2OH$ 1×10^{-11}	[96]
955	$C_2H + CH_3OH \rightarrow C_2H_2 + CH_3O$ 2×10^{-12}	[96]
956	$C_2H + CH_3OO \rightarrow CH_3O + HCCO$ 4×10^{-11}	[25]
957	$C_2H_4 + HCO^+ \rightarrow C_2H_5^+ + CO$ 1.4×10^{-9}	[13]
958	$C_2H_3 + HCO^+ \rightarrow C_2H_4^+ + CO$ 1.4×10^{-9}	[13]
959	$C_2H_2 + HCO^+ \rightarrow C_2H_3^+ + CO$ 1.4×10^{-9}	[38]
960	$C_2H + HCO^+ \rightarrow C_2H_2^+ + CO$ 7.8×10^{-10}	[1]
961	$C_2H_2^+ + HCO \rightarrow C_2H_2 + HCO^+$ 5×10^{-10}	[1]
962	$C_2H_2^+ + HCO \rightarrow C_2H_3^+ + CO$ 3.7×10^{-10}	[1]
963	$C_2H_2^+ + HCHO \rightarrow C_2H_3 + HCO^+$ 5.375×10^{-10}	[87]
964	$C_2H_2^+ + HCHO \rightarrow C_2H_4^+ + CO$ 2.795×10^{-10}	[87]
965	$C_2H^+ + HCO \rightarrow C_2H_2^+ + CO$ 7.6×10^{-10}	[1]

#	Reaction / Rate equation	Ref.
966	$H + HCCO \rightarrow CH_2 + CO$ $9.92 \times 10^{-13} \cdot T_g^{0.76} \cdot exp\left(\frac{4.38 \times 10^2}{T_g}\right)$	[119]
967	$CH_2CO + H \rightarrow CH_3 + CO$ $\frac{1.11 \times 10^7}{N_A} \cdot T_g^2 \cdot exp\left(\frac{-2 \times 10^3 \cdot 4.184}{R \cdot T_g}\right)$	[120]
968	$CH_2CO + H \rightarrow H_2 + HCCO$ $\frac{1.8 \times 10^{14}}{N_A} \cdot exp\left(\frac{-8.6 \times 10^3 \cdot 4.184}{R \cdot T_g}\right)$	[120]
969	$CH_2CO + H \rightarrow CH_3CO$ $\frac{1.63 \times 10^9}{N_A} \cdot T_g^{1.3766} \cdot exp\left(\frac{-1.664 \times 10^3 \cdot 4.184}{R \cdot T_g}\right)$	[121]
970	$CH_3CO + H \rightarrow CH_3 + HCO$ $\frac{0.65 \cdot 2 \times 10^{13}}{N_A}$	[122, 123]
971	$CH_3CO + H \rightarrow CH_2CO + H_2$ $\frac{0.35 \cdot 2 \times 10^{13}}{N_A}$	[122, 123]
972	$CH_3CO + H \rightarrow CH_3CHO$ $6.02 \times 10^{-11} \cdot T_g^{0.16}$	[110]
973	$CH_3CO + H_2 \rightarrow CH_3CHO + H$ $6.8 \times 10^{-18} \cdot T_g^{1.82} \cdot exp\left(\frac{-8.862 \times 10^3}{T_g}\right)$	[25]
974	$CH_3CHO + H \rightarrow CH_3CO + H_2$ $2.18 \times 10^{-19} \cdot T_g^{2.58} \cdot exp\left(\frac{-6.14 \times 10^2}{T_g}\right)$	[124]
975	$CH_3CHO + H \rightarrow CH_3CH_2O$ $7.66 \times 10^{-17} \cdot T_g^{1.71} \cdot exp\left(\frac{-3.57 \times 10^3}{T_g}\right)$	[124]
976	$CH_3CHO + H \rightarrow CH_3CHOH$ $2.89 \times 10^{-18} \cdot T_g^{2.2} \cdot exp\left(\frac{-3.78 \times 10^3}{T_g}\right)$	[124]
977	$CH_3CH_2O + H \rightarrow CH_2OH + CH_3$ $2.26 \times 10^{-12} \cdot T_g^{0.701} \cdot exp\left(\frac{-1.74 \times 10^2}{T_g}\right)$	[125]
978	$CH_3CH_2O + H \rightarrow CH_3CH_2OH$ $5.11 \times 10^{-13} \cdot T_g^{0.894} \cdot exp\left(\frac{-6.5}{T_g}\right)$	[125]
979	$CH_3CH_2O + H \rightarrow C_2H_5 + OH$ $9.04 \times 10^{-16} \cdot T_g^{1.27} \cdot exp\left(\frac{-1.57 \times 10^2}{T_g}\right)$	[125]
980	$CH_3CH_2O + H \rightarrow CH_3CHOH + H$ $1.33 \times 10^{-22} \cdot T_g^{3.1} \cdot exp\left(\frac{-1.42 \times 10^2}{T_g}\right)$	[125]

#	Reaction / Rate equation	Ref.
981	$CH_3CH_2O + H \rightarrow C_2H_4 + H_2O$ $9.95 \times 10^{-10} \cdot T_g^{-0.813} \cdot exp\left(\frac{-3.59 \times 10^2}{T_g}\right)$	[125]
982	$CH_3CH_2O + H \rightarrow CH_3CHO + H_2$ $1.25 \times 10^{-20} \cdot T_g^{1.78} \cdot exp\left(\frac{-4.07 \times 10^1}{T_g}\right)$ $+1.24 \times 10^{-14} \cdot T_g^{1.15} \cdot exp\left(\frac{-3.39 \times 10^2}{T_g}\right)$	[125]
983	$CH_3CH_2O + H \rightarrow CH_4 + HCHO$ $1.32 \times 10^{-21} \cdot T_g^{2.21} \cdot exp\left(\frac{9.05 \times 10^1}{T_g}\right)$	[125]
984	$CH_3CHOH + H \rightarrow CH_3CH_2OH$ $5.99 \times 10^{-11} \cdot T_g^{0.06} \cdot exp\left(\frac{-2.2 \times 10^2}{T_g}\right)$	[125]
985	$CH_3CHOH + H \rightarrow CH_2OH + CH_3$ $1.44 \times 10^{-7} \cdot T_g^{-0.891} \cdot exp\left(\frac{-1.461 \times 10^3}{T_g}\right)$	[125]
986	$CH_3CHOH + H \rightarrow C_2H_5 + OH$ $4.02 \times 10^{-9} \cdot T_g^{-0.83} \cdot exp\left(\frac{-2.414 \times 10^3}{T_g}\right)$	[125]
987	$CH_3CHOH + H \rightarrow CH_3CH_2O + H$ $4.95 \times 10^{-23} \cdot T_g^{2.94} \cdot exp\left(\frac{-4.266 \times 10^3}{T_g}\right)$	[125]
988	$CH_3CHOH + H \rightarrow C_2H_4 + H_2O$ $7.81 \times 10^{-3} \cdot T_g^{-3.02} \cdot exp\left(\frac{-1.432 \times 10^3}{T_g}\right)$	[125]
989	$CH_3CHOH + H \rightarrow CH_3CHO + H_2$ $7.42 \times 10^{-21} \cdot T_g^{1.62} \cdot exp\left(\frac{5.4}{T_g}\right)$ $+2.26 \times 10^{-15} \cdot T_g^{1.29} \cdot exp\left(\frac{-1.421 \times 10^3}{T_g}\right)$	[125]
990	$CH_3CHOH + H \rightarrow CH_4 + HCHO$ $5.56 \times 10^{-22} \cdot T_g^{2.1} \cdot exp\left(\frac{-1.07 \times 10^2}{T_g}\right)$	[125]
991	$CH_3CH_2OH + H \rightarrow C_2H_5 + H_2O$ $\frac{5.9 \times 10^{11}}{N_A} \cdot exp\left(\frac{-3.45 \times 10^3 \cdot 4.184}{R \cdot T_g}\right)$	[126]
992	$CH_3CH_2OH + H \rightarrow CH_3CHOH + H_2$ $1.46 \times 10^{-19} \cdot T_g^{2.68} \cdot exp\left(\frac{-1.467 \times 10^3}{T_g}\right)$	[127]
993	$CH_3CH_2OH + H \rightarrow CH_2CH_2OH + H_2$ $8.82 \times 10^{-20} \cdot T_g^{2.81} \cdot exp\left(\frac{-3.772 \times 10^3}{T_g}\right)$	[127]
994	$CH_3CH_2OH + H \rightarrow CH_3CH_2O + H_2$ $1.57 \times 10^{-21} \cdot T_g^{3.14} \cdot exp\left(\frac{-4.379 \times 10^3}{T_g}\right)$	[127]

#	Reaction / Rate equation	Ref.
995	$CH_3CHO + H_3^+ \rightarrow C_2H_3^+ + H_2 + H_2O$ 8.97×10^{-10}	[100]
996	$CH_3CHO + H_3^+ \rightarrow C_2H_5^+ + H_2O$ 7.59×10^{-10}	[100]
997	$CH_3CHO + H_3^+ \rightarrow CH_3OH + CH_3^+$ 1.449×10^{-9}	[100]
998	$CH_3CHO + H_3^+ \rightarrow CH_5^+ + CO + H_2$ 8.28×10^{-10}	[100]
999	$CH_3CHO + H_3^+ \rightarrow C_2H_4 + H_3O^+$ 1.035×10^{-9}	[100]
1000	$CH_3CH_2OH + H_3^+ \rightarrow CH_3^+ + CH_4 + H_2O$ 1.5×10^{-9}	[100]
1001	$CH_3CH_2OH + H_3^+ \rightarrow C_2H_3^+ + H_2 + H_2 + H_2O$ 4×10^{-10}	[100]
1002	$CH_3CH_2OH + H_3^+ \rightarrow CH_4 + H_2 + H_2 + HCO^+$ 1.1×10^{-9}	[100]
1003	$CH_3CH_2OH + H_3^+ \rightarrow C_2H_5^+ + H_2 + H_2O$ 1.1×10^{-9}	[100]
1004	$HCCO + OH \rightarrow CH_2CO + O$ $2.1 \times 10^{-18} \cdot T_g^{1.99} \cdot exp\left(\frac{-1.128 \times 10^4 \cdot 4.184}{R \cdot T_g}\right)$	[128]
1005	$CH_2CO + OH \rightarrow CH_2OH + CO$ $0.6 \cdot 2.8 \times 10^{-12} \cdot exp\left(\frac{5.1 \times 10^2}{T_g}\right)$	[5]
1006	$CH_2CO + OH \rightarrow H_2O + HCCO$ $0.01 \cdot 2.8 \times 10^{-12} \cdot exp\left(\frac{5.1 \times 10^2}{T_g}\right)$	[5]
1007	$CH_2CO + OH \rightarrow HCHO + HCO$ $0.02 \cdot 2.8 \times 10^{-12} \cdot exp\left(\frac{5.1 \times 10^2}{T_g}\right)$	[5]
1008	$CH_2CO + OH \rightarrow CH_3 + CO_2$ $0.37 \cdot 2.8 \times 10^{-12} \cdot exp\left(\frac{5.1 \times 10^2}{T_g}\right)$	[5]
1009	$CH_3CO + OH \rightarrow CH_2CO + H_2O$ 2×10^{-11}	[25]
1010	$CH_3CO + H_2O_2 \rightarrow CH_3CHO + HO_2$ $3 \times 10^{-13} \cdot exp\left(\frac{-4.14 \times 10^3}{T_g}\right)$	[25]
1011	$CH_3CHO + OH \rightarrow CH_3CO + H_2O$ $0.93 \cdot 4.8 \times 10^{-16} \cdot T_g^{1.35} \cdot exp\left(\frac{7.92 \times 10^2}{T_g}\right)$	[5]
1012	$CH_3CHO + OH \rightarrow CH_3 + HCOOH$ $0.03 \cdot 4.8 \times 10^{-16} \cdot T_g^{1.35} \cdot exp\left(\frac{7.92 \times 10^2}{T_g}\right)$	[5, 129]

#	Reaction / Rate equation	Ref.
1013	$CH_3CHO + OH \rightarrow CH_3COOH + H$ $0.02 \cdot 4.8 \times 10^{-16} \cdot T_g^{1.35} \cdot exp\left(\frac{7.92 \times 10^2}{T_g}\right)$	[5, 129]
1014	$CH_3CHO + HO_2 \rightarrow CH_3CO + H_2O_2$ $6.8 \times 10^{-20} \cdot T_g^{2.5} \cdot exp\left(\frac{-5.135 \times 10^3}{T_g}\right)$	[5]
1015	$CH_3CH_2OH + OH \rightarrow CH_2CH_2OH + H_2O$ $\frac{1.74 \times 10^{11}}{N_A} \cdot T_g^{0.27} \cdot exp\left(\frac{-6 \times 10^2 \cdot 4.184}{R \cdot T_g}\right)$	[130]
1016	$CH_3CH_2OH + OH \rightarrow CH_3CHOH + H_2O$ $\frac{4.64 \times 10^{11}}{N_A} \cdot T_g^{0.15}$	[130]
1017	$CH_3CH_2OH + OH \rightarrow CH_3CH_2O + H_2O$ $\frac{7.46 \times 10^{11}}{N_A} \cdot T_g^{0.3} \cdot exp\left(\frac{-1.634 \times 10^3 \cdot 4.184}{R \cdot T_g}\right)$	[130]
1018	$CH_3CH_2OH + HO_2 \rightarrow CH_3CHOH + H_2O_2$ $\frac{5.544 \times 10^{18}}{N_A} \cdot T_g^{-1.808} \cdot exp\left(\frac{-8.29197 \times 10^3}{T_g}\right)$	[131]
1019	$HCCO + O \rightarrow CH + CO_2$ $4.9 \times 10^{-11} \cdot exp\left(\frac{-5.6 \times 10^2}{T_g}\right)$	[5]
1020	$CH_2CO + O \rightarrow HCCO + OH$ $3.11 \times 10^{-10} \cdot exp\left(\frac{-1.669 \times 10^4 \cdot 4.184}{R \cdot T_g}\right)$	[128]
1021	$CH_2CO + O \rightarrow CO + HCHO$ $0.2 \cdot 3 \times 10^{-12} \cdot exp\left(\frac{-6.8 \times 10^2}{T_g}\right)$	[5]
1022	$CH_2CO + O \rightarrow HCO + HCO$ $0.1 \cdot 3 \times 10^{-12} \cdot exp\left(\frac{-6.8 \times 10^2}{T_g}\right)$	[5]
1023	$CH_2CO + O \rightarrow CH_2 + CO_2$ $0.6 \cdot 3 \times 10^{-12} \cdot exp\left(\frac{-6.8 \times 10^2}{T_g}\right)$	[5]
1024	$CH_3CO + O \rightarrow CH_2CO + OH$ 8.75×10^{-11}	[5]
1025	$CH_3CO + O \rightarrow CH_3 + CO_2$ 2.625×10^{-10}	[5]
1026	$CH_3CHO + O \rightarrow CH_3CO + OH$ $\frac{5 \times 10^{12}}{N_A} \cdot exp\left(\frac{-7.5 \times 10^3}{R \cdot T_g}\right)$	[123]
1027	$CH_3CHO + O_2 \rightarrow CH_3CO + HO_2$ $2 \times 10^{-19} \cdot T_g^{2.5} \cdot exp\left(\frac{-1.89 \times 10^4}{T_g}\right)$	[5]
1028	$CH_3CH_2O + O_2 \rightarrow CH_3CHO + HO_2$ $3.8 \times 10^{-14} \cdot exp\left(\frac{-4.4 \times 10^2}{T_g}\right)$	[5]

#	Reaction / Rate equation	Ref.
1029	$CH_3CHOH + O \rightarrow CH_3 + HCOOH$ $3.9 \times 10^{-10} \cdot \left(\frac{T_g}{3 \times 10^2}\right)^{0.18} \cdot exp\left(\frac{-0.49}{T_g}\right)$	[132]
1030	$CH_3CHOH + O \rightarrow CH_3CHO + OH$ $4.8 \times 10^{-11} \cdot \left(\frac{T_g}{3 \times 10^2}\right)^{0.19} \cdot exp\left(\frac{-0.39}{T_g}\right)$	[132]
1031	$CH_3CHOH + O \rightarrow CH_3COOH + H$ $2.2 \times 10^{-10} \cdot \left(\frac{T_g}{3 \times 10^2}\right)^{0.16} \cdot exp\left(\frac{-0.59}{T_g}\right)$	[132]
1032	$CH_3CHOH + O_2 \rightarrow CH_3CHO + HO_2$ $\frac{5.28 \times 10^{17}}{N_A} \cdot T_g^{-1.638} \cdot exp\left(\frac{-0.839 \cdot 4.184 \times 10^3}{R \cdot T_g}\right)$	[133]
1033	$CH_2CH_2OH + O \rightarrow CH_2OH + HCHO$ $4.6 \times 10^{-10} \cdot \left(\frac{T_g}{3 \times 10^2}\right)^{0.17} \cdot exp\left(\frac{-0.51}{T_g}\right)$	[132]
1034	$CH_3CH_2OH + O \rightarrow CH_3CHOH + OH$ $0.99 \cdot 1 \times 10^{-18} \cdot T_g^{2.5} \cdot exp\left(\frac{-9.3 \times 10^2}{T_g}\right)$	[5]
1035	$CH_3CH_2OH + O \rightarrow CH_2CH_2OH + OH$ $0.005 \cdot 1 \times 10^{-18} \cdot T_g^{2.5} \cdot exp\left(\frac{-9.3 \times 10^2}{T_g}\right)$	[5]
1036	$CH_3CH_2OH + O \rightarrow CH_3CH_2O + OH$ $0.005 \cdot 1 \times 10^{-18} \cdot T_g^{2.5} \cdot exp\left(\frac{-9.3 \times 10^2}{T_g}\right)$	[5]
1037	$CH_3CH_2OH + O_2 \rightarrow CH_3CHOH + HO_2$ $4 \times 10^{-19} \cdot T_g^{2.5} \cdot exp\left(\frac{-2.217 \times 10^4}{T_g}\right)$	[5]
1038	$CH_3CH_2OH + O_2 \rightarrow CH_2CH_2OH + HO_2$ $6 \times 10^{-19} \cdot T_g^{2.5} \cdot exp\left(\frac{-2.403 \times 10^4}{T_g}\right)$	[5]
1039	$CH_3CH_2OH + O_2 \rightarrow CH_3CH_2O + HO_2$ $2 \times 10^{-19} \cdot T_g^{2.5} \cdot exp\left(\frac{-2.653 \times 10^4}{T_g}\right)$	[5]
1040	$CH_2CO + CH_3 \rightarrow C_2H_5 + CO$ $\frac{1.24 \times 10^5}{N_A} \cdot T_g^{2.29} \cdot exp\left(\frac{-1.0642 \times 10^4 \cdot 4.184}{R \cdot T_g}\right)$	[134]
1041	$CH_2CO + CH_3 \rightarrow CH_4 + HCCO$ $\frac{1.55 \times 10^2}{N_A} \cdot T_g^{3.38} \cdot exp\left(\frac{-1.0512 \times 10^4 \cdot 4.184}{R \cdot T_g}\right)$	[134]
1042	$CH_2 + CH_2CO \rightarrow C_2H_4 + CO$ $\frac{1 \times 10^{12}}{N_A}$	[135]
1043	$CH_2 + CH_2CO \rightarrow CH_3 + HCCO$ $\frac{3.6 \times 10^{13}}{N_A} \cdot exp\left(\frac{-1.1 \times 10^4 \cdot 4.184}{R \cdot T_g}\right)$	[120]

#	Reaction / Rate equation	Ref.
1044	$CH_3CO + CH_4 \rightarrow CH_3 + CH_3CHO$ $3.6 \times 10^{-21} \cdot T_g^{2.88} \cdot exp\left(\frac{-1.08 \times 10^4}{T_g}\right)$	[25]
1045	$CH_3 + CH_3CO \rightarrow CH_2CO + CH_4$ $\frac{6.1 \times 10^9 \cdot 1 \times 10^3}{N_A}$	[136]
1046	$CH_2 + CH_3CO \rightarrow CH_2CO + CH_3$ 3×10^{-11}	[25]
1047	$CH_3 + CH_3CHO \rightarrow CH_3CO + CH_4$ $0.993 \cdot 5.8 \times 10^{-32} \cdot T_g^{6.21} \cdot exp\left(\frac{-8.2 \times 10^2}{T_g}\right)$	[5]
1048	$CH_3 + CH_3CH_2OH \rightarrow CH_3CHOH + CH_4$ $\frac{2.476 \times 10^1}{N_A} \cdot T_g^{3.368} \cdot exp\left(\frac{-3.95579 \times 10^3}{T_g}\right)$	[131]
1049	$CH_3 + CH_3CH_2OH \rightarrow CH_2CH_2OH + CH_4$ $\frac{1.861 \times 10^2}{N_A} \cdot T_g^{3.45} \cdot exp\left(\frac{-5.54285 \times 10^3}{T_g}\right)$	[131]
1050	$CH_3 + CH_3CH_2OH \rightarrow CH_3CH_2O + CH_4$ $\frac{0.09533}{N_A} \cdot T_g^{4.159} \cdot exp\left(\frac{-4.119 \times 10^3}{T_g}\right)$	[131]
1051	$C_2H_6 + CH_3CO \rightarrow C_2H_5 + CH_3CHO$ $3 \times 10^{-20} \cdot T_g^{2.75} \cdot exp\left(\frac{-8.82 \times 10^3}{T_g}\right)$	[25]
1052	$C_2H_5 + CH_3CHO \rightarrow C_2H_6 + CH_3CO$ $\frac{1.25892541 \times 10^{12}}{N_A} \cdot exp\left(\frac{-8.5 \cdot 4.184 \times 10^3}{R \cdot T_g}\right)$	[137]
1053	$CH_3CO + HCO \rightarrow CH_3CHO + CO$ 1.5×10^{-11}	[25]
1054	$CH_3CO + HCHO \rightarrow CH_3CHO + HCO$ $3 \times 10^{-13} \cdot exp\left(\frac{-6.5 \times 10^3}{T_g}\right)$	[25]
1055	$CH_3CO + CH_3O \rightarrow CH_2CO + CH_3OH$ 1×10^{-11}	[25]
1056	$CH_3CO + CH_3O \rightarrow CH_3CHO + HCHO$ 1×10^{-11}	[25]
1057	$CH_3CO + CH_3OH \rightarrow CH_2OH + CH_3CHO$ $8.06 \times 10^{-21} \cdot T_g^{2.99} \cdot exp\left(\frac{-6.21 \times 10^3}{T_g}\right)$	[96]
1058	$CH_3CHO + CH_3O \rightarrow CH_3CO + CH_3OH$ $\frac{1.69 \times 10^5}{N_A} \cdot T_g^{2.04} \cdot exp\left(\frac{-2.353 \times 10^3 \cdot 4.184}{R \cdot T_g}\right)$ $+\frac{9.62 \times 10^3}{N_A} \cdot T_g^{2.5} \cdot exp\left(\frac{-1.59 \times 10^2 \cdot 4.184}{R \cdot T_g}\right)$	[138]

#	Reaction / Rate equation	Ref.
1059	$CH_3CHO + CH_3OO \rightarrow CH_3CO + CH_3OOH$ $\frac{0.322}{N_A} \cdot T_g^{3.94} \cdot exp\left(\frac{-9.503 \times 10^3 \cdot 4.184}{R \cdot T_g}\right)$ $+\frac{4.99 \times 10^{-6}}{N_A} \cdot T_g^{4.98} \cdot exp\left(\frac{-5.2682 \times 10^3 \cdot 4.184}{R \cdot T_g}\right)$	[138]
1060	$CH_3CO + CH_3CO \rightarrow CH_2CO + CH_3CHO$ $\frac{9 \times 10^9 \cdot 1 \times 10^3}{N_A}$	[136]
1061	$COOH \rightarrow CO + OH$ $k_0 = \frac{10^{2.5137 \times 10^1}}{N_A} \cdot T_g^{-2.396} \cdot exp\left(\frac{-1.8862 \times 10^4}{T_g}\right)$ $k_\infty = 10^{1.4074 \times 10^1} \cdot T_g^{0.132} \cdot exp\left(\frac{-1.8349 \times 10^4}{T_g}\right)$ $F_c = 0.729 \cdot exp\left(\frac{-5.13 \times 10^2}{T_g}\right)$ $+exp\left(\frac{-T_g}{5.4 \times 10^2}\right)$	[139]a
1062	$COOH \rightarrow CO_2 + H$ $k_0 = \frac{10^{2.6775 \times 10^1}}{N_A} \cdot T_g^{-3.148} \cdot exp\left(\frac{-1.8629 \times 10^4}{T_g}\right)$ $k_\infty = 10^{1.1915 \times 10^1} \cdot T_g^{0.413} \cdot exp\left(\frac{-1.7783 \times 10^4}{T_g}\right)$ $F_c = 1.049 \cdot exp\left(\frac{-2.407 \times 10^3}{T_g}\right)$ $+exp\left(\frac{-T_g}{8.23 \times 10^2}\right)$	[139]a
1063	$HCHO \rightarrow H + HCO$ $8.09 \times 10^{-9} \cdot exp\left(\frac{-3.805 \times 10^4}{T_g}\right) \cdot n_M$	[5]
1064	$CH_2OH \rightarrow H + HCHO$ $k_0 = \frac{6.01 \times 10^{33}}{N_A} \cdot T_g^{-5.39} \cdot exp\left(\frac{-3.62 \times 10^4 \cdot 4.184}{R \cdot T_g}\right)$ $k_\infty = 2.8 \times 10^{14} \cdot T_g^{-0.73} \cdot exp\left(\frac{-3.282 \times 10^4 \cdot 4.184}{R \cdot T_g}\right)$ $F_c = (1 - 0.96) \cdot exp\left(\frac{-T_g}{6.76 \times 10^1}\right)$ $+0.96 \cdot exp\left(\frac{-T_g}{1.855 \times 10^3}\right)$ $+exp\left(\frac{-7.543 \times 10^3}{T_g}\right)$	[140]a

#	Reaction / Rate equation	Ref.
1065	$CH_3OH \rightarrow CH_3 + OH$ $0.8 \cdot k$ $k_0 = 1.1 \times 10^{-7} \cdot exp\left(\frac{-3.308 \times 10^4}{T_g}\right)$ $k_\infty = 2.5 \times 10^{19} \cdot T_g^{-0.94} \cdot exp\left(\frac{-4.703 \times 10^4}{T_g}\right)$ $F_c = 0.18 \cdot exp\left(\frac{-T_g}{2 \times 10^2}\right)$ $+0.82 \cdot exp\left(\frac{-T_g}{1.438 \times 10^3}\right)$	[5, 141][a]
1066	$CH_3OH \rightarrow CH_2 + H_2O$ $0.15 \cdot k$ $k_0 = 1.1 \times 10^{-7} \cdot exp\left(\frac{-3.308 \times 10^4}{T_g}\right)$ $k_\infty = 2.5 \times 10^{19} \cdot T_g^{-0.94} \cdot exp\left(\frac{-4.703 \times 10^4}{T_g}\right)$ $F_c = 0.18 \cdot exp\left(\frac{-T_g}{2 \times 10^2}\right)$ $+0.82 \cdot exp\left(\frac{-T_g}{1.438 \times 10^3}\right)$	[5, 141][a]
1067	$CH_3OH \rightarrow CH_2OH + H$ $0.05 \cdot k$ $k_0 = 1.1 \times 10^{-7} \cdot exp\left(\frac{-3.308 \times 10^4}{T_g}\right)$ $k_\infty = 2.5 \times 10^{19} \cdot T_g^{-0.94} \cdot exp\left(\frac{-4.703 \times 10^4}{T_g}\right)$ $F_c = 0.18 \cdot exp\left(\frac{-T_g}{2 \times 10^2}\right)$ $+0.82 \cdot exp\left(\frac{-T_g}{1.438 \times 10^3}\right)$	[5, 141][a]
1068	$CH_3OOH \rightarrow CH_3O + OH$ $6 \times 10^{14} \cdot exp\left(\frac{-2.13 \times 10^4}{T_g}\right)$	[5]
1069	$HCCO \rightarrow CH + CO$ $\frac{6 \times 10^{15}}{N_A} \cdot exp\left(\frac{-2.96 \times 10^4}{T_g}\right) \cdot n_M$	[142]
1070	$CH_2CO \rightarrow CH_2 + CO$ $\frac{2.3 \times 10^{15}}{N_A} \cdot exp\left(\frac{-2.899 \times 10^4}{T_g}\right) \cdot n_M$	[135]
1071	$CH_3CO \rightarrow CH_3 + CO$ $k_0 = 1 \times 10^{-8} \cdot exp\left(\frac{-7.08 \times 10^3}{T_g}\right)$ $k_\infty = 2 \times 10^{13} \cdot exp\left(\frac{-8.63 \times 10^3}{T_g}\right)$ $F_c = 0.5$	[5][a]

#	Reaction / Rate equation	Ref.
1072	$CH_3CO \rightarrow CH_2CO + H$ $1.36 \times 10^8 \cdot T_g^{1.9433} \cdot exp\left(\frac{-4.6005 \times 10^4 \cdot 4.184}{R \cdot T_g}\right)$	[121]
1073	$CH_3CHO \rightarrow CH_3CO + H$ $5 \times 10^{14} \cdot exp\left(\frac{-8.79 \times 10^4 \cdot 4.184}{R \cdot T_g}\right)$	[143]
1074	$CH_3CHO \rightarrow CH_3 + HCO$ $2.1 \times 10^{16} \cdot exp\left(\frac{-4.1135 \times 10^4}{T_g}\right)$	[5]
1075	$CH_3COOH \rightarrow CH_3 + COOH$ $10^{5.7 \times 10^1} \cdot T_g^{-1.204 \times 10^1} \cdot exp\left(\frac{-1.1313 \times 10^5 \cdot 4.182}{R \cdot T_g}\right)$	[144]
1076	$CH_3CH_2O \rightarrow CH_3CHO + H$ $\frac{5.43 \times 10^{15}}{N_A} \cdot T_g^{-0.69} \cdot exp\left(\frac{-2.223 \times 10^4 \cdot 4.184}{R \cdot T_g}\right)$	[93]
1077	$CH_3CH_2O \rightarrow CH_3 + HCHO$ $k_0 = \frac{4.7 \times 10^{25}}{N_A} \cdot T_g^{-3} \cdot exp\left(\frac{-8.32 \times 10^3}{T_g}\right)$ $k_\infty = 6.31 \times 10^{10} \cdot T_g^{0.93} \cdot exp\left(\frac{-8.605 \times 10^3}{T_g}\right)$ $F_c = (1 - 0.426) \cdot exp\left(\frac{-T_g}{0.3}\right)$ $+0.426 \cdot exp\left(\frac{-T_g}{2.278 \times 10^3}\right)$ $+exp\left(\frac{-1 \times 10^5}{T_g}\right)$	[145][a]
1078	$CH_3CHOH \rightarrow CH_3CHO + H$ $k_0 = \frac{1.77 \times 10^{16}}{N_A} \cdot exp\left(\frac{-1.0458 \times 10^4}{T_g}\right)$ $k_\infty = 6.17 \times 10^9 \cdot T_g^{1.31} \cdot exp\left(\frac{-1.6998 \times 10^4}{T_g}\right)$ $F_c = (1 - 0.187) \cdot exp\left(\frac{-T_g}{6.52 \times 10^1}\right)$ $+0.187 \cdot exp\left(\frac{-T_g}{2.568 \times 10^3}\right)$ $+exp\left(\frac{-4.1226 \times 10^4}{T_g}\right)$	[145][a]

#	Reaction / Rate equation	Ref.
1079	$CH_3CHOH \rightarrow CH_3 + HCHO$ $k_0 = \frac{5.86 \times 10^{15}}{N_A} \cdot exp\left(\frac{-1.0735 \times 10^4}{T_g}\right)$ $k_\infty = 2.22 \times 10^9 \cdot T_g^{1.18} \cdot exp\left(\frac{-1.7103 \times 10^4}{T_g}\right)$ $F_c = (1 - 0.124) \cdot exp\left(\frac{-T_g}{1}\right)$ $+0.124 \cdot exp\left(\frac{-T_g}{1.729 \times 10^3}\right)$ $+exp\left(\frac{-5 \times 10^4}{T_g}\right)$	[145]a
1080	$CH_3CH_2OH \rightarrow CH_2OH + CH_3$ $k_0 = \frac{2.88 \times 10^{85}}{N_A} \cdot T_g^{-1.89 \times 10^1} \cdot exp\left(\frac{-5.5317 \times 10^4}{T_g}\right)$ $k_\infty = 5.94 \times 10^{23} \cdot T_g^{-1.68} \cdot exp\left(\frac{-4.588 \times 10^4}{T_g}\right)$ $F_c = 0.5 \cdot exp\left(\frac{-T_g}{2 \times 10^2}\right)$ $+0.5 \cdot exp\left(\frac{-T_g}{8.9 \times 10^2}\right)$ $+exp\left(\frac{-4.6 \times 10^3}{T_g}\right)$	[130]a
1081	$e + HCO^+ \rightarrow CO + H$ $0.88 \cdot 2.4 \times 10^{-7} \cdot \left(\frac{T_e}{3 \times 10^2}\right)^{-0.69}$	[146, 147]
1082	$e + HCO^+ \rightarrow C + OH$ $0.06 \cdot 2.4 \times 10^{-7} \cdot \left(\frac{T_e}{3 \times 10^2}\right)^{-0.69}$	[146, 147]
1083	$e + HCO^+ \rightarrow CH + O$ $0.06 \cdot 2.4 \times 10^{-7} \cdot \left(\frac{T_e}{3 \times 10^2}\right)^{-0.69}$	[146, 147]
1084	$C + OH \rightarrow e + HCO^+$ $\frac{1.12 \times 10^{13}}{N_A} \cdot exp\left(\frac{-8.06 \times 10^4}{T_g}\right)$	d
1085	$CO + H \rightarrow e + HCO^+$ $\frac{1.12 \times 10^{13}}{N_A} \cdot exp\left(\frac{-8.06 \times 10^4}{T_g}\right)$	d
1086	$e + O \rightarrow e + e + O^+$ $f(\sigma)$	[24]
1087	$e + O^- \rightarrow e + e + O$ $f(\sigma)$	[148]
1088	$e + O_2 \rightarrow e + e + O_2^+$ $f(\sigma)$	[24]
1089	$e + O_2 \rightarrow e + e + O + O^+$ $f(\sigma)$	[149]

#	Reaction / Rate equation	Ref.
1090	$e + O_2 \rightarrow e + O + O$ $f(\sigma)$	[24]
1091	$e + O_2 \rightarrow e + O + O$ $f(\sigma)$	[24]
1092	$e + O_2 \rightarrow O + O^-$ $f(\sigma)$	[24]
1093	$e + O_3 \rightarrow O + O_2^-$ $f(\sigma)$	[148]
1094	$e + O_3 \rightarrow O_2 + O^-$ $f(\sigma)$	[148]
1095	$M + e + O \rightarrow M + O^-$ 1×10^{-31}	[52, 150]
1096	$M + e + O_2 \rightarrow M + O_2^-$ 1×10^{-31}	[52, 150]
1097	$M + e + O_3 \rightarrow M + O_3^-$ 1×10^{-31}	[52, 150]
1098	$e + e + O^+ \rightarrow e + O$ $7 \times 10^{-20} \cdot \left(\frac{3.0 \times 10^2}{T_e}\right)^{4.5}$	[52]
1099	$M + e + O^+ \rightarrow M + O$ $6 \times 10^{-27} \cdot \left(\frac{3.0 \times 10^2}{T_e}\right)^{1.5}$	[52, 150]
1100	$e + e + O_2^+ \rightarrow e + O_2$ $1 \times 10^{-19} \cdot \left(\frac{3.0 \times 10^2}{T_e}\right)^{4.5}$	[150]
1101	$M + e + O_2^+ \rightarrow M + O_2$ $6 \times 10^{-27} \cdot \left(\frac{3.0 \times 10^2}{T_e}\right)^{1.5}$	[52, 150]
1102	$e + O_2^+ \rightarrow O + O$ $2.7 \times 10^{-7} \cdot \left(\frac{3.0 \times 10^2}{T_e}\right)^{0.7}$	[52]
1103	$M + O + O \rightarrow M + O_2$ $5.2 \times 10^{-35} \cdot exp\left(\frac{9 \times 10^2}{T_g}\right)$	[25]
1104	$O + O \rightarrow e + O_2^+$ $\frac{1.12 \times 10^{13}}{N_A} \cdot exp\left(\frac{-8.06 \times 10^4}{T_g}\right)$	[151]
1105	$O + O^- \rightarrow e + O_2$ 2.3×10^{-10}	[152]
1106	$M + O + O^+ \rightarrow M + O_2^+$ 1×10^{-29}	[52, 150]
1107	$O + O_2^- \rightarrow O_2 + O^-$ 3.3×10^{-10}	[52, 150]

#	Reaction / Rate equation	Ref.
1108	$O + O_2^- \rightarrow e + O_3$ 1.5×10^{-10}	[52, 150]
1109	$O + O_3^- \rightarrow e + O_2 + O_2$ 1×10^{-13}	[153]
1110	$O + O_3^- \rightarrow O_2 + O_2^-$ 2.5×10^{-10}	[154]
1111	$O + O_3 \rightarrow O_2 + O_2$ $8 \times 10^{-12} \cdot exp\left(\frac{-2.060 \times 10^3}{T_g}\right)$	[54]
1112	$M + O + O_2 \rightarrow M + O_3$ $5.4 \times 10^{-34} \cdot \left(\frac{3 \times 10^2}{T_g}\right)^{1.9}$	[52]
1113	$O_2 + O^+ \rightarrow O + O_2^+$ $2 \times 10^{-11} \cdot \left(\frac{T_g}{3.0 \times 10^2}\right)^{-0.5}$	[52]
1114	$O_3 + O^+ \rightarrow O_2 + O_2^+$ 1×10^{-10}	[52, 150]
1115	$O^- + O^+ \rightarrow O + O$ $2 \times 10^{-7} \cdot \left(\frac{3.0 \times 10^2}{T_g}\right)^{0.5}$	[150]
1116	$O_2^- + O^+ \rightarrow O + O_2$ $2 \times 10^{-7} \cdot \left(\frac{3.0 \times 10^2}{T_g}\right)^{0.5}$	[150]
1117	$O_3^- + O^+ \rightarrow O + O_3$ $2 \times 10^{-7} \cdot \left(\frac{3.0 \times 10^2}{T_g}\right)^{0.5}$	[150]
1118	$M + O_2^- + O^+ \rightarrow M + O + O_2$ $2 \times 10^{-25} \cdot \left(\frac{3.0 \times 10^2}{T_g}\right)^{2.5}$	[150]
1119	$M + O^- + O^+ \rightarrow M + O + O$ $2 \times 10^{-25} \cdot \left(\frac{3.0 \times 10^2}{T_g}\right)^{2.5}$	[150]
1120	$M + O_2^- + O^+ \rightarrow M + O_3$ $2 \times 10^{-25} \cdot \left(\frac{3.0 \times 10^2}{T_g}\right)^{2.5}$	[150]
1121	$M + O^- + O^+ \rightarrow M + O_2$ $2 \times 10^{-25} \cdot \left(\frac{3.0 \times 10^2}{T_g}\right)^{2.5}$	[150]
1122	$M + O_3^- + O^+ \rightarrow M + O + O_3$ $2 \times 10^{-25} \cdot \left(\frac{3.0 \times 10^2}{T_g}\right)^{2.5}$	[155]
1123	$O_2^+ + O^- \rightarrow O + O + O$ 1×10^{-7}	[150]

#	Reaction / Rate equation	Ref.
1124	$O_2^+ + O^- \rightarrow O + O_2$ $2 \times 10^{-7} \cdot \left(\frac{3.0 \times 10^2}{T_g}\right)^{0.5}$	[150]
1125	$O_2 + O^- \rightarrow e + O_3$ 5×10^{-15}	[52, 150]
1126	$M + O_2 + O^- \rightarrow M + O_3^-$ $1.1 \times 10^{-30} \cdot \left(\frac{T_g}{3.0 \times 10^2}\right)^{-1}$	[52, 150, 156]
1127	$O_3 + O^- \rightarrow e + O_2 + O_2$ 3×10^{-10}	[52, 157]
1128	$O_3 + O^- \rightarrow O + O_3^-$ 8×10^{-10}	[52]
1129	$M + O^- \rightarrow M + e + O$ $6.9 \times 10^{-10} \cdot \left(\frac{T_g}{3 \times 10^2}\right)^{0.5}$	[158]
1130	$M + O_2^+ + O^- \rightarrow M + O + O_2$ $2 \times 10^{-25} \cdot \left(\frac{3.0 \times 10^2}{T_g}\right)^{2.5}$	[150]
1131	$M + O_2^+ + O^- \rightarrow M + O_3$ $2 \times 10^{-25} \cdot \left(\frac{3.0 \times 10^2}{T_g}\right)^{2.5}$	[150]
1132	$O_2 + O_2 \rightarrow O + O_3$ $2 \times 10^{-11} \cdot exp\left(\frac{-4.980 \times 10^4}{T_g}\right)$	[52]
1133	$M + O_2 \rightarrow M + O + O$ $3 \times 10^{-6} \cdot T_g^{-1} \cdot exp\left(\frac{-5.938 \times 10^4}{T_g}\right)$	[25]
1134	$M + O_2^+ + O_3^- \rightarrow M + O_2 + O_3$ $2 \times 10^{-25} \cdot \left(\frac{3.0 \times 10^2}{T_g}\right)^{2.5}$	[155]
1135	$O_2^+ + O_3^- \rightarrow O + O + O_3$ 1×10^{-7}	[150]
1136	$O_2^+ + O_3^- \rightarrow O_2 + O_3$ $2 \times 10^{-7} \cdot \left(\frac{3.0 \times 10^2}{T_g}\right)^{0.5}$	[150]
1137	$M + O_2^- + O_2^+ \rightarrow M + O_2 + O_2$ $2 \times 10^{-25} \cdot \left(\frac{3.0 \times 10^2}{T_g}\right)^{2.5}$	[150]
1138	$O_2^- + O_2^+ \rightarrow O + O + O_2$ 1×10^{-7}	[150]
1139	$O_2^- + O_2^+ \rightarrow O_2 + O_2$ $2 \times 10^{-7} \cdot \left(\frac{3.0 \times 10^2}{T_g}\right)^{0.5}$	[150, 159]

#	Reaction / Rate equation	Ref.
1140	$M + O_2^- \rightarrow M + e + O_2$ $2 \times 10^{-10} \cdot \left(\frac{T_g}{3 \times 10^2}\right)^{0.5}$	[158]
1141	$O_2^- + O_3 \rightarrow O_2 + O_3^-$ 3.5×10^{-10}	[52]
1142	$O_3 + O_3^- \rightarrow e + O_2 + O_2 + O_2$ 3×10^{-10}	[154]
1143	$M + O_3 \rightarrow M + O + O_2$ $6.6 \times 10^{-10} \cdot exp\left(\frac{-1.160 \times 10^4}{T_g}\right)$	[52]
1144	$M + O_3^- \rightarrow M + e + O_3$ $2 \times 10^{-10} \cdot \left(\frac{T_g}{3 \times 10^2}\right)^{0.5}$	c
1145	$O_2 + O_3^- \rightarrow e + O_2 + O_3$ 2.3×10^{-11}	[160]
1146	$CO_2 + e \rightarrow CO_2^+ + e + e$ $f(\sigma)$	[24]
1147	$CO_2 + e \rightarrow CO + e + O$ $f(\sigma)$	[161]
1148	$CO_2 + e \rightarrow CO + e + O$ $f(\sigma)$	[161]
1149	$CO_2 + e \rightarrow CO + O^-$ $f(\sigma)$	[162]
1150	$CO + e \rightarrow CO^+ + e + e$ $f(\sigma)$	[24]
1151	$CO + e \rightarrow C + O^-$ $f(\sigma)$	[24]
1152	$CO + e \rightarrow C + e + O$ $f(\sigma)$	[24]
1153	$CO^+ + e \rightarrow C + O$ $6.8 \times 10^{-7} \cdot \left(\frac{T_e}{3 \times 10^2}\right)^{-0.4}$	[160]
1154	$CO_2^+ + e \rightarrow CO + O$ $0.5 \cdot 3.4 \times 10^{-6} \cdot \left(\frac{T_e}{3 \times 10^2}\right)^{-0.4}$	[160]
1155	$CO_2^+ + e \rightarrow C + O_2$ $0.5 \cdot 3.4 \times 10^{-6} \cdot \left(\frac{T_e}{3 \times 10^2}\right)^{-0.4}$	[160]
1156	$CO + O \rightarrow CO_2^+ + e$ $\frac{1.12 \times 10^{13}}{N_A} \cdot exp\left(\frac{-8.06 \times 10^4}{T_g}\right)$	d
1157	$C + O_2 \rightarrow CO_2^+ + e$ $\frac{1.12 \times 10^{13}}{N_A} \cdot exp\left(\frac{-8.06 \times 10^4}{T_g}\right)$	d

#	Reaction / Rate equation	Ref.
1158	$C + O \rightarrow CO^+ + e$ $\frac{5.28 \times 10^{12}}{N_A} \cdot exp\left(\frac{-3.2 \times 10^4}{T_g}\right)$	[151, 163]
1159	$CO^+ + e + e \rightarrow CO + e$ $1 \times 10^{-19} \cdot \left(\frac{3 \times 10^2}{T_e}\right)^{4.5}$	e
1160	$M + CO^+ + e \rightarrow M + CO$ $6 \times 10^{-27} \cdot \left(\frac{3 \times 10^2}{T_e}\right)^{1.5}$	f
1161	$CO_2^+ + e + e \rightarrow CO_2 + e$ $1 \times 10^{-19} \cdot \left(\frac{3 \times 10^2}{T_e}\right)^{4.5}$	e
1162	$M + CO_2^+ + e \rightarrow M + CO_2$ $6 \times 10^{-27} \cdot \left(\frac{3 \times 10^2}{T_e}\right)^{1.5}$	f
1163	$M + C + O \rightarrow M + CO$ $9.1 \times 10^{-22} \cdot T_g^{-3.08} \cdot exp\left(\frac{-2.114 \times 10^3}{T_g}\right)$	[160]
1164	$C + O_2 \rightarrow CO + O$ $\frac{1.2 \times 10^{14}}{N_A} \cdot exp\left(\frac{-2.01 \times 10^3}{T_g}\right)$	[164]
1165	$M + C + O^+ \rightarrow M + CO^+$ $1 \times 10^{-19} \cdot T_g^{-3.08} \cdot exp\left(\frac{-2.114 \times 10^3}{T_g}\right)$	[165]
1166	$C + O_2^+ \rightarrow CO^+ + O$ 5.2×10^{-11}	[1]
1167	$C + O_2^+ \rightarrow C^+ + O_2$ 5.2×10^{-11}	[1]
1168	$C + O^- \rightarrow CO + e$ 5×10^{-10}	[1]
1169	$M + C^+ + O \rightarrow M + CO^+$ $1 \times 10^{-19} \cdot T_g^{-3.08} \cdot exp\left(\frac{-2.114 \times 10^3}{T_g}\right)$	[165]
1170	$C^+ + O_2 \rightarrow CO + O^+$ 6.138×10^{-10}	[56]
1171	$C^+ + O_2 \rightarrow CO^+ + O$ 3.762×10^{-10}	[56]
1172	$CO_2 + O \rightarrow CO + O_2$ $\frac{1.7 \times 10^{13}}{N_A} \cdot exp\left(\frac{-2.65 \times 10^4}{T_g}\right)$	[160]
1173	$CO_2 + O^+ \rightarrow CO_2^+ + O$ 4.5×10^{-10}	[56]
1174	$CO_2 + O^+ \rightarrow CO + O_2^+$ 4.5×10^{-10}	[56]

#	Reaction / Rate equation	Ref.
1175	$M + CO + O \rightarrow M + CO_2$ $8.3 \times 10^{-34} \cdot exp\left(\frac{-1.51 \times 10^3}{T_g}\right)$	[25]
1176	$CO + O_2 \rightarrow CO_2 + O$ $4.2 \times 10^{-12} \cdot exp\left(\frac{-2.4 \times 10^4}{T_g}\right)$	[25]
1177	$CO + O_3 \rightarrow CO_2 + O_2$ 4×10^{-25}	[166]
1178	$CO + O^+ \rightarrow CO^+ + O$ $2 \times 10^{-11} \cdot \left(\frac{T_g}{5 \times 10^3}\right)^{0.5} \cdot exp\left(\frac{-4.58 \times 10^3}{T_g}\right)$	[165]
1179	$CO + O^- \rightarrow CO_2 + e$ $6 \times 10^{-10} \cdot \left(\frac{T_g}{3 \times 10^2}\right)^{-0.39}$	[167]
1180	$CO_2^+ + O \rightarrow CO_2 + O^+$ 9.62×10^{-11}	[56]
1181	$CO_2^+ + O \rightarrow CO + O_2^+$ 1.638×10^{-10}	[56]
1182	$CO_2^+ + O_2 \rightarrow CO_2 + O_2^+$ 5.3×10^{-11}	[83]
1183	$CO^+ + O \rightarrow CO + O^+$ 1.4×10^{-10}	[168]
1184	$CO^+ + O_2 \rightarrow CO + O_2^+$ 1.2×10^{-10}	[91]
1185	$C + CO_2 \rightarrow CO + CO$ 1×10^{-15}	[169]
1186	$CO_2 + C^+ \rightarrow CO + CO^+$ 1.1×10^{-9}	[170]
1187	$C + CO^+ \rightarrow CO + C^+$ 1.1×10^{-10}	[1]
1188	$M + CO_2 \rightarrow M + CO + O$ $\frac{3.65 \times 10^{14}}{N_A} \cdot exp\left(\frac{-5.2525 \times 10^4}{T_g}\right)$	[171]
1189	$CO_2 + CO^+ \rightarrow CO + CO_2^+$ 1×10^{-9}	[91]
1190	$M + CO \rightarrow M + C + O$ $1.46 \times 10^6 \cdot T_g^{-3.52} \cdot exp\left(\frac{-1.287 \times 10^5}{T_g}\right)$	[160]
1191	$e + H \rightarrow e + e + H^+$ $f(\sigma)$	[24]
1192	$e + H_2 \rightarrow e + e + H_2^+$ $f(\sigma)$	[24]

#	Reaction / Rate equation	Ref.
1193	$e + H_2 \rightarrow e + H + H$ $f(\sigma)$	[149]
1194	$e + H_2 \rightarrow e + e + H + H^+$ $f(\sigma)$	[149]
1195	$e + H_2 \rightarrow H + H^-$ $f(\sigma)$	[149]
1196	$e + H_2^+ \rightarrow H + H$ $7.51 \times 10^{-09} - 1.12 \times 10^{-09} \cdot \frac{T_e}{1.16045052e4}$ $+1.03 \times 10^{-10} \cdot \left(\frac{T_e}{1.16045052 \times 10^4}\right)^{2.0}$ $-4.15 \times 10^{-12} \cdot \left(\frac{T_e}{1.16045052 \times 10^4}\right)^{3.0}$ $+5.86 \times 10^{-14} \cdot \left(\frac{T_e}{1.16045052 \times 10^4}\right)^{4.0}$	[172]
1197	$e + H_3^+ \rightarrow H + H + H$ $5 \times 10^{-01} \cdot \left(8.39 \times 10^{-09} + 3.02 \times 10^{-09} \cdot \frac{T_e}{1.16045052e4}\right)$ $+5 \times 10^{-01} \cdot \left(-3.8 \times 10^{-10} \cdot \left(\frac{T_e}{1.16045052 \times 10^4}\right)^{2.0}\right)$ $+5 \times 10^{-01} \cdot \left(1.31 \times 10^{-11} \cdot \left(\frac{T_e}{1.16045052 \times 10^4}\right)^{3.0}\right)$ $+5 \times 10^{-01} \cdot \left(2.42 \times 10^{-13} \cdot \left(\frac{T_e}{1.16045052 \times 10^4}\right)^{4.0}\right)$ $+5 \times 10^{-01} \cdot \left(-2.3 \times 10^{-14} \cdot \left(\frac{T_e}{1.16045052 \times 10^4}\right)^{5.0}\right)$ $+5 \times 10^{-01} \cdot \left(3.55 \times 10^{-16} \cdot \left(\frac{T_e}{1.16045052 \times 10^4}\right)^{6.0}\right)$	[172]
1198	$e + H_3^+ \rightarrow H + H_2$ $5 \times 10^{-01} \cdot \left(8.39 \times 10^{-09} + 3.02 \times 10^{-09} \cdot \frac{T_e}{1.16045052e4}\right)$ $+5 \times 10^{-01} \cdot \left(-3.8 \times 10^{-10} \cdot \left(\frac{T_e}{1.16045052 \times 10^4}\right)^{2.0}\right)$ $+5 \times 10^{-01} \cdot \left(1.31 \times 10^{-11} \cdot \left(\frac{T_e}{1.16045052 \times 10^4}\right)^{3.0}\right)$ $+5 \times 10^{-01} \cdot \left(2.42 \times 10^{-13} \cdot \left(\frac{T_e}{1.16045052 \times 10^4}\right)^{4.0}\right)$ $+5 \times 10^{-01} \cdot \left(-2.3 \times 10^{-14} \cdot \left(\frac{T_e}{1.16045052 \times 10^4}\right)^{5.0}\right)$ $+5 \times 10^{-01} \cdot \left(3.55 \times 10^{-16} \cdot \left(\frac{T_e}{1.16045052 \times 10^4}\right)^{6.0}\right)$	[172]

#	Reaction / Rate equation	Ref.
1199	$H + H_2^+ \rightarrow H_2 + H^+$ 6.4×10^{-10}	[27]
1200	$M + H + H \rightarrow M + H_2$ $\frac{1.5 \times 10^{-29}}{N_A} \cdot T_g^{-1.3}$	[25]
1201	$H + H \rightarrow e + H_2^+$ $\frac{1.12 \times 10^{13}}{N_A} \cdot exp\left(\frac{-8.06 \times 10^4}{T_g}\right)$	d
1202	$M + H^- \rightarrow M + e + H$ $8 \times 10^{-12} \cdot \left(\frac{T_g}{3 \times 10^2}\right)^{0.5}$	[173]
1203	$H_2^+ + H^- \rightarrow H + H + H$ $2 \times 10^{-7} \cdot \frac{3.0 \times 10^2}{T_g}$	[174]
1204	$H_3^+ + H^- \rightarrow H + H + H_2$ $2 \times 10^{-7} \cdot \frac{3.0 \times 10^2}{T_g}$	[174]
1205	$H^- + H^+ \rightarrow H + H$ $7.51 \times 10^{-8} \cdot \left(\frac{T_g}{3 \times 10^2}\right)^{-0.5}$	[2, 3]
1206	$H_2 + H_2^+ \rightarrow H + H_3^+$ 2×10^{-9}	[27]
1207	$M + H_2 \rightarrow M + H + H$ $\frac{7.6 \times 10^{-5}}{N_A} \cdot T_g^{-1.4} \cdot exp\left(\frac{-5.253 \times 10^4}{T_g}\right)$	[25]
1208	$C + e \rightarrow C^+ + e + e$ $f(\sigma)$	[148]
1209	$C + H_2 \rightarrow CH + H$ $k_{rev} \cdot K_{eq}$	b
1210	$C_2H_4 \rightarrow C + CH_4$ $k_{rev} \cdot K_{eq}$	b
1211	$C_2H_2 + H \rightarrow C + CH_3$ $k_{rev} \cdot K_{eq}$	b
1212	$C_2H + H \rightarrow C + CH_2$ $k_{rev} \cdot K_{eq}$	b
1213	$C_2H_6 + H \rightarrow CH_3 + CH_4$ $k_{rev} \cdot K_{eq}$	b
1214	$C_2H_5 + H_2 \rightarrow CH_3 + CH_4$ $k_{rev} \cdot K_{eq}$	b
1215	$C_2H_4 + H \rightarrow CH + CH_4$ $k_{rev} \cdot K_{eq}$	b
1216	$C_2H_4 + H \rightarrow CH_2 + CH_3$ $k_{rev} \cdot K_{eq}$	b

#	Reaction / Rate equation	Ref.
1217	$C_2H_2 + H_2 \rightarrow CH_2 + CH_2$ $k_{rev} \cdot K_{eq}$	b
1218	$C_2H_2 \rightarrow CH + CH$ $k_{rev} \cdot K_{eq}$	b
1219	$CH_2 + H \rightarrow CH_3$ $k_{rev} \cdot K_{eq}$	b
1220	$CH + H \rightarrow CH_2$ $k_{rev} \cdot K_{eq}$	b
1221	$C + H_2 \rightarrow CH_2$ $k_{rev} \cdot K_{eq}$	b
1222	$C + H \rightarrow CH$ $k_{rev} \cdot K_{eq}$	b
1223	$C_2H_2 + CH_2 \rightarrow C + C_2H_4$ $k_{rev} \cdot K_{eq}$	b
1224	$C_2H_4 + CH_3 \rightarrow C_2H_6 + CH$ $k_{rev} \cdot K_{eq}$	b
1225	$C_2H_4 + CH_4 \rightarrow C_2H_5 + CH_3$ $k_{rev} \cdot K_{eq}$	b
1226	$C_2H_4 + CH_3 \rightarrow C_2H_5 + CH_2$ $k_{rev} \cdot K_{eq}$	b
1227	$C_2H_2 + CH_4 \rightarrow C_2H_3 + CH_3$ $k_{rev} \cdot K_{eq}$	b
1228	$C_2H_2 + CH_3 \rightarrow C_2H_3 + CH_2$ $k_{rev} \cdot K_{eq}$	b
1229	$C_2H_2 + CH \rightarrow C_2H + CH_2$ $k_{rev} \cdot K_{eq}$	b
1230	$C_2H_4 + C_2H_6 \rightarrow C_2H_5 + C_2H_5$ $k_{rev} \cdot K_{eq}$	b
1231	$C_2H_2 + C_2H_6 \rightarrow C_2H_3 + C_2H_5$ $k_{rev} \cdot K_{eq}$	b
1232	$C_2H_2 + C_2H_4 \rightarrow C_2H + C_2H_5$ $k_{rev} \cdot K_{eq}$	b
1233	$C_2H_2 + C_2H_3 \rightarrow C_2H + C_2H_4$ $k_{rev} \cdot K_{eq}$	b
1234	$H_2 + O_2 \rightarrow OH + OH$ $k_{rev} \cdot K_{eq}$	b
1235	$OH + OH \rightarrow H_2O_2$ $k_{rev} \cdot K_{eq}$	b
1236	$M + H + OH \rightarrow M + H_2O$ $k_{rev} \cdot K_{eq}$	b
1237	$H_2O_2 + O \rightarrow H_2O + O_2$ $k_{rev} \cdot K_{eq}$	b

#	Reaction / Rate equation	Ref.
1238	$M + HO_2 \rightarrow M + H + O_2$ $k_{rev} \cdot K_{eq}$	b
1239	$HO_2 + O \rightarrow H + O_3$ $k_{rev} \cdot K_{eq}$	b
1240	$HO_2 + OH \rightarrow H_2 + O_3$ $k_{rev} \cdot K_{eq}$	b
1241	$CO + H \rightarrow C + OH$ $k_{rev} \cdot K_{eq}$	b
1242	$HCO \rightarrow CO + H$ $k_{rev} \cdot K_{eq}$	b
1243	$CO_2 + OH \rightarrow CO + HO_2$ $k_{rev} \cdot K_{eq}$	b
1244	$COOH + OH \rightarrow CO + H_2O_2$ $k_{rev} \cdot K_{eq}$	b
1245	$H + HCHO \rightarrow CH_3 + O$ $k_{rev} \cdot K_{eq}$	b
1246	$HCHO + OH \rightarrow CH_3 + O_2$ $k_{rev} \cdot K_{eq}$	b
1247	$CH_3OO \rightarrow CH_3 + O_2$ $k_{rev} \cdot K_{eq}$	b
1248	$CO + H_2 \rightarrow CH_2 + O$ $k_{rev} \cdot K_{eq}$	b
1249	$HCHO + O \rightarrow CH_2 + O_2$ $k_{rev} \cdot K_{eq}$	b
1250	$CO + H_2O \rightarrow CH_2 + O_2$ $k_{rev} \cdot K_{eq}$	b
1251	$CO + H \rightarrow CH + O$ $k_{rev} \cdot K_{eq}$	b
1252	$CO_2 + H \rightarrow CH + O_2$ $k_{rev} \cdot K_{eq}$	b
1253	$CO + OH \rightarrow CH + O_2$ $k_{rev} \cdot K_{eq}$	b
1254	$HCO + O \rightarrow CH + O_2$ $k_{rev} \cdot K_{eq}$	b
1255	$CO + HCHO \rightarrow CH_2 + CO_2$ $k_{rev} \cdot K_{eq}$	b
1256	$CO + HCO \rightarrow CH + CO_2$ $k_{rev} \cdot K_{eq}$	b
1257	$CH_3O + H \rightarrow CH_3 + OH$ $k_{rev} \cdot K_{eq}$	b
1258	$H_2 + HCHO \rightarrow CH_3 + OH$ $k_{rev} \cdot K_{eq}$	b

#	Reaction / Rate equation	Ref.
1259	$CH_3O + OH \rightarrow CH_3 + HO_2$ $k_{rev} \cdot K_{eq}$	b
1260	$H + HCHO \rightarrow CH_2 + OH$ $k_{rev} \cdot K_{eq}$	b
1261	$HCHO + OH \rightarrow CH_2 + HO_2$ $k_{rev} \cdot K_{eq}$	b
1262	$CH_3 + HO_2 \rightarrow CH_2 + H_2O_2$ $k_{rev} \cdot K_{eq}$	b
1263	$C + H_2O \rightarrow CH + OH$ $k_{rev} \cdot K_{eq}$	b
1264	$H + HCO \rightarrow CH + OH$ $k_{rev} \cdot K_{eq}$	b
1265	$H + HCHO \rightarrow CH + H_2O$ $k_{rev} \cdot K_{eq}$	b
1266	$CO_2 + HCO \rightarrow CO + COOH$ $k_{rev} \cdot K_{eq}$	b
1267	$CH_3 + CO_2 \rightarrow CH_3O + CO$ $k_{rev} \cdot K_{eq}$	b
1268	$HCHO + HCO \rightarrow CH_3O + CO$ $k_{rev} \cdot K_{eq}$	b
1269	$CH_3O + CO_2 \rightarrow CH_3OO + CO$ $k_{rev} \cdot K_{eq}$	b
1270	$CO + H_2 \rightarrow H + HCO$ $k_{rev} \cdot K_{eq}$	b
1271	$CH_2 + O \rightarrow H + HCO$ $k_{rev} \cdot K_{eq}$	b
1272	$H_2 + HCO \rightarrow H + HCHO$ $k_{rev} \cdot K_{eq}$	b
1273	$CH_3O \rightarrow H + HCHO$ $k_{rev} \cdot K_{eq}$	b
1274	$H_2 + HCHO \rightarrow CH_3O + H$ $k_{rev} \cdot K_{eq}$	b
1275	$CH_3OH \rightarrow CH_3O + H$ $k_{rev} \cdot K_{eq}$	b
1276	$CH_3OH + H \rightarrow CH_3O + H_2$ $k_{rev} \cdot K_{eq}$	b
1277	$H_2 + HCHO \rightarrow CH_2OH + H$ $k_{rev} \cdot K_{eq}$	b
1278	$CH_3 + H_2O \rightarrow CH_3OH + H$ $k_{rev} \cdot K_{eq}$	b
1279	$CH_3O + OH \rightarrow CH_3OO + H$ $k_{rev} \cdot K_{eq}$	b

#	Reaction / Rate equation	Ref.
1280	$CH_3OOH + H \rightarrow CH_3OO + H_2$ $k_{rev} \cdot K_{eq}$	b
1281	$CO + H_2O \rightarrow HCO + OH$ $k_{rev} \cdot K_{eq}$	b
1282	$H + HCOOH \rightarrow HCHO + OH$ $k_{rev} \cdot K_{eq}$	b
1283	$COOH + H_2O \rightarrow HCOOH + OH$ $k_{rev} \cdot K_{eq}$	b
1284	$H_2O + HCHO \rightarrow CH_3O + OH$ $k_{rev} \cdot K_{eq}$	b
1285	$H_2O_2 + HCHO \rightarrow CH_3O + HO_2$ $k_{rev} \cdot K_{eq}$	b
1286	$CH_3OH + O_2 \rightarrow CH_3O + HO_2$ $k_{rev} \cdot K_{eq}$	b
1287	$H_2O + HCHO \rightarrow CH_2OH + OH$ $k_{rev} \cdot K_{eq}$	b
1288	$CH_3OH + OH \rightarrow CH_2OH + H_2O$ $k_{rev} \cdot K_{eq}$	b
1289	$H_2O_2 + HCHO \rightarrow CH_2OH + HO_2$ $k_{rev} \cdot K_{eq}$	b
1290	$H_2O + HCOOH \rightarrow CH_2OH + HO_2$ $k_{rev} \cdot K_{eq}$	b
1291	$CH_3O + H_2O_2 \rightarrow CH_3OH + HO_2$ $k_{rev} \cdot K_{eq}$	b
1292	$CH_3OO + H_2O \rightarrow CH_3OOH + OH$ $k_{rev} \cdot K_{eq}$	b
1293	$CH_3OH + O_2 \rightarrow CH_3OO + OH$ $k_{rev} \cdot K_{eq}$	b
1294	$CH_3OOH + O_2 \rightarrow CH_3OO + HO_2$ $k_{rev} \cdot K_{eq}$	b
1295	$CH_3OOH + HO_2 \rightarrow CH_3OO + H_2O_2$ $k_{rev} \cdot K_{eq}$	b
1296	$CO + OH \rightarrow HCO + O$ $k_{rev} \cdot K_{eq}$	b
1297	$CO_2 + H \rightarrow HCO + O$ $k_{rev} \cdot K_{eq}$	b
1298	$CO + HO_2 \rightarrow HCO + O_2$ $k_{rev} \cdot K_{eq}$	b
1299	$HCO + OH \rightarrow HCHO + O$ $k_{rev} \cdot K_{eq}$	b
1300	$HCO + HO_2 \rightarrow HCHO + O_2$ $k_{rev} \cdot K_{eq}$	b

#	Reaction / Rate equation	Ref.
1301	$HCHO + OH \rightarrow CH_3O + O$ $k_{rev} \cdot K_{eq}$	b
1302	$HCHO + HO_2 \rightarrow CH_3O + O_2$ $k_{rev} \cdot K_{eq}$	b
1303	$CH_2OH + OH \rightarrow CH_3OH + O$ $k_{rev} \cdot K_{eq}$	b
1304	$CH_3O + O_2 \rightarrow CH_3OO + O$ $k_{rev} \cdot K_{eq}$	b
1305	$CH_4 + CO \rightarrow CH_3 + HCO$ $k_{rev} \cdot K_{eq}$	b
1306	$CH_3 + CO \rightarrow CH_2 + HCO$ $k_{rev} \cdot K_{eq}$	b
1307	$CH_2CO + H_2O \rightarrow CH_3 + COOH$ $k_{rev} \cdot K_{eq}$	b
1308	$CH_4 + CO_2 \rightarrow CH_3 + COOH$ $k_{rev} \cdot K_{eq}$	b
1309	$CH_3 + HCO \rightarrow CH_2 + HCHO$ $k_{rev} \cdot K_{eq}$	b
1310	$CH_2CO + H \rightarrow CH + HCHO$ $k_{rev} \cdot K_{eq}$	b
1311	$CH_4 + HCHO \rightarrow CH_3 + CH_3O$ $k_{rev} \cdot K_{eq}$	b
1312	$CH_3 + HCHO \rightarrow CH_2 + CH_3O$ $k_{rev} \cdot K_{eq}$	b
1313	$CH_4 + HCHO \rightarrow CH_2OH + CH_3$ $k_{rev} \cdot K_{eq}$	b
1314	$C_2H_4 + OH \rightarrow CH_2 + CH_2OH$ $k_{rev} \cdot K_{eq}$	b
1315	$CH_3 + HCHO \rightarrow CH_2 + CH_2OH$ $k_{rev} \cdot K_{eq}$	b
1316	$CH_2OH + CH_3 \rightarrow CH_2 + CH_3OH$ $k_{rev} \cdot K_{eq}$	b
1317	$CH_3 + CH_3O \rightarrow CH_2 + CH_3OH$ $k_{rev} \cdot K_{eq}$	b
1318	$CH_3 + CH_3OOH \rightarrow CH_3OO + CH_4$ $k_{rev} \cdot K_{eq}$	b
1319	$CH_3O + CH_3O \rightarrow CH_3 + CH_3OO$ $k_{rev} \cdot K_{eq}$	b
1320	$CH_3O + HCHO \rightarrow CH_2 + CH_3OO$ $k_{rev} \cdot K_{eq}$	b
1321	$C_2H_5 + O_2 \rightarrow CH_2 + CH_3OO$ $k_{rev} \cdot K_{eq}$	b

#	Reaction / Rate equation	Ref.
1322	$CO + HCHO \rightarrow HCO + HCO$ $k_{rev} \cdot K_{eq}$	b
1323	$CH_3OH + CO \rightarrow CH_3O + HCO$ $k_{rev} \cdot K_{eq}$	b
1324	$CH_3OH + CO \rightarrow CH_2OH + HCO$ $k_{rev} \cdot K_{eq}$	b
1325	$HCHO + HCHO \rightarrow CH_2OH + HCO$ $k_{rev} \cdot K_{eq}$	b
1326	$CH_3OH + HCHO \rightarrow CH_3O + CH_3O$ $k_{rev} \cdot K_{eq}$	b
1327	$CH_3OH + HCHO \rightarrow CH_2OH + CH_3O$ $k_{rev} \cdot K_{eq}$	b
1328	$CH_3OH + HCHO \rightarrow CH_2OH + CH_2OH$ $k_{rev} \cdot K_{eq}$	b
1329	$CH_3OOH + HCHO \rightarrow CH_3O + CH_3OO$ $k_{rev} \cdot K_{eq}$	b
1330	$CH_2OH + CH_3OOH \rightarrow CH_3OH + CH_3OO$ $k_{rev} \cdot K_{eq}$	b
1331	$CH_3O + CH_3OOH \rightarrow CH_3OH + CH_3OO$ $k_{rev} \cdot K_{eq}$	b
1332	$CH_3OOH + HCHO \rightarrow CH_2OH + CH_3OO$ $k_{rev} \cdot K_{eq}$	b
1333	$CH_3OH + HCOOH \rightarrow CH_2OH + CH_3OO$ $k_{rev} \cdot K_{eq}$	b
1334	$CH_3OOH + HCO \rightarrow CH_3OO + HCHO$ $k_{rev} \cdot K_{eq}$	b
1335	$C_2H_4 + H_2O \rightarrow C_2H_5 + OH$ $k_{rev} \cdot K_{eq}$	b
1336	$C_2H_4 + H_2O_2 \rightarrow C_2H_5 + HO_2$ $k_{rev} \cdot K_{eq}$	b
1337	$CH_3 + HCHO \rightarrow C_2H_4 + OH$ $k_{rev} \cdot K_{eq}$	b
1338	$CH_3CHO + H \rightarrow C_2H_4 + OH$ $k_{rev} \cdot K_{eq}$	b
1339	$CH_2CH_2OH \rightarrow C_2H_4 + OH$ $k_{rev} \cdot K_{eq}$	b
1340	$CH_3 + HCO \rightarrow C_2H_3 + OH$ $k_{rev} \cdot K_{eq}$	b
1341	$CH_3CO + H \rightarrow C_2H_3 + OH$ $k_{rev} \cdot K_{eq}$	b
1342	$C_2H_2 + H_2O \rightarrow C_2H_3 + OH$ $k_{rev} \cdot K_{eq}$	b

#	Reaction / Rate equation	Ref.
1343	$CH_2CO + H_2 \rightarrow C_2H_3 + OH$ $k_{rev} \cdot K_{eq}$	b
1344	$CH_4 + CO \rightarrow C_2H_3 + OH$ $k_{rev} \cdot K_{eq}$	b
1345	$C_2H_4 + OH \rightarrow C_2H_3 + H_2O$ $k_{rev} \cdot K_{eq}$	b
1346	$C_2H_4 + HO_2 \rightarrow C_2H_3 + H_2O_2$ $k_{rev} \cdot K_{eq}$	b
1347	$CH_2CO + H \rightarrow C_2H_2 + OH$ $k_{rev} \cdot K_{eq}$	b
1348	$C_2H_2 + O \rightarrow C_2H + OH$ $k_{rev} \cdot K_{eq}$	b
1349	$CH_2 + CO \rightarrow C_2H + OH$ $k_{rev} \cdot K_{eq}$	b
1350	$C_2H_2 + O_2 \rightarrow C_2H + HO_2$ $k_{rev} \cdot K_{eq}$	b
1351	$HCCO + OH \rightarrow C_2H + HO_2$ $k_{rev} \cdot K_{eq}$	b
1352	$CH_3CHO + H \rightarrow C_2H_5 + O$ $k_{rev} \cdot K_{eq}$	b
1353	$CH_3 + HCHO \rightarrow C_2H_5 + O$ $k_{rev} \cdot K_{eq}$	b
1354	$C_2H_4 + OH \rightarrow C_2H_5 + O$ $k_{rev} \cdot K_{eq}$	b
1355	$CH_3 + HCO \rightarrow C_2H_4 + O$ $k_{rev} \cdot K_{eq}$	b
1356	$CH_2CO + H_2 \rightarrow C_2H_4 + O$ $k_{rev} \cdot K_{eq}$	b
1357	$C_2H_3 + HO_2 \rightarrow C_2H_4 + O_2$ $k_{rev} \cdot K_{eq}$	b
1358	$C_2H_2 + OH \rightarrow C_2H_3 + O$ $k_{rev} \cdot K_{eq}$	b
1359	$CH_3 + CO \rightarrow C_2H_3 + O$ $k_{rev} \cdot K_{eq}$	b
1360	$CH_2 + HCO \rightarrow C_2H_3 + O$ $k_{rev} \cdot K_{eq}$	b
1361	$HCHO + HCO \rightarrow C_2H_3 + O_2$ $k_{rev} \cdot K_{eq}$	b
1362	$CH_2 + CO \rightarrow C_2H_2 + O$ $k_{rev} \cdot K_{eq}$	b
1363	$H + HCCO \rightarrow C_2H_2 + O$ $k_{rev} \cdot K_{eq}$	b

#	Reaction / Rate equation	Ref.
1364	$HCO + HCO \rightarrow C_2H_2 + O_2$ $k_{rev} \cdot K_{eq}$	b
1365	$CH + CO \rightarrow C_2H + O$ $k_{rev} \cdot K_{eq}$	b
1366	$CO + HCO \rightarrow C_2H + O_2$ $k_{rev} \cdot K_{eq}$	b
1367	$CH + CO_2 \rightarrow C_2H + O_2$ $k_{rev} \cdot K_{eq}$	b
1368	$C_2H_5 + CH_3OOH \rightarrow C_2H_6 + CH_3OO$ $k_{rev} \cdot K_{eq}$	b
1369	$C_2H_6 + CO \rightarrow C_2H_5 + HCO$ $k_{rev} \cdot K_{eq}$	b
1370	$C_2H_6 + HCHO \rightarrow C_2H_5 + CH_3O$ $k_{rev} \cdot K_{eq}$	b
1371	$C_2H_4 + CH_3OH \rightarrow C_2H_5 + CH_2OH$ $k_{rev} \cdot K_{eq}$	b
1372	$C_2H_6 + HCHO \rightarrow C_2H_5 + CH_2OH$ $k_{rev} \cdot K_{eq}$	b
1373	$CH_3CH_2O + CH_3O \rightarrow C_2H_5 + CH_3OO$ $k_{rev} \cdot K_{eq}$	b
1374	$C_2H_5 + CO_2 \rightarrow C_2H_4 + COOH$ $k_{rev} \cdot K_{eq}$	b
1375	$C_2H_5 + HCHO \rightarrow C_2H_4 + CH_2OH$ $k_{rev} \cdot K_{eq}$	b
1376	$C_2H_4 + HCO \rightarrow C_2H_3 + HCHO$ $k_{rev} \cdot K_{eq}$	b
1377	$C_2H_4 + HCHO \rightarrow C_2H_3 + CH_3O$ $k_{rev} \cdot K_{eq}$	b
1378	$C_2H_4 + HCHO \rightarrow C_2H_3 + CH_2OH$ $k_{rev} \cdot K_{eq}$	b
1379	$C_2H_4 + CH_2OH \rightarrow C_2H_3 + CH_3OH$ $k_{rev} \cdot K_{eq}$	b
1380	$C_2H_4 + CH_3O \rightarrow C_2H_3 + CH_3OH$ $k_{rev} \cdot K_{eq}$	b
1381	$C_2H_3 + CO_2 \rightarrow C_2H_2 + COOH$ $k_{rev} \cdot K_{eq}$	b
1382	$C_2H_3 + HCHO \rightarrow C_2H_2 + CH_2OH$ $k_{rev} \cdot K_{eq}$	b
1383	$C_2H_2 + HCHO \rightarrow C_2H + CH_3O$ $k_{rev} \cdot K_{eq}$	b
1384	$C_2H_2 + HCHO \rightarrow C_2H + CH_2OH$ $k_{rev} \cdot K_{eq}$	b

#	Reaction / Rate equation	Ref.
1385	$C_2H_2 + CH_2OH \rightarrow C_2H + CH_3OH$ $k_{rev} \cdot K_{eq}$	b
1386	$C_2H_2 + CH_3O \rightarrow C_2H + CH_3OH$ $k_{rev} \cdot K_{eq}$	b
1387	$CH_3O + HCCO \rightarrow C_2H + CH_3OO$ $k_{rev} \cdot K_{eq}$	b
1388	$CH_2 + CO \rightarrow H + HCCO$ $k_{rev} \cdot K_{eq}$	b
1389	$CH_3 + CO \rightarrow CH_2CO + H$ $k_{rev} \cdot K_{eq}$	b
1390	$H_2 + HCCO \rightarrow CH_2CO + H$ $k_{rev} \cdot K_{eq}$	b
1391	$CH_3 + HCO \rightarrow CH_3CO + H$ $k_{rev} \cdot K_{eq}$	b
1392	$CH_2CO + H_2 \rightarrow CH_3CO + H$ $k_{rev} \cdot K_{eq}$	b
1393	$CH_2OH + CH_3 \rightarrow CH_3CH_2O + H$ $k_{rev} \cdot K_{eq}$	b
1394	$CH_3CH_2OH \rightarrow CH_3CH_2O + H$ $k_{rev} \cdot K_{eq}$	b
1395	$C_2H_5 + OH \rightarrow CH_3CH_2O + H$ $k_{rev} \cdot K_{eq}$	b
1396	$C_2H_4 + H_2O \rightarrow CH_3CH_2O + H$ $k_{rev} \cdot K_{eq}$	b
1397	$CH_3CHO + H_2 \rightarrow CH_3CH_2O + H$ $k_{rev} \cdot K_{eq}$	b
1398	$CH_4 + HCHO \rightarrow CH_3CH_2O + H$ $k_{rev} \cdot K_{eq}$	b
1399	$CH_3CH_2OH \rightarrow CH_3CHOH + H$ $k_{rev} \cdot K_{eq}$	b
1400	$CH_2OH + CH_3 \rightarrow CH_3CHOH + H$ $k_{rev} \cdot K_{eq}$	b
1401	$C_2H_5 + OH \rightarrow CH_3CHOH + H$ $k_{rev} \cdot K_{eq}$	b
1402	$C_2H_4 + H_2O \rightarrow CH_3CHOH + H$ $k_{rev} \cdot K_{eq}$	b
1403	$CH_3CHO + H_2 \rightarrow CH_3CHOH + H$ $k_{rev} \cdot K_{eq}$	b
1404	$CH_4 + HCHO \rightarrow CH_3CHOH + H$ $k_{rev} \cdot K_{eq}$	b
1405	$C_2H_5 + H_2O \rightarrow CH_3CH_2OH + H$ $k_{rev} \cdot K_{eq}$	b

#	Reaction / Rate equation	Ref.
1406	$CH_3CHOH + H_2 \rightarrow CH_3CH_2OH + H$ $k_{rev} \cdot K_{eq}$	b
1407	$CH_2CH_2OH + H_2 \rightarrow CH_3CH_2OH + H$ $k_{rev} \cdot K_{eq}$	b
1408	$CH_3CH_2O + H_2 \rightarrow CH_3CH_2OH + H$ $k_{rev} \cdot K_{eq}$	b
1409	$CH_2OH + CO \rightarrow CH_2CO + OH$ $k_{rev} \cdot K_{eq}$	b
1410	$H_2O + HCCO \rightarrow CH_2CO + OH$ $k_{rev} \cdot K_{eq}$	b
1411	$HCHO + HCO \rightarrow CH_2CO + OH$ $k_{rev} \cdot K_{eq}$	b
1412	$CH_3 + CO_2 \rightarrow CH_2CO + OH$ $k_{rev} \cdot K_{eq}$	b
1413	$CH_2CO + H_2O \rightarrow CH_3CO + OH$ $k_{rev} \cdot K_{eq}$	b
1414	$CH_3CO + H_2O \rightarrow CH_3CHO + OH$ $k_{rev} \cdot K_{eq}$	b
1415	$CH_3 + HCOOH \rightarrow CH_3CHO + OH$ $k_{rev} \cdot K_{eq}$	b
1416	$CH_3COOH + H \rightarrow CH_3CHO + OH$ $k_{rev} \cdot K_{eq}$	b
1417	$CH_2CH_2OH + H_2O \rightarrow CH_3CH_2OH + OH$ $k_{rev} \cdot K_{eq}$	b
1418	$CH_3CHOH + H_2O \rightarrow CH_3CH_2OH + OH$ $k_{rev} \cdot K_{eq}$	b
1419	$CH_3CH_2O + H_2O \rightarrow CH_3CH_2OH + OH$ $k_{rev} \cdot K_{eq}$	b
1420	$CH_3CHOH + H_2O_2 \rightarrow CH_3CH_2OH + HO_2$ $k_{rev} \cdot K_{eq}$	b
1421	$CH + CO_2 \rightarrow HCCO + O$ $k_{rev} \cdot K_{eq}$	b
1422	$CO + HCHO \rightarrow CH_2CO + O$ $k_{rev} \cdot K_{eq}$	b
1423	$HCO + HCO \rightarrow CH_2CO + O$ $k_{rev} \cdot K_{eq}$	b
1424	$CH_2 + CO_2 \rightarrow CH_2CO + O$ $k_{rev} \cdot K_{eq}$	b
1425	$CH_2CO + OH \rightarrow CH_3CO + O$ $k_{rev} \cdot K_{eq}$	b
1426	$CH_3 + CO_2 \rightarrow CH_3CO + O$ $k_{rev} \cdot K_{eq}$	b

#	Reaction / Rate equation	Ref.
1427	$CH_3CO + OH \rightarrow CH_3CHO + O$ $k_{rev} \cdot K_{eq}$	b
1428	$CH_3CO + HO_2 \rightarrow CH_3CHO + O_2$ $k_{rev} \cdot K_{eq}$	b
1429	$CH_3CHO + HO_2 \rightarrow CH_3CH_2O + O_2$ $k_{rev} \cdot K_{eq}$	b
1430	$CH_3 + HCOOH \rightarrow CH_3CHOH + O$ $k_{rev} \cdot K_{eq}$	b
1431	$CH_3CHO + OH \rightarrow CH_3CHOH + O$ $k_{rev} \cdot K_{eq}$	b
1432	$CH_3COOH + H \rightarrow CH_3CHOH + O$ $k_{rev} \cdot K_{eq}$	b
1433	$CH_3CHO + HO_2 \rightarrow CH_3CHOH + O_2$ $k_{rev} \cdot K_{eq}$	b
1434	$CH_2OH + HCHO \rightarrow CH_2CH_2OH + O$ $k_{rev} \cdot K_{eq}$	b
1435	$CH_3CHOH + OH \rightarrow CH_3CH_2OH + O$ $k_{rev} \cdot K_{eq}$	b
1436	$CH_2CH_2OH + OH \rightarrow CH_3CH_2OH + O$ $k_{rev} \cdot K_{eq}$	b
1437	$CH_3CH_2O + OH \rightarrow CH_3CH_2OH + O$ $k_{rev} \cdot K_{eq}$	b
1438	$CH_3CHOH + HO_2 \rightarrow CH_3CH_2OH + O_2$ $k_{rev} \cdot K_{eq}$	b
1439	$CH_2CH_2OH + HO_2 \rightarrow CH_3CH_2OH + O_2$ $k_{rev} \cdot K_{eq}$	b
1440	$CH_3CH_2O + HO_2 \rightarrow CH_3CH_2OH + O_2$ $k_{rev} \cdot K_{eq}$	b
1441	$C_2H_5 + CO \rightarrow CH_2CO + CH_3$ $k_{rev} \cdot K_{eq}$	b
1442	$CH_4 + HCCO \rightarrow CH_2CO + CH_3$ $k_{rev} \cdot K_{eq}$	b
1443	$C_2H_4 + CO \rightarrow CH_2 + CH_2CO$ $k_{rev} \cdot K_{eq}$	b
1444	$CH_3 + HCCO \rightarrow CH_2 + CH_2CO$ $k_{rev} \cdot K_{eq}$	b
1445	$CH_2CO + CH_4 \rightarrow CH_3 + CH_3CO$ $k_{rev} \cdot K_{eq}$	b
1446	$CH_2CO + CH_3 \rightarrow CH_2 + CH_3CO$ $k_{rev} \cdot K_{eq}$	b
1447	$CH_3CHOH + CH_4 \rightarrow CH_3 + CH_3CH_2OH$ $k_{rev} \cdot K_{eq}$	b

#	Reaction / Rate equation	Ref.
1448	$CH_2CH_2OH + CH_4 \rightarrow CH_3 + CH_3CH_2OH$ $k_{rev} \cdot K_{eq}$	b
1449	$CH_3CH_2O + CH_4 \rightarrow CH_3 + CH_3CH_2OH$ $k_{rev} \cdot K_{eq}$	b
1450	$CH_3CHO + CO \rightarrow CH_3CO + HCO$ $k_{rev} \cdot K_{eq}$	b
1451	$CH_3CHO + HCO \rightarrow CH_3CO + HCHO$ $k_{rev} \cdot K_{eq}$	b
1452	$CH_2CO + CH_3OH \rightarrow CH_3CO + CH_3O$ $k_{rev} \cdot K_{eq}$	b
1453	$CH_3CHO + HCHO \rightarrow CH_3CO + CH_3O$ $k_{rev} \cdot K_{eq}$	b
1454	$CH_2OH + CH_3CHO \rightarrow CH_3CO + CH_3OH$ $k_{rev} \cdot K_{eq}$	b
1455	$CH_3CO + CH_3OH \rightarrow CH_3CHO + CH_3O$ $k_{rev} \cdot K_{eq}$	b
1456	$CH_3CO + CH_3OOH \rightarrow CH_3CHO + CH_3OO$ $k_{rev} \cdot K_{eq}$	b
1457	$CH_2CO + CH_3CHO \rightarrow CH_3CO + CH_3CO$ $k_{rev} \cdot K_{eq}$	b
1458	$CO + OH \rightarrow COOH$ $k_{rev} \cdot K_{eq}$	b
1459	$CO_2 + H \rightarrow COOH$ $k_{rev} \cdot K_{eq}$	b
1460	$H + HCO \rightarrow HCHO$ $k_{rev} \cdot K_{eq}$	b
1461	$H + HCHO \rightarrow CH_2OH$ $k_{rev} \cdot K_{eq}$	b
1462	$CH_2 + H_2O \rightarrow CH_3OH$ $k_{rev} \cdot K_{eq}$	b
1463	$CH_2OH + H \rightarrow CH_3OH$ $k_{rev} \cdot K_{eq}$	b
1464	$CH_3O + OH \rightarrow CH_3OOH$ $k_{rev} \cdot K_{eq}$	b
1465	$CH_3 + COOH \rightarrow CH_3COOH$ $k_{rev} \cdot K_{eq}$	b
1466	$CH_3 + HCHO \rightarrow CH_3CHOH$ $k_{rev} \cdot K_{eq}$	b
1467	$CO + O \rightarrow C + O_2$ $k_{rev} \cdot K_{eq}$	b
1468	$CO_2 + O_2 \rightarrow CO + O_3$ $k_{rev} \cdot K_{eq}$	b

#	Reaction / Rate equation	Ref.
1469	$CO + CO \rightarrow C + CO_2$ $k_{rev} \cdot K_{eq}$	b

Constants:

$N_A = 6.02214076 \times 10^{23} mol^{-1}$
$k_B = 1.38064852 \times 10^{-23} J/K$
$R = 8.31446261815324 JK^{-1} mol^{-1}$
$n_M =$ total number density of neutral species (cm^{-3})

Notes:

[a] falloff expression, Lindemann-Hinshelwood expression with broadening factor:

$$k = \frac{k_0[M]k_\infty}{k_0[M] + k_\infty} F; logF = \frac{logF_c}{1 + \left[\frac{log(k_0[M]/k_\infty)}{N}\right]^2}; N = 0.75 - 1.27 logF_c$$

[b] rate expression calculated from equilibrium constant and reverse reaction rate:

$$K_{eq} = e^{\left(\frac{-\Delta G_r}{RT}\right)} \cdot \left(\frac{p}{R \cdot T}\right)^{\Delta v}; p = 1bar; \Delta v = \sum \mu_P - \sum \mu_R$$

[c] estimated: equal to $O^- + M \rightarrow e + O + M$ [158]
[d] estimated: equal to $O + O \rightarrow O_2^+ + e$ [163]
[e] estimated: equal to $e + e + A^+ \rightarrow e + A$ [150]
[f] estimated: equal to $e + A^+ + M \rightarrow A + M$ [150]

Table D-2 Cross sections reference list

#	Process	Type	Ref.
1	$C \rightarrow C$	$effective$	[148]
2	$C \rightarrow C(1D)(1.264eV)$	$excitation$	[148]
3	$C \rightarrow C(1S)(2.684eV)$	$excitation$	[148]
4	$CH \rightarrow CH$	$effective$	[148]
5	$CH_2 \rightarrow CH_2$	$effective$	[148]
6	$CH_3 \rightarrow CH_3$	$effective$	[148]
7	$CH_4 \rightarrow CH_4$	$elastic$	[24]
8	$CH_4 \rightarrow CH_4(V24)(0.162eV)$	$excitation$	[24]
9	$CH_4 \rightarrow CH_4(V13)(0.361eV)$	$excitation$	[24]
10	$C_2H_2 \rightarrow C_2H_2$	$elastic$	[175]
11	$C_2H_2 \rightarrow C_2H_2(v5)(0.09eV)$	$excitation$	[175]
12	$C_2H_2 \rightarrow C_2H_2(V2)(0.255eV)$	$excitation$	[175]
13	$C_2H_2 \rightarrow C_2H_2(V31)(0.407eV)$	$excitation$	[175]
14	$C_2H_2 \rightarrow C_2H_2 * (1.911ev)$	$excitation$	[175]
15	$C_2H_2 \rightarrow C_2H_2 * (5.089eV)$	$excitation$	[175]
16	$C_2H_2 \rightarrow C_2H_2 * (7.902eV)$	$excitation$	[175]
17	$C_2H_4 \rightarrow C_2H_4$	$elastic$	[175]
18	$C_2H_4 \rightarrow C_2H_4(V1)(0.11eV)$	$excitation$	[175]
19	$C_2H_4 \rightarrow C_2H_4(V2)(0.36eV)$	$excitation$	[175]
20	$C_2H_4 \rightarrow C_2H_4(3.8eV)$	$excitation$	[175]
21	$C_2H_4 \rightarrow C_2H_4(5eV)$	$excitation$	[175]
22	$C_2H_4 \rightarrow C_2H_4(7eV)$	$excitation$	[175]
23	$C_2H_6 \rightarrow C_2H_6$	$elastic$	[175]
24	$C_2H_6 \rightarrow C_2H_6(V24)(0.16eV)$	$excitation$	[175]
25	$C_2H_6 \rightarrow C_2H_6(v13)(0.371eV)$	$excitation$	[175]
26	$C_2H_6 \rightarrow C_2H_6 * (7.53eV)$	$excitation$	[175]
27	$C_2H_6 \rightarrow C_2H_6 * (10.12eV)$	$excitation$	[175]
28	$CO \rightarrow CO$	$elastic$	[24]
29	$CO \rightarrow CO(J = 0 - J = 1)(0.000479992eV)$	$rotational$	[46]
30	$CO \rightarrow CO(J = 1 - J = 2)(0.000959985eV)$	$rotational$	[46]
31	$CO \rightarrow CO(J = 2 - J = 3)(0.00143998eV)$	$rotational$	[46]
32	$CO \rightarrow CO(J = 3 - J = 4)(0.00191997eV)$	$rotational$	[46]
33	$CO \rightarrow CO(J = 4 - J = 5)(0.00239996eV)$	$rotational$	[46]
34	$CO \rightarrow CO(J = 5 - J = 6)(0.00287995eV)$	$rotational$	[46]
35	$CO \rightarrow CO(J = 6 - J = 7)(0.00335995eV)$	$rotational$	[46]
36	$CO \rightarrow CO(J = 7 - J = 8)(0.00383994eV)$	$rotational$	[46]
37	$CO \rightarrow CO(J = 8 - J = 9)(0.00431993eV)$	$rotational$	[46]
38	$CO \rightarrow CO(J = 9 - J = 10)(0.00479992eV)$	$rotational$	[46]
39	$CO \rightarrow CO(J = 10 - J = 11)(0.00527992eV)$	$rotational$	[46]
40	$CO \rightarrow CO(J = 11 - J = 12)(0.00575991eV)$	$rotational$	[46]
41	$CO \rightarrow CO(J = 12 - J = 13)(0.0062399eV)$	$rotational$	[46]
42	$CO \rightarrow CO(J = 13 - J = 14)(0.00671989eV)$	$rotational$	[46]
43	$CO \rightarrow CO(J = 14 - J = 15)(0.00719989eV)$	$rotational$	[46]
44	$CO \rightarrow CO(J = 15 - J = 16)(0.00767988eV)$	$rotational$	[46]
45	$CO \rightarrow CO(J = 16 - J = 17)(0.00815987eV)$	$rotational$	[46]

#	Process	Type	Ref.
46	$CO \rightarrow CO(v0-v1)(0.266eV)$	$excitation$	[24]
47	$CO \rightarrow CO(v0-v2)(0.54eV)$	$excitation$	[24]
48	$CO \rightarrow CO(v0-v3)(0.81eV)$	$excitation$	[24]
49	$CO \rightarrow CO(v0-v4)(1.07eV)$	$excitation$	[24]
50	$CO \rightarrow CO(v0-v5)(1.33eV)$	$excitation$	[24]
51	$CO \rightarrow CO(v0-v6)(1.59eV)$	$excitation$	[24]
52	$CO \rightarrow CO(v0-v7)(1.84eV)$	$excitation$	[24]
53	$CO \rightarrow CO(v0-v8)(2.09eV)$	$excitation$	[24]
54	$CO \rightarrow CO(v0-v9)(2.33eV)$	$excitation$	[24]
55	$CO \rightarrow CO(v0-v10)(2.58eV)$	$excitation$	[24]
56	$CO \rightarrow CO(a3P)(6.006eV)$	$excitation$	[24]
57	$CO \rightarrow CO(a'3Su+)(6.8eV)$	$excitation$	[24]
58	$CO \rightarrow CO(A1P)(8.024eV)$	$excitation$	[24]
59	$CO \rightarrow CO(b3Su+)(10.399eV)$	$excitation$	[24]
60	$CO \rightarrow CO(B1Su+)(10.777eV)$	$excitation$	[24]
61	$CO \rightarrow CO(C1Su+)(11.396eV)$	$excitation$	[24]
62	$CO \rightarrow CO(E1P)(11.524eV)$	$excitation$	[24]
63	$CO_2 \rightarrow CO_2$	$effective$	[24]
64	$CO_2 \rightarrow CO_2(v010)(0.083eV)$	$excitation$	[24]
65	$CO_2 \rightarrow CO_2(v020)(0.167eV)$	$excitation$	[24]
66	$CO_2 \rightarrow CO_2(v100)(0.167eV)$	$excitation$	[24]
67	$CO_2 \rightarrow CO_2(v030+110)(0.252eV)$	$excitation$	[24]
68	$CO_2 \rightarrow CO_2(v001)(0.291eV)$	$excitation$	[24]
69	$CO_2 \rightarrow CO_2(v040+120+011)(0.339eV)$	$excitation$	[24]
70	$CO_2 \rightarrow CO_2(Xv200)(0.339eV)$	$excitation$	[24]
71	$CO_2 \rightarrow CO_2(Xv050+210+130+021+101)(0.422eV)$	$excitation$	[24]
72	$CO_2 \rightarrow CO_2(Xv300)(0.5eV)$	$excitation$	[24]
73	$CO_2 \rightarrow CO_2(Xv060+220+140)(0.505eV)$	$excitation$	[24]
74	$CO_2 \rightarrow CO_2(Xv0n0+n00)(2.5eV)$	$excitation$	[24]
75	$CO_2 \rightarrow CO_2(e1)(7eV)$	$excitation$	[24]
76	$CO_2 \rightarrow CO_2(e2)(10.5eV)$	$excitation$	[24]
77	$H \rightarrow H$	$elastic$	[24]
78	$H \rightarrow H(1p)(10.21eV)$	$excitation$	[24]
79	$H \rightarrow H(2s)(10.21eV)$	$excitation$	[24]
80	$H \rightarrow H(3)(12.11eV)$	$excitation$	[24]
81	$H \rightarrow H(4)(12.76eV)$	$excitation$	[24]
82	$H \rightarrow H(5)(13.11eV)$	$excitation$	[24]
83	$H_2 \rightarrow H_2$	$elastic$	[24]
84	$H_2 \rightarrow H_2(J=0-J=2)(0.044eV)$	$rotational$	[46]
85	$H_2 \rightarrow H_2(J=1-J=3)(0.073eV)$	$rotational$	[46]
86	$H_2 \rightarrow H_2(J=2-J=4)(0.1eV)$	$rotational$	[46]
87	$H_2 \rightarrow H_2(J=3-J=5)(0.12eV)$	$rotational$	[46]
88	$H_2 \rightarrow H_2(v0-v1)(0.516eV)$	$excitation$	[24]
89	$H_2 \rightarrow H_2(v0-v2)(1eV)$	$excitation$	[24]
90	$H_2 \rightarrow H_2(v0-v3)(1.5eV)$	$excitation$	[24]
91	$H_2 \rightarrow H_2(b3Su)(8.9eV)$	$excitation$	[24]
92	$H_2 \rightarrow H_2(B1Su)(11.4eV)$	$excitation$	[24]

#	Process	Type	Ref.
93	$H_2 \rightarrow H_2(c3Pu)(11.75eV)$	$excitation$	[24]
94	$H_2 \rightarrow H_2(a3Sg)(11.8eV)$	$excitation$	[24]
95	$H_2 \rightarrow H_2(C1Pu)(12.4eV)$	$excitation$	[24]
96	$H_2 \rightarrow H_2(E1Sg, F1Sg)(12.4eV)$	$excitation$	[24]
97	$H_2 \rightarrow H_2(e3Su)(13.4eV)$	$excitation$	[24]
98	$H_2 \rightarrow H_2(B'1Su)(13.8eV)$	$excitation$	[24]
99	$H_2 \rightarrow H_2(D1Pu)(14eV)$	$excitation$	[24]
100	$H_2 \rightarrow H_2(B'1Su)(14.6eV)$	$excitation$	[24]
101	$H_2 \rightarrow H_2(D'1Pu)(14.6eV)$	$excitation$	[24]
102	$H_2O \rightarrow H_2O$	$elastic$	[46]
103	$H_2O \rightarrow H_2O(R)(0.04eV)$	$excitation$	[46]
104	$H_2O \rightarrow H_2O(VA)(0.198eV)$	$excitation$	[46]
105	$H_2O \rightarrow H_2O(V1)(0.453eV)$	$excitation$	[46]
106	$O \rightarrow O$	$elastic$	[24]
107	$O \rightarrow O(1D)(1.96eV)$	$excitation$	[24]
108	$O \rightarrow O(1S)(4.18eV)$	$excitation$	[24]
109	$O \rightarrow O(4S0)(9.2eV)$	$excitation$	[24]
110	$O \rightarrow O(2D0)(12.5eV)$	$excitation$	[24]
111	$O \rightarrow O(2P0)(14.1eV)$	$excitation$	[24]
112	$O \rightarrow O(3P0)(15.7eV)$	$excitation$	[24]
113	$O_2 \rightarrow O_2$	$effective$	[24]
114	$O_2 \rightarrow O_2(v0 - v1)(0.19eV)$	$excitation$	[24]
115	$O_2 \rightarrow O_2(v0 - v2)(0.38eV)$	$excitation$	[24]
116	$O_2 \rightarrow O_2(v0 - v3)(0.6eV)$	$excitation$	[24]
117	$O_2 \rightarrow O_2(v0 - v4)(0.8eV)$	$excitation$	[24]
118	$O_2 \rightarrow O_2(a1Dg)(0.977eV)$	$excitation$	[24]
119	$O_2 \rightarrow O_2(b1Sg+)(1.627eV)$	$excitation$	[24]
120	$O_2 \rightarrow O_2(A3Su+, C3Du, c1Su-)(4.5eV)$	$excitation$	[24]
121	$O_2 \rightarrow O_2(9.97eV)$	$excitation$	[24]
122	$O_2 \rightarrow O_2(14.7eV)$	$excitation$	[24]
123	$O_3 \rightarrow O_3$	$effective$	[148]

(1) S. S. Prasad and J. H. W. T., 1980, **43**, 1, DOI: 10.1086/190665.

(2) N. Harada and E. Herbst, 2008, **685**, 272–280, DOI: 10.1086/590468.

(3) D. McElroy, C. Walsh, A. J. Markwick, M. A. Cordiner, K. Smith and T. J. Millar, *Astronomy and Astrophysics*, 2013, **550**, A36, DOI: 10.1051/0004-6361/201220465.

(4) M. J. Rabinowitz, J. W. Sutherland, P. M. Patterson and R. B. Klemm, *The Journal of Physical Chemistry*, 1991, **95**, 674–681, DOI: 10.1021/j100155a033.

(5) D. L. Baulch, C. T. Bowman, C. J. Cobos, R. A. Cox, T. Just, J. A. Kerr, M. J. Pilling, D. Stocker, J. Troe, W. Tsang, R. W. Walker and J. Warnatz, 2005, **34**, 757–1397, DOI: 10.1063/1.1748524.

(6) K.-W. Lu, H. Matsui, C.-L. Huang, P. Raghunath, N.-S. Wang and M. C. Lin, 2010, **114**, 5493–5502, DOI: 10.1021/jp100535r.

(7) J. K. Kim and W. T. Huntress, 1975, **62**, 2820–2825, DOI: 10.1063/1.430817.

(8) M. J. McEwan, G. B. I. Scott, N. G. Adams, L. M. Babcock, R. Terzieva and E. Herbst, *The Astrophysical Journal*, 1999, **513**, 287–293, DOI: 10.1086/306861.

(9) N. Adams and D. Smith, *Chemical Physics Letters*, 1977, **47**, 383–387, DOI: 10.1016/0009-2614(77)80043-2.

(10) W. Braun, A. M. Bass, D. D. Davis, J. D. Simmons, G. Porter and M. J. Lighthill, *Proceedings of the Royal Society of London. A. Mathematical and Physical Sciences*, 1969, **312**, 417–434, DOI: 10.1098/rspa.1969.0168.

(11) A. J. Dean and R. K. Hanson, 1992, **24**, 517–532, DOI: 10.1002/kin.550240602.

(12) J. Oscar Martinez, N. B. Betts, S. M. Villano, N. Eyet, T. P. Snow and V. M. Bierbaum, 2008, **686**, 1486–1492, DOI: 10.1086/591548.

(13) C. M. Leung, E. Herbst and W. F. Huebner, 1984, **56**, 231, DOI: 10.1086/190982.

(14) K. Tabayashi and S. Bauer, 1979, **34**, 63–83, DOI: 10.1016/0010-2180(79)90079-8.

(15) T. Bohland, S. Dobe, F. Temps and H. G. Wagner, 1985, **89**, 1110–1116, DOI: 10.1002/bbpc.19850891018.

(16) P. Han, K. Su, Y. Liu, Y. Wang, X. Wang, Q. Zeng, L. Cheng and L. Zhang, 2011, **32**, 2745–2755, DOI: 10.1002/jcc.21854.

(17) S. Bauerle, M. Klatt and H. G. G. Wagner, 1995, **99**, 870–879, DOI: 10.1002/bbpc.19950990612.

(18) W. Braun, J. R. McNesby and A. M. Bass, 1967, **46**, 2071–2080, DOI: 10.1063/1.1841003.

(19) H. Tahara, K. ichiro Minami, A. Murai, T. Yasui and T. Y. T. Yoshikawa, *Japanese Journal of Applied Physics*, 1995, **34**, 1972, DOI: 10.1143/jjap.34.1972.

(20) D. Smith and N. Adams, 1978, **54**, 535–540, DOI: 10.1016/0009-2614(78)85279-8.

(21) K Tachibana, M Nishida, H Harima and Y Urano, *Journal of Physics D: Applied Physics*, 1984, **17**, 1727–1742, DOI: 10.1088/0022-3727/17/8/026.

(22) R. K. Janev and D. Reiter, 2002, **9**, 4071–4081, DOI: 10.1063/1.1500735.

(23) D. Reiter and R. K. Janev, *Contributions to Plasma Physics*, 2010, **50**, 986–1013, DOI: 10.1002/ctpp.201000090.

(24) Obtained from LXCAT (IST-Lisbon database), www.lxcat.net.

(25) W. Tsang and R. F. Hampson, 1986, **15**, 1087–1279, DOI: 10.1063/1.555759.

(26) V. D. Knyazev, A. Bencsura, S. I. Stoliarov and I. R. Slagle, *The Journal of Physical Chemistry*, 1996, **100**, 11346–11354, DOI: 10.1021/jp9606568.

(27) V. G. Anicich, 1993, **22**, 1469–1569, DOI: 10.1063/1.555940.

(28) G. I. Mackay, H. I. Schiff and D. K. Bohme, 1981, **59**, 1771–1778, DOI: 10.1139/v81-265.

(29) D. Smith, P. Spanel and C. A. Mayhew, 1992, **117**, 457–473, DOI: 10.1016/0168-1176(92)80108-d.

(30) J. Kim, L. Theard and W. Huntress, *International Journal of Mass Spectrometry and Ion Physics*, 1974, **15**, 223–244, DOI: 10.1016/0020-7381(74)85001-1.

(31) V. G. Anicich, J. H. Futrell, W. T. Huntress and J. Kim, *International Journal of Mass Spectrometry and Ion Physics*, 1975, **18**, 63–64, DOI: 10.1016/0020-7381(75)87007-0.

(32) M. Mandal, S. Ghosh and B. Maiti, *The Journal of Physical Chemistry A*, 2018, **122**, 3556–3562, DOI: 10.1021/acs.jpca.8b01386.

(33) A. Bergeat and J.-C. Loison, *Physical Chemistry Chemical Physics*, 2001, **3**, 2038–2042, DOI: 10.1039/b100656h.

(34) N. Galland, F. Caralp, Y. Hannachi, A. Bergeat and J.-C. Loison, *The Journal of Physical Chemistry A*, 2003, **107**, 5419–5426, DOI: 10.1021/jp027465r.

(35) Y. Ge, M. S. Gordon, F. Battaglia and R. O. Fox, *The Journal of Physical Chemistry A*, 2010, **114**, 2384–2392, DOI: 10.1021/jp911673h.

(36) S. I. Stoliarov, V. D. Knyazev and I. R. Slagle, *The Journal of Physical Chemistry A*, 2000, **104**, 9687–9697, DOI: 10.1021/jp992476e.

(37) A. Fiaux, D. Smith and J. Futrell, *International Journal of Mass Spectrometry and Ion Physics*, 1974, **15**, 9–21, DOI: 10.1016/0020-7381(74)80082-3.

(38) G. I. Mackay, K. Tanaka and D. K. Bohme, 1977, **24**, 125–136, DOI: 10.1016/0020-7381(77)80020-x.

(39) J. K. Kim, V. G. Anicich and W. T. Huntress, *The Journal of Physical Chemistry*, 1977, **81**, 1798–1805, DOI: 10.1021/j100534a002.

(40) T. Ibuki and Y. Takezaki, *Bulletin of the Chemical Society of Japan*, 1975, **48**, 769–773, DOI: 10.1246/bcsj.48.769.

(41) A. Fahr and D. C. Tardy, *The Journal of Physical Chemistry A*, 2002, **106**, 11135–11140, DOI: 10.1021/jp021497x.

(42) M. R. Dash and B. Rajakumar, *Physical Chemistry Chemical Physics*, 2015, **17**, 3142–3156, DOI: 10.1039/c4cp04677c.

(43) R. K. Janev and D. Reiter, *Physics of Plasmas*, 2004, **11**, 780–829, DOI: 10.1063/1.1630794.

(44) P. Stewart, C. Larson and D. Golden, *Combustion and Flame*, 1989, **75**, 25–31, DOI: 10.1016/0010-2180(89)90084-9.

(45) A. M. Dean, *The Journal of Physical Chemistry*, 1985, **89**, 4600–4608, DOI: 10.1021/j100267a038.

(46) C Verheyen, T Silva, V Guerra and A Bogaerts, *Plasma Sources Science and Technology*, 2020, **29**, 095009, DOI: 10.1088/1361-6595/aba1c8.

(47) Y. Itikawa and N. Mason, *Journal of Physical and Chemical Reference Data*, 2005, **34**, 1–22, DOI: 10.1063/1.1799251.

(48) Obtained from LXCAT (TRINITI database), www.lxcat.net.

(49) D. Nandi, E. Krishnakumar, A. Rosa, W.-F. Schmidt and E. Illenberger, *Chemical Physics Letters*, 2003, **373**, 454–459, DOI: 10.1016/s0009-2614(03)00622-5.

(50) R. Riahi, P. Teulet, Z. B. Lakhdar and A. Gleizes, *The European Physical Journal D*, 2006, **40**, 223–230, DOI: 10.1140/epjd/e2006-00159-2.

(51) S. D. T. Axford and A. N. Hayhurst, *Proc. R. Soc. A: Math. Phys. Eng. Sci.*, 1996, **452**, 1007–1033, DOI: 10.1098/rspa.1996.0051.

(52) M. Capitelli, C. M. Ferreira, B. F. Gordiets and A. I. Osipov, Springer Berlin Heidelberg, 2000, DOI: 10.1007/978-3-662-04158-1.

(53) S. P. Karkach and V. I. Osherov, *The Journal of Chemical Physics*, 1999, **110**, 11918–11927, DOI: 10.1063/1.479131.

(54) R. Atkinson, D. L. Baulch, R. A. Cox, J. N. Crowley, R. F. Hampson, R. G. Hynes, M. E. Jenkin, M. J. Rossi and J. Troe, *Atmospheric Chemistry and Physics*, 2004, **4**, 1461–1738, DOI: 10.5194/acp-4-1461-2004.

(55) E. E. Ferguson, *Atomic Data and Nuclear Data Tables*, 1973, **12**, 159–178, DOI: 10.1016/0092-640x(73)90017-x.

(56) D. Albritton, *Atomic Data and Nuclear Data Tables*, 1978, **22**, 1–89, DOI: 10.1016/0092-640x(78)90027-x.

(57) W. V. Gaens and A Bogaerts, *Journal of Physics D: Applied Physics*, 2013, **46**, 275201, DOI: 10.1088/0022-3727/46/27/275201.

(58) D. L. Baulch, C. J. Cobos, R. A. Cox, P. Frank, G. Hayman, T. Just, J. A. Kerr, T. Murrells, M. J. Pilling, J. Troe, R. W. Walker and J. Warnatz, *Journal of Physical and Chemical Reference Data*, 1994, **23**, 847–848, DOI: 10.1063/1.555953.

(59) R. Atkinson, D. L. Baulch, R. A. Cox, R. F. Hampson, J. A. K. (Chairman) and J. Troe, *Journal of Physical and Chemical Reference Data*, 1989, **18**, 881–1097, DOI: 10.1063/1.555832.

(60) T. Murakami, K. Niemi, T. Gans, D. O. Connell and W. G. Graham, *Plasma Sources Science and Technology*, 2012, **22**, 015003, DOI: 10.1088/0963-0252/22/1/015003.

(61) A. B. Rakshit and P. Warneck, 1980, **76**, 1084, DOI: 10.1039/f29807601084.

(62) N. Harada, E. Herbst and V. Wakelam, *The Astrophysical Journal*, 2010, **721**, 1570–1578, DOI: 10.1088/0004-637x/721/2/1570.

(63) C. J. Howard and B. J. Finlayson-Pitts, *The Journal of Chemical Physics*, 1980, **72**, 3842–3843, DOI: 10.1063/1.439601.

(64) A. W. Sleight, J. D. Bierlein and P. E. Bierstedt, *The Journal of Chemical Physics*, 1975, **62**, 2826–2827, DOI: 10.1063/1.430818.

(65) R. P. A. Bettens, T. A. Hansen and M. A. Collins, *The Journal of Chemical Physics*, 1999, **111**, 6322–6332, DOI: 10.1063/1.479937.

(66) P. Glarborg, J. A. Miller, B. Ruscic and S. J. Klippenstein, 2018, **67**, 31–68, DOI: 10.1016/j.pecs.2018.01.002.

(67) V. G. Anicich, W. T. Huntress and J. H. Futrell, 1976, **40**, 233–236, DOI: 10.1016/0009-2614(76)85066-x.

(68) S. J. Klippenstein, Y. Georgievskii and B. J. McCall, 2009, **114**, 278–290, DOI: 10.1021/jp908500h.

(69) O. Martinez, Z. Yang, N. J. Demarais, T. P. Snow and V. M. Bierbaum, 2010, **720**, 173–177, DOI: 10.1088/0004-637x/720/1/173.

(70) P. Tosi, S. Iannotta, D. Bassi, H. Villinger, W. Dobler and W. Lindinger, 1984, **80**, 1905–1906, DOI: 10.1063/1.446951.

(71) W. Federer, H. Villinger, F. Howorka, W. Lindinger, P. Tosi, D. Bassi and E. Ferguson, 1984, **52**, 2084–2086, DOI: 10.1103/physrevlett.52.2084.

(72) G. B. Scott, D. A. Fairley, C. G. Freeman, M. J. McEwan, P. Spanel and D. Smith, 1997, **106**, 3982–3987, DOI: 10.1063/1.473116.

(73) V. Lissianski, H. Yang, Z. Qin, M. Mueller, K. Shin and W. Gardiner, *Chemical Physics Letters*, 1995, **240**, 57–62, DOI: 10.1016/0009-2614(95)00496-q.

(74) P. Glarborg, M. U. Alzueta, K. Dam-Johansen and J. A. Miller, 1998, **115**, 1–27, DOI: 10.1016/s0010-2180(97)00359-3.

(75) P. Glarborg and P. Marshall, 2009, **475**, 40–43, DOI: 10.1016/j.cplett.2009.05.028.

(76) J. Jones, K. Birkinshaw and N. Twiddy, 1981, **77**, 484–488, DOI: 10.1016/0009-2614(81)85191-3.

(77) Z. Karpas, V. Anicich and W. Huntress, 1978, **59**, 84–86, DOI: 10.1016/0009-2614(78)85620-6.

(78) J. H. W. T., V. G. Anicich, M. J. McEwan and Z. Karpas, 1980, **44**, 481, DOI: 10.1086/190701.

(79) G. Bogdanchikov, A. Baklanov and D. Parker, 2004, **385**, 486–490, DOI: 10.1016/j.cplett.2004.01.015.

(80) C. Dombrowsky, S. M. Hwang, M. Rohrig and H. G. Wagner, 1992, **96**, 194–198, DOI: 10.1002/bbpc.19920960215.

(81) A. A. Viggiano, D. L. Albritton, F. C. Fehsenfeld, N. G. Adams, D. Smith and F. Howorka, 1980, **236**, 492, DOI: 10.1086/157766.

(82) F. C. Felisenfeld, 1976, **209**, 638, DOI: 10.1086/154761.

(83) N. Copp, M. Hamdan, J. Jones, K. Birkinshaw and N. Twiddy, 1982, **88**, 508–511, DOI: 10.1016/0009-2614(82)83164-3.

(84) N. K. Srinivasan, M.-C. Su, J. W. Sutherland and J. V. Michael, 2005, **109**, 1857–1863, DOI: 10.1021/jp040679j.

(85) N. Cohen and K. R. Westberg, 1991, **20**, 1211–1311, DOI: 10.1063/1.555901.

(86) N. Cohen and K. R. Westberg, 1983, **12**, 531–590, DOI: 10.1063/1.555692.

(87) J. H. W. T., 1977, **33**, 495, DOI: 10.1086/190439.

(88) J. T. Petty, J. A. Harrison and C. B. Moore, 1993, **97**, 11194–11198, DOI: 10.1021/j100145a013.

(89) B. Wang, H. Hou and Y. Gu, 1999, **103**, 8021–8029, DOI: 10.1021/jp991203g.

(90) S. P. Sander and R. T. Watson, 1980, **84**, 1664–1674, DOI: 10.1021/j100450a002.

(91) N. Adams, D. Smith and D. Grief, 1978, **26**, 405–415, DOI: 10.1016/0020-7381(78)80059-x.

(92) T. Tsuboi and K. Hashimoto, 1981, **42**, 61–76, DOI: 10.1016/0010-2180(81)90142-5.

(93) H. J. Curran, 2006, **38**, 250–275, DOI: 10.1002/kin.20153.

(94) K. Brudnik, A. A. Gola and J. T. Jodkowski, 2009, **15**, 1061–1066, DOI: 10.1007/s00894-009-0461-x.

(95) J. T. Jodkowski, M.-T. Rayez, J.-C. Rayez, T. Berces and S. Dobe, 1999, **103**, 3750–3765, DOI: 10.1021/jp984367q.

(96) W. Tsang, 1987, **16**, 471–508, DOI: 10.1063/1.555802.

(97) Y. Hidaka, T. Oki, H. Kawano and T. Higashihara, 1989, **93**, 7134–7139, DOI: 10.1021/j100357a022.

(98) A. D. Sen, V. G. Anicich and S. R. Federman, 1992, **391**, 141, DOI: 10.1086/171331.

(99) G. I. Mackay, A. C. Hopkinson and D. K. Bohme, 1978, **100**, 7460–7464, DOI: 10.1021/ja00492a003.

(100) H. S. Lee, M. Drucker and N. G. Adams, 1992, **117**, 101–114, DOI: 10.1016/0168-1176(92)80088-i.

(101) R. A. Yetter, H. Rabitz, F. L. Dryer, R. G. Maki and R. B. Klemm, 1989, **91**, 4088–4097, DOI: 10.1063/1.456838.

(102) A. Galano, J. R. Alvarez-Idaboy, M. E. Ruiz-Santoyo and A. Vivier-Bunge, 2002, **106**, 9520–9528, DOI: 10.1021/jp020297i.

(103) E. Assaf, C. Schoemaecker, L. Vereecken and C. Fittschen, 2018, **20**, 10660–10670, DOI: 10.1039/c7cp05770a.

(104) S. H. Mousavipour and Z. Homayoon, 2011, **115**, 3291–3300, DOI: 10.1021/jp112081r.

(105) M. Altarawneh, A. H. Al-Muhtaseb, B. Z. Dlugogorski, E. M. Kennedy and J. C. Mackie, 2011, **32**, 1725–1733, DOI: 10.1002/jcc.21756.

(106) H.-G. Yu and J. S. Francisco, 2009, **113**, 3844–3849, DOI: 10.1021/jp809730j.

(107) H. M. T. Nguyen, H. T. Nguyen, T.-N. Nguyen, H. V. Hoang and L. Vereecken, 2014, **118**, 8861–8871, DOI: 10.1021/jp506175k.

(108) Z. Zhao, J. Song, B. Su, X. Wang and Z. Li, 2018, **122**, 5078–5088, DOI: 10.1021/acs.jpca.7b09988.

(109) F. Xiao, X. Sun, Z. Li and X. Li, *ACS Omega*, 2020, **5**, 12777–12788, DOI: 10.1021/acsomega.0c00400.

(110) V. D. Knyazev, 2017, **685**, 165–170, DOI: 10.1016/j.cplett.2017.07.040.

(111) A. M. Mebel, E. W. G. Diau, M. C. Lin and K. Morokuma, 1996, **118**, 9759–9771, DOI: 10.1021/ja961476e.

(112) S. A. Carl, H. M. T. Nguyen, R. M. I. Elsamra, M. T. Nguyen and J. Peeters, 2005, **122**, 114307, DOI: 10.1063/1.1861887.

(113) D. K. Bohme and G. I. Mackay, 1981, **103**, 2173–2175, DOI: 10.1021/ja00399a006.

(114) Y. Hidaka, T. Nishimori, K. Sato, Y. Henmi, R. Okuda, K. Inami and T. Higashihara, 1999, **117**, 755–776, DOI: 10.1016/s0010-2180(98)00128-x.

(115) J. Gimenez-Lopez, C. T. Rasmussen, H. Hashemi, M. U. Alzueta, Y. Gao, P. Marshall, C. F. Goldsmith and P. Glarborg, 2016, **48**, 724–738, DOI: 10.1002/kin.21028.

(116) A. Raksit, 1986, **69**, 45–65, DOI: 10.1016/0168-1176(86)87041-0.

(117) B. K. Decker, N. G. Adams and L. M. Babcock, 2000, **195-196**, 185–201, DOI: 10.1016/s1387-3806(99)00146-3.

(118) G. B. I. Scott, D. B. Milligan, D. A. Fairley, C. G. Freeman and M. J. McEwan, 2000, **112**, 4959–4965, DOI: 10.1063/1.481050.

(119) P.-C. Nam, P. Raghunath, L. K. Huynh, S. Xu and M. C. Lin, 2016, **188**, 1095–1114, DOI: 10.1080/00102202.2016.1151878.

(120) Y. Hidaka, K. Kimura and H. Kawano, 1994, **99**, 18–28, DOI: 10.1016/0010-2180(94)90079-5.

(121) L. K. Huynh and A. Violi, 2007, **73**, 94–101, DOI: 10.1021/jo701824n.

(122) K. Ohmori, A. Miyoshi, H. Matsui and N. Washida, 1990, **94**, 3253–3255, DOI: 10.1021/j100371a006.

(123) J. Warnatz, in Springer New York, 1984, pp. 197–360, DOI: 10.1007/978-1-4684-0186-8_5.

(124) R. Sivaramakrishnan, J. V. Michael and S. J. Klippenstein, 2009, **114**, 755–764, DOI: 10.1021/jp906918z.

(125) Z. F. Xu, K. Xu and M. C. Lin, 2011, **115**, 3509–3522, DOI: 10.1021/jp110580r.

(126) W.-K. Aders and H. G. Wagner, 1973, **77**, 332–335, DOI: https://doi.org/10.1002/bbpc.19730770509.

(127) R. Sivaramakrishnan, M.-C. Su, J. V. Michael, S. J. Klippenstein, L. B. Harding and B. Ruscic, 2010, **114**, 9425–9439, DOI: 10.1021/jp104759d.

(128) S.-Z. Xiong, Q. Yao, Z.-R. Li and X.-Y. Li, 2014, **161**, 885–897, DOI: 10.1016/j.combustflame.2013.10.013.

(129) M. Cameron, V. Sivakumaran, T. J. Dillon and J. N. Crowley, 2002, **4**, 3628–3638, DOI: 10.1039/b202586h.

(130) N. M. Marinov, 1999, **31**, 183–220, DOI: 10.1002/(sici)1097-4601(1999)31:3<183::aid-kin3>3.0.co;2-x.

(131) C. Olm, T. Varga, E. Valko, S. Hartl, C. Hasse and T. Turanyi, 2016, **48**, 423–441, DOI: 10.1002/kin.20998.

(132) D. Skouteris, N. Balucani, C. Ceccarelli, F. Vazart, C. Puzzarini, V. Barone, C. Codella and B. Lefloch, 2018, **854**, 135, DOI: 10.3847/1538-4357/aaa41e.

(133) G. da Silva, J. W. Bozzelli, L. Liang and J. T. Farrell, 2009, **113**, 8923–8933, DOI: 10.1021/jp903210a.

(134) A. S. Semenikhin, E. G. Shubina, A. S. Savchenkova, I. V. Chechet, S. G. Matveev, A. A. Konnov and A. M. Mebel, 2018, **50**, 273–284, DOI: 10.1002/kin.21156.

(135) P. Frank, K. A. Bhaskaran and T. Just, 1986, **90**, 2226–2231, DOI: 10.1021/j100401a046.

(136) E. Hassinen, K. Kalliorinne and J. Koskikallio, 1990, **22**, 741–745, DOI: 10.1002/kin.550220709.

(137) G. Hoehlein and G. R. Freeman, 1970, **92**, 6118–6125, DOI: 10.1021/ja00724a004.

(138) X. Zhang, L. Ye, Y. Li, Y. Zhang, C. Cao, J. Yang, Z. Zhou, Z. Huang and F. Qi, 2018, **191**, 431–441, DOI: 10.1016/j.combustflame.2018.01.027.

(139) D. M. Golden, G. P. Smith, A. B. McEwen, C.-L. Yu, B. Eiteneer, M. Frenklach, G. L. Vaghjiani, A. R. Ravishankara and F. P. Tully, 1998, **102**, 8598–8606, DOI: 10.1021/jp982110m.

(140) T. J. Held and F. L. Dryer, 1998, **30**, 805–830, DOI: 10.1002/(sici)1097-4601(1998)30:11<805::aid-kin4>3.0.co;2-z.

(141) C. Dombrowsky, A. Hoffmann, M. Klatt and H. G. Wagner, *Berichte der Bunsengesellschaft fur physikalische Chemie*, 1991, **95**, 1685–1687, DOI: 10.1002/bbpc.19910951217.

(142) P. Frank, K. Bhaskaran and T. Just, 1988, **21**, 885–893, DOI: 10.1016/s0082-0784(88)80320-5.

(143) K. Yasunaga, S. Kubo, H. Hoshikawa, T. Kamesawa and Y. Hidaka, 2007, **40**, 73–102, DOI: 10.1002/kin.20294.

(144) C. Cavallotti, M. Pelucchi and A. Frassoldati, *Proceedings of the Combustion Institute*, 2019, **37**, 539–546, DOI: 10.1016/j.proci.2018.06.137.

(145) E. E. Dames, 2014, **46**, 176–188, DOI: 10.1002/kin.20844.

(146) B. Ganguli, M. A. Biondi, R. Johnsen and J. L. Dulaney, *Physical Review A*, 1988, **37**, 2543–2547, DOI: 10.1103/physreva.37.2543.

(147) W. D. Geppert, R. Thomas, A. Ehlerding, J. Semaniak, F. Osterdahl, M. af Ugglas, N. Djuric, A. Paal and M. Larsson, *Faraday Discuss.*, 2004, **127**, 425–437, DOI: 10.1039/b314005a.

(148) Obtained from LXCAT (Morgan database), www.lxcat.net.

(149) Obtained from LXCAT (Itikawa database), www.lxcat.net.

(150) I. A. Kossyi, A. Y. Kostinsky, A. A. Matveyev and V. P. Silakov, *Plasma Sources Science and Technology*, 1992, **1**, 207–220, DOI: 10.1088/0963-0252/1/3/011.

(151) C. PARK, in *24th Thermophysics Conference*, DOI: 10.2514/6.1989-1740.

(152) S. G. Belostotsky, D. J. Economou, D. V. Lopaev and T. V. Rakhimova, *Plasma Sources Science and Technology*, 2005, **14**, 532–542, DOI: 10.1088/0963-0252/14/3/016.

(153) A. Cenian, A. Chernukho and V. Borodin, *Contributions to Plasma Physics*, 1995, **35**, 273–296, DOI: 10.1002/ctpp.2150350309.

(154) L. E. Khvorostovskaya and V. A. Yankovsky, *Contributions to Plasma Physics*, 1991, **31**, 71–88, DOI: 10.1002/ctpp.2150310109.

(155) W. Wang, R. Snoeckx, X. Zhang, M. S. Cha and A. Bogaerts, *The Journal of Physical Chemistry C*, 2018, **122**, 8704–8723, DOI: 10.1021/acs.jpcc.7b10619.

(156) H. Hokazono, M. Obara, K. Midorikawa and H. Tashiro, *Journal of Applied Physics*, 1991, **69**, 6850–6868, DOI: 10.1063/1.347675.

(157) C. Lifshitz, R. L. C. Wu, J. C. Haartz and T. O. Tiernan, *The Journal of Chemical Physics*, 1977, **67**, 2381, DOI: 10.1063/1.435078.

(158) D. S. Stafford and M. J. Kushner, *Journal of Applied Physics*, 2004, **96**, 2451–2465, DOI: 10.1063/1.1768615.

(159) J. T. Gudmundsson and E. G. Thorsteinsson, *Plasma Sources Science and Technology*, 2007, **16**, 399–412, DOI: 10.1088/0963-0252/16/2/025.

(160) T. G. Beuthe and J.-S. Chang, *Japanese Journal of Applied Physics*, 1997, **36**, 4997–5002, DOI: 10.1143/jjap.36.4997.

(161) L. Polak and D. Slovetsky, *International Journal for Radiation Physics and Chemistry*, 1976, **8**, 257–282, DOI: 10.1016/0020-7055(76)90070-x.

(162) Obtained from LXCAT (Biagi database), www.lxcat.net.

(163) C. Park, J. T. Howe, R. L. Jaffe and G. V. Candler, *Journal of Thermophysics and Heat Transfer*, 1994, **8**, 9–23, DOI: 10.2514/3.496.

(164) A. J. Dean, D. F. Davidson and R. K. Hanson, *The Journal of Physical Chemistry*, 1991, **95**, 183–191, DOI: 10.1021/j100154a037.

(165) S. J. Petuchowski, E. Dwek, J. A. J. E. and I. N. J. A., *The Astrophysical Journal*, 1989, **342**, 406, DOI: 10.1086/167601.

(166) L. M. Arin and P. Warneck, *The Journal of Physical Chemistry*, 1972, **76**, 1514–1516, DOI: 10.1021/j100655a002.

(167) M. McFarland, D. L. Albritton, F. C. Fehsenfeld, E. E. Ferguson and A. L. Schmeltekopf, *The Journal of Chemical Physics*, 1973, **59**, 6629–6635, DOI: 10.1063/1.1680043.

(168) F. C. Fehsenfeld and E. E. Ferguson, *The Journal of Chemical Physics*, 1972, **56**, 3066–3070, DOI: 10.1063/1.1677642.

(169) D. Husain and A. N. Young, *Journal of the Chemical Society, Faraday Transactions 2*, 1975, **71**, 525, DOI: 10.1039/f29757100525.

(170) D. W. Fahey, F. C. Fehsenfeld and E. E. Ferguson, *Geophysical Research Letters*, 1981, **8**, 1115–1117, DOI: 10.1029/gl008i010p01115.

(171) M. Burmeister and P. Roth, *AIAA Journal*, 1990, **28**, 402–405, DOI: 10.2514/3.10406.

(172) I. Mendez, F. J. Gordillo-Vazquez, V. J. Herrero and I. Tanarro, *The Journal of Physical Chemistry A*, 2006, **110**, 6060–6066, DOI: 10.1021/jp057182+.

(173) D. X. Liu, P Bruggeman, F Iza, M. Z. Rong and M. G. Kong, *Plasma Sources Science and Technology*, 2010, **19**, 025018, DOI: 10.1088/0963-0252/19/2/025018.

(174) B Gordiets, C. M. Ferreira, M. J. Pinheiro and A Ricard, *Plasma Sources Science and Technology*, 1998, **7**, 363–378, DOI: 10.1088/0963-0252/7/3/015.

(175) Obtained from LXCAT (Hayashi database), www.lxcat.net.

List of publications

As first author

- **Slaets, J.**; Aghaei, M.; Ceulemans, S.; Van Alphen, S.; Bogaerts, A. CO_2 and CH_4 conversion in "real" gas mixtures in a gliding arc plasmatron: how do N_2 and O_2 affect the performance? *Green Chemistry* **2020**, *22* (4), 1366–1377. https://doi.org/10.1039/c9gc03743h.

- Van Alphen, S.*; **Slaets, J.***; Ceulemans, S.; Aghaei, M.; Snyders, R.; Bogaerts, A. Effect of N_2 on CO_2-CH_4 conversion in a gliding arc plasmatron: Can this major component in industrial emissions improve the energy efficiency? Journal of CO2 Utilization **2021**, 54, 101767. https://doi.org/10.1016/j.jcou.2021.101767.

- **Slaets, J.**; Loenders, B.; Bogaerts, A. Plasma-based dry reforming of CH_4: Plasma effects vs. thermal conversion. *Fuel* **2024**, *360*, 130650. https://doi.org/10.1016/j.fuel.2023.130650.

- Van Alphen, S.*; Wanten, B.*; Girard-Sahun, F.*; **Slaets, J.***; Creel, J.; Aghaei, M.; Bogaerts, A. The role of CH_4 in Plasma-Assisted CO_2 and CH_4 conversion in a rotating gliding arc plasma: Insights revealed by experiments and modeling. *ACS Sustainable Chemistry & Engineering* **2024**. https://doi.org/10.1021/acssuschemeng.4c06627.

- **Slaets, J.**; Morais, E.; Bogaerts, A. Afterglow quenching in plasma-based dry reforming of methane: a detailed analysis of the post-plasma chemistry via kinetic modelling. Submitted to Fuel.

* shared first author

As Co-author

- Wanten, B.; Maerivoet, S.; Vantomme, C.; **Slaets, J.**; Trenchev, G.; Bogaerts, A. Dry reforming of methane in an atmospheric pressure glow discharge: Confining the plasma to expand the performance. *Journal of CO2 Utilization* **2022**, *56*, 101869. https://doi.org/10.1016/j.jcou.2021.101869.

- Maerivoet, S.; Tsonev, I.; **Slaets, J.**; Reniers, F.; Bogaerts, A. Coupled multi-dimensional modelling of warm plasmas: Application and validation for an atmospheric pressure glow discharge in $CO_2/CH_4/O_2$. *Chemical Engineering Journal* **2024**, *492*, 152006. https://doi.org/10.1016/j.cej.2024.152006.

Conference contributions

- Poster presentation: Kerogreen workshop (15/11/2019) "Gliding arc plasma: a promising approach for CO_2 and CH_4 conversion into value-added chemicals", Eindhoven, The Netherlands
- Oral presentation: UCRA 2022 (22/09/2022) "Plasma-based reforming of CO_2 and CH_4 under atmospheric pressures, a chemical breakdown through 0D kinetics modelling", Leamington Spa, United Kingdom

Other achievements

- Supervisor for the bachelor's thesis of Stein Maerivoet at PLASMANT (2020)
- Supervisor for the master's thesis of Bart Wanten at PLASMANT (2020)
- Supervisor for the bachelor's thesis of Maxim Biscop at PLASMANT (2021)
- Supervisor for the bachelor's thesis of Keyo Aubry at PLASMANT (2022)
- Supervisor for the bachelor's thesis of Amira Vandenbroucke at PLASMANT (2023)